EXPERIMENTAL TANK AND GATING SYSTEM (ETAGS)

Final Report

Contract No. 26-3425

to

UNITED STATES DEPARTMENT OF AGRICULTURE
FOREST SERVICE
INTERMOUNTAIN FOREST & RANGE EXPERIMENT STATION
OGDEN, UTAH 84401

A REPORT OF RESEARCH PERFORMED UNDER THE AUSPICES OF THE INTERMOUNTAIN FOREST AND RANGE EXPERIMENT STATION, OGDEN, UTAH.

Honeywell
600 2ND STREET NORTHEAST
HOPKINS, MINNESOTA 55343

EXPERIMENTAL TANK AND GATING SYSTEM (ETAGS)

Final Report
by D.H. Swanson, A.D. Luedecke
and T.N.Helvig

Contract No. 26-3425

1 September 1978

U.S. Department of Agriculture
Forest Service
Intermountain Forest and Range Experiment Station
Ogden, Utah 84401

HONEYWELL DEFENSE SYSTEMS DIVISION - 600 Second Street Northeast, Hopkins, Minnesota 55343

47361

TABLE OF CONTENTS

Section		Page
I	INTRODUCTION AND SUMMARY	1
	Background	1
	Summary	2
II	TANK DESIGN	4
	Conceptual Design	4
	Structural Design	7
	Filling System	7
	Venting System	9
	Gating System	10
	Opening and Closing Mechanism	11
	Drive System	11
	Door Seals	14
	Hydraulic Control System	18
	Electrical System	23
	Tank Control System	27
	Instrumentation System	32
	Supplemental Fixtures	38
	Loading Indicator	38
	Downloading Fixture	38
	Aircraft Installation	38
III	FLOW RATE STUDIES	41
	Background	41
	Summary	43
	Initial Studies	43
	Door Fluid Studies	46
IV	FLIGHT TEST PLAN	58
V	VERIFICATION OF FLIGHT DATA	62
	Drop Conditions	62
	Drop Heights	62
	Aircraft Velocity	62
	Tank Performance	63
	Door Performance	64
	Flow Rate Measurement	69
	Matched Flow Rates from Configuration Drops	76
VI	SELECTION OF ANALYSIS TECHNIQUES	79
	Chi-Square Analysis	79
	Alternative Techniques	82
	Replicate Analysis	83
	Fourier Analysis	86
	Distributional Studies	97
	Modified PATSIM	109

TABLE OF CONTENTS (Concluded)

Section		Page
VII	MATRIX ANALYSIS	123
	Measures of Pattern Performance	123
	Length of Inner 90% of Pattern	123
	Area Above 1 gpc	125
	Weighted Average Concentration	125
	Three-Dimensional Pattern Concentration Plots	125
	Interpretive Graphics for Inner 90% Pattern Length	126
	Linear Regression Statistics	126
	Flow Rate (Time out of Tank) Studies (Test Matrix 1)	127
	Tank Configuration Studies (Test Matrix 2)	128
	920-Gallon Load Size Configuration (Test Matrix 3)	149
	Head Height Experiment (Test Matrix 4)	149
	Load Size Test Series (Test Matrix 5)	161
	Airspeed Test Series (Test Matrix 6)	165
	Additional Door Rate Studies (Test Matrix 7)	173
	Retardant Downrange Distance Traveled	191
VIII	DATA ANALYSIS SUMMARY	206
	Aircraft-Induced Spread	206
	Time out of Tank	206
	Exit Geometry	208
	Aircraft Velocity	210
	Retardant Quantity	212
	Tank Separation	213
	Head-Height	216
	Comparison of Matrix Results	218
IX	CONCLUSIONS AND RECOMMENDATIONS	221
	Model Elements	221
	Flow Rate	221
	Tank Configuration	225
	Approximate Effects of the Propositions on Pattern Formation	230
REFERENCES		232
APPENDIX A.	ETAGS STRUCTURAL ANALYSIS	A-1
APPENDIX B.	FLOW RATE OFF-LINE PROGRAM LISTING AND PROGRAM FLOW	B-1
APPENDIX C.	ETAGS PROGRAM TEST DROPS	C-1
APPENDIX D.	TEST MATRICES	D-1

LIST OF ILLUSTRATIONS

Figure		Page
1	ETAGS Tank in Test Data Matrix	5
2	Tank Layout and Capabilities	6
3	Tank Design Details	8
4	Tank Fill System	9
5	Door Arrangement - Top View	10
6	Door Design Details	12
7	Door Operating Mechanism	13
8	Door Drive System	15
9	Door Sealing Technique	17
10	Door Closure Tuning Mechanisms	18
11	Door Control Hydraulics	19
12	Hydraulic System Schematic	21
13	Door Actuator Electrical Connections	24
14	Door Actuator System Electrical Schematic	25
15	Door Limit Switch Connections	28
16	Tank Control System Components	29
17	Pilot's Control Panel Layout	30
18	Test Setup Panel Layout	31
19	ETAGS Instrumentation Schematic	33
20	Instrumentation Patch Panel	34
21	Pressure Instrumentation Manifold	34
22	Float System	37
23	Tank Fillmeter	39
24	Downloading Fixture	39
25	ETAGS Installation on P2V-5F Aircraft	40
26	Comparison of Actual and Theoretical Flow Rate	44
27	High-Speed Door Sequence Showing Phenomena at the Door-to-Fluid Interface	47

LIST OF ILLUSTRATIONS (Continued)

Figure		Page
28	Four Different Door Conditions	48
29	Comparison of Actual and Simulated Single Unit Tank, Full Door Release for Two Door Rates	49
30	Simulation Printout for Figure 29(a) - Fast Door	50
31	Simulation Printout for Figure 29(b) - Slow Door	50
32	Comparison of Actual and Simulated Four-Unit Tank, 1/2-Door Release for Two Door Rates	51
33	Simulation Printout for Figure 32(a) - Fast Door	52
34	Simulation Printout for Figure 32(b) - Slow Door	53
35	Comparison of Actual and Simulated Four-Unit Tank, 1/4-Door Release	54
36	Simulation Printout for Figure 35	55
37	ETAGS Tank in Test Data Matrix	60
38	Data Analysis Elements	61
39	Door 1 Performance Summary	65
40	Door 2 Performance Summary	66
41	Door 3 Performance Summary	67
42	Door 4 Performance Summary	68
43	Flow Rates and Pressures for Full-Door Drop, Tank 5, Rate 6	70
44	Flow Rate and Three-Dimensional Ground Pattern for 3/4-Door Drop, Rate 6	71
45	Flow Rates and Pressures for Full-Door Drops Tank 5, Rate 2	72
46	Flow Rates and Pressures for 1/2-Door Drops Tank 5, Rate 6	73
47	Flow Rates, Pressures and Ground Pattern Cross Section for 1/2-Door Drops, Rate 2	74
48	Flow Rates and Ground Pattern Cross Section for 1/4-Door Drops	75
49	Combined and Single-Door Performance	78
50	Comparison of Three Replicate Drops - Full-Door, Rate 6, Water	84
51	Comparison of Two Replicate Drops - 3/4-Door, Rate 6, Phos-Chek	85

LIST OF ILLUSTRATIONS (Continued)

Figure		Page
52	Replicate Analysis - Low-Speed Group	87
53	Replicate Analysis - High-Speed Group	89
54	Steps in the Fourier Simulation	94
55	Fourier Transfer Functions for Selected Configuration Drops	95
56	Marginal Distribution Definition	98
57	Weibul Distribution Model as Applied to Retardant Pattern Analysis	101
58	Tests for Normal Distribution of Crossrange Patterns	104
59	Confirmation of Normal Distributions in Extreme Patterns	105
60	Crossrange Marginals of Selected Drops	106
61	Cumulative Marginal Distribution Using Beta	111
62	Sample Distribution of Actual Drop	111
63	Range Marginals and Distance from Release to Impact - Water	114
64	Range Marginals and Distance from Release to Impact - Phos-Chek	114
65	Tank Configuration Geometries	115
66	Range Marginals for Phos-Chek Drops of Three Configurations ("means" forced)	116
67	Pattern Length Parameters as a Function of Velocity for All Phos-Chek Drops of Tank Configuration C1	117
68	Tank Configuration C1 Water Drops Compared with Phos-Chek (PX) and Simulation (S) Drops	119
69	Three-Dimensional Plots of Retardant Concentration from Flow Rate Study - Phos-Chek	129
70	Three-Dimensional Plots of Retardant Concentration from Flow Rate Study - Water	131
71	Flow Rate Study Results for Phos-Chek Drops at 150 and 300 Feet	133
72	Three-Dimensional Plots of Retardant Concentrations from Tank Configuration Studies - Phos-Chek	137
73	Three-Dimensional Plots of Retardant Concentrations from Tank Configuration Studies - Water	139
74	Pattern Length versus Tank Configuration at Two Drop Heights and Two Drop Speeds - Phos-Chek	142

LIST OF ILLUSTRATIONS (Continued)

Figure		Page
75	Pattern Length versus Tank Configuration at Two Drop Heights and Two Drop Speeds - Water	143
76	Pattern Length versus Compartment Length-to-Width Ratio for Two Drop Heights and Two Drop Speeds - Phos-Chek	144
77	Pattern Length versus Compartment Length-to-Width Ratio for Two Drop Heights and Two Drop Speeds - Water	145
78	Least-Squares Fit of Length of Inner 90% as a Function of Compartment Length-to-Width Ratio	146
79	Pattern Length as a Function of Compartment Length	147
80	Three-Dimensional Plots of Retardant Concentration from 920-gallon Load Size Studies, 300-foot Drop Height - Phos-Chek	151
81	Three-Dimensional Plots of Retardant Concentration from 920-gallon Load Size Studies, 300-foot Drop Height - Water	153
82	Pattern Length versus Tank Configuration (920-gallon load) at 300-foot Drop Height and Two Door Rates - Phos-Chek	155
83	Pattern Length versus Tank Configuration (920-gallon load) at 300-foot Drop Height and Two Door Rates - Water	155
84	Three-Dimensional Plots of Retardant Concentration from Head-Height Experiment - Phos-Chek	157
85	Three-Dimensional Plots of Retardant Concentration from Head-Height Experiment - Water	159
86	Pattern Length versus Head Height and Time-Out-of Tank - Phos-Chek	162
87	Pattern Length versus Head Height and Time-Out-of Tank - Water	163
88	Effects of Tank Length-to-Width Ratio on Head Height Experiment	164
89	Error from Use of Length as a Predictor of 90% Pattern Length	165
90	Three Dimensional Plots of Retardant Concentration from Load-Size Test Series - Phos-Chek	167
91	Three Dimensional Plots of Retardant Concentration from Load-Size Test Series - Water	169
92	Pattern Length versus Load Size for Two Drop Heights - Phos-Chek	171
93	Three-Dimensional Plots of Retardant Concentration from Airspeed Test Series - Phos-Chek	175

LIST OF ILLUSTRATIONS (Continued)

Figure		Page
94	Three-Dimensional Plots of Retardant Concentration from Airspeed Test Series - Water	177
95	Pattern Length versus Drop Speed for Two Drop Heights - Configuration C3, Phos-Chek	179
96	Pattern Length versus Drop Speed for Two Drop Heights - Configuration C3, Water	179
97	Pattern Length versus Drop Speed for Two Drop Heights - Configuration C1, Phos-Chek	180
98	Pattern Length versus Drop Speed for Two Drop Heights - Configuration C1, Water	181
99	Three-Dimensional Plots of Retardant Concentration from Additional Door Rate Studies - Phos-Chek	185
100	Three-Dimensional Plots of Retardant Concentration from Additional Door Rate Studies - Water	187
101	Pattern Length versus Time Out of Tank for Configuration C1 and Two Drop Heights - Phos-Chek	189
102	Pattern Length versus Time Out of Tank for Configuration C3 and Two Drop Heights - Phos-Chek	190
103	Retardant Downrange Distance Traveled versus Tank Configuration for Two Drop Heights and Two Drop Speeds - Phos-Chek	194
104	Retardant Downrange Distance Traveled versus Head Height at Two Drop Heights - Phos-Chek and Water	195
105	Retardant Downrange Distance Traveled versus Load Size at Two Drop Heights - Phos-Chek and Water	196
106	Retardant Downrange Distance Traveled versus Drop Speed for Two Drop Heights - Configuration C1, Phos-Chek and Water	197
107	Retardant Downrange Distance Traveled versus Drop Speed for Two Drop Heights - Configuration C3, Phos-Chek and Water	198
108	Retardant Downrange Distance Traveled versus Time Out of Tank for Two Drop Heights - Phos-Chek	199
109	Retardant Downrange Distance Traveled versus Time Out of Tank for Two Drop Heights - Water	200
110	Definitions, Parameters and Factors Pertaining to Data Analysis Summary	207
111	Rate of Pattern Length Increase versus Quantity Buildup	213

LIST OF ILLUSTRATIONS (Concluded)

Figure		Page
112	Mixing of Fluid from Various Tank Compartments - 160-foot Drop Height	215
113	Pattern Formation from Tanks Separated Along the Flight Path - 300-foot Drop Height	215
114	Mixing of Fluid from Laterally Separated Tanks	217
115	Sensitivity of Baseline Pattern to Test Parameters in Terms of Pattern Length Divided by Available Retardant	219
116	Forms of Retardant Distribution	220
117	Location of Fluid Head During Tank Evacuation	223
118	Fluid Elongation at Tank Evacuation	223
119	Example of How Fluid Column Reforms to Maintain Equal Volume while Increasing in Length	223
120	Faucet Example	223
121	Approximate Shape of Fluid Mass on Full Exit from Tank	224
122	Vertical Fluid Elongation Due to Flow Rate and its Effect on Breakup	226
123	Fluid Contraction as a Function of Time Out of Tank	226
124	Theoretical Breakup Length	227
125	Approximate Model for Fluid Column Breakup	227
126	Fluid Breakup as a Function of Time and Tank Configuration	229
127	Sequence of Tank Evacuation	230
128	Pattern Formations Generated Using an Approximate Model	231

LIST OF TABLES

Table		Page
1	Pressure Sensor Calibrations	36
2	Evacuation Time Summary	77
3	Range Marginal Distribution	81
4	Replicate Drops	86
5	Pattern Statistics	96
6	Examples of Weibull Analysis	102
7	Calculations for Beta Distribution	110
8	Inner 90% Pattern Length Comparison	112
9	Matrices of Lengths Generated by K_1 and K_2 Combinations	121
10	PATSIM Comparisons	122
11	Linear Regression Analysis Data - Test Matrix 1, Weighted Average	134
12	Linear Regression Analysis Data - Test Matrix 1, Area	135
13	Linear Regression Analysis Data - Test Matrix 1, Length of Inner 90%	136
14	Linear Regression Analysis Data - Test Matrix 3, Length of Inner 90%	156
15	Linear Regression Analysis Data - Test Matrix 4, Length of Inner 90%	166
16	Linear Regression Analysis Data - Test Matrix 5, Length of Inner 90%	172
17	Linear Regression Analysis Data - Test Matrix 6, Length of Inner 90%, Configuration C1	182
18	Linear Regression Analysis Data - Test Matrix 6, Length of Inner 90%, Configuration C3	183
19	Linear Regression Analysis Data - Test Matrix 7, Length of Inner 90%, Configuration C3	
20	Linear Regression Analysis Data - Test Matrix 7, Length of Inner 90%, Configuration C1	193
21	Linear Regression Analysis Data - Test Matrix 1, Distance Traveled	201
22	Linear Regression Analysis Data - Test Matrix 4, Distance Traveled	202
23	Linear Regression Analysis Data - Test Matrix 5, Distance Traveled	203
24	Linear Regression Analysis Data - Test Matrix 6, Distance Traveled, Configuration C3	204
25	Linear Regression Analysis Data - Test Matrix 6, Distance Traveled, Configuration C1	205

SECTION I
INTRODUCTION AND SUMMARY

The Experimental Tank and Gating System (ETAGS) Program was initiated in 1974 as a means to a better understanding of the effect of aircraft tank and gating characteristics on retardant dispersion and ground pattern formation. The original contract required the design and fabrication of the experimental tank to be instrumented and installed in a Forest Service P2V aircraft and data collected on tank performance in ground and flight tests. The contract was subsequently modified and extended to include analysis of the resulting tank and ground data and the preparation of a Tank Design Guide incorporating the knowledge gained through the experiment.

BACKGROUND

The Forest Service has long recognized the need for increased safety and improved efficiency in the aerial delivery of retardants. The ETAGS program is one of several projects to obtain analytical insight into the behavior of retardant as it is released from the aircraft, spreads, drops, and coats the fuel. The ETAGS experiment was initially recommended by Honeywell during the High Altitude Retardant Drop Mechanization Study as a means of providing definitive answers to key questions of tank design.

The general objectives of such an experiment are twofold:

- First, to provide independent contractors with source data and design information that will enable them to tank diverse aircraft with effective, near-optimum systems.
- Second, to provide the basis for critique and improvement of existing tankers through practical design changes or more knowledgeable use by operating personnel.

Work on the High Altitude Retardant Drop Mechanization Study and the ensuing User Guideline Program had demonstrated that the flow-rate distribution from the tank, retardant quantity, and the retardant rheological system so dominate the pattern formation process that it is relatively insensitive to subordinate parameters other than aircraft velocity and altitude. The effects of other factors – exit geometry, tank separation, etc. – are difficult to resolve without drop data

from a calibrated tank. In addition, tank characteristics affecting flow rate, such as door area, opening rate, hydraulic head, tank geometry and venting, though they yield to approximate modeling, require more precise data.

Specifically, then, ETAGS provides the basis for the release of retardant under known and well controlled initial conditions. These initial conditions are directly relatable to pattern performance collected on the ground plane.

The ETAGS system is a calibrated and instrumented test bed for conducting the experiments plus additional tests to examine retardant rheological factors or other tank-control variables. It is a system for the generalized evaluation of tank, gating, and retardant parameters that could potentially become a standard test bed for research purposes with usage extending beyond the immediately envisioned test program.

SUMMARY

ETAGS is a hydrodynamically clean design capable of simulating performance of a wide range of tanks and their variations, including tank length, height, width, volume, door speed, door area, and compartment separation. It was flown in a series of 245 flight tests in a Forest Service P2V-5 aircraft in Chico, California, during 1975. In each flight, door-opening rates, fluid evacuation rate, and tank internal pressure were recorded as related to an initial release time signaled to ground cameras by a flash-bulb mounted externally on the aircraft. Trajectory data on each drop were recorded by Forest Service ground cameras. The resulting coverage levels were determined by weighing the retardant (or water) captured in a grid of cups in the drop area.

The test series resulted directly in a large body of data on important design questions including issues of retardant rheology under investigation in a separate program.

Analysis of the data from these drops yields confirmation of many conclusions on the effect of tank performance previously outlined. Among these are both the effect of flow rate and its methods of control. The analysis also yielded information on the phenomena of retardant pattern formation not previously described. Foremost of these is the contribution of the exit geometry (door shape) to the pattern distribution, a factor not clearly apparent in prior tests on specific tanks. Second, considerable insight was generated on the effect of simultaneous

release of retardant from physically separated compartments. Finally, new insight was provided on the breakup process itself in a small series of drops using diversely colored water in separate tank compartments. Details of the results presented here have been used to generate a Tank Design Guide published under separate cover.

SECTION II
TANK DESIGN

The Experimental Tank and Gating System (ETAGS) was designed to provide capability for testing a large number of tank-controlled retardant delivery parameters. In effect, the tank's combination of separately releasable retardant volumes and wide dynamic range of door rates enables it to imitate the performance of most known tanks under controlled conditions. Figure 1 shows the various release configurations enabled in the tank. The tank was designed to implement a preplanned test series when installed in a U.S. Forest Service-owned P2V-5F aircraft.

CONCEPTUAL DESIGN

Aircraft installation in the bomb or fuel bay of the P2V-5F limits the tank width to 70 inches and the length to 132 inches without aircraft modification. The test concept required that self-contained volumes be used like building blocks to produce the various drops of the experiment. As a result, all compartments are constrained to straight-sided multiples of a single unit. Additionally, the tank compartments were to be mechanically "clean", with no mechanisms to interrupt fluid flow. This was achieved by employing a double-wall construction so that door-opening mechanisms could operate outside of the fluid. The plan of the tank after allocation of space to the double walls is shown in Figure 2.

This plan establishes a door width of 16.96 inches to cover one row of single-unit compartments. The full-open door in conjunction with aircraft ground clearance determines the allowable extension of the tank below the aircraft fuselage. Upward extension into the bomb bay is limited by aircraft wing structure. This results in a maximum tank height of 62 inches.

Attachment to the aircraft is by a structural angle iron along each side of the fuselage. This provision had been employed to support the previous tank. The distance between these support points is about 90 inches. As a result, the tank structure must extend an additional 10 inches beyond the tank walls on

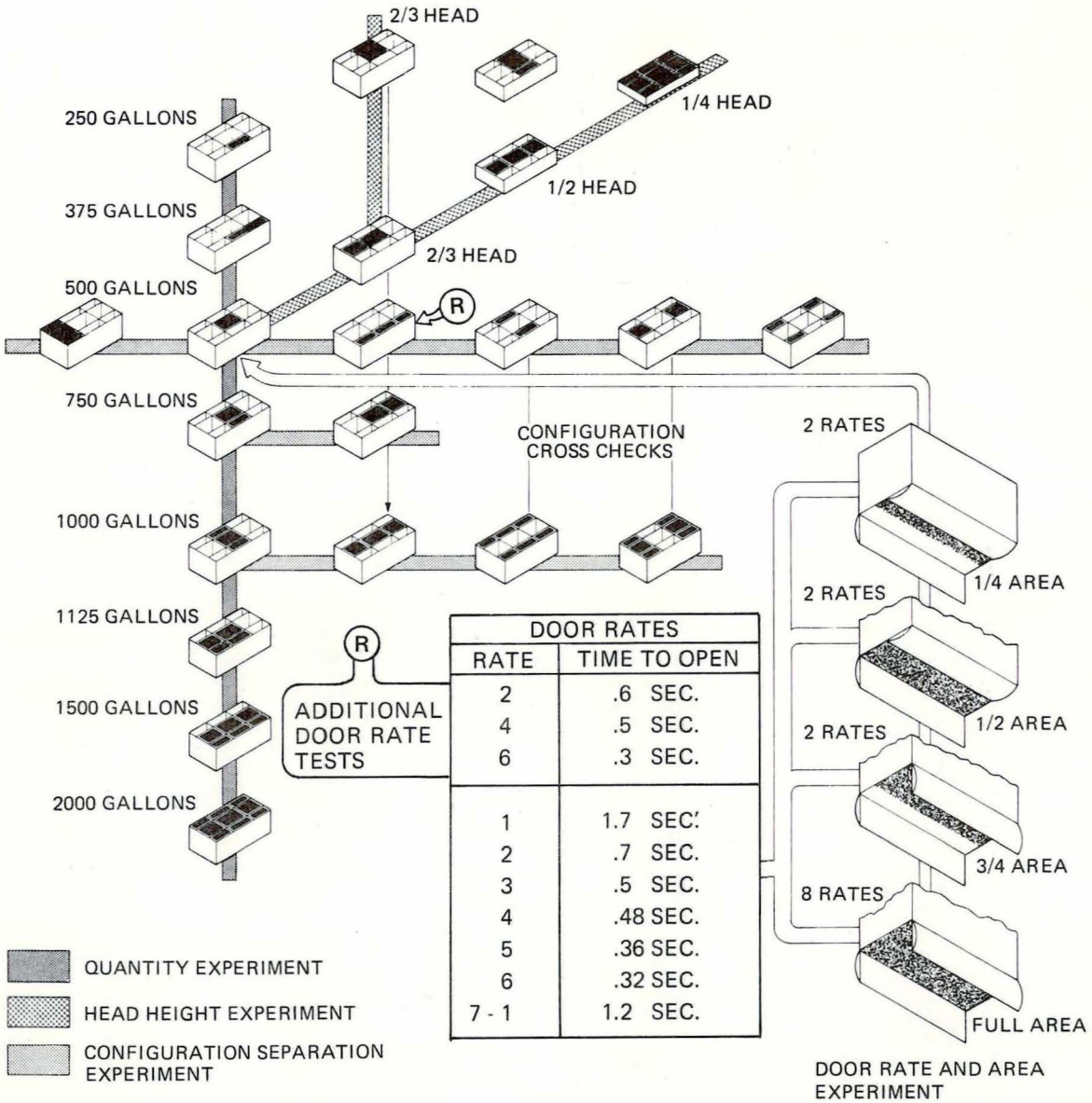

Figure 1. ETAGS Tank in Test Data Matrix

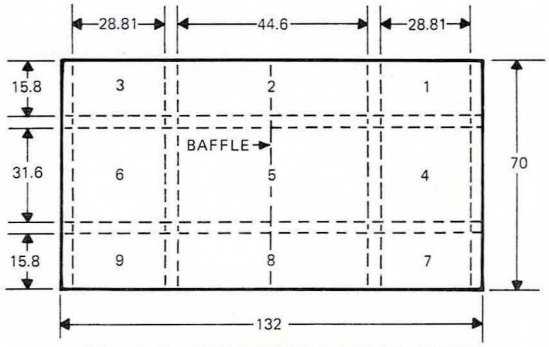

PLAN VIEW – COMPARTMENT LAYOUT FROM TOP
(DIMENSIONS IN INCHES)

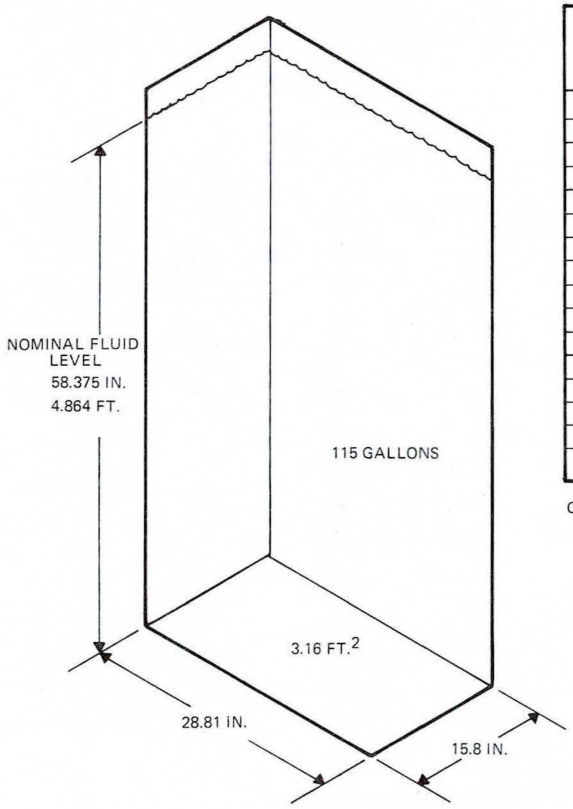

BASIC TANK UNIT

CAPABILITIES

UNITS	TANKS	GALLONS	DOOR AREA (ft^2)	DOOR CONSTRICTIONS (ft^2)		
				¼	½	¾
1	1, 3, 7, 9	115	3.16			
2	2, 4, 6, 8	230	6.32			
3	C	345	9.48			
4	5	460	12.64	3.16	6.32	9.48
5	C	575				
6	C	690	18.96			
7	C	805				
8	C	920	25.28			
9	C	1035	28.44			
10	C	1150				
11	C	1265				
12	C	1380	37.92			
13	C	1495				
14	C	1610				
15	C	1725				
16	C	1840	50.56			

C = COMBINATIONS

Figure 2. Tank Layout and Capabilities

each side to pick up the aircraft support structure. It was decided to use this extension to provide greater rigidity in the structure and to fair the sides of the tank. As a result, the tank cross section was established as shown below.

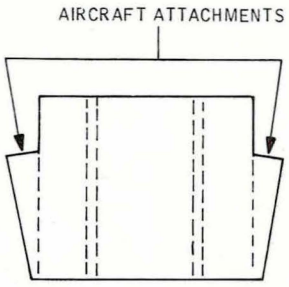

STRUCTURAL DESIGN

The tank was designed for riveted construction using 6061-T6 aluminum. Welding is limited for structural purposes to the door sill frame where it is subject to inspection. The double-wall over channel construction provides excellent rigidity. The tank is designed with an ultimate safety factor for inertial loads of 1.5 and for pressure loads of 2.0. Limit load conditions with a full retardant load are 3g down and forward, ± 1.5g lateral and 1g up, treated generally as separate conditions. (A full stress analysis is presented in Appendix A.) Tank construction details are shown in Figure 3.

FILLING SYSTEM

The test program required that each of the nine compartments be separately fillable (see Figure 4). The fill pipes are aluminum capped with Evertite® 3-inch aluminum male firehose fittings. They are welded to the tank

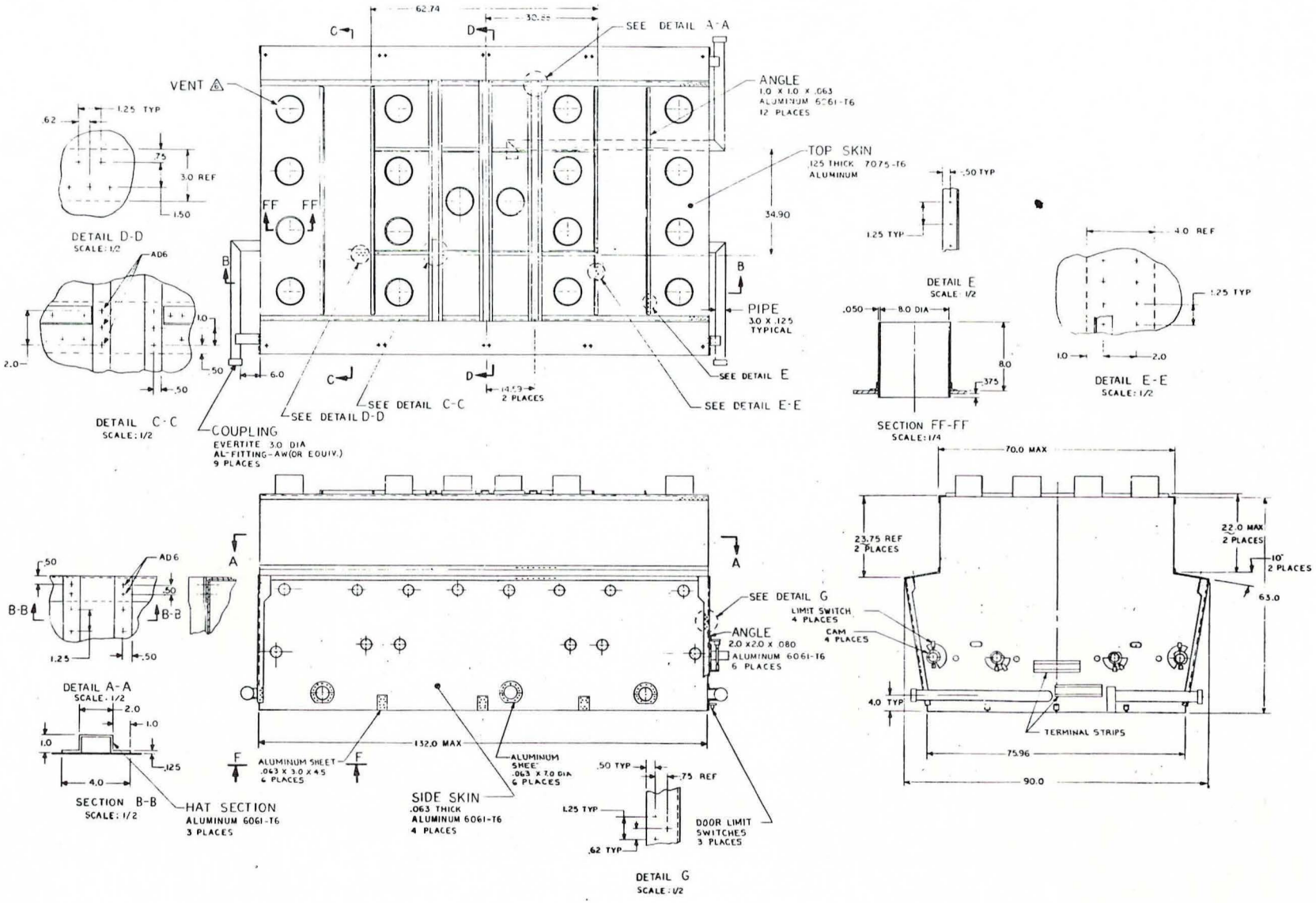

Figure 3. Tank Design Details

structure entering the tank about 4 inches from the bottom. The opening inside the tank is closed by a spring-loaded flapper valve. All paths are direct except for tank 5. In this case the 3-inch aluminum pipe is reduced to connect with a square pipe fitting between the tank walls. Tanks 4, 5, and 6 have flapper valves installed in special assemblies at the fill end. This allows the tanks to be downloaded or their quantity adjusted by use of a downloading fixture that enables the operator to open the flapper valve from the fill connector.

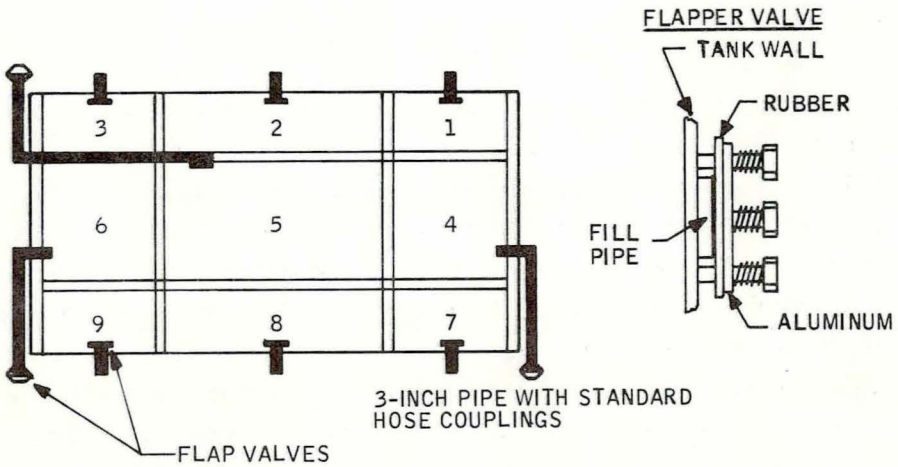

Figure 4. Tank Fill System

VENTING SYSTEM

The design basis for tank venting was to achieve not more than 0.5 psi at the highest evacuation rate. On this basis, one 8-inch-diameter stack vent was installed for each unit volume. This provides about 50 square inches of air entry or about one-ninth of the fluid exit area. Each stack extended originally 8 inches above the tank. On installation however, the stacks were found, in some cases, to interfere with structure, and they were modified by cutting them down as necessary. Each valve is fitted with a spring-loaded splash valve. These valves are set to pull gently shut to prevent retardant from

splashing out of the tank during takeoff or landing. Subsequent data show that pressures are generally under 0.5 psi.

Since the flapper valves are not accessible during loading, a separate fill vent system was added. This system consists of 1-1/2-inch flexible plastic hose, connected to the top of each tank compartment and leading to the outside through the tanks' fairings. Although these pipes can be closed with thermos caps, they appear not to leak in flight and consequently may be left open.

GATING SYSTEM

The ETAGS experiment requires the ability to deliver retardant quantities under a range of release conditions, with fast door opening, slow door opening (to restrain fluid flow), and with varying degrees of flow restriction. The nine-compartment tank is fitted with four doors or gates, one on each outboard row of compartments and two on the wider central compartment row. All doors were hinged on their outboard edge to open down and away from the tank centerline. This configuration requires the two central doors to join in an overlapping seal. It also allows for a drop with half of the compartment's exit area restricted by opening only one of the two doors on the center-row compartments. To provide additional experiments on restricted flow, tank 5 was fitted with a removable shelf covering a fourth of the tank width above door 2. The door arrangement is shown in Figure 5.

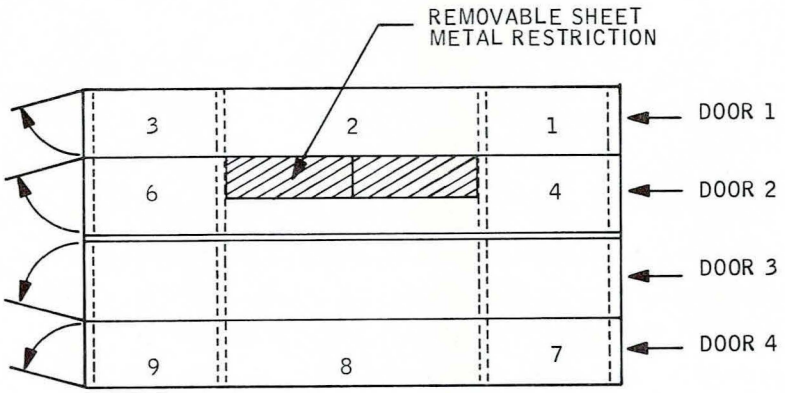

Figure 5. Door Arrangement - Top View

The need to locate the door opening mechanism out of the fluid within the tank walls caused considerable difficulty in achieving door opening to a full 90 degrees and in sealing. (In retrospect, this feature was unnecessary. Restrictions up to a fourth of the bottom door area did not significantly influence flow rate or the patterns generated.)

Door rigidity is provided by a basic box structure formed by welding a 2-inch-deep, 14 1/2-inch-wide aluminum channel to the 1/2-inch sheet-aluminum door plate. One-inch-wide spacers are included in the channel running across the door at each end and at each attachment point for the opening system. They are secured with six bolts. They support the eyebolts attaching the opening mechanism and provide stiffness for transmitting opening torque. This door design is shown in Figure 6. The doors are attached to the tank with an extruded piano hinge, MS 20001-16, bolted to the door plate and the tank sills.

Opening and Closing Mechanism

The opening and closing mechanism is buried in the tank walls to eliminate clutter in the fluid flow stream. It consists of four torque tubes, located in the walls about 17 inches above the bottom of the tank, that operate the doors through a two-lever linkage. The tubes are 2.5-inch OD, 2-inch ID aluminum supported in six places by glass-fitted Teflon® bushings that serve as bearings. The design is shown in Figure 7. The linkage is designed to permit over-center latching of the doors, i.e., so that the pull line between the eye bolt on the door and the pivot point between the crank arms and door lever pass outside of the torque tube center line. This allows the tank to remain closed without power and retain the retardant load. This feature was not used in the ETAGS tests for two reasons. First, the time required between the release signal and the passage of the door linkage over center was undesirable for instrumentation purposes. Second, the over-center linkage made it difficult to extend the doors to the full 90 degrees over the full stroke. The system is thus limited to holding the retardant load only in the power-up condition. This is suitable for experimental purposes but not suited to operational aircraft.

Drive System

The torque tubes are driven and held by four hydraulic cylinders, anchored to aluminum blocks on the bottom front of the tank, that operate bell cranks bolted to the forward end of each torque tube. Some difficulty was encountered in

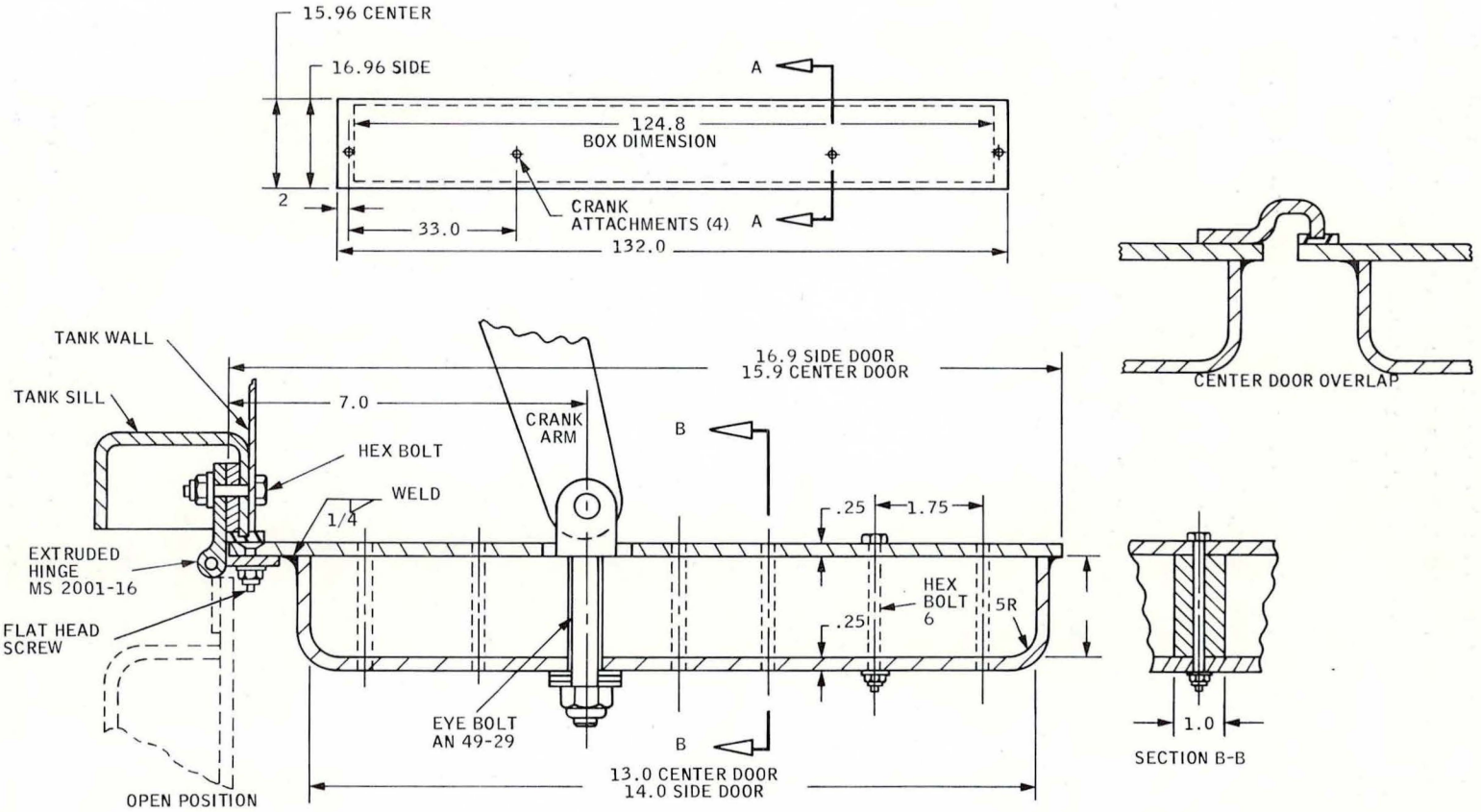

Figure 6. Door Design Details

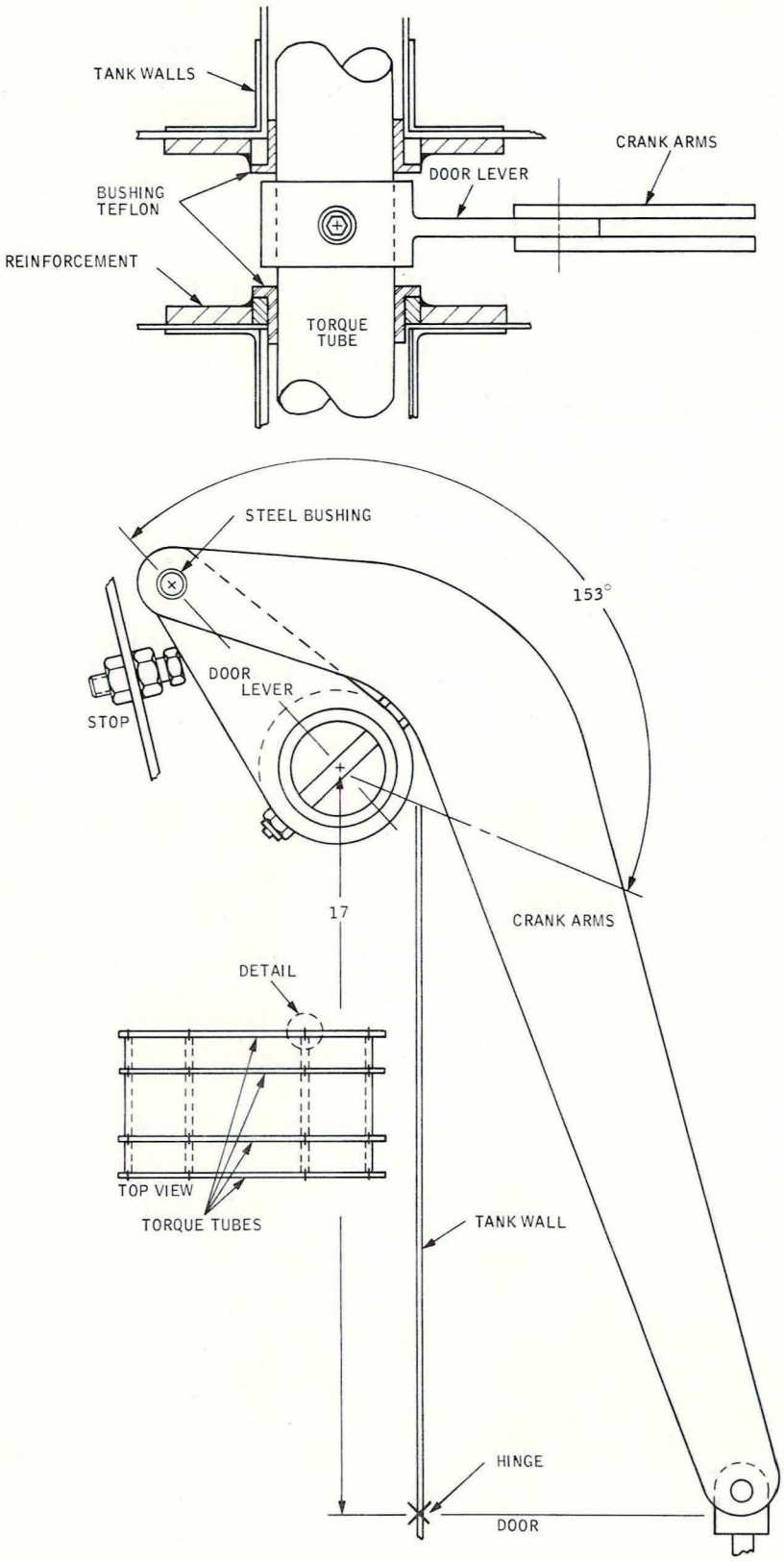

Figure 7. Door Operating Mechanism

providing adequate structural rigidity between the anchor blocks and the torque tube supports. As a result, half-inch aluminum plates were added between the tiedown blocks and the forward torque tube bearings to minimize flexure. This arrangement is shown in Figure 8.

Door Seals

The combination of rigid door structure (to restrain fluid flow), the movement of lever arms out of the tank area proper (to preserve a clutter-free compartment), and the overlapping closure of the central doors presents some unique problems in sealing the tank.

The rigidity of the door structure prevents the door itself from taking up any irregularities in the compartment sills. It also causes sill ridges or high points to take up considerable amounts of closing force. This situation is aggravated because of the location geometry of the lever arms - their pull is least effective at the closed position. As a result, the take-up to close off leak paths must be relegated to the rubber seal. In addition, there are about 320 running inches of sill contact for each door unit - about 40 square inches of contact area, which is larger than most tanks due to the double-wall compartment construction. As a result, the hard rubbers typically used in seals provide a substantial resistance to closure. The solution to providing a workable seal under these conditions has been to lay a strip of soft, conventional seal rubber, and top it with a closed-pore gasket rubber. The harder underseal serves mainly to minimize cutting of the softer material trapped between the door and the sill. It is likely that the soft rubber alone would seal the tank, but this was not tried, except in some local areas, during the course of seal maintenance on ETAGS.

A peculiarity of sealing exists in the overlapping of the central door system. A lip on door 3 contacts a seal on door 2 as it pulls closed. This seal has been surprisingly effective, but problems occur at the butt joints sealing the ends and between compartments. The sealing technique is shown in Figure 9.

The door opening system is designed to provide clutter-free interior tanks, and is somewhat less than optimum for sealing. All driving forces are applied at the forward end of the torque tube. Therefore, the closing force on the door is highest at the forward bell crank position and lower by some degree at the aft due to deflection in the torque tube. During the course of the ETAGS flight tests,

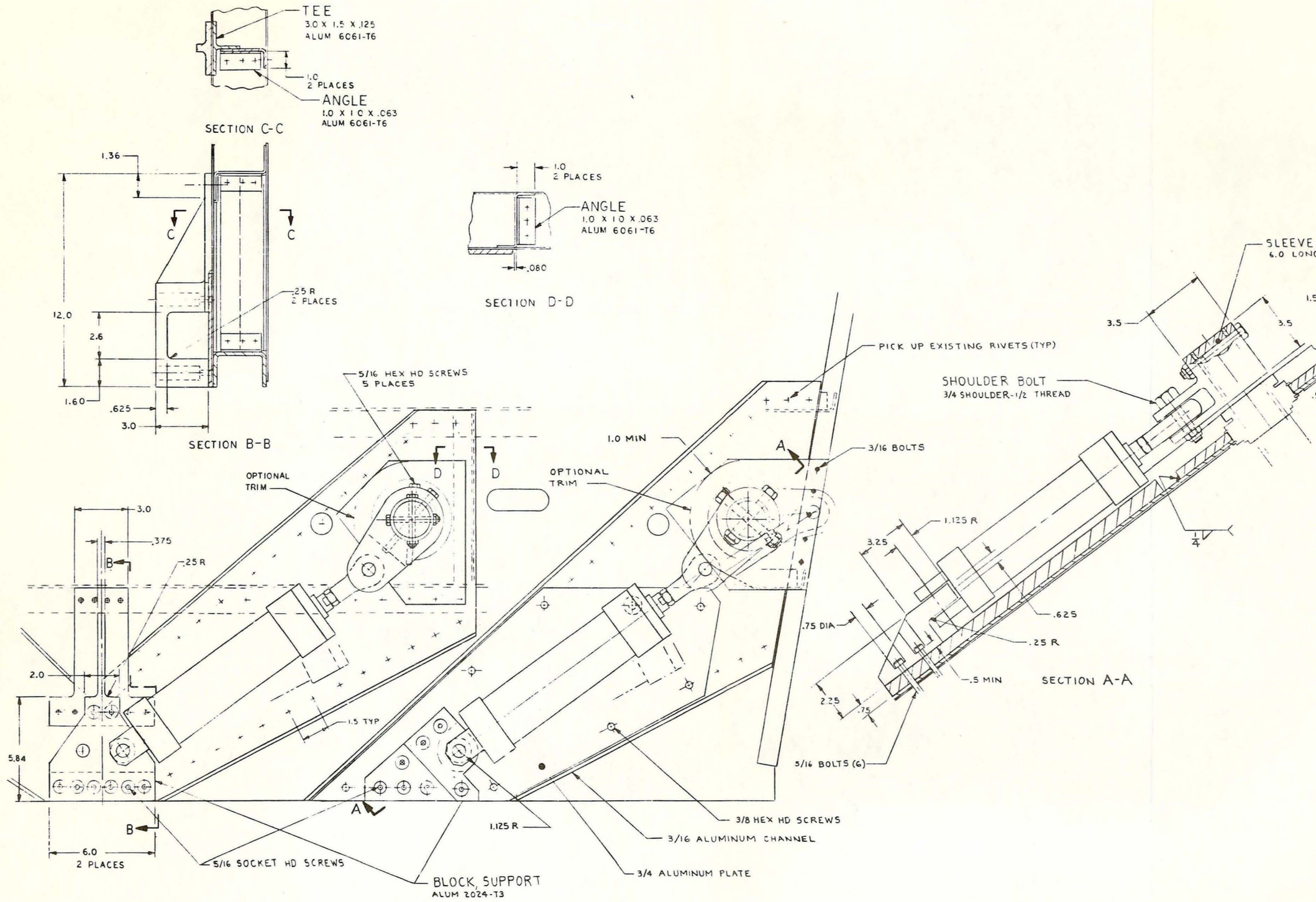

Figure 8. Door Drive System

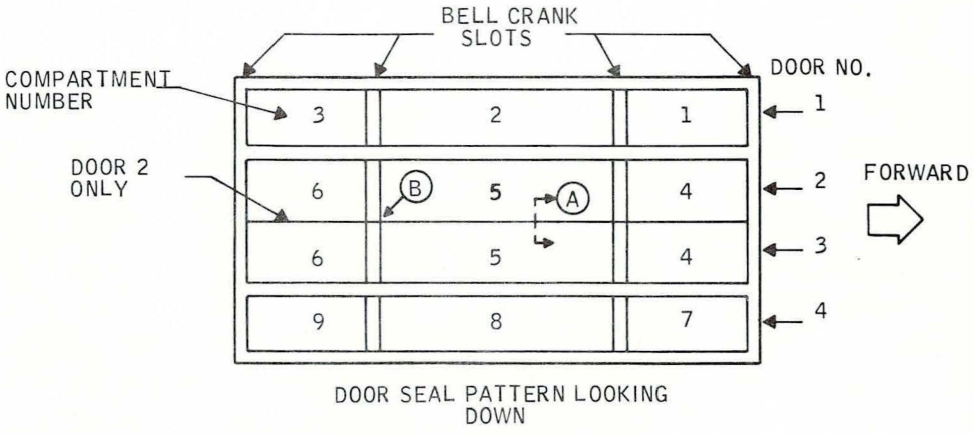

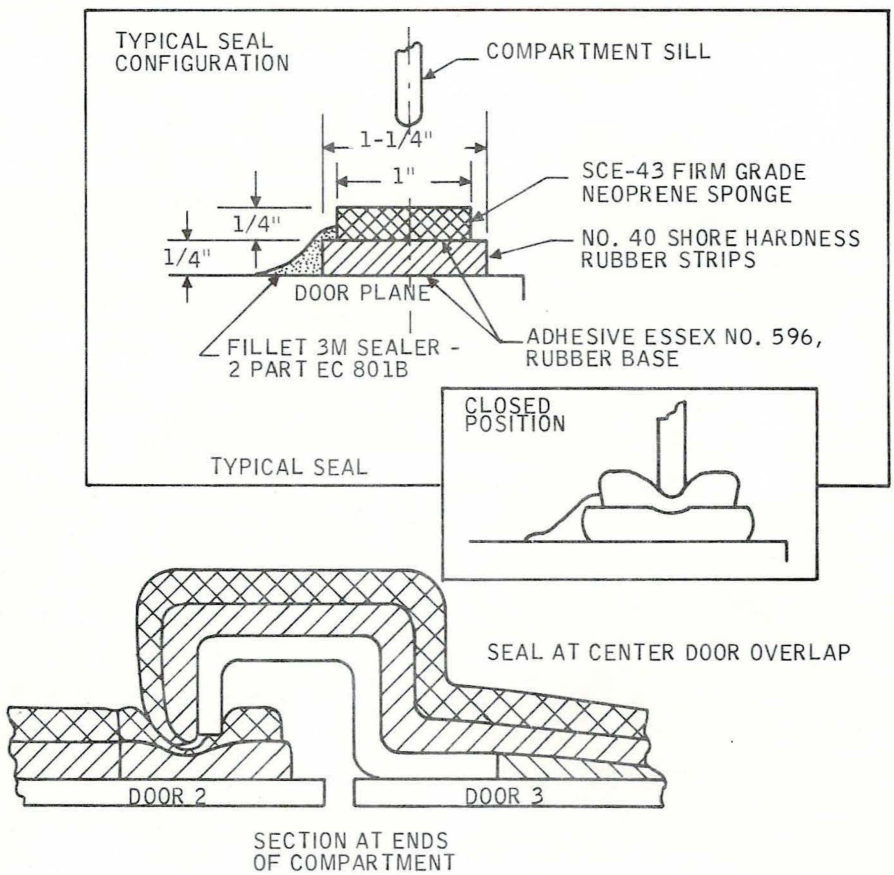

Figure 9. Door Sealing Technique

seal maintenance was conducted without adjustments to the operating systems. Nonetheless, tuning is possible and may be required periodically. The mechanisms for tuning are shown in Figure 10.

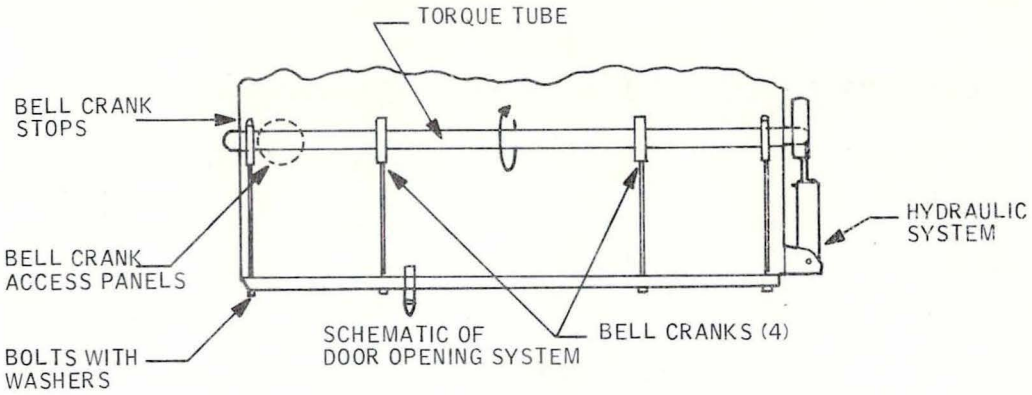

Figure 10. Door Closure Tuning Mechanism

Access panels are provided to the bell crank attachments on the torque tube. These are preset and can only be changed with difficulty due to the confined space. It is not recommended that these adjustments be attempted unless a radical overhaul of the tank is required. This is also true of the stops that are, in theory, adjustable to yield over-center door locking.

Hydraulic Control System

A hydraulic system of controlling the doors was selected over pneumatic systems to yield more positive response (considered necessary for experimental purposes) and to provide the power required to restrain operation of the doors against the fluid in the slow-door experiments. Figure 11 shows the basic layout of the system. Physically the system consists of (1) a block-mounted assembly containing the motor-driven pump, accumulator and control manifold assembly, (2) a separate hydraulic reservoir, (3) connector hoses, and (4) the hydraulic cylinders. The system is independent of the aircraft hydraulic system, requiring only electrical power to operate the pump and control solenoids. It is mounted in the aircraft in the radar compartment immediately in front of the bomb bays. Although the doors would open on loss of power as a result of internal bleeding through the

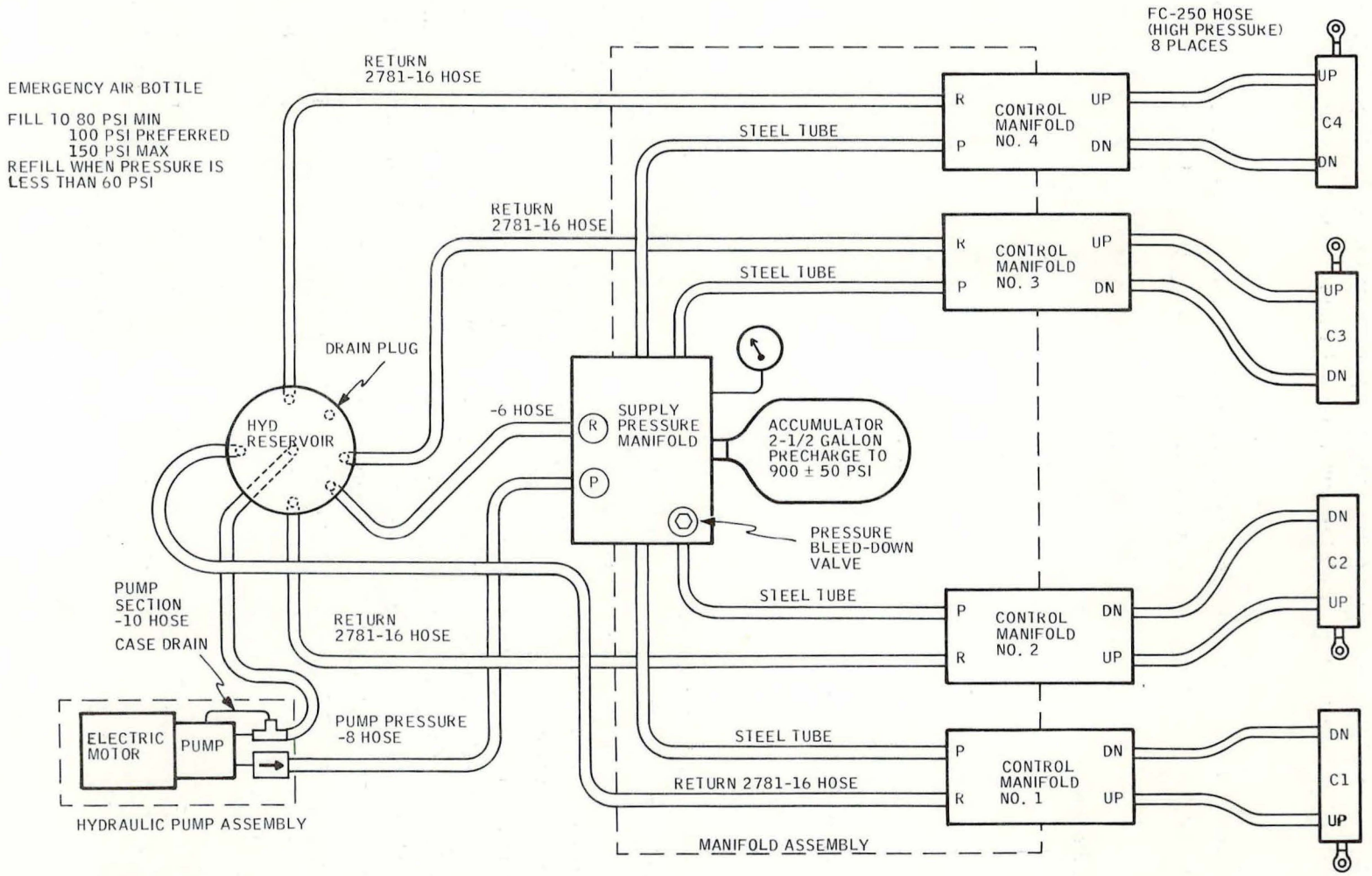

Figure 11. Door Control Hydraulics

lines, the process was considered too slow to meet emergency dump requirements. As a result, an emergency release system was included to permit injecting air (from an air bottle) into the down control lines through the control manifold.

The doors implement up to seven rates inboard and three rates outboard. The original rates were set to provide the following opening times (in seconds):

	Rate	Original	Revised
Inboard	1	1.5	2.10
	2	.75	.83
	3	.50	.60
	4	.40	.55
	5	.32	.44
	6	.26	.33
	7	.22	.29
Outboard	2	.75	.74
	4	.40	.55
	6	.26	.32

After static tests and a review of the effect these rates had on flow-rate it was decided to reduce the maximum rates (that had little effect on flow) to achieve a greater range of flow rate effect. They were revised insofar as design change permitted to the second set of rates shown above. Although the doors open to 90 degrees, measured time values are taken at 60 degrees. This results from (1) instrumentation on torque tube travel that yields imprecise calibration at the less critical full angle (60 to 90 degrees), and (2) the self-snubbing feature of the hydraulic cylinders as they reach the end of their strokes. The instrumentation tradeoff was made to preserve maximum accuracy at the critical initial angles of door operation while protecting the pots from retardant spray. The self-snubbing feature prevents sudden deceleration as the door achieves full extension, and it operates in conjunction with limit switches that power the system down as they reach full extension.

The rates are achieved by activating any one or both of two flow restrictors in the control manifold for the outboard doors or any combination of three on the inboard doors. The full hydraulic schematic is shown in Figure 12.

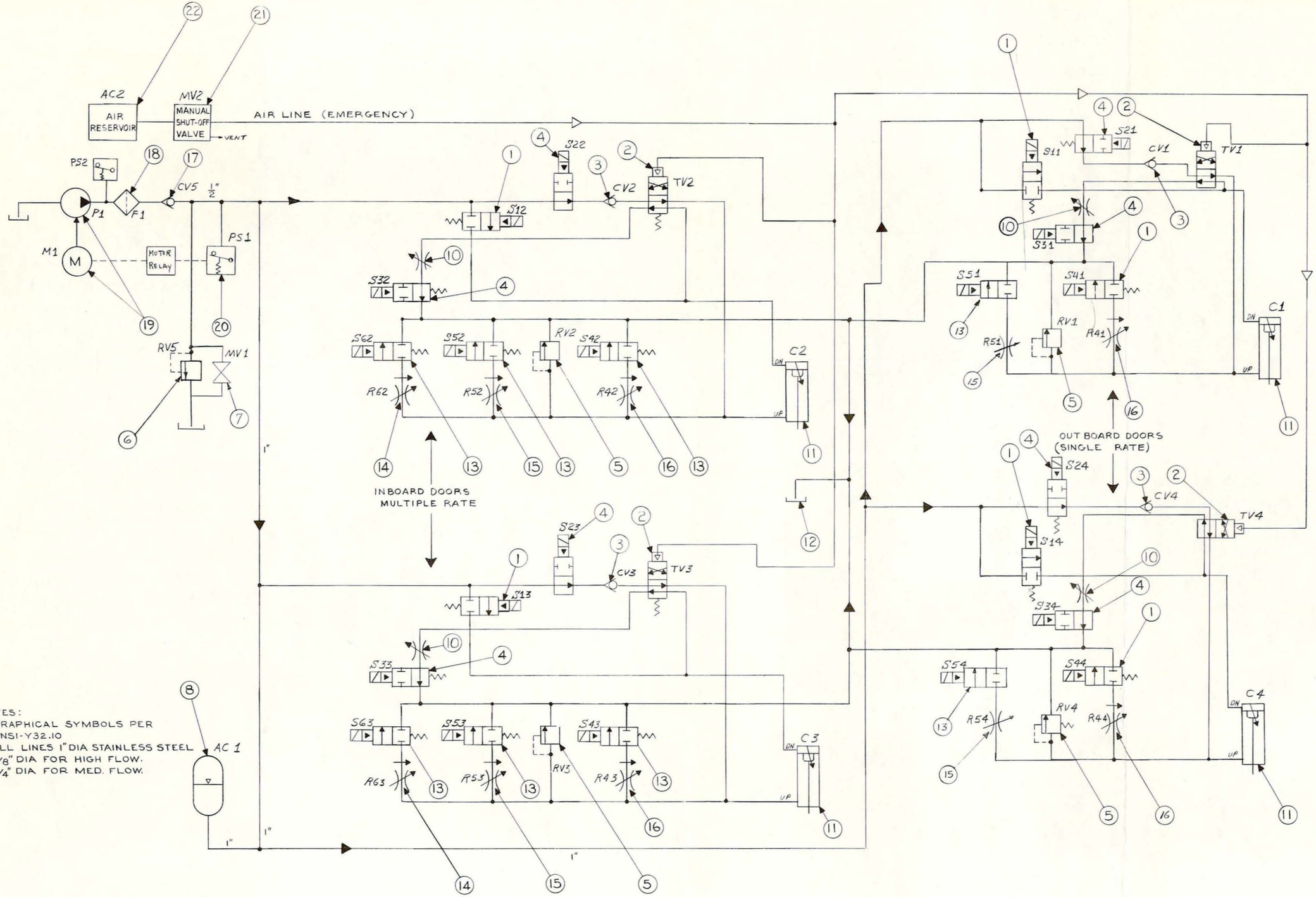

NOTES:
1- GRAPHICAL SYMBOLS PER ANSI-Y32.10
2- ALL LINES 1" DIA STAINLESS STEEL
3- 7/8" DIA FOR HIGH FLOW.
3/4" DIA FOR MED. FLOW.

Figure 12. Hydraulic System Schematic

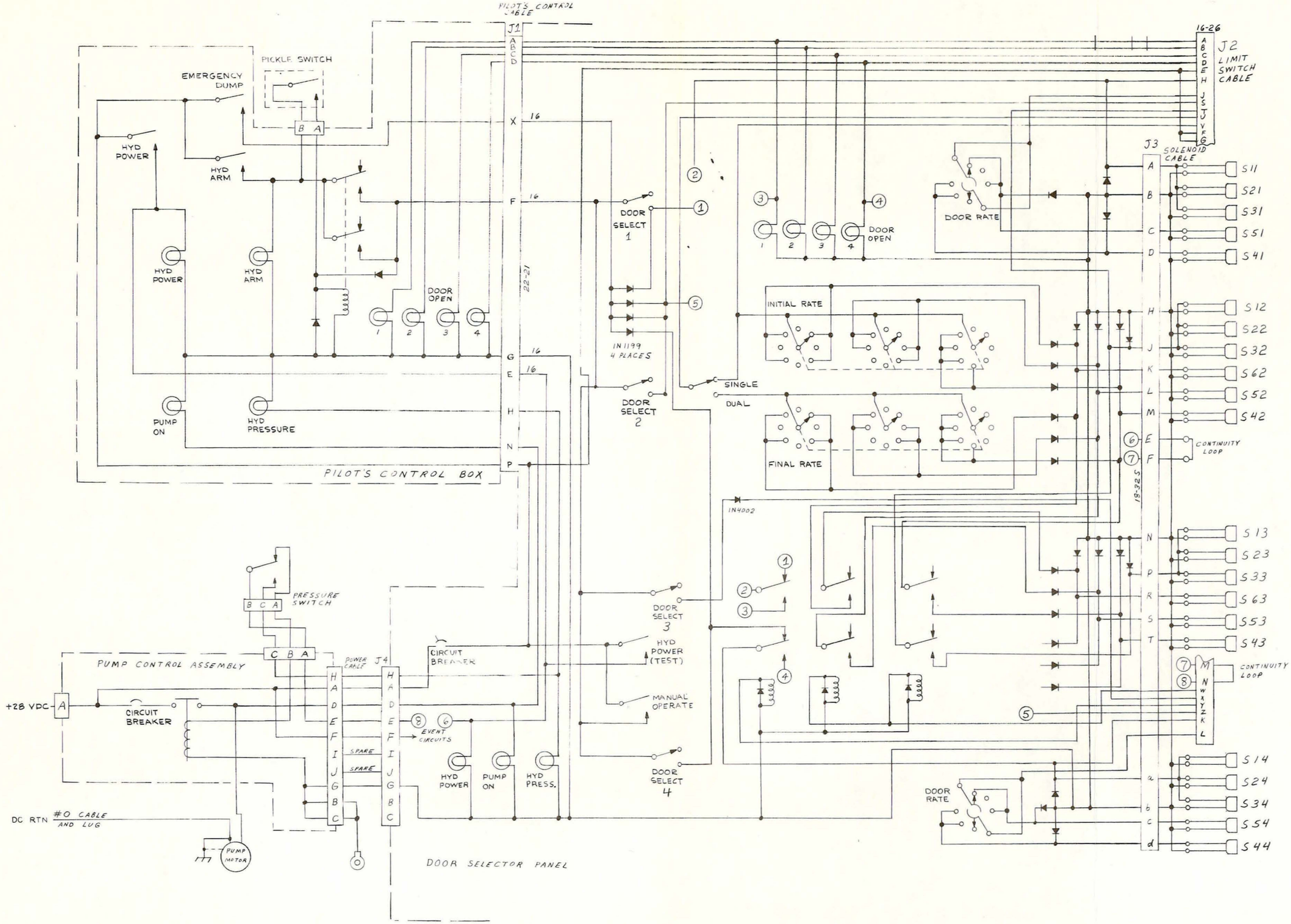

Figure 14. Door Actuator System Electrical Schematic

- Door 3 will close fully prior to door 2 closure. This protects the overlapping area from misclosure.

Locations and wiring are shown in Figure 15.

TANK CONTROL SYSTEM

The tank control system consists of four separate components as shown in Figure 16:

- Pilot's Control Panel - The Pilot's Control Panel (Figure 17) is mounted in the cockpit. It provides controls for (1) actuating the hydraulic pump, (2) arming the pickle switch and closing the doors, (3) emergency dump through the electrical/hydraulic system, and (4) status monitoring lights.

- Test Setup Panel - The Test Setup Panel (Figure 18) is the master distribution box for electrical control of the hydraulic system. It allows pre-programming of the selected test by selecting the appropriate doors and their rates. It contains subsidiary controls and status indicators in parallel with the Pilot's Control Panel for checkout purposes. These are not normally used in the air test sequences.

- Pickle Switch - The Pickle Switch allows the pilot to trigger the retardant drop when ARMED by means of the Pilot's Control Panel master arming switch. Doors will remain open after pickling until the arming switch is turned off.

- Emergency Dump Air Switch - The Emergency Dump Air Switch applies stored air pressure to the hydraulic system, causing evacuation of all tanks regardless of programmed test setting. The system should be used only if emergency dump through the electrical/hydraulic system fails.

  WARNING: Doors cannot be closed after actuation of the Emergency Air Dump System. Care must be taken in landing to avoid tail-down, strut-compressed conditions.

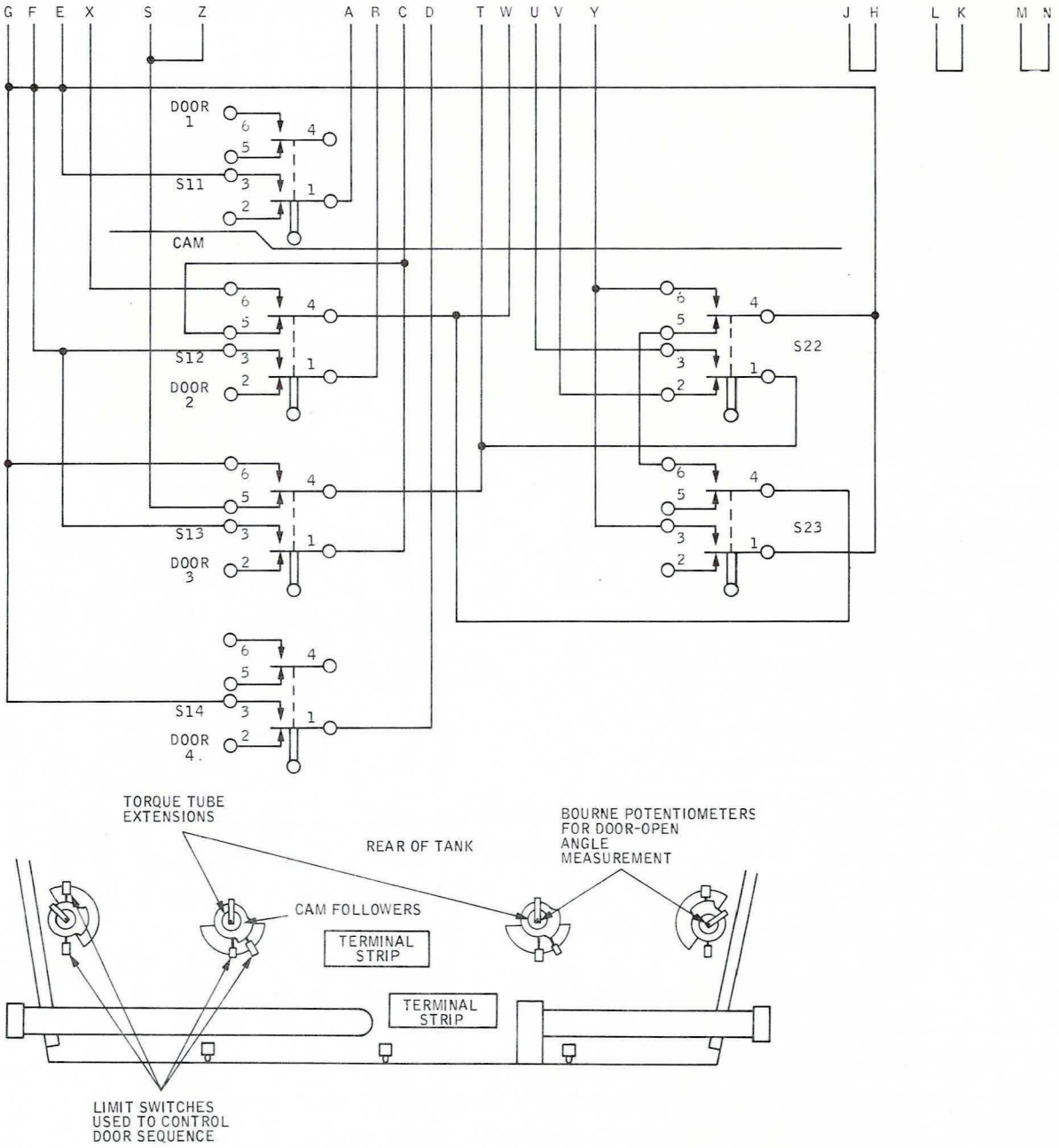

Figure 15. Door Limit Switch Connections

The system operates from a precharged (900 ± 500 psi) accumulator. It is set to operate at 2000-psi hydraulic pressure. All solenoid valves are spring loaded to the door-closed position. They will not open unless electrical power is applied. The tank is safed hydraulically by means of a mechanical bypass valve (7/16-inch hex head) located on the manifold assembly. This valve must be open before any maintenance on the door is attempted.

The system is unique in its ability to provide a wide range of control over door-opening rates. Pressure at 2000 psi is dictated by the need to hold against fluid flow to provide slow opening options. The large tubing is required to create adequate flow without frictional losses in achieving fast door opening. It is consequently a high-flow, high-pressure system, not generally desirable in an operational tank.

Electrical System

The electrical system is contained in two boxes located in the pilot's compartment and one located in the aircraft crew compartment forward of the wing. Pilot access is limited to those aspects of the drop that must be under his control. The parameters controlling the test are set up in the control panel before the flight begins.

Connections for the panels are shown in Figure 13. An electrical schematic, Figure 14, shows the components of the system.

Two features of the system require additional commentary. First, to assure that the doors would not over-power in the open condition, limit switches were positioned on cams attached to the torque tubes. Additional switches tested the door closed conditions at the rear of the tank. Switching logic was arranged to provide the following:

- Outboard doors cannot close (or open) while inboard doors are full open. At the 90-degree extension, the box structure on the inboard doors interferes with outboard door closure.
- Door 3 will not open until the overlapping portion of door 2 has passed the interference condition (about 6 degrees).

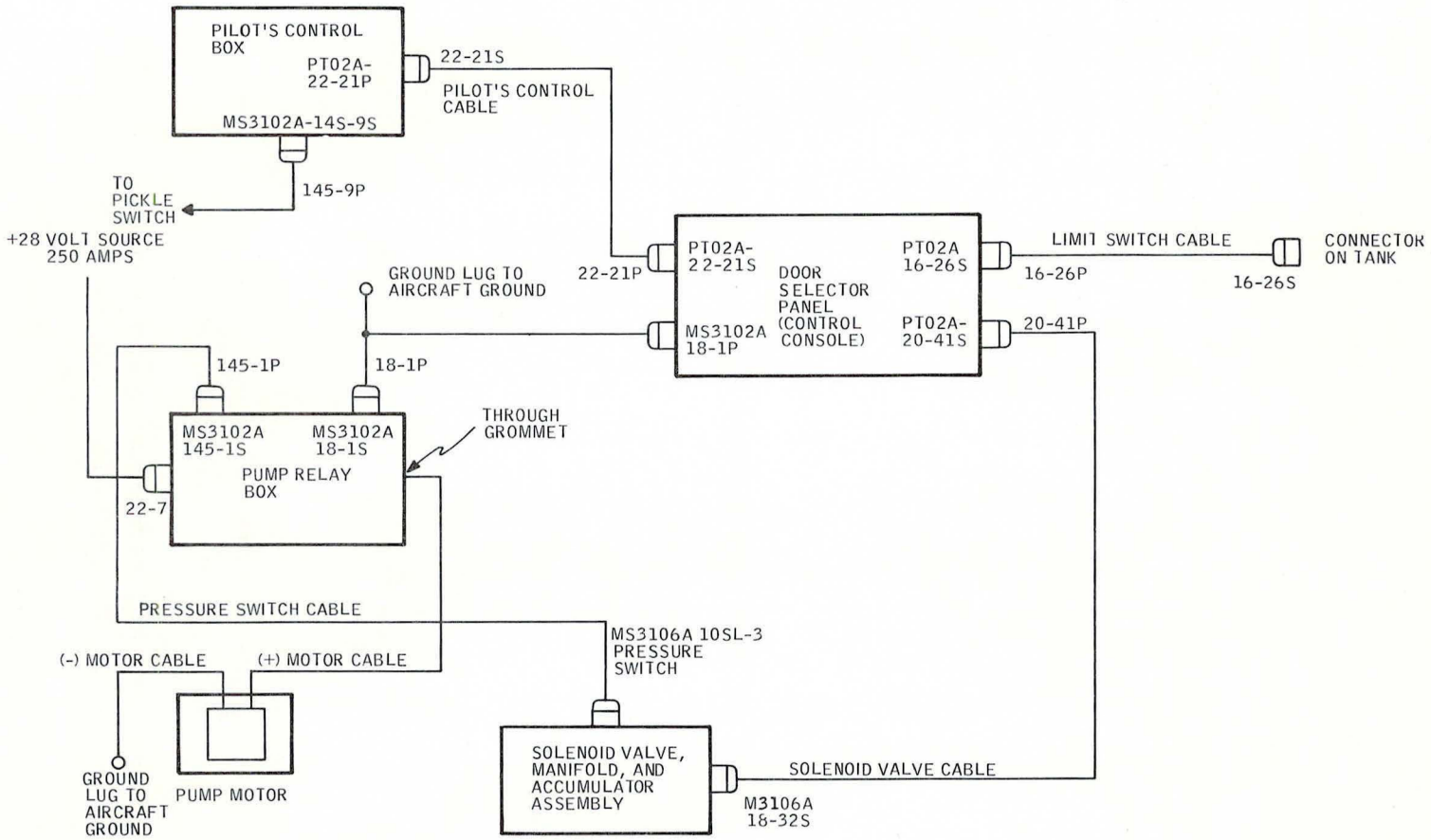

Figure 13. Door Actuator Electrical Connections

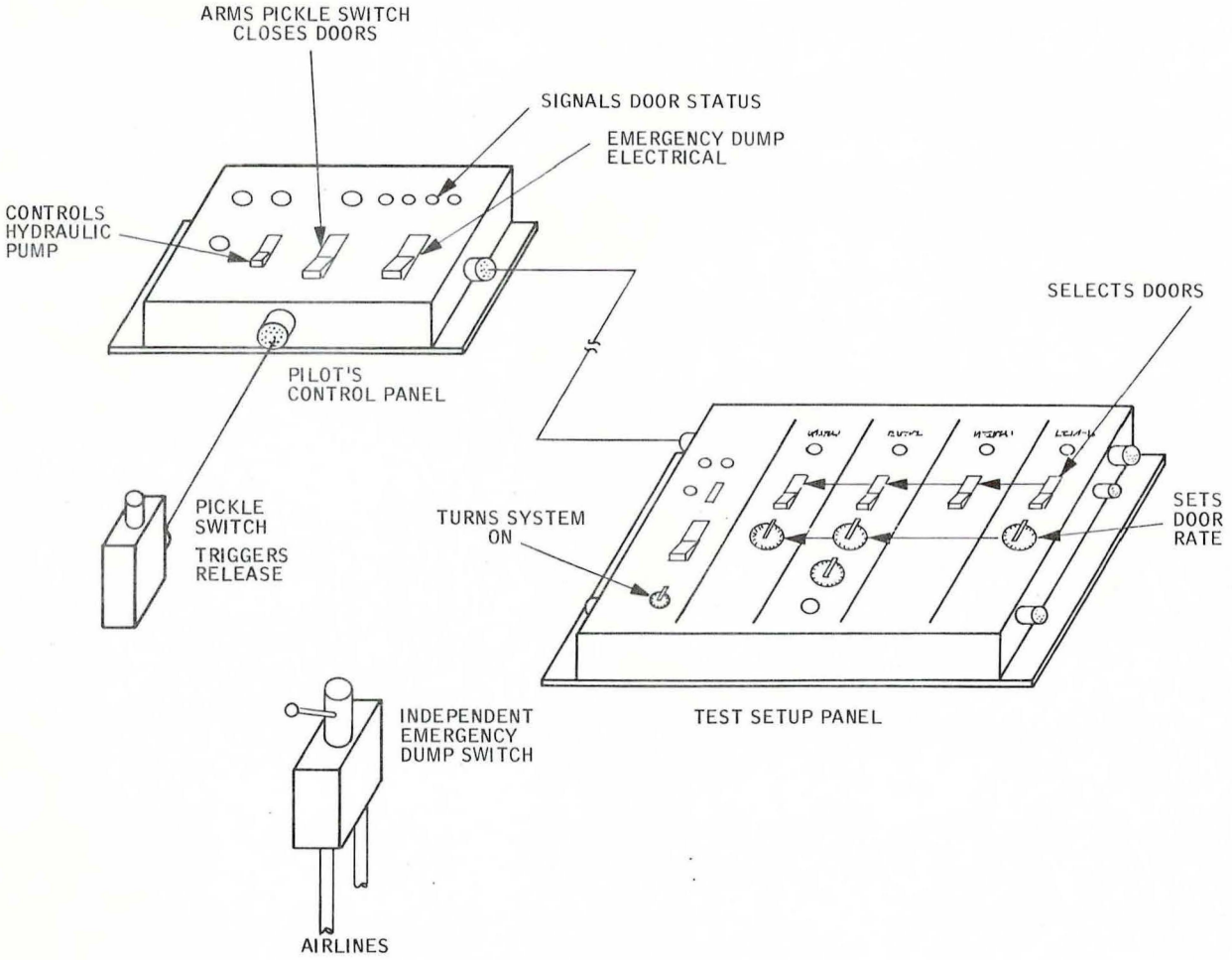

Figure 16. Tank Control System Components

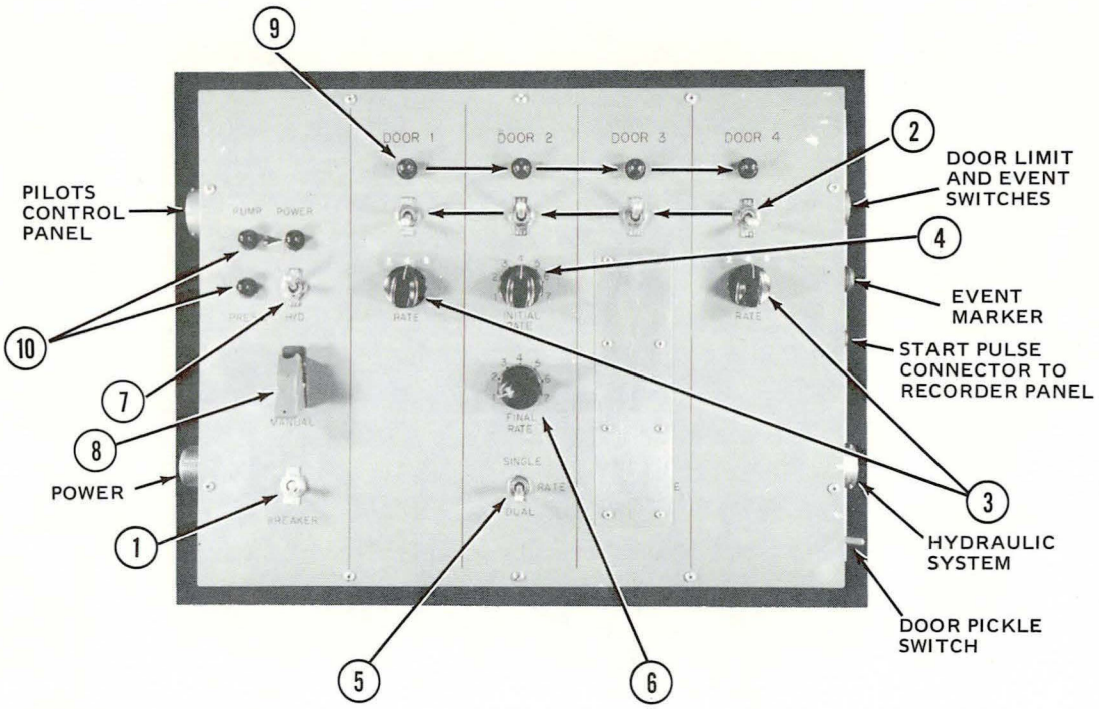

SWITCH CONTROLS:

(1) Circuit Breaker: When ON (up) powers the hydraulic system. The switch must be ON during loading and flight operations.

(2) Door Selector Switches (4): When ON (up), the switches enable opening of the selected doors (numbered 1 through 4 from the pilot's left to right) on release of the armed pickle switch. Door 3 will NOT Open unless Door 2 opens.

(3) Outboard Door Rate Switches (2): Select one of three rates for outboard door opening.

(4) Initial Rate Switch: Selects one of seven rates for the two inboard doors. When Rate Switch 5 is SINGLE (up), the selected rate prevails through the sequential opening of doors 2 and 3. When Rate Switch 5 is DUAL (down), the switch sets the rate of the first 45-degree travel of door 2.

(5) Rate Mode Switch: Selects single-rate opening of doors 2 and 3 (up), or a programmed rate change (DUAL or DOWN).

(6) Final Rate Switch: Selects one of seven rates switched in when door 2 reaches 45 degrees. Normally a lower rate than that selected on the Initial Rate Switch.

(7) Hydraulic Pump Switch: Normally OFF (down) for flight operations. Parallels control on pilot's panel.

(8) Manual: Normally OFF (down). Cover closed for flight operations. Parallels ARM switch on Pilot's Control panel. Used for checkout purposes to open selected doors (ON) or close them (OFF).

INDICATOR LIGHTS

(9) Door Status Lamps (4-Red): ON when door is open.

(10) Dump, Press, Power Lamps (3-Green): Parallel operation of indicators on Pilot's Control panel.

Figure 17. Pilot's Control Panel Layout

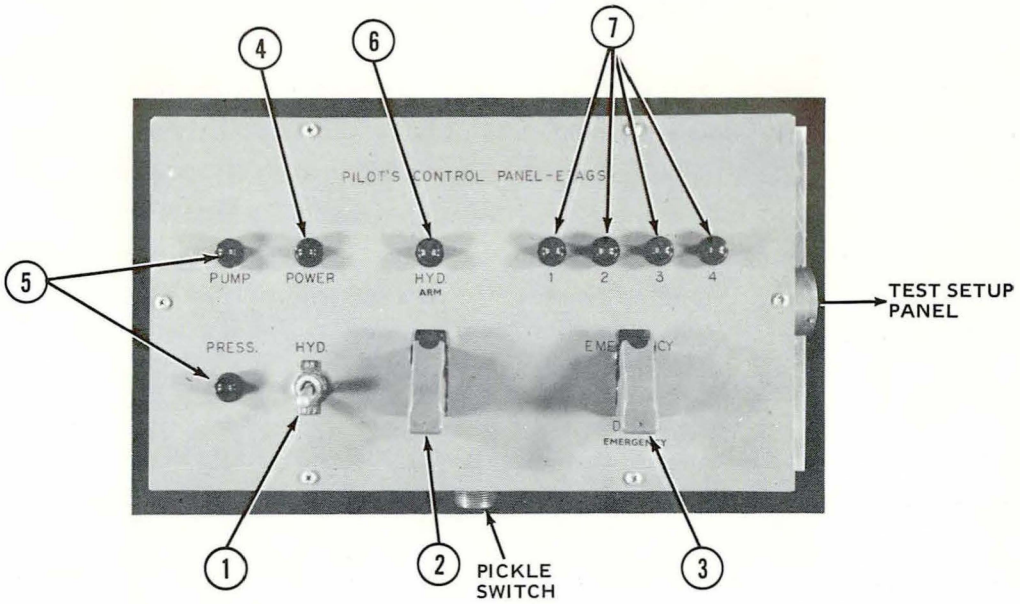

SWITCH CONTROLS:

(1) Hydaulic Pump Switch: Normally ON (up) when system is in operation. Doors will eventually open with loss of pressure when pump is off.

(2) Hydraulic Arm Switch: Cover UP; Switch ON (up) arms pickle switch. Pressing pickle switch will then cause selected doors to open. Switch OFF (down), cover DOWN to close doors.

(3) Emergency Switch: Cover UP, switch ON (up) opens doors on all tanks regardless of pre-programmed setup on Test Control Panel.
Operates through electrical hydraulic system.

STATUS LIGHTS:

(4) Power Lamp (Green): ON when hydraulic pump is powered.

(5) Pump/Pressure Lamps (Green): Pump lamp ON when pump is running. Pressure lamp ON when hydraulic pressures exceeds 1700 psi and pump is NOT running. If either lamp is ON, hydraulic system is operating.

(6) Arm Lamp (Red): ON when pickle switch is armed.

(7) Door Status Lamps (RED): ON when door is open. Doors are numbered 1 through 4 starting on pilot's left. Either door 2 or 3 evacuates central tank row.

Figure 18. Test Setup Panel Layout

INSTRUMENTATION SYSTEM

A primary requirement of the ETAGS tank is to provide instrumentation of each drop so that flow rate, door opening, and pressure can be analyzed in association with ground data. The instrumentation scheme is shown in Figure 19. Data records were collected on a Honeywell 5600, 14-channel FM tape recorder and verified by previewing data played back on a two-channel Brush recorder. Test records were used on the voice track prior to each flight. Since there are potentially 25 channels of data, only the 14 instruments of most interest are selected when the data exceeds the recording capability. To conserve tape, the recorder was started remotely by the copilot prior to each drop. A flash bulb located immediately in front of the forward fairing and visible to ground cameras was used to provide a time zero for film data analysis.

The patch panel (Figure 20), located in the compartment just forward of the wing, contains jacks for each item of instrumentation to allow selection of data for recording. The instrumentation is described as follows:

- Accelerometer - A PCB 308 A02 accelerometer was mounted near the control panel above the tank center of gravity. The location proved to be noisy, and the accelerations caused by load release were not sufficient to extract from the vibration noise. These data were not useful and the instrumentation was abandoned.

- Door Opening Angle - Door angle was measured by four TRW-type 7501 1 Kohm, single-turn, linear potentiometers mounted on sheet-metal extensions over the rear ends of the torque tubes. The potentiometer shaft engaged an aluminum block in the torque tube. Torque tube to actual door angle was calibrated with a separate potentiometer fixture affixed to the door hinge. This calibration curve was stored for use in computer analysis. The only difficulty with this approach was poor resolution at the end of the door cycle (60 to 90 degrees).

- Pressure Measurement - Pressure taps were inserted in the top of each tank compartment. Plastic tubing was run from each tap across the top of the tank to an aluminum manifold (Figure 21) located in an accessible position at the tank front. Each was connected to a National Semiconductor LX 3701D (-5 to +5 psi) temperature-compensated differential pressure transducer. Reference pressures were taken in

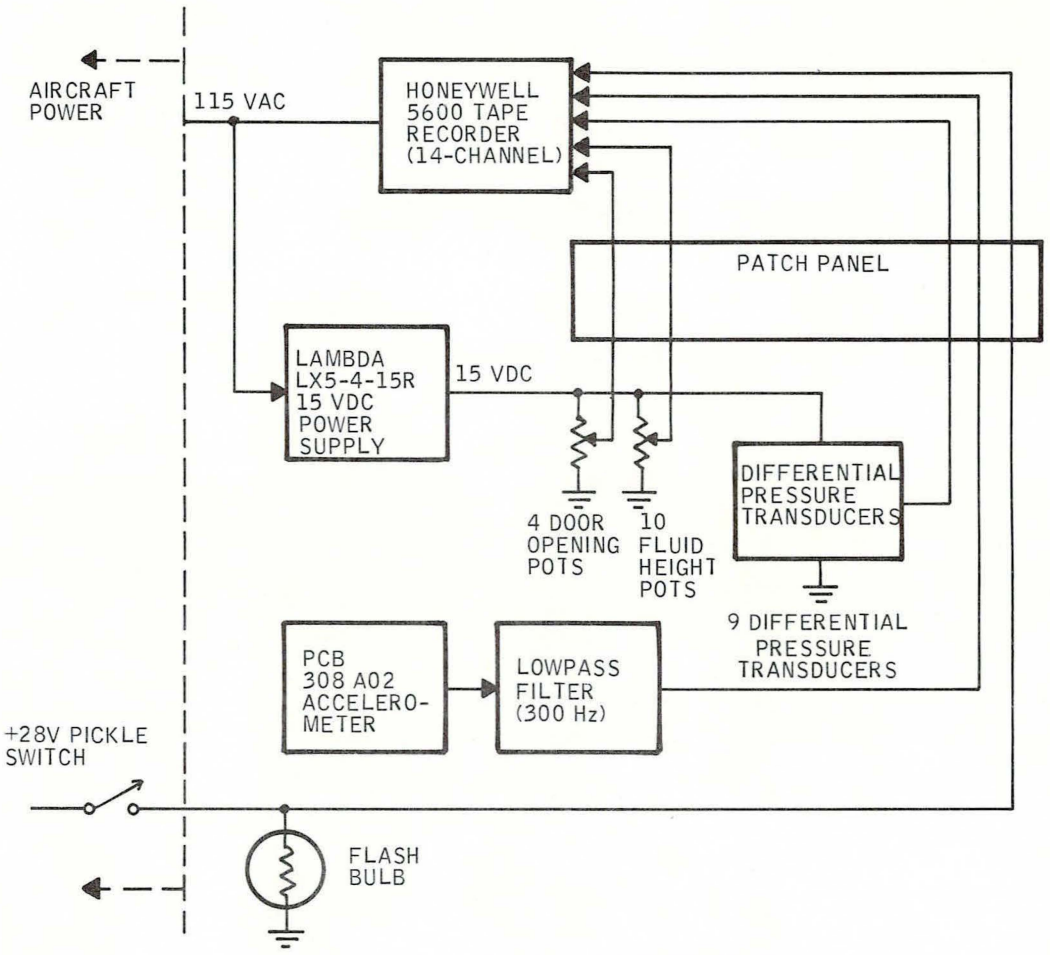

Figure 19. ETAGS Instrumentation Schematic

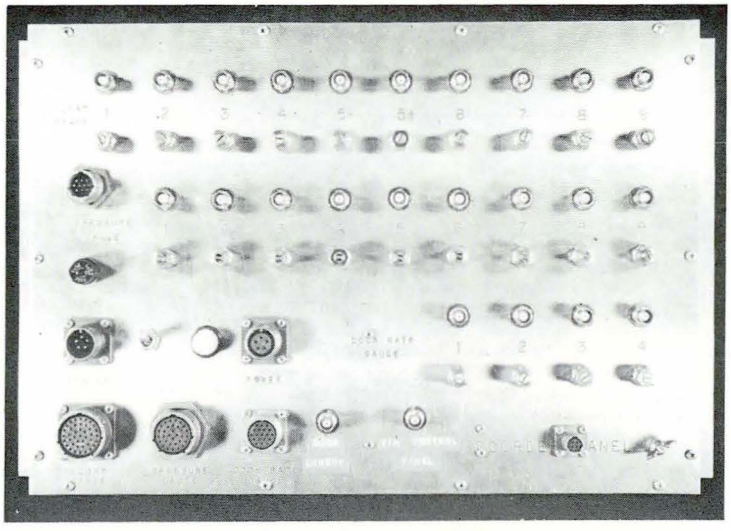

Figure 20. Instrumentation Patch Panel

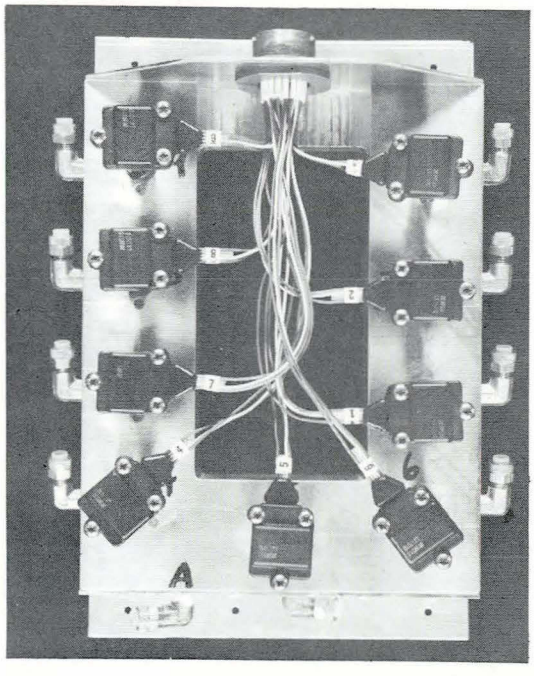

Figure 21. Pressure Instrumentation Manifold

the aircraft cabin. Calibration for the instrumentation was as shown in Table 1. One transducer designated for tank 9 could not be calibrated. Although a replacement was ordered, it was not available until the test series was completed. During the course of testing, the transducer in tank 4 developed a failure that was not discovered in the course of verification. Very little valid data was obtained from this tank. Since the nonworking gauges were replicated in similar compartments, this lack of data was not significant.

- Float System - The top surface of the fluid was monitored during drops by the float system shown in Figure 22. Several difficulties were encountered in achieving a workable float system. The first design utilized sprockets instead of pulleys, with a chain drive returning through the square channel. This system recorded flow rates that appeared to decrease as door opening rates were increased. High-speed photographs through the vent holes showed clearly that the floats were not tracking the fluid. This was found to be caused by fluid drag on the chain returning upward against the fluid flow. The system was then modified to that shown, with aircraft cable winding up on each pulley. Skirts made of formed sheetmetal and wired over the floats were added during this period to increase fluid drag on the float - the skirts normally reside below the surface. This practice was retained in the operating system.

  The wire modification proved effective but difficult to maintain. Part of the problem was in retaining adequate tension on the floatwire to prevent its whipping off the pulley track when subjected to the airstream after the drop. Float maintenance was continuous, and drops were selected based on working floats to preserve maximum data. Results in terms of data were excellent. There were, however, more difficulties in tank loading, where fill levels were controlled by the floats. In this case, float failures could, and occasionally did, result in over filling. This situation was corrected by means of a downloading fixture, but on several occasions it blew seals. An improved float system is highly recommended in any future drop series.

Table 1. Pressure Sensor Calibrations (Zero Pressure Adjusted to 1.00 $^{+0.002}_{-0.008}$ Volt)

Tank	Pressure (psi)								
	-5	-4	-3	-2	-1	0	+1	+2	+3
1	0.37	0.50	0.63	0.77	0.89	1.01	1.16	1.29	1.42
2	0.34	0.47	0.61	0.74	0.87	1.01	1.14	1.28	1.42
3	0.33	0.47	0.60	0.73	0.87	1.01	1.14	1.28	1.41
4	0.35	0.48	0.61	0.75	0.88	1.02	1.15	1.28	1.42
5	0.34	0.47	0.60	0.74	0.87	1.00	1.13	1.27	1.41
6	0.32	0.46	0.60	0.73	0.87	1.00	1.15	1.28	1.42
7	0.33	0.46	0.60	0.73	0.86	1.00	1.13	1.26	1.40
8	0.34	0.47	0.61	0.74	0.88	1.01	1.15	1.28	1.41
9	Would not come up to 1.00 cal volts								

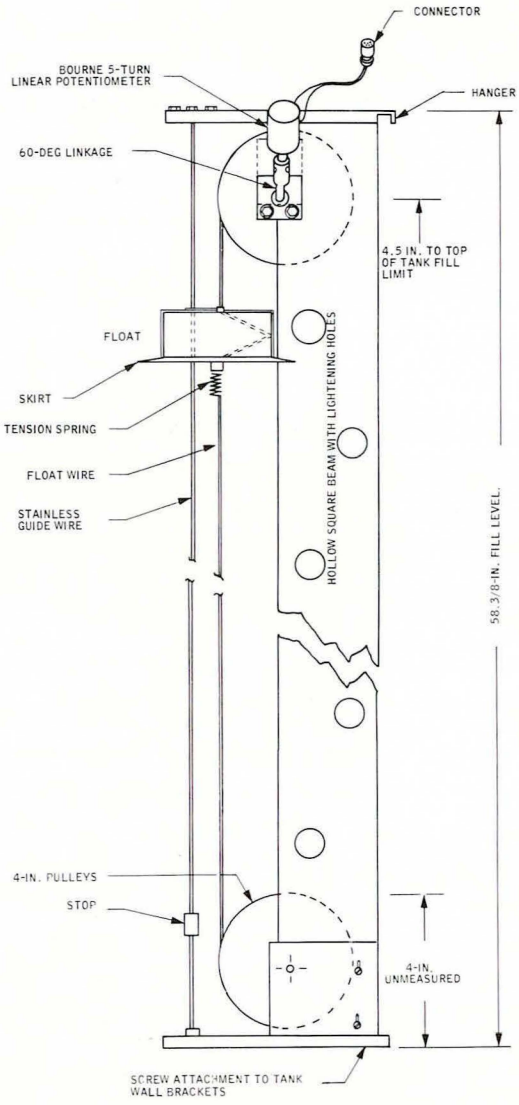

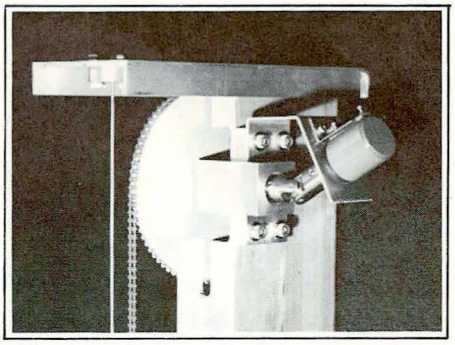

TOP ASSEMBLY
SHOWING ORIGINAL CHAIN DRIVE

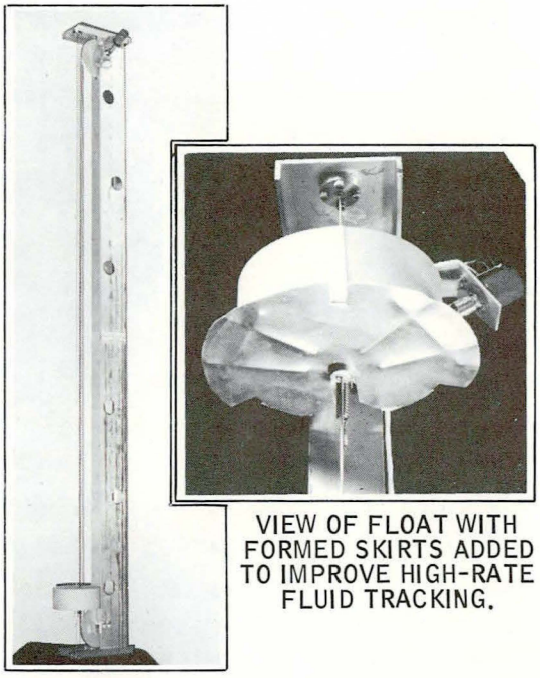

VIEW OF FLOAT WITH FORMED SKIRTS ADDED TO IMPROVE HIGH-RATE FLUID TRACKING.

Figure 22. Float System

NOTE: The tank was subsequently fitted with rubber encapsulated float switches to indicate the full condition, but not fill levels, for possible use and evaluation in an operational role.

SUPPLEMENTAL FIXTURES

Loading Indicator

Figure 23 shows the fill indicator box built to read float position in a selected compartment from outside the aircraft. The box attaches via a long cable to a connector on the right side-fairing. It produces a continuous readout of the selected float position to allow the control of full and partially filled compartments.

Downloading Fixture

A downloading fixture was built to enable load tailoring by subverting the flapper valve to drain fluid from the tank. The fixture shown in Figure 24 is based on a modified hose coupling fitted with a plunger assembly and a drain.

AIRCRAFT INSTALLATION

Aircraft ferrying, refurbishment, tank installation and flight-test operation were subcontracted to Aero Union Corporation, Chico, California, whose competence and consultation were highly valued throughout the course of the program. The aircraft was ferried from Missoula, Montana, to Chico, California, and was ready for tank installation about two weeks before the start of the tests. Aero Union installed the tank and outfitted the installation with fairings. The completed installation is shown in Figure 25.

A weight and balance study (furnished to the Forest Service under separate cover*) showed the net aircraft weight with tank installed as 47,572 pounds including 400 pounds of ballast added in the tail to correct the cg with respect to the tank. The tank system accounts for about 3100 pounds of the total weight. The aircraft with a full load (20,000 pounds of retardant) has no special limitation due to its tank configuration.

*Aero Union Document

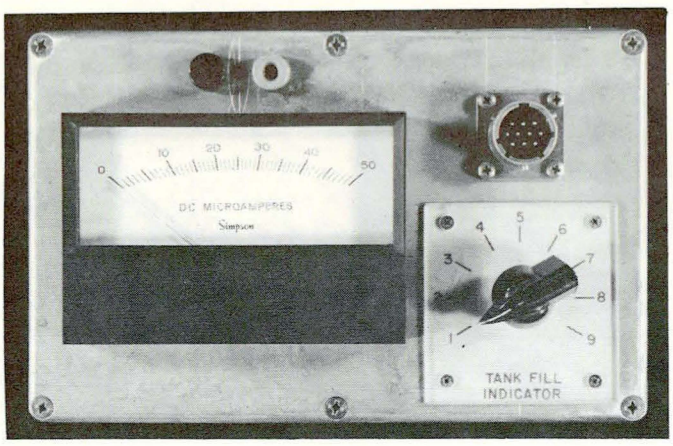

Figure 23. Tank Fillmeter

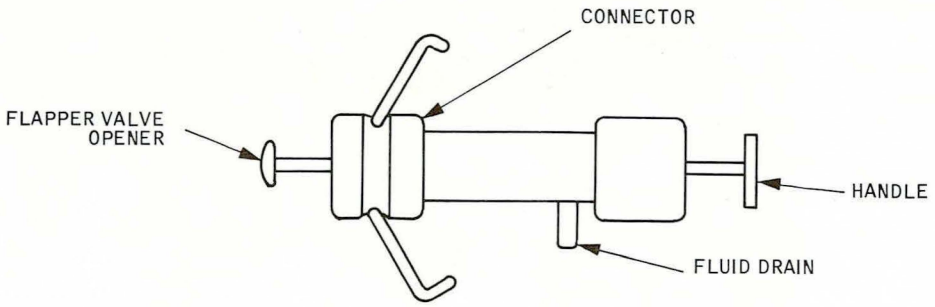

Figure 24. Downloading Fixture

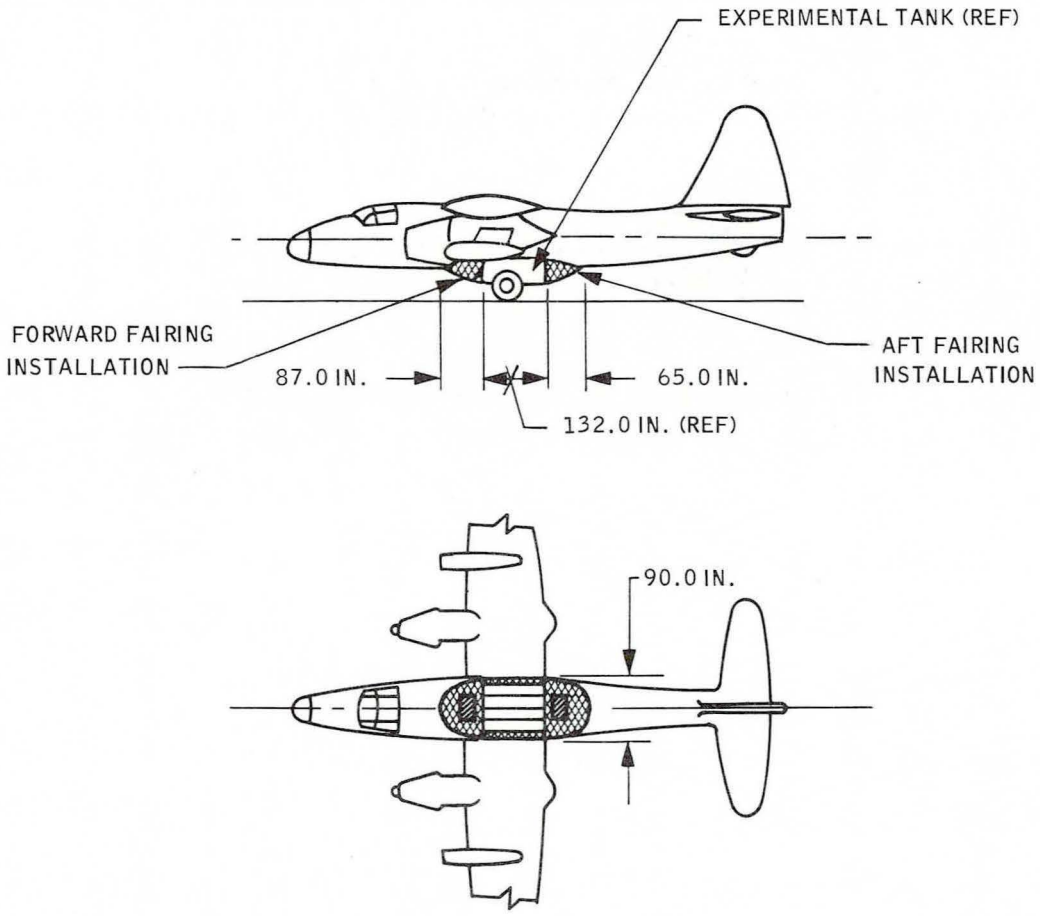

Figure 25. ETAGS Installation on P2V-5F Aircraft

SECTION III
FLOW RATE STUDIES

Because of the significance of flow rate in determining pattern formation and distribution, an objective of the ETAGS experiment was to obtain a more definitive understanding of the tank parameters as they affect the flow. To this end, an exhaustive set of tank ground tests was planned with full instrumentation and high-speed (500 frames per second) camera coverage of fluid flow including the falling surface within the tank and emergence at the door area. During the course of these tests it was determined that float instrumentation did not track the fluid surface. As a result, emphasis in the test series was directed more toward instrumentation changes than the collection of flow data itself. The primary source of flow-rate data, therefore, was derived from the actual flight test series.

BACKGROUND

Simultaneous work under the User Guidelines Contract (Ref. 1) had revised the Bernoulli flow simulation contained in the original MacPhearson simulation (Ref. 2). Briefly, the principles of tank flow were revised to view the tank as being dominated by either steady-state (Bernoulli) flow or acceleration (Newtonian) flow. This represents a numerical approximation to the source partial differential equation, in which one term or the other is negligible:

$$\frac{\partial u}{\partial t} + \frac{u \partial u}{\partial x} = g \qquad (1)$$

where u is the velocity and x is distance (head height). When the acceleration term is negligible, the integral of the resulting ordinary differential equation yields the Bernoulli equation:

$$V_{efflux} = \sqrt{2gx} \qquad (2)$$

When the steady-state term is negligible, the acceleration term integrates to g.

This work showed that there are two types of tanks, those with only minor restrictions and fast doors where the fluid continually accelerates out of the tank and those sufficiently restricted that they reach and sustain a steady-state flow performance. The resulting simulation computes the instantaneous flow rate under both conditions and selectes the lower velocity case for calculating the new fluid

position. The equations are further elaborated to include the effects of pressure buildup due to venting restrictions, yielding three equations:

- Bernoulli velocity: $V_E = \sqrt{\frac{2g\rho h - 2P + V_2^2}{\rho}}$ (3)

- Free-fall velocity: $V_E = V_2 + \Delta t \left(6 + \frac{P}{\rho}\right)$ (4)

- Pressure: $P = \frac{K_1 L (Q)^2}{D^5}$ (5)

  or Pressure: $P = \frac{K_2 (Q)^2}{D^4}$ (6)

where

V_E = velocity of efflux (ft/sec)

g = acceleration of gravity (32.2 ft/sec^2)

ρ = retardant density (lb/ft^3)

h = fluid height (ft)

P = pressure (psf)

V_2 = initial velocity (ft/sec)

K_1 = an accumulation of constants (Ref. 3) = 0.00278

K_2 = an accumulation of constants (Ref. 3) = 0.0019275

L = length of vent (ft)

D = diameter of vent (ft)

Q = volume fluid evacuated in the last time increment (ft^3/sec)

The alternative pressure generators result from viewing the vent system as a duct (of significant length) or as a straight orifice where losses due to flow through a pipe can be ignored.

This model to approximate tank flow had been shown to account for most aspects of tank flow far better than the Bernoulli system alone. It did have numeric instability at the changeover between acceleration and Bernoulli flow when pressures approach stopping. One objective of the ETAGS study was to refine this work in terms of considerable new data resulting from the tests.

SUMMARY

The study showed that the simulation scheme would yield good predictions of performance. The flow-rate subroutine was removed from PATSIM for interactive operation on a time-share for convenience of study. It was then used to duplicate results from selected ETAGS drops. This resulted in four items of significance:

- Door area (exit area) equations were corrected to reflect the observation in film analysis that fast doors exceed the rate of fluid fall from the tank. This corrects the overprediction of previous simulations in the early phase of evacuation.

- The source of the numeric instability when the tank nears pressure stoppage is inherent in the model approximation and cannot be damped out in a simple simulation. Since this is the condition of "pop bottling" that should be avoided in tank design, it should be sufficient for the simulation to identify the condition without actually driving to a stop.

- Pressure is not easily calibrated due to unexplained variations in recorded pressures (generally increasing), as the tank gets larger even though the vent area increases proportionately. In the pure case (tank 7) the constant in the velocity pressure equation (K_2) appears to predict the correct values.

- In a truly free-fall tank, the program will switch from the acceleration routine to the Bernoulli toward the end of evacuation. This switch departs from the actual flow rate and introduces an error in the fastest material to leave the tank. As a result, it is desirable not to allow the steady-state case when we can clearly identify an unrestricted tank. Where the tank is restricted to the Bernoulli, choice of routines is the more valid predictive approach.

INITIAL STUDIES

The initial studies on flow rate were to confirm tank performance. They are reported in Section VII . Thereafter the actual flow rates and pressures were examined to determine relative conformance to the ideas of flow rate development as they had been previously developed. Figure 26 shows the flow rate from a fast

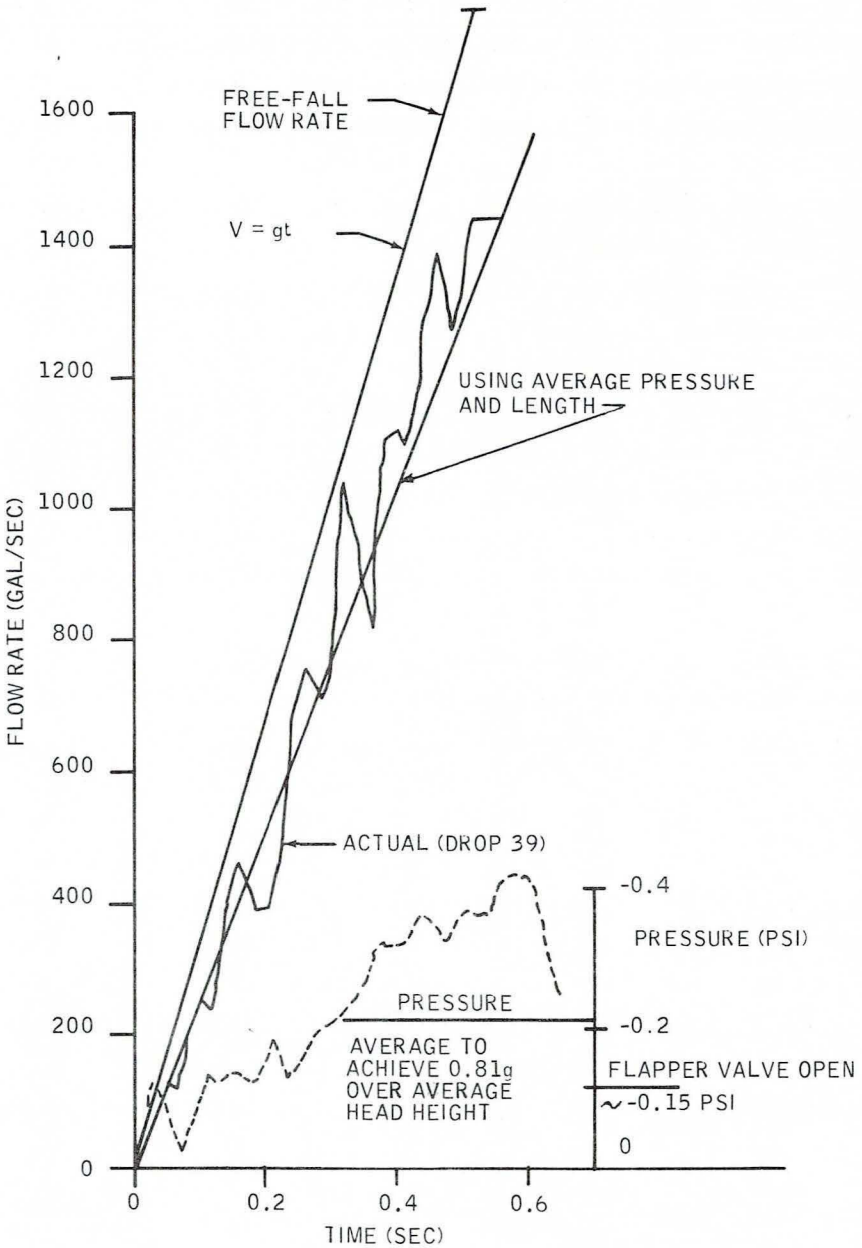

Figure 26. Comparison of Actual and Theoretical Flow Rate

opening door for drop 39. Although flow rate itself is somewhat more noisy than head versus time, the amplification of error provided by differentiation makes it useful for comparing with theoretical values. The figure shows the actual flow rate compared with the theoretical flow under gravity.

Actual flow rate approximates 0.81g. If the 0.19g difference in acceleration is attributed to pressure, we can estimate the average pressure/length combination that yields this difference from the equation:

$$a = 32.2\left(1 - \frac{psi}{0.46\overline{L}}\right)$$

where $\overline{L}$ is the average head or about 2.432 feet. The average pressure to yield 0.19 psi is then 0.212 psi. This value appears to reasonably account for the deflection in the flow-rate curve.

We can also examine the implications on pressure from Equation (6). Since the vent area is approximately 1/19th of the bottom area, peak air velocity will be about 158 ft/sec. This is associated with a pressure drop of 0.20 psi. Actual pressures recorded were about twice this value. This would suggest that the effective vent area is more like 1:12. Re-evaluation shows that this is about the case. Webbing to hold the splash valve is composed of 1/2-inch sheet metal in three arms intersecting centrally, occupying about 0.08 ft^2 of the 0.34 ft^2 available. There is then 0.264 ft^2 per vent and about a 1:11.8 area ratio.

It appears, as a result of the above, that the mechanisms of pressure buildup and their effect on the tank are reasonably well understood. Unfortunately, there was a great deal of variation in pressures measured from tank to tank. It is not known if these were due to calibration changes in the transducer or flow restrictions through the aircraft structure above the tank. Flapper valves and structure need to clear the stack vent orifices less than 2 inches to assure that the vent itself is the limiting factor. It is more probable, therefore, that the differences may relate to the way flapper valves operated or their operation in combination that created these difficulties.

Similar analysis was conducted on other configurations. Of particular interest is the 9.6-foot long by 1.2-foot wide exit configuration at door rate 6. This, due to the single-door operation, is the fastest release configuration. Flow rate peak was 1440 gal/sec. Based on an average pressure and length, and recognizing a 9% measurement error from the last 4 to 6 inches of travel (below the float), the theoretical value is 1432 gal/sec. Thus, there is essentially no effect of door on the release.

DOOR FLUID STUDIES

Door-open area (area of efflux) in association with velocity of efflux is used in the simulation to determine the incremental quantity of retardant released. The equation programmed in PATSIM to calculate this value is

$$A_E = L_D W_D \sin\alpha \qquad (7)$$

where α is the angle between the door and the bottom of the tank. This is physically viewed as the surface defined by door length and a line drawn from the point of the tank opposite the hinge perpendicular to the door surface, an increasing fraction of the door width. Although PATSIM also carries the additional area of the two triangles at each end of the door, this feature introduces considerable error in the free-fall tank (where it should not be included) and adds insignificantly to restricted or slow door performance for most tanks.

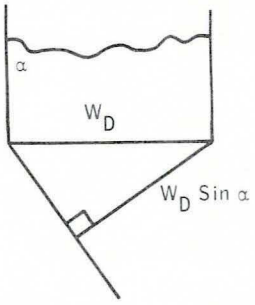

Figure 27 shows the performance of the fluid at the door interface for a very fast, powered door reconstructed from high-speed photographs from the ETAGS Static Test Series. Note that the door actually pulls away from the fluid as it exceeds the free-fall velocity of the fluid surface. The emergence of turbulence coincides with the passage of the free-fall line. This is clearly a complex flow dynamic. It is significant in predicting flow, not because the initial quantities are themselves significant, but because they establish the conditions for subsequent flow.

This aspect of performance was included in an off-line simulation of the ETAGS tank by specifying and recognizing four different conditions of door effects as shown in Figure 28.

The conditions are selected and control is transferred by relationships of the free-fall surface with respect to the door angle. A program listing appears as Appendix B. This program was not re-introduced to PATSIM because the significance of predicting the fine structure of flow rates on pattern prediction is not great.

(A) The fluid at the base of the tank falls at or slightly less than free-fall velocity. In the initial period the angular rate of the door runs ahead of the fluid over most of its length. It actually pulls against surface tension, forming the curve on the face of the fluid. Even in a door free to fall as driven by the fluid, the tip farthest from the hinge will attempt to exceed the free-fall velocity of the fluid. As a result, the door will open at a rate that balances fluid resistance acting on a long moment in front of the door's center of gravity, with the fluid's inertial forces acting aft at the door's center of gravity. As a result, a free-fall door is held back by the fluid and opens slightly slower than would be predicted by free-fall calculations alone.

(B) Surface tension failures in the fluid develop at the front edge. Turbulence starts near the hinge where the fluid's free-fall surface pushes against the door.

(C) The plume off the door tip increases, and the turbulence moves down the door.

(D) As the door approaches the full-open position, turbulence emanating in the restricted area flows over the bell crank, obscuring the detachment area. Note however, that only the plume has dropped below the tip of the door.

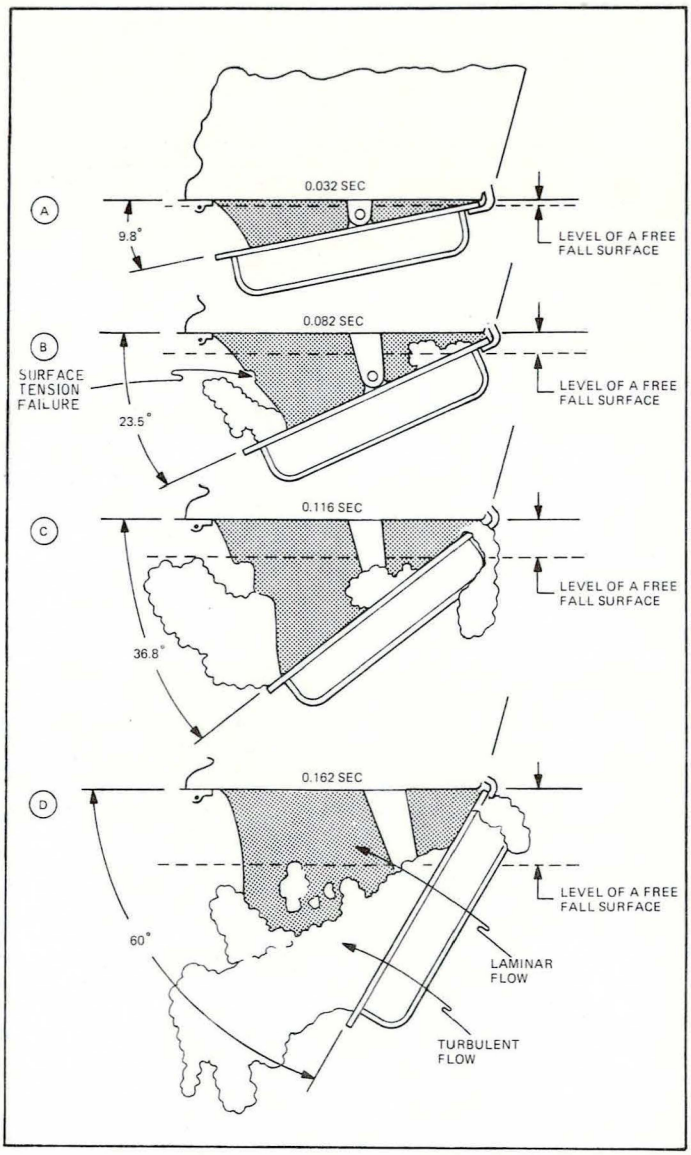

Figure 27. High-Speed Door Sequence Showing Phenomena at the Door-to-Fluid Interface

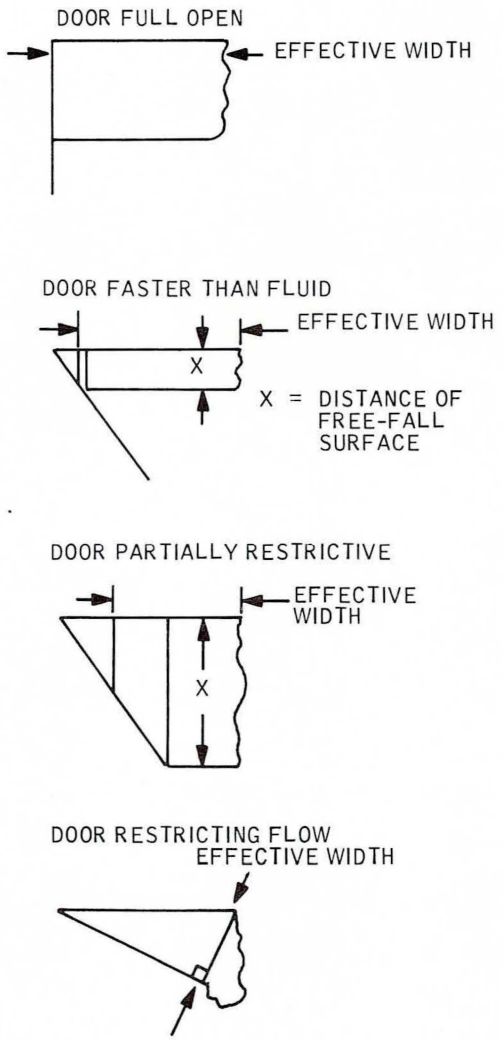

Figure 28. Four Different Door Conditions

The results of the program are shown on the following pages with illustrations accompanied by printouts. Figure 29 shows the single-unit (tank 7) simulation with fast and slow doors in terms of volume out and times as overlays to the actual. Note that pressures are actually lower than recorded. (This aspect was investigated separately). Computer printouts of the simulations are reproduced as Figures 30 and 31.

Figures 32 through 34 show the simulation applied to the four-unit tank (tank 5) with only one door opening (the 1/2-door arrangement), both fast- and slow-door versions. In this case, tracking is reasonable up to the last 60 gallons, where the Bernoulli equation predicts considerably slower evacuation than actually occurs.

Figures 35 and 36 show the four-unit tank with 1/4 door. Again, tracking is good up to the final 60 gallons. It is possible that this under-prediction results from the strength of the fluid below the tank that may provide apparent head greater than that within the tank limits.

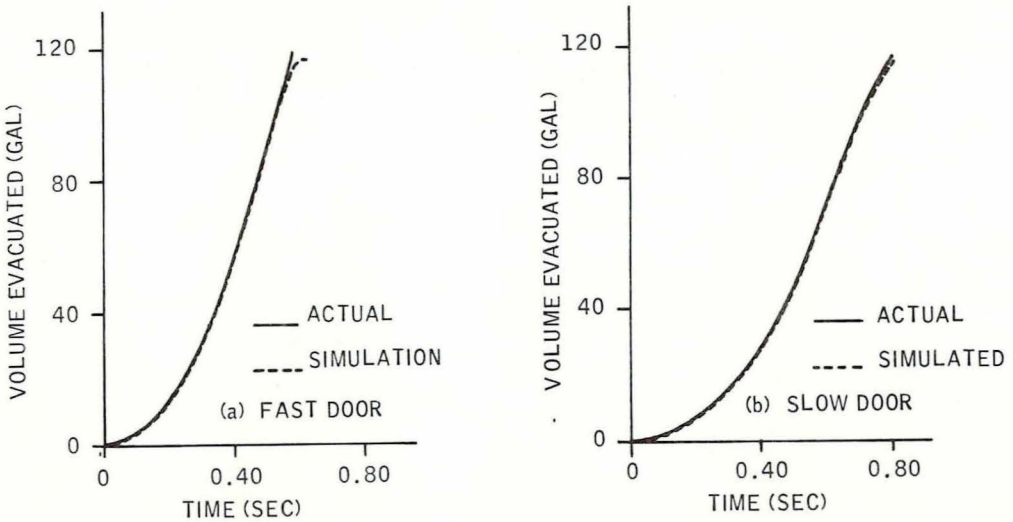

Figure 29. Comparison of Actual and Simulated Single Unit Tank, Full Door Release for Two Door Rates

```
?LIST PARAM1

H=4.864                    HEAD HEIGHT (FT)
LD=2.4                     DOOR LENGHT (FT)
WD=1.317                   DOOR WIDTH (FT)
LT=2.4                     LENGHT FLUID TOP (FT)
WT=1.317                   WIDTH FLUID TOP (FT)
DV=0.677                   EQUIVALENT VENT DIA. (FT)
LV=0.500                   LENGTH OF VENT (FT)
RHO=2.072                  RETARDANT DENSITY (PSF/FT)
K=0.0019275
G=32.2                     GRAVITY CONSTANT (FT/SEC**2)
HT=5.17                    TANK HEIGHT (FT)


?COPY DOOR2 DOOR

?COPY PARAM1 PARAM

?RUN FLO
```

TIME (SEC)	HEAD (FT)	VEL EXIT	VEL TOP	RATE GALS/SEC	VOLUME OUT	PRESS PSI		
0.04	4.85	0.64	0.56	13.16	0.26	-0.000	A	1
0.06	4.83	1.29	1.24	29.41	0.85	-0.001	A	1
0.08	4.79	1.93	1.90	44.95	1.75	-0.002	A	1
0.10	4.74	2.58	2.55	60.25	2.96	-0.004	A	1
0.12	4.68	3.22	3.19	75.36	4.46	-0.006	A	1
0.14	4.60	3.86	3.82	90.44	6.27	-0.008	A	1
0.16	4.51	4.50	4.47	105.61	8.38	-0.011	A	1
0.18	4.41	5.14	5.11	120.79	10.80	-0.014	A	1
0.20	4.29	5.78	5.75	135.94	13.52	-0.018	A	1
0.22	4.16	6.42	6.39	151.07	16.54	-0.023	A	1
0.24	4.02	7.06	7.06	166.86	19.88	-0.028	A	0
0.26	3.87	7.69	7.69	181.86	23.51	-0.033	A	0
0.28	3.70	8.32	8.32	196.80	27.45	-0.039	A	0
0.30	3.52	8.95	8.95	211.69	31.68	-0.045	A	0
0.32	3.33	9.58	9.58	226.49	36.21	-0.052	A	0
0.34	3.13	10.20	10.20	241.20	41.04	-0.060	A	0
0.36	2.91	10.82	10.82	255.80	46.15	-0.067	A	0
0.38	2.68	11.43	11.43	270.27	51.56	-0.076	A	0
0.40	2.44	12.03	12.03	284.57	57.25	-0.084	A	0
0.42	2.19	12.63	12.63	298.67	63.22	-0.093	A	0
0.44	1.93	13.22	13.22	312.50	69.47	-0.102	A	0
0.46	1.65	13.79	13.79	325.99	75.99	-0.112	A	0
0.48	1.36	14.34	14.34	339.00	82.77	-0.121	A	0
0.50	1.07	14.86	14.86	351.31	89.80	-0.130	A	0
0.52	0.76	15.33	15.33	362.52	97.05	-0.139	A	0
0.54	0.45	15.72	15.72	371.72	104.48	-0.147	A	0
0.56	0.13	15.91	15.91	376.11	112.01	-0.151	A	0
0.58	-0.17	14.90	14.90	352.34	119.05	-0.133	A	0

```
STOP,
?DELETE DOOR
```

Figure 30. Simulation Printout for Figure 29(a) - Fast Door

```
?RUN FLO
```

TIME (SEC)	HEAD (FT)	VEL EXIT	VEL TOP	RATE GALS/SEC	VOLUME OUT	PRESS PSI		
0.06	4.86	0.64	0.43	10.13	0.20	-0.000	A	1
0.08	4.83	1.29	1.06	25.16	0.71	-0.001	A	1
0.10	4.80	1.93	1.73	40.90	1.52	-0.002	A	1
0.12	4.75	2.58	2.38	56.34	2.65	-0.003	A	1
0.14	4.72	3.22	1.62	38.33	3.42	-0.002	A	2
0.16	4.68	3.86	1.95	46.13	4.34	-0.002	A	2
0.18	4.63	4.51	2.28	54.00	5.42	-0.003	A	2
0.20	4.58	5.15	2.62	61.95	6.66	-0.004	A	2
0.22	4.52	5.79	2.96	70.00	8.06	-0.005	A	2
0.24	4.46	6.43	3.31	78.17	9.62	-0.006	A	2
0.26	4.38	7.08	3.66	86.50	11.35	-0.008	A	2
0.28	4.30	7.72	4.02	95.00	13.25	-0.009	A	2
0.30	4.22	8.36	4.39	103.73	15.33	-0.011	A	2
0.32	4.12	9.00	4.77	112.68	17.58	-0.013	A	2
0.34	4.02	9.64	5.16	122.10	20.02	-0.015	A	2
0.36	3.91	10.28	5.55	131.83	22.66	-0.018	A	2
0.38	3.79	10.91	6.01	142.15	25.50	-0.021	A	2
0.40	3.66	11.55	6.47	152.86	28.56	-0.024	A	2
0.42	3.52	12.19	6.93	163.81	31.84	-0.028	A	2
0.44	3.37	12.82	7.41	175.14	35.34	-0.032	A	2
0.46	3.21	13.45	7.92	187.37	39.09	-0.037	A	2
0.48	3.04	14.08	8.46	200.12	43.09	-0.042	A	2
0.50	2.86	14.70	9.03	213.61	47.36	-0.048	A	2
0.52	2.67	15.32	9.63	227.69	51.91	-0.054	A	2
0.54	2.46	15.94	10.30	243.63	56.79	-0.062	A	2
0.56	2.25	16.00	10.65	251.79	61.82	-0.067	B	2
0.58	2.03	15.78	10.87	256.96	66.96	-0.070	B	2
0.60	1.81	15.47	11.03	260.85	72.18	-0.072	B	2
0.62	1.59	15.11	11.16	263.94	77.46	-0.074	B	2
0.64	1.36	14.72	11.26	266.26	82.78	-0.076	B	2
0.66	1.14	14.28	11.20	264.79	88.08	-0.075	B	2
0.68	0.92	13.72	11.02	260.55	93.29	-0.073	B	2
0.70	0.71	13.05	10.55	249.35	98.28	-0.067	B	2
0.72	0.51	12.14	9.87	233.32	102.94	-0.059	B	2
0.74	0.33	11.04	9.03	213.62	107.22	-0.050	B	2
0.76	0.17	9.79	8.05	190.64	111.03	-0.040	B	2
0.78	0.03	8.38	6.98	164.99	114.33	-0.030	B	2
0.80	-0.09	0.81	5.73	135.46	117.04	-0.020	B	2

```
STOP,
?OFF
OFF AT 15:45  05/23/77
COMPUTE SEC. - 11.5
CONNECT MIN. - 05
```

Figure 31. Simulation Printout for Figure 29(b) - Slow Door

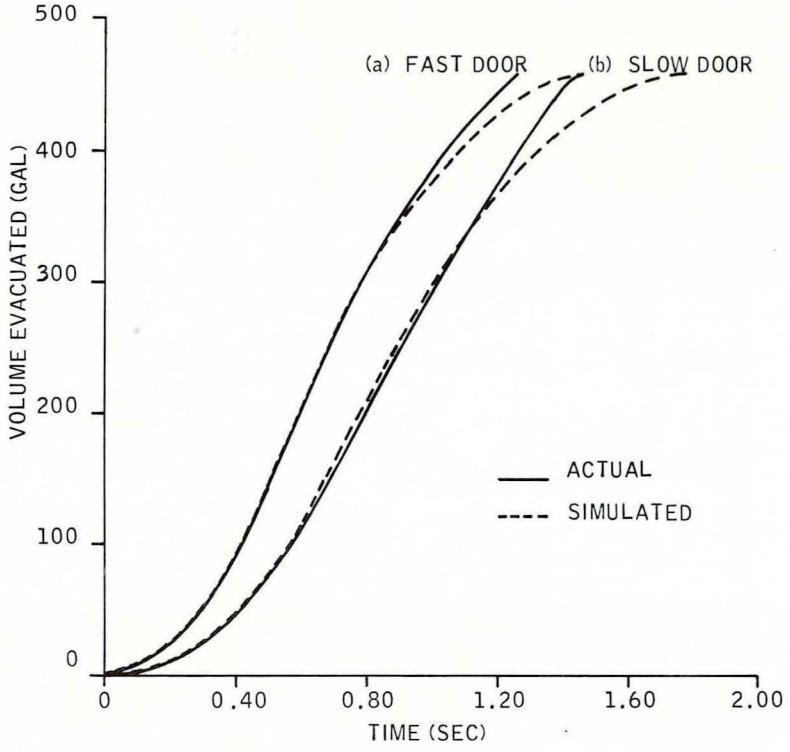

Figure 32. Comparison of Actual and Simulated Four-Unit Tank, 1/2-Door Release for Two Door Rates

```
?DELETE DOOR

?COPY DOOR2 DOOR

?RUN
LOAD RL
```

TIME (SEC)	HEAD (FT)	VEL EXIT	VEL TOP	RATE GALS/SEC	VOLUME OUT	PRESS PSI		
0.04	4.66	0.64	0.22	21.06	0.42	-0.000	A	1
0.06	4.65	1.29	0.50	47.06	1.36	-0.000	A	1
0.08	4.63	1.93	0.76	71.92	2.80	-0.000	A	1
0.10	4.61	2.58	1.02	96.42	4.73	-0.001	A	1
0.12	4.79	3.22	1.28	120.63	7.14	-0.001	A	1
0.14	4.76	3.86	1.53	144.82	10.04	-0.001	A	1
0.16	4.72	4.51	1.79	169.17	13.42	-0.002	A	1
0.18	4.68	5.15	2.05	193.56	17.29	-0.002	A	1
0.20	4.64	5.79	2.30	217.95	21.65	-0.003	A	1
0.22	4.58	6.44	2.56	242.35	26.50	-0.004	A	1
0.24	4.53	7.08	2.83	267.85	31.86	-0.005	A	0
0.26	4.47	7.72	3.09	292.16	37.70	-0.006	A	0
0.28	4.40	8.36	3.35	316.46	44.03	-0.007	A	0
0.30	4.33	9.01	3.60	340.74	50.84	-0.008	A	0
0.32	4.25	9.65	3.86	365.02	58.14	-0.009	A	0
0.34	4.17	10.29	4.12	389.27	65.93	-0.010	A	0
0.36	4.08	10.93	4.37	413.51	74.20	-0.011	A	0
0.38	3.99	11.57	4.63	437.73	82.95	-0.013	A	0
0.40	3.89	12.21	4.88	461.93	92.19	-0.014	A	0
0.42	3.79	12.85	5.14	486.11	101.91	-0.016	A	0
0.44	3.68	13.49	5.39	510.26	112.12	-0.017	A	0
0.46	3.57	14.12	5.65	534.38	122.81	-0.019	A	0
0.48	3.45	14.76	5.90	558.46	133.98	-0.021	A	0
0.50	3.32	15.40	6.16	582.51	145.63	-0.023	A	0
0.52	3.20	15.78	6.31	596.66	157.58	-0.024	B	0
0.54	3.07	15.67	6.23	589.14	169.35	-0.023	B	0
0.56	2.95	15.28	6.11	576.13	180.91	-0.022	B	0
0.58	2.83	14.98	5.99	566.62	192.24	-0.022	B	0
0.60	2.71	14.67	5.87	555.04	203.34	-0.021	B	0
0.62	2.60	14.36	5.75	543.44	214.21	-0.020	B	0
0.64	2.49	14.06	5.62	531.84	224.85	-0.019	B	0
0.66	2.38	13.75	5.50	520.24	235.25	-0.019	B	0
0.68	2.27	13.44	5.38	508.64	245.43	-0.018	B	0
0.70	2.16	13.14	5.25	497.03	255.37	-0.017	B	0
0.72	2.06	12.83	5.13	485.43	265.08	-0.016	B	0
0.74	1.96	12.52	5.01	473.82	274.55	-0.015	B	0
0.76	1.86	12.22	4.89	462.20	283.80	-0.015	B	0
0.78	1.77	11.91	4.76	450.59	292.81	-0.014	B	0
0.80	1.68	11.60	4.64	438.96	301.59	-0.013	B	0
0.82	1.59	11.30	4.52	427.34	310.13	-0.013	B	0
0.84	1.50	10.99	4.40	415.71	318.45	-0.012	B	0
0.86	1.41	10.68	4.27	404.07	326.53	-0.011	B	0
0.88	1.33	10.37	4.15	392.43	334.38	-0.011	B	0
0.90	1.25	10.06	4.03	380.78	341.99	-0.010	B	0
0.92	1.17	9.76	3.90	369.12	349.38	-0.010	B	0
0.94	1.09	9.45	3.78	357.46	356.52	-0.009	B	0
0.96	1.02	9.14	3.66	345.79	363.44	-0.008	B	0
0.98	0.95	8.83	3.53	334.11	370.12	-0.008	B	0
1.00	0.88	8.52	3.41	322.42	376.57	-0.007	B	0
1.02	0.82	8.21	3.29	310.72	382.79	-0.007	B	0
1.04	0.75	7.90	3.16	299.01	388.77	-0.006	B	0
1.06	0.69	7.59	3.04	287.29	394.51	-0.006	B	0
1.08	0.63	7.28	2.91	275.56	400.02	-0.005	B	0
1.10	0.58	6.97	2.79	263.81	405.30	-0.005	B	0
1.12	0.53	6.66	2.66	252.05	410.34	-0.004	B	0
1.14	0.47	6.35	2.54	240.27	415.14	-0.004	B	0
1.16	0.43	6.04	2.42	228.47	419.71	-0.004	B	0
1.18	0.38	5.73	2.29	216.65	424.05	-0.003	B	0
1.20	0.34	5.41	2.17	204.80	428.14	-0.003	B	0
1.22	0.30	5.10	2.04	192.94	432.00	-0.003	B	0
1.24	0.26	4.79	1.91	181.04	435.62	-0.002	B	0
1.26	0.22	4.47	1.79	169.10	439.00	-0.002	B	0
1.28	0.19	4.15	1.66	157.13	442.15	-0.002	B	0
1.30	0.16	3.84	1.53	145.11	445.05	-0.001	B	0
1.32	0.13	3.52	1.41	133.03	447.71	-0.001	B	0
1.34	0.10	3.20	1.28	120.89	450.13	-0.001	B	0
1.36	0.08	2.87	1.15	108.66	452.30	-0.001	B	0
1.38	0.06	2.55	1.02	96.33	454.23	-0.001	B	0
1.40	0.04	2.22	0.89	83.87	455.91	-0.000	B	0
1.42	0.03	1.88	0.75	71.21	457.33	-0.000	B	0
1.44	0.02	1.54	0.62	58.28	458.50	-0.000	B	0
1.46	0.01	1.19	0.47	44.90	459.39	-0.000	B	0
1.48	0.00	0.81	0.32	30.66	460.01	-0.000	B	0
1.50	-0.00	0.36	0.14	13.61	460.28	-0.000	B	0

```
STOP.
?
```

Figure 33. Simulation Printout for Figure 32(a) - Fast Door

TIME (SEC)	HEAD (FT)	VEL EXIT	VEL TOP	RATE GALS/SEC	VOLUME OUT	PRESS PSI		
0.06	4.86	0.64	0.17	16.21	0.32	-0.000	A	1
0.08	4.85	1.29	0.43	40.25	1.13	-0.000	A	1
0.10	4.84	1.93	0.69	65.44	2.44	-0.000	A	1
0.12	4.82	2.56	0.95	90.17	4.24	-0.001	A	1
0.14	4.81	3.22	0.65	81.36	5.47	-0.000	A	2
0.16	4.79	3.86	0.78	73.83	6.95	-0.000	A	2
0.18	4.77	4.51	0.91	86.44	8.67	-0.001	A	2
0.20	4.75	5.15	1.05	99.17	10.66	-0.001	A	2
0.22	4.73	5.80	1.19	112.08	12.90	-0.001	A	2
0.24	4.70	6.44	1.32	125.17	15.40	-0.001	A	2
0.26	4.67	7.08	1.46	138.55	18.17	-0.001	A	2
0.28	4.64	7.73	1.61	152.17	21.22	-0.002	A	2
0.30	4.60	8.37	1.76	166.21	24.54	-0.002	A	2
0.32	4.57	9.01	1.91	180.58	28.15	-0.002	A	2
0.34	4.52	9.66	2.07	195.73	32.07	-0.003	A	2
0.36	4.48	10.30	2.24	211.41	36.30	-0.003	A	2
0.38	4.43	10.94	2.41	228.03	40.86	-0.003	A	2
0.40	4.38	11.59	2.59	245.36	45.76	-0.004	A	2
0.42	4.32	12.23	2.78	263.03	51.02	-0.005	A	2
0.44	4.27	12.87	2.97	281.38	56.65	-0.005	A	2
0.46	4.20	13.51	3.18	301.22	62.68	-0.006	A	2
0.48	4.13	14.16	3.40	321.97	69.12	-0.007	A	2
0.50	4.06	14.80	3.64	343.99	76.00	-0.008	A	2
0.52	3.98	15.44	3.88	367.06	83.34	-0.009	A	2
0.54	3.90	16.08	4.16	393.25	91.20	-0.010	A	2
0.56	3.81	16.34	4.35	411.38	99.43	-0.011	B	2
0.58	3.72	16.21	4.47	422.50	107.88	-0.012	B	2
0.60	3.63	16.07	4.58	433.49	116.55	-0.013	B	2
0.62	3.54	15.91	4.70	444.69	125.44	-0.013	B	2
0.64	3.44	15.75	4.82	456.03	134.56	-0.014	B	2
0.66	3.34	15.59	4.89	462.28	143.81	-0.014	B	2
0.68	3.24	15.40	4.95	467.93	153.17	-0.015	B	2
0.70	3.15	15.21	4.92	464.91	162.47	-0.015	B	2
0.72	3.05	14.99	4.87	460.95	171.68	-0.014	B	2
0.74	2.95	14.77	4.83	457.02	180.83	-0.014	B	2
0.76	2.86	14.54	4.79	452.96	189.84	-0.014	B	2
0.78	2.76	14.32	4.77	450.78	198.90	-0.014	B	2
0.80	2.67	14.09	4.74	448.58	207.87	-0.014	B	2
0.82	2.57	13.87	4.72	446.54	216.81	-0.014	B	2
0.84	2.48	13.64	4.74	448.17	225.77	-0.014	B	2
0.86	2.38	13.42	4.63	437.70	234.53	-0.013	B	2
0.88	2.29	13.16	4.60	435.50	243.24	-0.013	B	2
0.90	2.20	12.92	4.59	433.94	251.91	-0.013	B	2
0.92	2.11	12.69	4.56	431.12	260.54	-0.013	B	2
0.94	2.02	12.44	4.52	427.89	269.09	-0.013	B	2
0.96	1.93	12.20	4.44	420.34	277.50	-0.012	B	2
0.98	1.84	11.93	4.36	412.20	285.75	-0.012	B	2
1.00	1.76	11.66	4.26	402.96	293.80	-0.011	B	2
1.02	1.67	11.39	4.18	393.58	301.68	-0.011	B	2
1.04	1.59	11.12	4.06	384.19	309.36	-0.010	B	2
1.06	1.51	10.85	3.96	374.78	316.86	-0.010	B	2
1.08	1.44	10.58	3.85	365.37	324.16	-0.009	B	2
1.10	1.36	10.30	3.76	355.96	331.28	-0.009	B	2
1.12	1.29	10.03	3.66	346.55	338.21	-0.008	B	2
1.14	1.22	9.76	3.56	337.13	344.96	-0.008	B	2
1.16	1.15	9.49	3.46	327.70	351.51	-0.008	B	2
1.18	1.08	9.21	3.36	318.27	357.88	-0.007	B	2
1.20	1.02	8.94	3.27	308.84	364.05	-0.007	B	2
1.22	0.95	8.67	3.17	299.40	370.04	-0.006	B	2
1.24	0.89	8.39	3.07	289.95	375.84	-0.006	B	2
1.26	0.83	8.12	2.97	280.50	381.45	-0.006	B	2
1.28	0.77	7.85	2.87	271.04	386.87	-0.005	B	2
1.30	0.72	7.57	2.77	261.58	392.10	-0.005	B	2
1.32	0.67	7.30	2.67	252.11	397.14	-0.004	B	2
1.34	0.61	7.02	2.57	242.63	402.00	-0.004	B	2
1.36	0.56	6.75	2.46	233.13	406.66	-0.004	B	2
1.38	0.52	6.47	2.36	223.63	411.13	-0.004	B	2
1.40	0.47	6.20	2.26	214.12	415.41	-0.003	B	2
1.42	0.43	5.92	2.16	204.60	419.51	-0.003	B	2
1.44	0.39	5.65	2.06	195.08	423.41	-0.003	B	2
1.46	0.35	5.37	1.96	185.51	427.12	-0.002	B	2
1.48	0.31	5.09	1.86	175.95	430.64	-0.002	B	2
1.50	0.28	4.82	1.76	166.36	433.96	-0.002	B	2
1.52	0.24	4.54	1.66	156.76	437.10	-0.002	B	2
1.54	0.21	4.26	1.56	147.13	440.04	-0.002	B	2
1.56	0.18	3.98	1.45	137.48	442.79	-0.001	B	2
1.58	0.16	3.70	1.35	127.79	445.35	-0.001	B	2
1.60	0.13	3.42	1.25	118.07	447.71	-0.001	B	2
1.62	0.11	3.13	1.15	108.31	449.87	-0.001	B	2
1.64	0.09	2.85	1.04	98.49	451.84	-0.001	B	2
1.66	0.07	2.57	0.94	88.62	453.62	-0.001	B	2
1.68	0.05	2.28	0.83	78.66	455.19	-0.000	B	2
1.70	0.04	1.99	0.73	68.61	456.56	-0.000	B	2
1.72	0.02	1.69	0.62	58.41	457.73	-0.000	B	2
1.74	0.01	1.39	0.51	48.00	458.69	-0.000	B	2
1.76	0.01	1.08	0.39	37.28	459.44	-0.000	B	2
1.78	0.00	0.75	0.27	25.93	459.95	-0.000	B	2
1.80	-0.00	0.37	0.14	12.79	460.21	-0.000	B	2

STOP,

Figure 34. Simulation Printout for Figure 32(b) - Slow Door

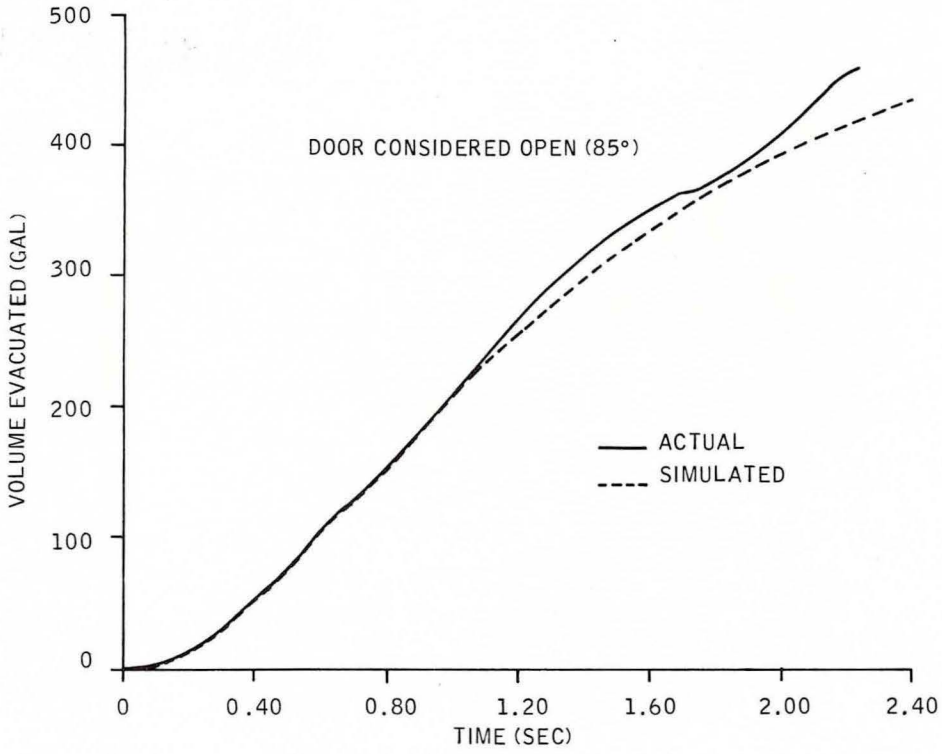

Figure 35. Comparison of Actual and Simulated Four-Unit Tank, 1/4-Door Release

TIME (SEC)	HEAD (FT)	VEL EXIT	VEL TOP	RATE GALS/SEC	VOLUME OUT	PRESS PSI		
0.02	4.66	0.64	0.12	11.57	0.23	-0.000	A	1
0.04	4.66	1.29	0.24	23.15	0.69	-0.000	A	0
0.06	4.65	1.93	0.37	34.72	1.39	-0.000	A	0
0.08	4.64	2.58	0.49	46.29	2.31	-0.000	A	0
0.10	4.63	3.22	0.61	57.86	3.47	-0.000	A	0
0.12	4.61	3.86	0.73	69.44	4.86	-0.000	A	0
0.14	4.60	4.51	0.86	81.01	6.48	-0.000	A	0
0.16	4.58	5.15	0.98	92.58	8.33	-0.001	A	0
0.18	4.55	5.80	1.10	104.15	10.42	-0.001	A	0
0.20	4.53	6.44	1.22	115.72	12.73	-0.001	A	0
0.22	4.50	7.08	1.35	127.29	15.28	-0.001	A	0
0.24	4.47	7.73	1.47	138.86	18.05	-0.001	A	0
0.26	4.44	8.37	1.59	150.42	21.06	-0.002	A	0
0.28	4.41	9.01	1.71	161.99	24.30	-0.002	A	0
0.30	4.37	9.66	1.83	173.55	27.77	-0.002	A	0
0.32	4.33	10.30	1.96	185.11	31.47	-0.002	A	0
0.34	4.29	10.94	2.08	196.67	35.41	-0.003	A	0
0.36	4.25	11.59	2.20	208.23	39.57	-0.003	A	0
0.38	4.20	12.23	2.32	219.79	43.97	-0.003	A	0
0.40	4.35	12.87	2.45	231.34	48.59	-0.004	A	0
0.42	4.30	13.52	2.57	242.90	53.45	-0.004	A	0
0.44	4.25	14.16	2.69	254.45	58.54	-0.004	A	0
0.46	4.19	14.80	2.81	265.99	63.86	-0.005	A	0
0.48	4.13	15.44	2.93	277.54	69.41	-0.005	A	0
0.50	4.07	16.09	3.06	289.08	75.19	-0.006	A	0
0.52	4.01	16.45	3.13	295.62	81.11	-0.006	B	0
0.54	3.94	16.34	3.10	293.63	86.95	-0.006	B	0
0.56	3.88	16.21	3.08	291.35	92.81	-0.006	B	0
0.58	3.82	16.09	3.06	289.07	98.59	-0.006	B	0
0.60	3.76	15.96	3.03	286.79	104.32	-0.006	B	0
0.62	3.70	15.83	3.01	284.50	110.01	-0.006	B	0
0.64	3.64	15.70	2.98	282.22	115.66	-0.006	B	0
0.66	3.58	15.58	2.96	279.93	121.26	-0.006	B	0
0.68	3.52	15.45	2.94	277.65	126.81	-0.006	B	0
0.70	3.47	15.32	2.91	275.36	132.32	-0.006	B	0
0.72	3.41	15.20	2.89	273.08	137.78	-0.006	B	0
0.74	3.35	15.07	2.86	270.79	143.19	-0.006	B	0
0.76	3.29	14.94	2.84	268.51	148.56	-0.006	B	0
0.78	3.24	14.81	2.81	266.22	153.89	-0.006	B	0
0.80	3.18	14.69	2.79	263.94	159.17	-0.006	B	0
0.82	3.13	14.56	2.77	261.65	164.40	-0.006	B	0
0.84	3.07	14.43	2.74	259.37	169.59	-0.006	B	0
0.86	3.02	14.31	2.72	257.08	174.73	-0.006	B	0
0.88	2.96	14.18	2.69	254.80	179.82	-0.006	B	0
0.90	2.91	14.05	2.67	252.51	184.88	-0.004	B	0
0.92	2.86	13.92	2.65	250.23	189.88	-0.004	B	0
0.94	2.80	13.80	2.62	247.94	194.84	-0.004	B	0
0.96	2.75	13.67	2.60	245.65	199.75	-0.004	B	0
0.98	2.70	13.54	2.57	243.37	204.62	-0.004	B	0
1.00	2.65	13.42	2.55	241.08	209.44	-0.004	B	0
1.02	2.60	13.29	2.52	238.80	214.22	-0.004	B	0
1.04	2.55	13.16	2.50	236.51	218.95	-0.004	B	0
1.06	2.50	13.03	2.48	234.23	223.63	-0.004	B	0
1.08	2.45	12.91	2.45	231.94	228.27	-0.004	B	0
1.10	2.40	12.78	2.43	229.65	232.86	-0.004	B	0
1.12	2.35	12.65	2.40	227.37	237.41	-0.004	B	0
1.14	2.31	12.52	2.38	225.08	241.91	-0.004	B	0
1.16	2.26	12.40	2.36	222.80	246.37	-0.003	B	0
1.18	2.21	12.27	2.33	220.51	250.78	-0.003	B	0
1.20	2.17	12.14	2.31	218.22	255.14	-0.003	B	0
1.22	2.12	12.02	2.28	215.94	259.46	-0.003	B	0
1.24	2.08	11.89	2.26	213.65	263.73	-0.003	B	0
1.26	2.03	11.76	2.23	211.36	267.96	-0.003	B	0
1.28	1.99	11.63	2.21	209.07	272.14	-0.003	B	0
1.30	1.94	11.51	2.19	206.79	276.28	-0.003	B	0
1.32	1.90	11.38	2.16	204.50	280.37	-0.003	B	0
1.34	1.86	11.25	2.14	202.21	284.41	-0.003	B	0
1.36	1.81	11.12	2.11	199.92	288.41	-0.003	B	0
1.38	1.77	11.00	2.09	197.64	292.36	-0.003	B	0
1.40	1.73	10.87	2.07	195.35	296.27	-0.003	B	0
1.42	1.69	10.74	2.04	193.06	300.13	-0.003	B	0
1.44	1.65	10.62	2.02	190.77	303.95	-0.003	B	0
1.46	1.61	10.49	1.99	188.48	307.72	-0.002	B	0
1.48	1.57	10.36	1.97	186.19	311.44	-0.002	B	0
1.50	1.53	10.23	1.94	183.90	315.12	-0.002	B	0
1.52	1.49	10.11	1.92	181.62	318.75	-0.002	B	0
1.54	1.46	9.98	1.90	179.33	322.34	-0.002	B	0
1.56	1.42	9.85	1.87	177.04	325.88	-0.002	B	0

Figure 36. Simulation Printout for Figure 35 (1 of 2)

```
1.58    1.38    9.72    1.85    174.75    329.37    -0.002  B  0
1.60    1.35    9.60    1.82    172.46    332.82    -0.002  B  0
1.62    1.31    9.47    1.80    170.17    336.23    -0.002  B  0
1.64    1.27    9.34    1.77    167.88    339.58    -0.002  B  0
1.66    1.24    9.21    1.75    165.59    342.90    -0.002  B  0
1.68    1.20    9.09    1.73    163.30    346.16    -0.002  B  0
1.70    1.17    8.96    1.70    161.00    349.38    -0.002  B  0
1.72    1.14    8.83    1.68    158.71    352.56    -0.002  B  0
1.74    1.10    8.70    1.65    156.42    355.68    -0.002  B  0
1.76    1.07    8.58    1.63    154.13    358.77    -0.002  B  0
1.78    1.04    8.45    1.61    151.84    361.80    -0.002  B  0
1.80    1.01    8.32    1.58    149.55    364.79    -0.002  B  0
1.82    0.98    8.19    1.56    147.25    367.74    -0.002  B  0
1.84    0.95    8.07    1.53    144.96    370.64    -0.001  B  0
1.86    0.92    7.94    1.51    142.67    373.49    -0.001  B  0
1.88    0.89    7.81    1.48    140.37    376.30    -0.001  B  0
1.90    0.86    7.68    1.46    138.08    379.06    -0.001  B  0
1.92    0.83    7.56    1.44    135.79    381.78    -0.001  B  0
1.94    0.80    7.43    1.41    133.49    384.45    -0.001  B  0
1.96    0.77    7.30    1.39    131.20    387.07    -0.001  B  0
1.98    0.74    7.17    1.36    128.90    389.65    -0.001  B  0
2.00    0.72    7.05    1.34    126.61    392.18    -0.001  B  0
2.02    0.69    6.92    1.31    124.31    394.67    -0.001  B  0
2.04    0.67    6.79    1.29    122.01    397.11    -0.001  B  0
2.06    0.64    6.66    1.27    119.72    399.50    -0.001  B  0
2.08    0.62    6.53    1.24    117.42    401.85    -0.001  B  0
2.10    0.59    6.41    1.22    115.12    404.15    -0.001  B  0
2.12    0.57    6.28    1.19    112.82    406.41    -0.001  B  0
2.14    0.54    6.15    1.17    110.52    408.62    -0.001  B  0
2.16    0.52    6.02    1.14    108.22    410.78    -0.001  B  0
2.18    0.50    5.89    1.12    105.92    412.90    -0.001  B  0
2.20    0.48    5.77    1.10    103.62    414.97    -0.001  B  0
2.22    0.46    5.64    1.07    101.32    417.00    -0.001  B  0
2.24    0.43    5.51    1.05     99.02    418.98    -0.001  B  0
2.26    0.41    5.38    1.02     96.72    420.92    -0.001  B  0
2.28    0.39    5.25    1.00     94.42    422.80    -0.001  B  0
2.30    0.37    5.13    0.97     92.11    424.65    -0.001  B  0
2.32    0.36    5.00    0.95     89.81    426.44    -0.001  B  0
2.34    0.34    4.87    0.93     87.50    428.19    -0.001  B  0
2.36    0.32    4.74    0.90     85.20    429.90    -0.001  B  0
2.38    0.30    4.61    0.88     82.89    431.55    -0.000  B  0
2.40    0.28    4.48    0.85     80.58    433.17    -0.000  B  0
2.42    0.27    4.36    0.83     78.27    434.73    -0.000  B  0
2.44    0.25    4.23    0.80     75.96    436.25    -0.000  B  0
2.46    0.24    4.10    0.78     73.65    437.72    -0.000  B  0
2.48    0.22    3.97    0.75     71.34    439.15    -0.000  B  0
2.50    0.21    3.84    0.73     69.02    440.53    -0.000  B  0
2.52    0.19    3.71    0.71     66.71    441.87    -0.000  B  0
2.54    0.18    3.58    0.68     64.39    443.15    -0.000  B  0
2.56    0.17    3.45    0.66     62.07    444.39    -0.000  B  0
2.58    0.15    3.33    0.63     59.75    445.59    -0.000  B  0
2.60    0.14    3.20    0.61     57.43    446.74    -0.000  B  0
2.62    0.13    3.07    0.58     55.11    447.84    -0.000  B  0
2.64    0.12    2.94    0.56     52.78    448.90    -0.000  B  0
2.66    0.11    2.81    0.53     50.45    449.91    -0.000  B  0
2.68    0.10    2.68    0.51     48.12    450.87    -0.000  B  0
2.70    0.09    2.55    0.48     45.79    451.78    -0.000  B  0
2.72    0.08    2.42    0.46     43.45    452.65    -0.000  B  0
2.74    0.07    2.29    0.43     41.11    453.47    -0.000  B  0
2.76    0.06
TIME=0002
?LIST DOOR PARAM

85.00

H=4.864                         REAL HEIGHT (FT)
LD=4.8                          DOOR LENGHT (FT)
WD=1.317                        DOOR WIDTH (FT)
LT=4.8                          LENGHT FLUID TOP (FT)
WT=2.634                        WIDTH FLUID TOP (FT)
DV=1.354                        EQUIVALENT VENT DIA. (FT)
LV=0.500                        LENGTH OF VENT (FT)
RHO=2.072                       RETARDANT DENSITY (PSF/FT)
K=0.0019275
G=32.2                          GRAVITY CONSTANT (FT/SEC**2)
HT=5.17                         TANK HEIGHT (FT)


?OFF
OFF AT 15:08  05/23/77
COMPUTE SEC. - 26.2
CONNECT MIN. - 09
```

Figure 36. Simulation Printout for Figure 35 (2 of 2)

It was noted that pressures predicted with the best-fit simulation did not achieve actual pressures. Even so, the best-fit performance was obtained using Equation (6). To match actual pressures, it was necessary to raise the value of K_2 to 0.00460. In this case however, the flow rate departs from the actual.

It was concluded that the influence of the Bernoulli equations on predictive flow are generally unfavorable, but no simple alternative can be proposed to accommodate the restricted tank. From the standpoint of simulation, PATSIM is adequate for most applications. The separate flow-rate program is potentially useful for tank design.

SECTION IV
FLIGHT TEST PLAN

The ETAGS test series consisted of 245 instrumented drops, exploring a wide variety of tank parameters and drop conditions using both water and a gum-thickened retardant (Phos-Chek XA*). More limited experiments were also conducted with different retardant characteristics. For each drop, both tank performance and ground data were collected, yielding a large amount of data. The basic test plan was conducted on a set of eight matrices as follows:

- Matrix 1: Flow Rate Study -- 460 gallons were dropped at eight different flow rates through changes in door rate and open area. The series was replicated at 150- and 300-foot nominal drop heights with both Phos-Chek* and water. Aircraft velocity was held at a nominal 125 knots.

- Matrix 2: Configuration Study -- 460 gallons were dropped with three different bulk geometries at three aircraft velocities; 100, 125 and 160 knots. The series was replicated at 150- and 300-foot nominal drop heights with both Phos-Check and water. Flow rate was held constant.

- Matrix 3: 920-Gallon Load Studies -- 920 gallons were dropped primarily from 300 feet to explore flow rate (controlled by door rate), two bulk geometries, and two cases of tank separation. The series replicated aspects of Matrix 1 and 2 with a larger quantity with both Phos-Chek and water. Velocity was held at a nomonal 125 knots.

- Matrix 4: Head-Height Studies -- 460 gallons were dropped with the head height reduced to 2/3, 1/2, and 1/4 of the nominally full head in five bulk geometry configurations at 150- and 300-foot drop heights, Phos-Chek and water, with velocity held at a nominal 125 knots.

- Matrix 5: Load Size Studies -- Supplemented baseline data on 460 and 920 gallons by exploring loads ranging from 230 to 1840 gallons at 150 and 300 feet for water and Phos-Chek, with the nominal 125-knot aircraft velocity.

---

*Phos-Chek XA and Phos-Chek are registered trademarks of the Monsanto Co.

- Matrix 6: Aircraft Velocity Studies -- A selected set of 460-gallon drops repeated at aircraft velocities ranging from a nominal 100 to 180 knots, for both Phos-Chek and water at 150- and 300-foot nominal altitudes, to provide performance data throughout the velocity range.

- Matrix 7: Door Opening Studies -- 460 gallons were dropped in two bulk configurations at a nominal 125 knots for each of two drop heights (150 and 300 feet) to expand data on the control of pattern by varying door opening rate.

- Matrix 8: Retardant Rheological Studies -- A selected set of 460-gallon drops from 300 feet drop height were repeated at aircraft velocities of 125 and 180 knots to evaluate retardant rheological properties. Flow rates were held constant. This matrix was conducted primarily for use in separate rheology studies and is not discussed in detail in this report, although data from the drops were used when they helped shed light on other phenomena.

The tank was designed to implement these experiments as shown in Figure 37. Flight-related variables included drop speed and altitude.

The original set of interlocking matrices was designed to yield multiple performance data using the previously developed PATSIM simulation, operating from recorded flow data and delivery characteristics to generate expected values. This approach did not yield adequate resolution to carry through on the analysis. As a result, the analysis strategy was changed to follow the approach outlined in Figure 38. Sections V through VIII discuss this analysis effort in some detail.

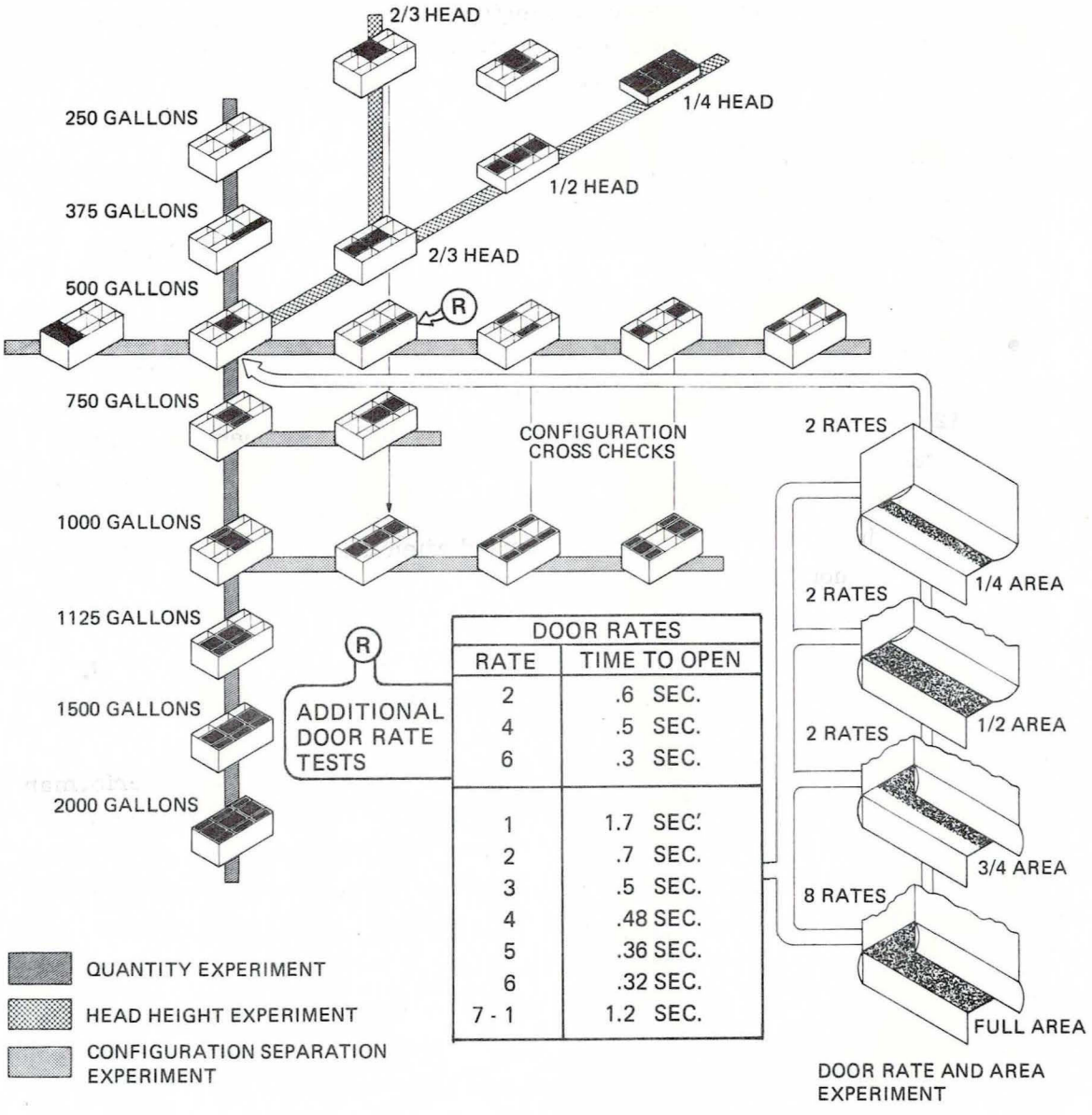

Figure 37. ETAGS Tank in Test Data Matrix

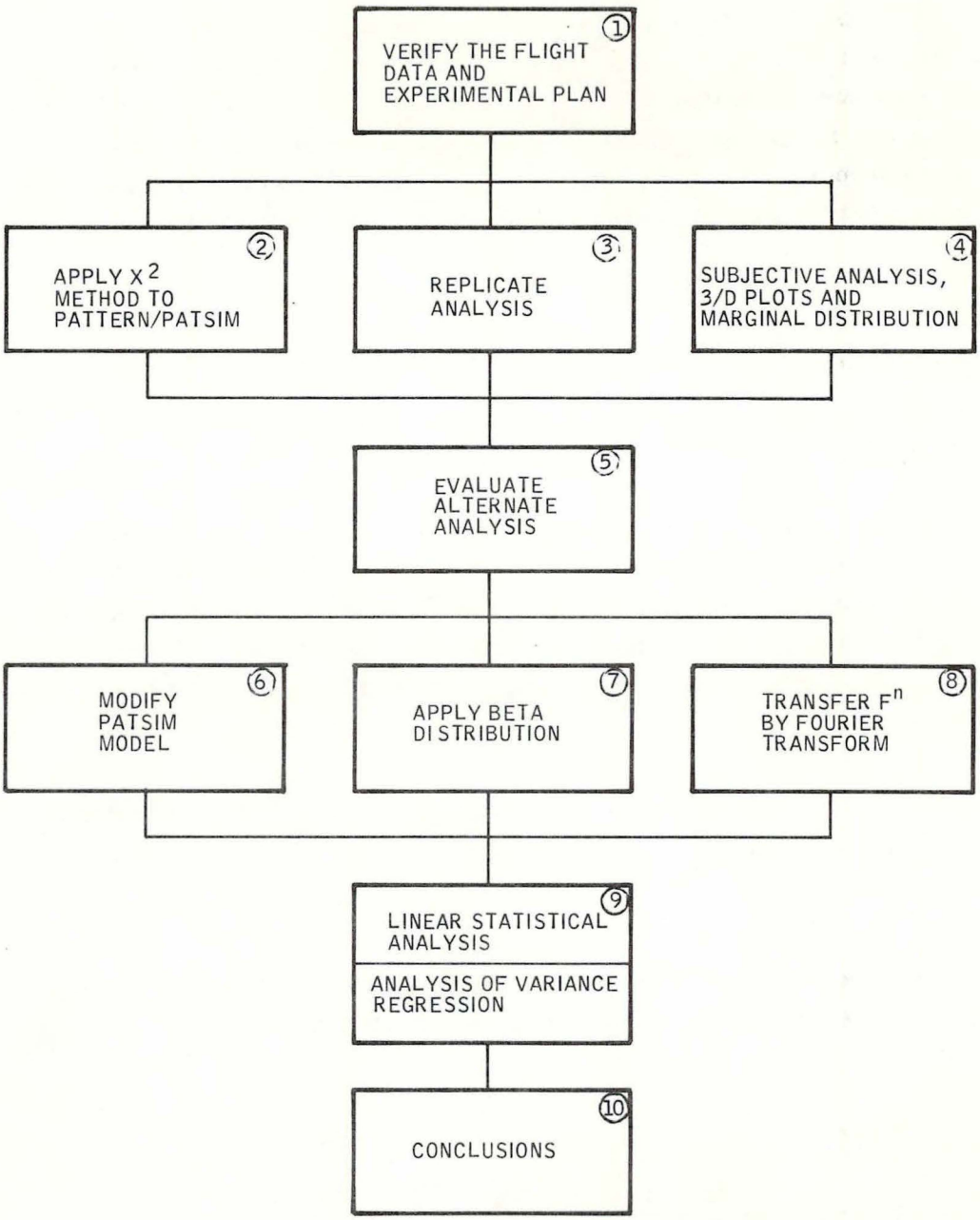

Figure 38. Data Analysis Elements

SECTION V
VERIFICATION OF FLIGHT DATA

The 245 drops were planned to provide nominal drop conditions within a predesigned test matrix. Prior to analysis, the planned conditions were compared with actual test conditions as verified by camera coverage and recorded data. As a result, it was verified that only a few drops departed significantly from the intended drop matrix. This subsection discusses the actual and planned conditions of controlled variables in the experiment. The drop record appears in Appendix C.

DROP CONDITIONS

Drop Heights

Aircraft drop heights were generally targeted for 150 feet or 300 feet in the total test series. They were controlled initially be an Inflight System Radar Altimeter, which performed erratically. Later a Honeywell Radar Altimeter was installed. Actual heights were provided by the Forest Service from analysis of the drop films. Examination of these data showed reasonably good conformance to plan as follows:

Nominal (ft)	Mean (ft)	Standard Deviation (ft)
150	149.8	19.7
300	318.6	30.3

Two drops were not within the "as planned" constraints. Drop 20 was at 288.7 feet, and Drop 120 was at 163.6 feet instead of 300 feet.

Aircraft Velocity

Aircraft velocities were targeted variously at 100 knots, 125 knots, 160 knots and 180 knots. Velocity was controlled by the pilot through his airspeed indicator, and actual ground speed was determined by Forest Service film analysis. Difficulty in attaining the desired aircraft speed was encountered only when there were significant winds and the airspeed did not approximate ground speed. In general, drops

under wind conditions were avoided except in terms of a duplicate matrix flown with a significant wind to contribute insight to performance under less than ideal conditions. Some other drops were wind influenced due to changing conditions. * They were generally repeated in more favorable weather. Despite this factor, velocities were held very close to the nominal values:

Ground Speed (kt)	Nominal Mean (kt)	Standard Deviation (kt)
100	103	9.95
125	123.65	7.68
160	156.6	4.85

Only five drops were not at the planned conditions:

Drops 57 through 59 were closer to 100 knots than the 125-knot target. Drop 198 was substantially lower than 125 knots at 81.9 knots. Drop 238 was at 107.7 knots rather than 125 knots. All were under high wind conditions (above 16.5 mph).

TANK PERFORMANCE

For most drops tank data were recorded on 14-track analog data tape. General performance of the system was confirmed after each drop by reading the tape on the tracing recorder. The data were subsequently digitized at Honeywell, and a complete set of plot data was furnished to the Forest Service. The tank was instrumented to provide the following information:

- Door rate on each of the four doors
- Top tank pressure on each compartment
- Fluid level (by means of floats) in each compartment (two in tank 5)
- Acceleration of the aircraft during the drop was also recorded; but vibration through the mount exceeded any signal that might have been obtained.

---

*Wind speed and direction were monitored at a weather station adjacent to the test grid at the time of each drop.

Of the 245 drops, no data were taken on 32. These drops were configurations which had been measured repeatedly, and these configurations were selected for tests:

- When the tape recorder was down for a short period
- When float repair would have slowed the retardant composition tests
- In a final drop series when the tape was expended.

On an additional 21 drops, data were not recovered due to various causes, producing a 90% yield.

Door Performance

Door rate was used as the primary operating mechanism to control flow rate and was therefore critical to controlling tank performance. Performance, as summarized in Figures 39 through 42, was good, and highly repeatable, particularly at the higher rates. At slower rates, particularly Rate 1, there was considerable variation. The curves presented are valid to about 60 degrees. Above this value there are multiple solutions to the calibration curve relating torque tube travel (measured) to the door open angle. As a result, the door appears to open only to 80 degrees, whereas actual values were close to 90 degrees. The particular calibration/measurement scheme yields somewhat better accuracy in the lower angles (thought to have a greater influence on flow) due to motion amplification through the torque tube linkage than more exposed pots operating on the door hinge itself.

Door 3 was designed to lag door 2 so that the overlapping sills could not collide. It performed like door 2 with a 6-degree lag, close to the value programmed in the opening mechanism.

Drops 148, 167, 183, 203, 223 produced rates that were not apparently as planned. Only Drop 148, however, showed an identifiable departure from the anticipated flow rate.

DOOR 1 WAS USED IN 57 DROPS, YIELDING DATA ON 46 DROPS (80%). RATES WERE DISTRIBUTED AS FOLLOWS:

	TOTAL	DATA	TIME TO 60° (SEC)	COMMENTS
RATE 2	53	41	0.52 - 0.68	4 classes, see notes
RATE 6	4	4	0.3	Traces identical

DOOR 1 NOTES: PERFORMANCE SPLITS INTO FOUR CLASSES AS SHOWN. THERE IS NO EVIDENCE OF PARAMETRIC DIFFERENCES IN THE FOUR-CLASS STRUCTURE. DROP 167 IS NOT SUPPOSED TO BE A DOOR 1.

RATE 2 24, 25, 29, 46*, 47, 50, 51, 52*, 53, 54, 59, 62, 65*, 66, 67, 68, 72, 73*, 74, 75, 79, 80, 81, 84, 90, 91, 92*, 94, 95*, 96, 102, 103, 104, 111*, 167, 176, 179, 185, 192*, 196, 199*, 201*, 202*, 204*, 205, 206, 207, 209, 212, 215, 220, 223, 224

* = NO DATA WERE OBTAINED

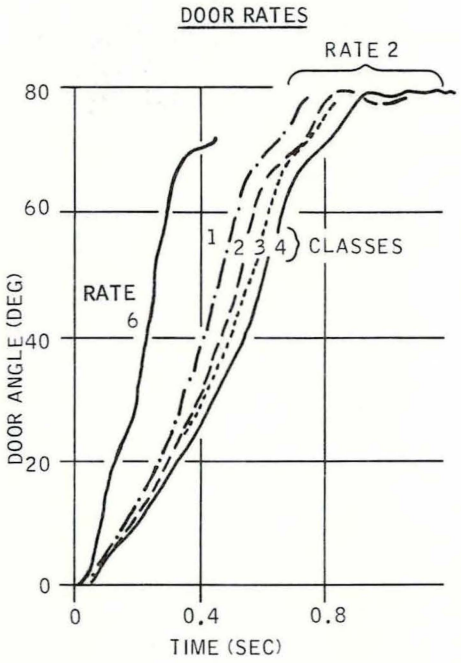

CLASS 1 (0.52 SEC) 62, 185)
CLASS 2 (0.56 SEC) 25, 47, 51, 53, 72, 79, 80 81, 91, 96, 179, 205, 206, 209, 212, 220
CLASS 3 (0.62 SEC) 24, 54, 59, 74, 75, 90, 103, 102 (167?)
CLASS 4 (0.68 SEC) 29, 50, 66, 67, 68, 84, 94, 104, 196, 215, 223, 224

Figure 39. Door 1 Performance Summary

DOOR 2 WAS USED IN 177 DROPS YIELDING DATA ON 128 DROPS (72%).
RATES WERE DISTRIBUTED AMONG THE FOLLOWING:

	TOTAL	DATA	TIME TO 60° (SEC)	COMMENTS
RATE 1	8	5	1.6 - 1.8	Considerably variable
RATE 2	25	19	7.2 - 7.7	Minor variations
RATE 3	3	3	0.5	Traces identical
RATE 4	6	4	0.48	Traces identical
RATE 5	1	1	0.36	
RATE 6	127	91	0.32	Consistent
RATE 6-1	1	1	0.32	
RATE 7-1	6	4	0.24 - 0.32	

RATE 1 137*, 139, 140, 142, 173*, 190, 222, 236*

RATE 2 5, 6, 7, 9*, 12, 13*, 14, 15*, 19, 28, 31, 33, 34, 35, 36, 41, 43*, 45, 147, 151, 152, 181, 219, 225*, 237*

RATE 3 141, 153, 180

RATE 4 145, 150, 174*, 178, 193, 195*

RATE 5 20

RATE 6 1, 2, 3*, 4, 8, 11*, 16, 17, 18, 22, 24, 25, 27, 29, 30, 32, 37, 38, 39, 40, 42, 44, 48, 49*, 57, 58, 63*, 64, 65*, 66, 67, 68, 69, 70, 82, 83, 85, 86, 87, 88, 89, 90, 91, 92*, 94, 95*, 97, 98, 109*, 110*, 112*, 118, 119, 120, 121*, 122, 124, 128, 131, 134*, 135, 138, 143, 148, 154, 155, 156, 157, 158*, 159*, 160*, 161*, 162*, 163, 164, 165*, 166, 167*, 168, 169, 175, 176, 177, 179, 183, 184, 185, 186, 187, 188, 189, 192*, 196, 197*, 199*, 200*, 201*, 202*, 203, 204*, 205, 206, 207, 208*, 209, 210, 211, 212, 213, 214, 215, 216, 217, 218, 223, 224*, 233, 234, 235*, 238, 239*, 240*, 241*, 242*, 243*, 244*, 245*

RATE 6-1 198

RATE 7-1 144, 182, 227*, 228*, 230, 231

* = NO DATA
XXX = DISCREPANT PERFORMANCE

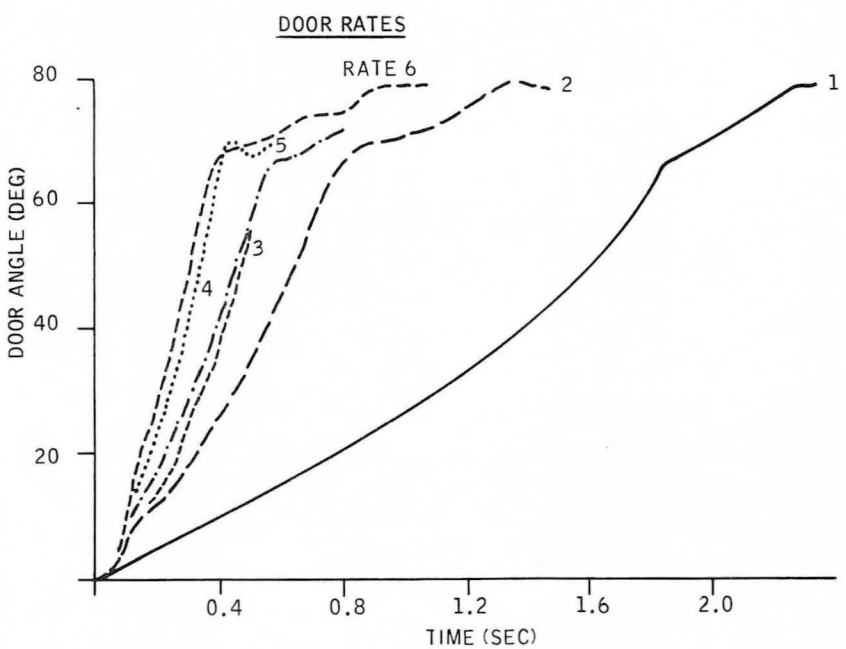

Figure 40. Door 2 Performance Summary

DOOR 3 WAS USED IN 159 DROPS YIELDING DATA ON 115 DROPS (72%).
RATES WERE DISTRIBUTED AS FOLLOWS:

	TOTAL	DATA	TIME TO 60° (SEC)	COMMENTS	OPENING DELAY (SEC)
RATE 1	7	6	2.0 - 2.28	Drop 222 short of range	0.56
RATE 2	16	10	0.94 - 0.98	In two groups	0.16
RATE 3	4	3	0.72	Traces identical	0.14
RATE 4	6	5	0.52	Traces identical	0.12
RATE 6	119	86	0.34	Traces identical	0.08
RATE 6-1	1	1	0.40	Essentially a slow Rate 6	0.12 0.12
RATE 7-1	6	4	1.2 - 1.7	230, 231 valid	0.14

RATE 1 139, 140, 142, 173, 190, 222, 236*

RATE 2 5, 9*, 13*, 14, 15*, 34*, 36, 41, 45, 147, 151, 152, 181, 219, 225*, 237*

RATE 3 137*, 141, 153, 180

RATE 4 145, 150, 174, 178, 193, 195*

RATE 6 1, 2, 3*, 4, 16, 18, 22, 24, 25, 29, 38, 39, 40, 44, 48, 49*, 57, 58, 63, 64, 65*, 66, 67, 68, 69, 70, 82, 83, 85, 86, 87, 88, 89, 90, 91, 92*, 94, 95*, 97, 98, 109*, 110*, 112*, 118, 119, 120, 121*, 122, 124, 128, 131, 134*, 164,*, 165*, 166, 167, 168, 169, 175, 176, 177, 179, 183, 184, 185, 186, 187, 188, 189, 192*, 196, 197*, 199*, 200*, 201*, 202*, 203, 204*, 205, 206, 207, 208*, 209, 210, 211, 212, 213, 214, 215, 216, 217, 218, 223, 224, 233, 234, 235*, 238, 239*, 240*, 241*, 242*, 243, 244*, 245*

RATE 6-1 198

RATE 7-1 144, 182, 227*, 228*, 230, 231

* NO DATA OBTAINED

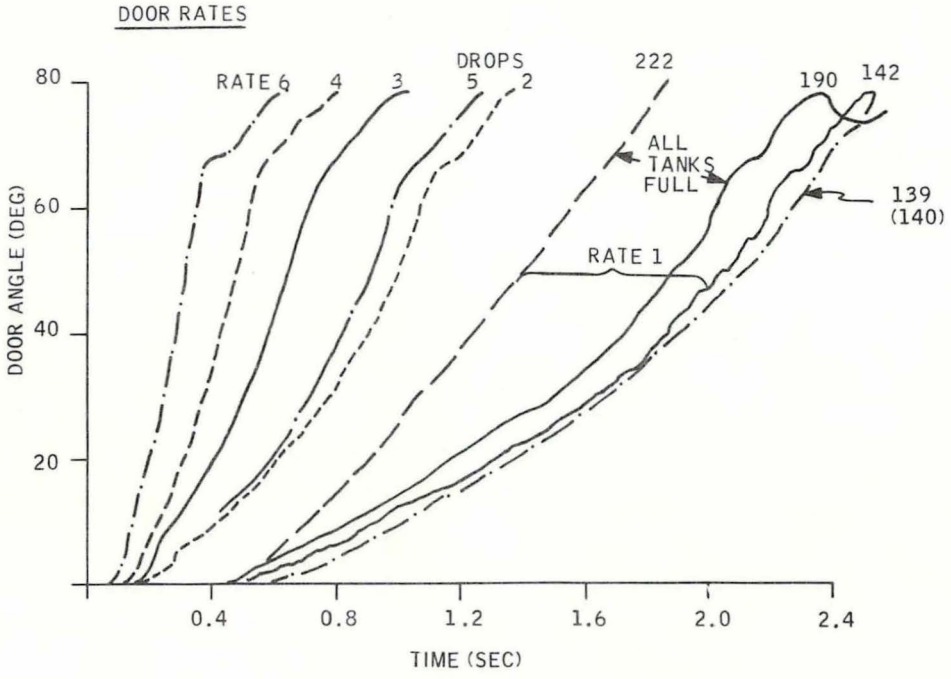

Figure 41. Door 3 Performance Summary

DOOR 4 WAS USED IN 99 DROPS YIELDING DATA ON 76 DROPS (76%)
RATES WERE DISTRIBUTED AS FOLLOWS:

	TOTAL	DATA	TIME TO 60° (SEC)	COMMENTS
RATE 2	86	64	0.62 - 0.72	3 classes, see notes
RATE 4	4	2	0.47	Traces identical
RATE 6	9	9	0.30 - 0.32	Minor difference in two drops

RATE 2 10, 21, 23, 24, 25, 26, 29, 46*, 47, 50, 51, 52, 53, 54, 55, 56, 59, 60, 61*, 62, 65*, 66, 67, 68, 71, 72, 73*, 74, 75, 76, 77, 78, 79, 80, 81, 84, 90, 91, 92*, 93, 94, 95*, 96, 99*, 100, 101, 102, 103, 104, 105*, 106*, 107*, 108*, 111*, 113*, 114, 115, 116, 117, 123, 125, 126, 133*, 149, 167*, 170*, 176*, 179, 184, 185, 189, 192*, 196, 199*, 201*, 202*, 206*, 207*, 209, 212, 213, 218, 220, 223, 224, 229.

RATE 4 136*, 146*, 171, 172

RATE 6 127, 129, 130, 132, 191, 194, 221, 226, 232

* NO DATA OBTAINED

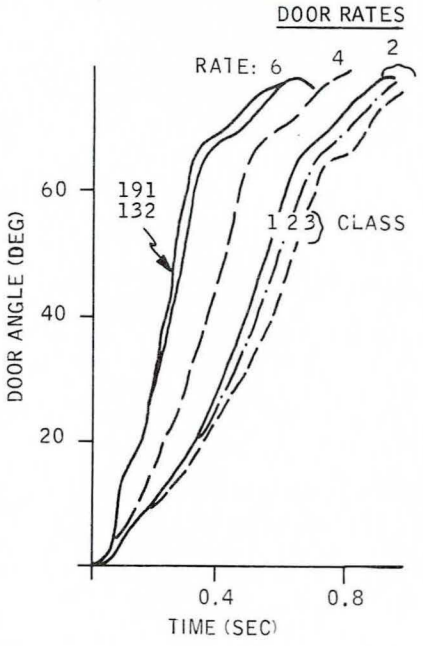

CLASS 1 (0.62 SEC) 23, 24, 25, 26, 47, 53, 54, 55, 56, 59, 60, 62, 67, 71, 72, 74, 75, 76, 77, 78, 79, 80 81, 90, 91, 96, 100, 101, 102, 103, 104, 123, 125, 126, 149, 179, 185, 189, 209, 212, 218, 220, 229, 170

CLASS 2 (0.67 SEC) 10, 21, 51, 66, 68, 84, 93, 94, 114, 115, 116, 117, 184, 196, 213, 223, 224

CLASS 3 (0.72 SEC) 29, 50

Figure 42. Door 4 Performance Summary

Flow Rate Measurement

Flow rate was computed from the fall of the top fluid surface as a function of time, as measured by a float system driving a linear potentiometer. The float was guided by a wire and connected to the potentiometer pulley so that is could respond to up and down changes in the fluid surface. This instrumentation proved difficult to maintain in the surge environment and the side loads after airstream exposure. Consequently, a number of discrete float data points were lost. Nonetheless, one or more valid float records were available to confirm general performance on 189 drops, or 88% of the drops for which data were taken. A full set of summary flow-rate data including plots of gallons versus time (distance), gallons per second versus time (velocity) and gallons per second^2 versus time (acceleration) was supplied to the Forest Service.

Flow rate was intially identified as the most significant variable in the control of the experiment, particularly since it was hypothesized that the frequency data in the pattern corresponded to similar frequency variations in the flow rate. During subsequent analysis, it was shown that the fine structure on the flow rate curve did not account for pattern performance, at least through the PATSIM Simulation, and there was little reason to assert that these variations were significant. They are probably more related to noise or surface perturbations around the float that are amplified by differentiation.

The contention was examined in some detail in Matrix 1 in part to check out the proposed method of analysis. Figure 43 shows the flow rate and pressure traces for the 460-gallon central tank (5) with a fast door, for both water and Phos-Chek. Both float and pressure curves exhibit similar frequency characteristics. They occur in about the same way in all cases. A look at the implied acceleration, however, shows values that are apparently unobtainable, ranging from +3g to minus 1g. The energy to achieve such accelerations of the liquid mass on any but a local basis is clearly unobtainable.

Figures 44 through 48 show typical flow rates from drops where the rate was controlled by combinations of open door area and door rate variations. Figure 44 compares the flow rate with the ground patterns. It thus illustrates the prior hypothesis that fine changes in flow rate might correlate directly with the resulting fluctuations in the pattern, since these, too, would be amplified presumably by the aerodynamic breakup process. Attempts to find a direct correlation were not rewarding. Figures 47 and 48 show in cross section the pattern fluctuations for direct comparison with flow rate fluctuations. They show both the "apparent"

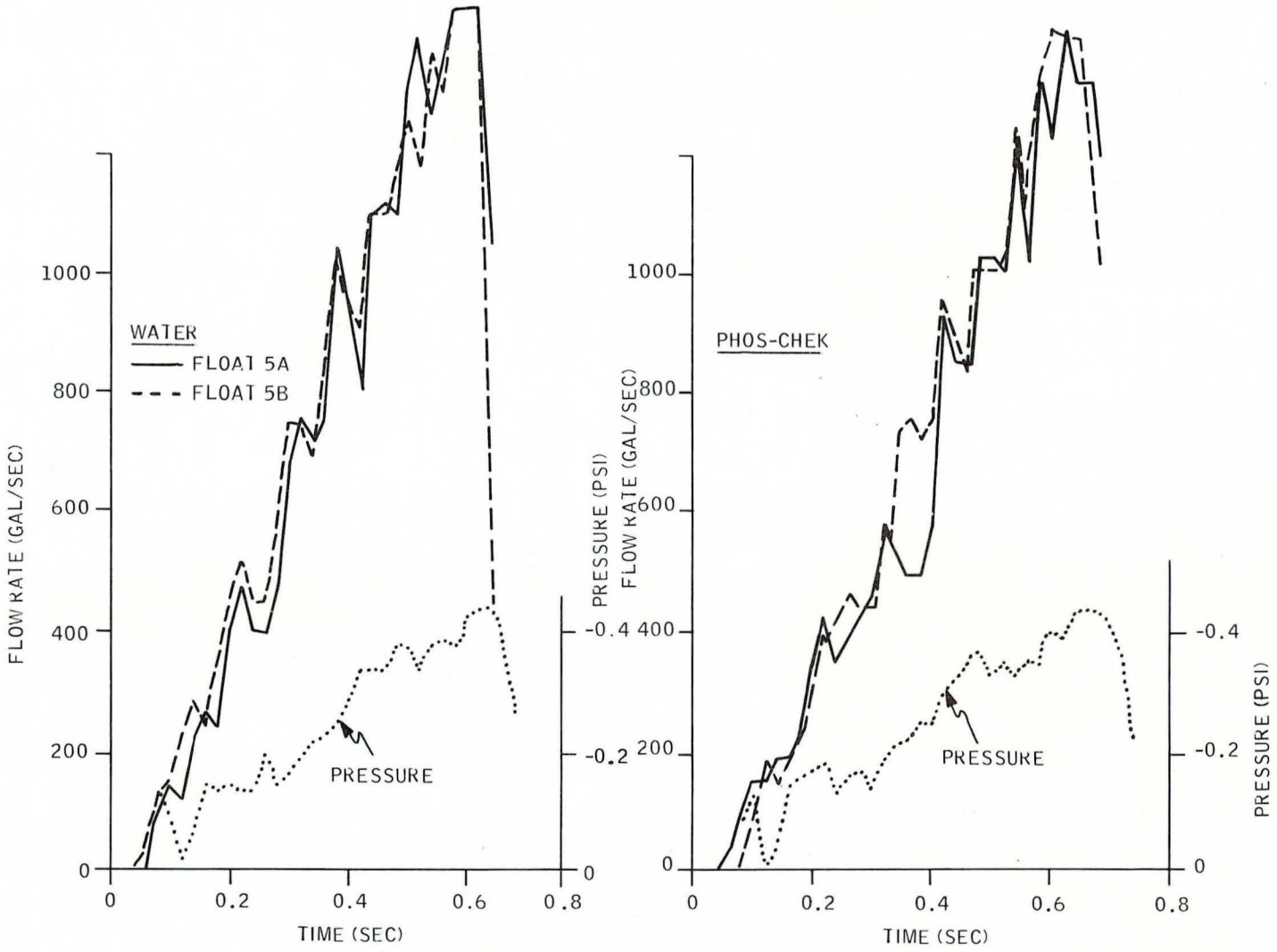

Figure 43. Flow Rates and Pressures for Full-Door Drop, Tank 5, Rate 6

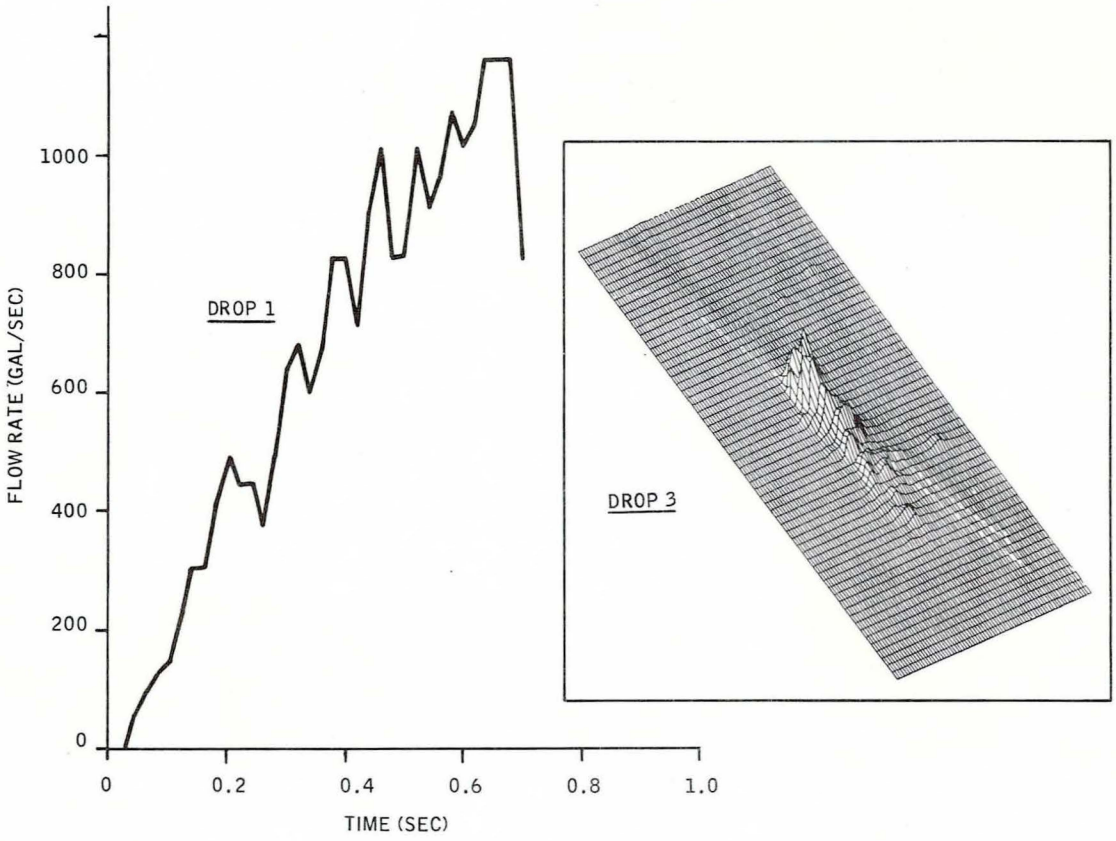

Figure 44. Flow Rate and Three-Dimensional Ground Pattern for 3/4-Door Drop, Rate 6

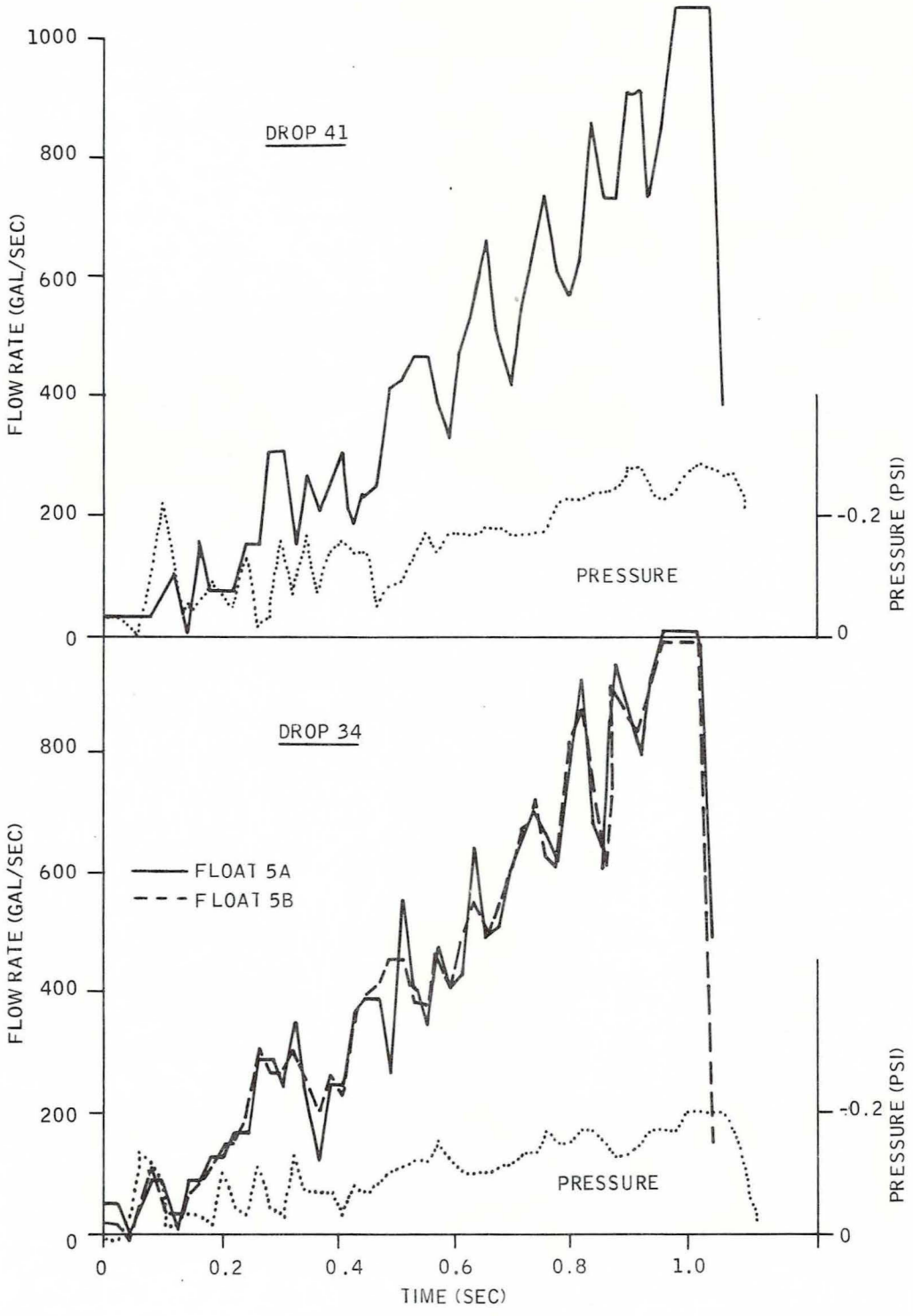

Figure 45. Flow Rates and Pressures for Full-Door Drops Tank 5, Rate 2

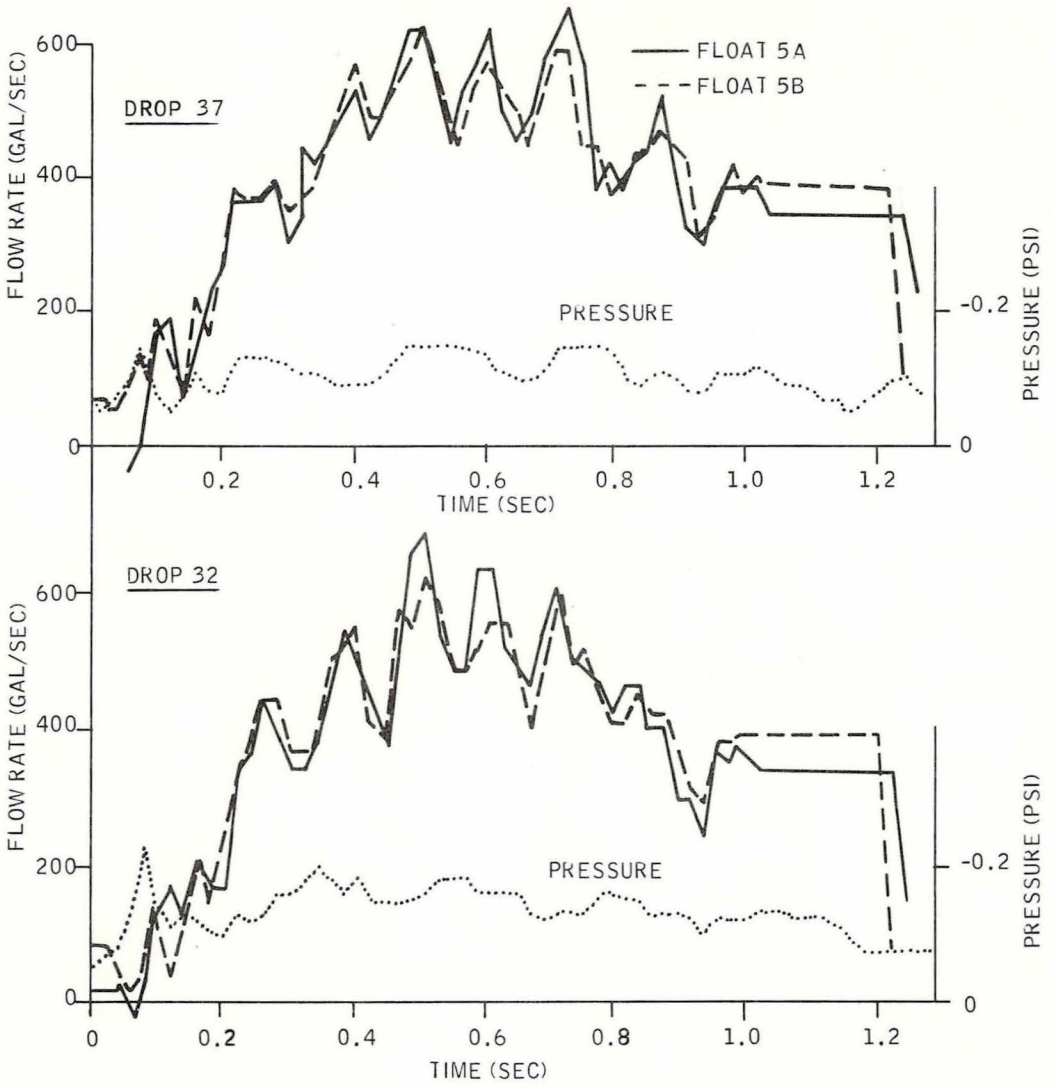

Figure 46. Flow Rates and Pressures for 1/2-Door Drops Tank 5, Rate 6

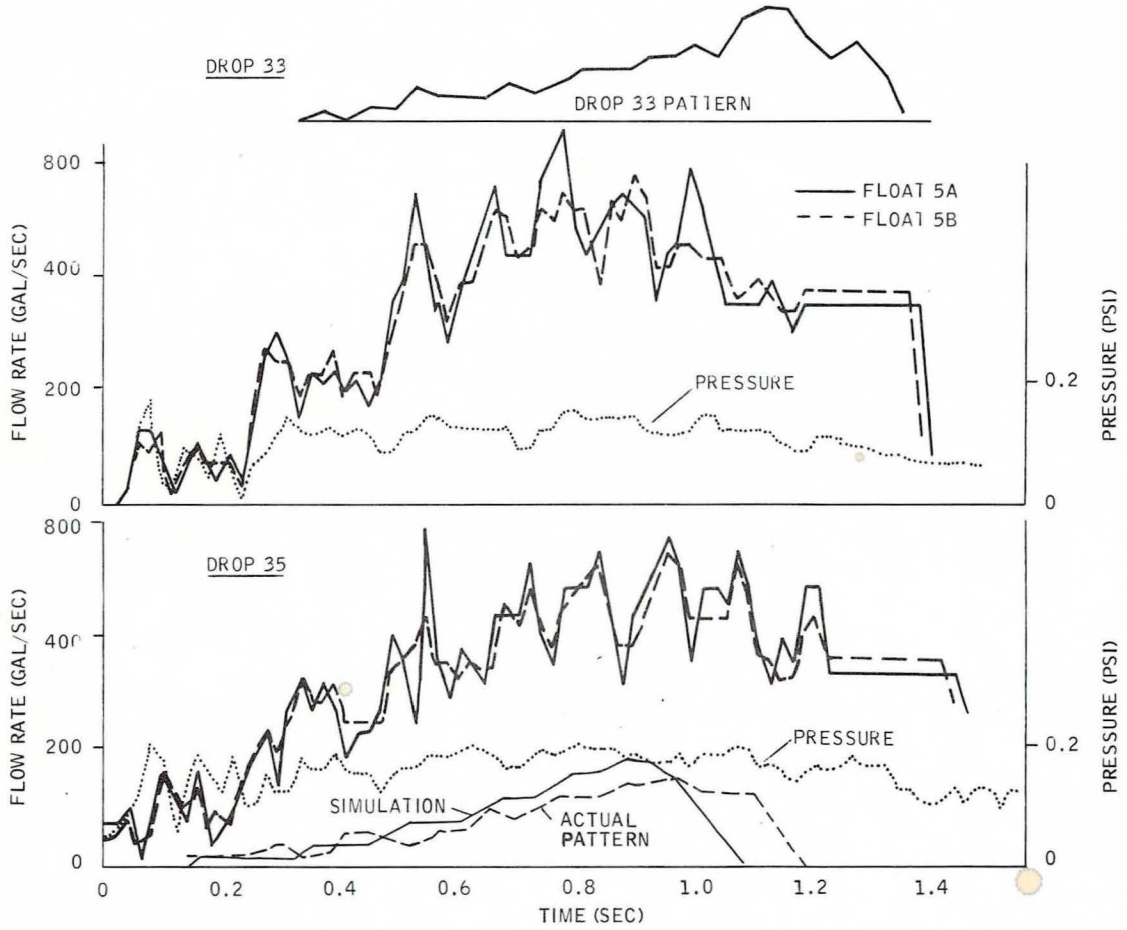

Figure 47. Flow Rates, Pressures and Ground Pattern Cross Section for 1/2-Door Drops, Rate 2

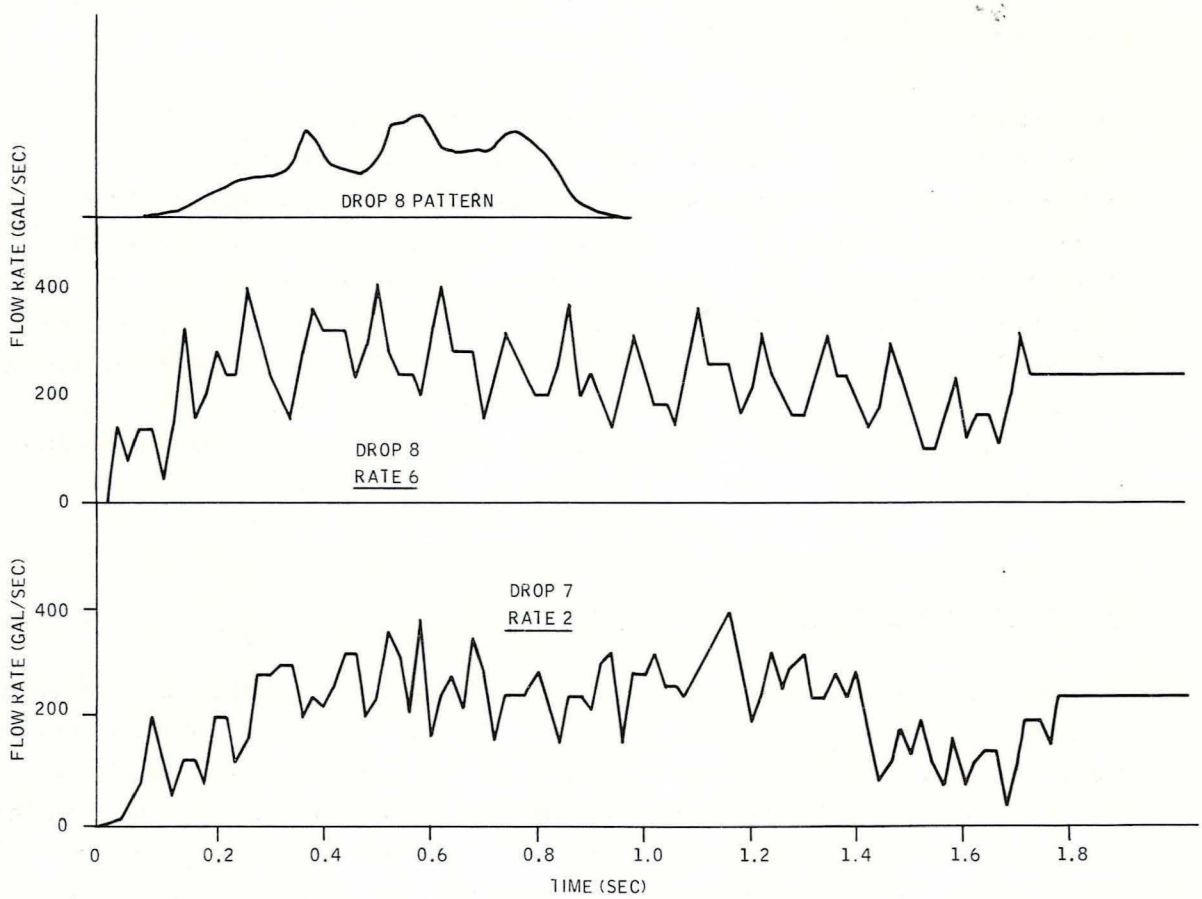

Figure 48. Flow Rates and Ground Pattern Cross Section for 1/4-Door Drops

similarity and striking differences. (Note particularly drop 8.) For drop 35, the simulation pattern from PATSIM driven directly from the actual flow rate is also shown. From this examination, it was tentatively concluded that the gross form of the flow rate was repeatable and that it does contribute to some degree to the pattern form. However, both the flow rate and the pattern exhibit noise characteristics in the fine structure that do not correlate with each other. (This contention was confirmed by Fourier analysis in later stages of the analysis.)

Significantly, examination of the full range of flow rates, both in multiple-float drops and in cross comparisons, revealed that there was remarkable repeatability and that they could be treated as a controlled constant throughout most of the analysis. The planned flow rates achieved the times out of the tank shown in Table 2. These times were reasonably constant, except as noted, regardless of the number of compartments filled. Most of the variability within range can be attributed to the ambiguity in the start pulse; i. e., if the curves are shifted slightly to best alignment, their forms and timing are nearly identical. As in the case of door opening data, there is more variation in the slower flow-rate drops than the fast ones.

Matched Flow Rates from Configuration Drops

An area of concern in the experiment was the ability to deliver different configurations at approximately equivalent flow rates. Due to the necessity of programming the overlapping center doors with a short delay to prevent collisions, the best match for composite flow rates was obtained with a slow outer door (rate 2) and a fast (rate 6) setting on the central door system. It was agreed early in the program that only an approximate match was required, in that analytic techniques were capable of separating the flow rate differences from configurational differences. Results of this analysis confirm that small variations in flow rate are, in fact, less influential as pattern determinents than previously believed. Figure 49 shows typical differences between the flow rates generated by the door differences.

Table 2. Evacuation Time Summary

Drop Condition	Rate	Time Out of Tank (seconds)		Comments
		Average	Range	
Doors 1 and/or 4	2	0.780	0.70 → 0.82	
	6	0.635	0.60 → 0.66	
1/4 Door (Door 2)	2	2.24	2.22 → 2.26	
	6	2.10	2.04 → 2.16	
1/2 Door (Door 2)	2	1.43	1.40 → 1.44	
	6	1.21	1.19 → 1.24	
3/4 Door (2 and 3)	2	1.15	1.12 → 1.16	
	6	0.77	0.72 → 0.80	
Doors 2 and 3	1	1.89	1.62 → 2.1	Drop 190 abnormal, rest 1.75 → 2.01
	2	1.11	1.00 → 1.60	
	3	0.81	0.72 → 0.86	
	4	0.78	0.76 → 0.82	Drop 36 abnormal; rest 1.0 → 1.20
	6	0.69	0.60 → 0.74	
	7/1	1.04		Drop 137 abnormal; rest 0.84 → 0.86
Combined Doors 2 and 3	6	0.76	0.70 → 0.80	Note 0.70 was limited to tanks 3-6-9. All others ranged 0.76 → 0.80.
Doors 1 and 4	2			
2/3 Head, Doors 2 and 3 Combined		0.53	0.56 → 0.62	
		0.67	0.66 → 0.68	
1/2 Head, Doors 2 and 3 Combined		0.54		
		0.64		
1/2 Head, Combined		6.56	0.50 → 0.62	

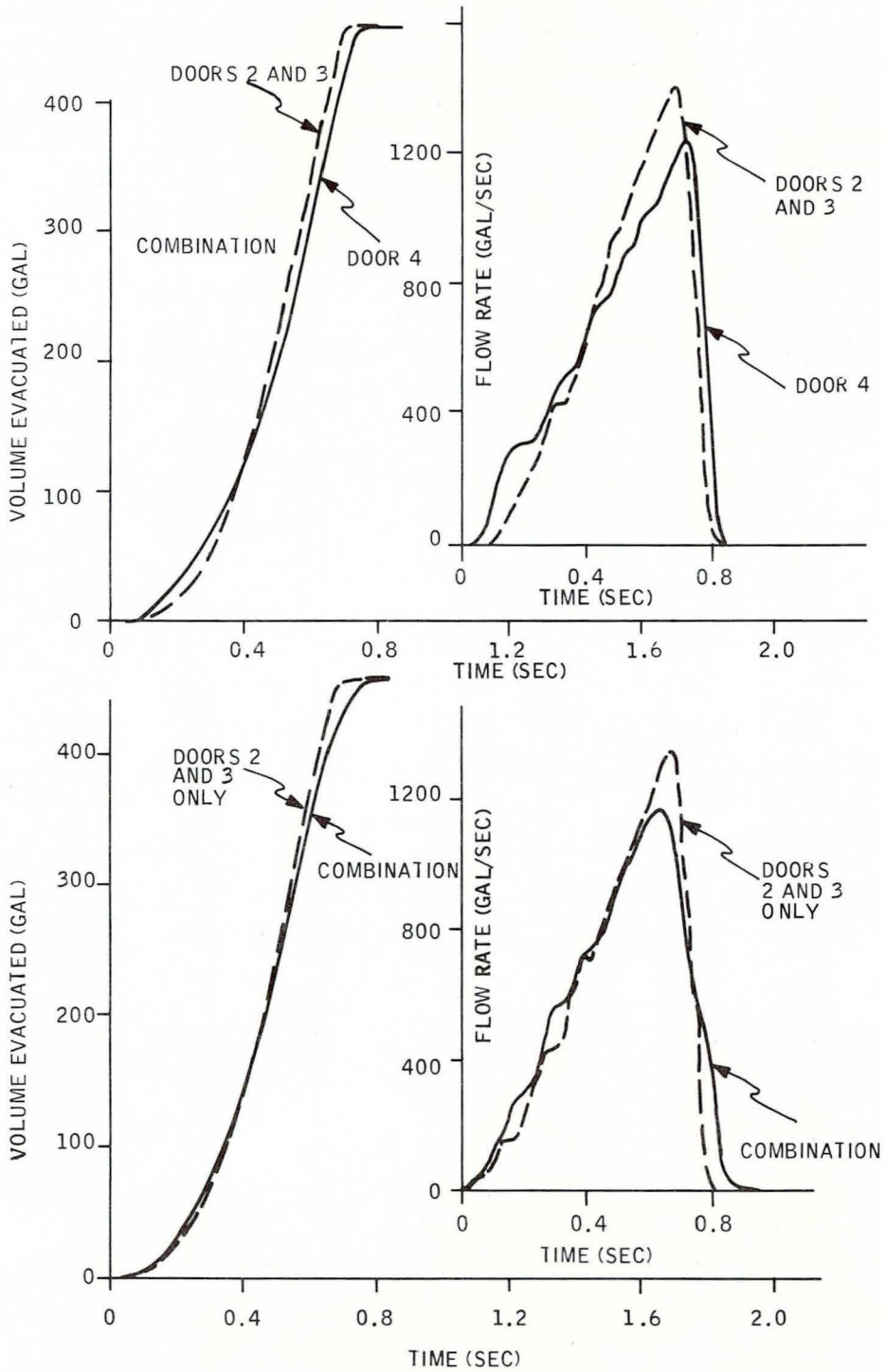

Figure 49. Combined and Single-Door Performance

SECTION VI
SELECTION OF ANALYSIS TECHNIQUES

The initial plan for data analysis was converted to computer programs prior to the test. This plan called for the use of the PATSIM program operating from measured flow rate data, with aircraft drop height and ground speed, to generate an expected value for the pattern distribution. The expected value apttern was then to be compared with the actual pattern generated by the Forest Service and "corrected" to align the data with the flight path used in the simulation system. The results yield multiparameter distributions of the difference between the predicted and real patterns. In essence, the difference data would represent a combination of:

(1) Parameters of significance not included in PATSIM, such as configuration, and

(2) An error term estimating the unaccounted phenomena present in the drop.

CHI-SQUARE ANALYSIS

Chi-square analysis is tranditionally employed to test whether observed frequencies differ significantly from expected frequencies. A measure of the discrepancy between observed and expected frequencies is given by the χ^2 statistic:

$$\chi^2 = \sum_{j=i}^{K} \frac{(\text{Observed}_j - \text{Expected}_j)^2}{\text{Expected}_j}$$

The sampling distribution of χ^2 is approximated closely by the chi-square distribution:

$$Y = Y_o X^{v-2} e^{-1/2 x^2}$$

where v = degrees of freedom

We will accept the hypothesis generating the expected value when the computed value of χ^2 is greater than some critical value such as $\chi^2_{.95}$. A side item of the test occurs when χ^2 is too close to zero (χ^2 less than $\chi^2_{.05}$ for instance). In this case the agreement is usually considered suspect since it is rare that observed frequencies agree this closely with predicted frequencies. In other words, we might suspect that the outcome is more determinate in nature than a frequency distribution, as originally assumed.

To apply this test in the data analysis, the PATSIM simulation is run with input conditions of the actual drop. One or more of the summary distributions are then generated to yield a set of expected values corresponding to, for example, the predicted density for each range cell in the pattern. This distribution is then aligned with the actual pattern distribution to yield the best fit χ^2 value. The value is accepted if it resides between the $\chi^2_{.95}$ criteria for rejection and the $\chi^2_{.05}$ value for extreme correspondence based on table values for the appropriate degrees of freedom. If, and only if, the values are accepted, they are then used as a scalar measure of the error between the simulation and pattern in a contingency table analysis of the specific test matrix. If they are rejected, we must find a similar accepted drop for use in the matrix analysis or disregard the cell in the contingency table.

This form of analysis was tested early in the program on a portion of Matrix 1 (door area and rate) as soon as data became available. The general analysis scheme of the matrix was to use a χ^2 technique to assess (1), the goodness of fit for each test distribution and (2) the effect of parameters. Table 3 shows the results of the matrix analysis.

The differences in the marginals as simulated from flow rate and the patterns in this matrix are not severe except in one high-altitude drop (37). This drop also appears out of form with respect to its low-altitude neighbor and with respect to the general set.

The analytic method requires first a check of the χ^2 value against table values for compliance for the appropriate degrees of freedom. For the values achieved in this matrix, it was possible to assert that the simulation and patterns were "good" fits. (In the total set of 16 patterns tested in this manner, only one fell out of the χ^2 range.)

Table 3. Range Marginal Distribution

Nominal Drop Height (ft)	1/2 Door				Full Door			
	Rate 2		Rate 6		Rate 2		Rate 6	
150	χ^2 = 22.51		12.7		15.89		5.33	
	Drop	Actual Alt.						
	33	157 (ft)	32	155 (ft)	41	139 (ft)	40	136 (ft)
300	χ^2 = 11.52		18.92		7.99		17.44	
	35	274 (ft)	37	272 (ft)	34	392 (ft)	38	353 (ft)

Best fit Difference between simulation and real pattern (less fringe)

$= \sum_s \frac{\chi^2}{}$ for (simulation - pattern) expressed as %

Indeterminate functions $\frac{\chi^2}{0}$ are arbitrarily set = $\frac{\chi^2}{1}$

The data showed generally adequate matches (no significant error), but analysis of effects using the method of Yeats showed mostly a very large noise content that may or may not be indigenous with the data set.

The Yeats method of evaluating the matrix is simply a mechanism for multiple linear regression. It yields coefficients for each parameter and its combinations. The coefficient associated with the final term combining all effects can be construed to represent the net variability. Significance of a parameter or cross effect is asserted only if the coefficient is considerably larger (by a factor of four or better) than the net variability depending on the confidence desired. In the test case, the combined error term was large (also in similar analysis of crossrange), and parametric coefficients were either less than or of about the same magnitude.

On the above basis it could be concluded either that (a) the PATSIM simulation contained no significant error with respect to the matrix variables or (b) the variability of the data with respect to the simulation was too great to allow

resolution of the test parameters. Subsequent analysis showed that both contentions were essentially true. The patterns predicted from real flow rate, though generally representative, did not exhibit the correspondence to the fine structure of the pattern that was expected. Secondly, as discussed later, examination of replicate drops that occurred (but were not planned) in the test showed considerable variability not attributable to the flow rate. Finally, tank configuration, a parameter not accounted for in the simulation, was recognized as having a significant effect on pattern formation. This combination of a known parametric deficiency in the simulation and variable performance of the actual pattern under identical situations precluded use of the simulation to generate an "expected value" adequate for χ^2 evaluation of the test matrixes. As a result, other techniques of analyzing the data were instituted as discussed in the following subsection.

ALTERNATIVE TECHNIQUES

Deficiencies in the planned method of analysis were a substantial setback to the data analysis tasks. Specifically, the difference data between an expected value, generated by the simulation, and a real pattern had provided a single metric for use in statistical analysis. It would have reduced the analysis problem from the complex evaluation and comparison of multidimensional distributions to a single net difference. Without this feature, the problem was considerably confounded. As a result, a number of recovery paths were evaluated:

- An analysis of replicate drops occurring by chance in the test matrix to determine the degree of correspondence that might be expected.
- Investigation of the Fourier transform as an alternative technique of generating expected values from flow rate for comparison with actual patterns.
- Exploration of the distributed form of the patterns to assess the most meaningful metrics for further analysis.
- Investigation of a quick fix to the PATSIM program to accommodate the configuration, thus preserving the initial data analysis scheme.

These studies are summarized in the following paragraphs.

Replicate Analysis

To examine the sources of variability, replicate pairs on altitude and velocity were examined. These pairs occurred by accident in the test plan and were sparse. Phos-Chek was selected because experience has suggested less variability than in water drops. The two replicate sets are shown with respect to their range distributions in Figures 50 and 51.

Most of the replicates were reasonably close in terms of the marginal distribution but not specifically in the fine structure, i.e., the ups and downs in the pattern. One drop of a triplicate pair, however, appears substantially different. No cause of the difference was found.

Two aspects of these paired drops are of significance: First, the frequency information, the ups and downs in the distributions, which we choose to call the fine structure, are substantially different between like drops, and they are not associated with variations in flow rate, even though the more general shapes of the patterns are similar and retain their flow rate identity. Second, drop 131 of the triplicate set is itself substantially different in the gross distribution from its replicates. Occurrences of these anomalous drops have been noted in prior tests at a frequency of about one in seven drops. Although not particularly significant in the field, in so far as occasional aberrant performance occurs, it contributes difficulties to data analysis.

The study was subsequently expanded to more thoroughly examine two sets of replicate drops in terms of drop conditions (Table 4) and pattern statistics (Table 5). Figures 52 and 53 show detailed pattern characteristics.

Parameters in Table 5 are values covered in other sections of the analysis, and they are to some extent related. Average coverage is the weighted average of concentration (gpc) divided by pattern area. It is similar to Eta in the Weibul-type distributions of a form indicated by Beta. Note that although drops 131 and 161 are the same in most parameters, they differ in the distributed form indicated by β, η, and the 90% length, a key parameter of the Beta distribution, which is discussed later.

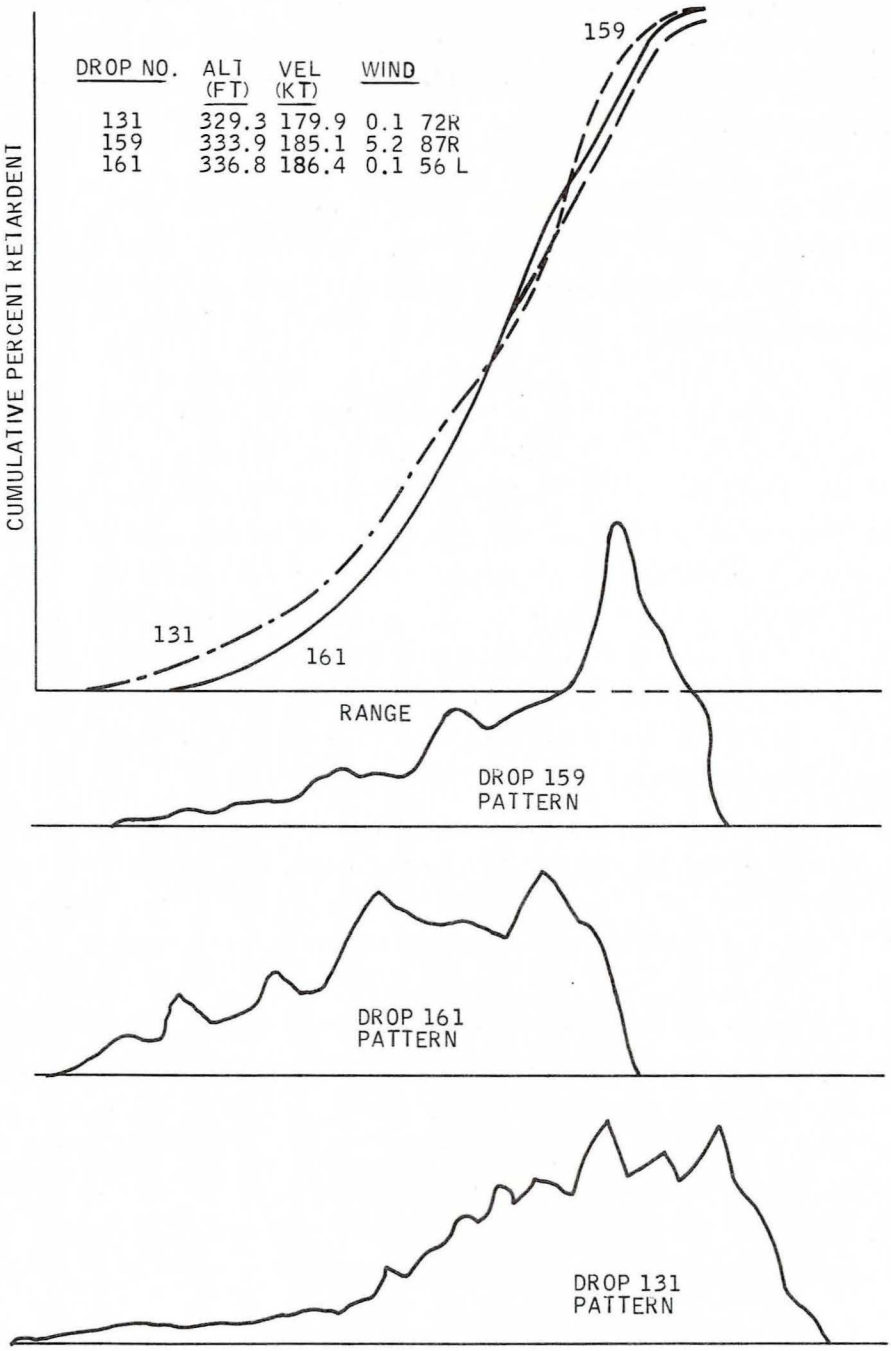

Figure 50. Comparison of Three Replicate Drops - Full-Door, Rate 6, Water

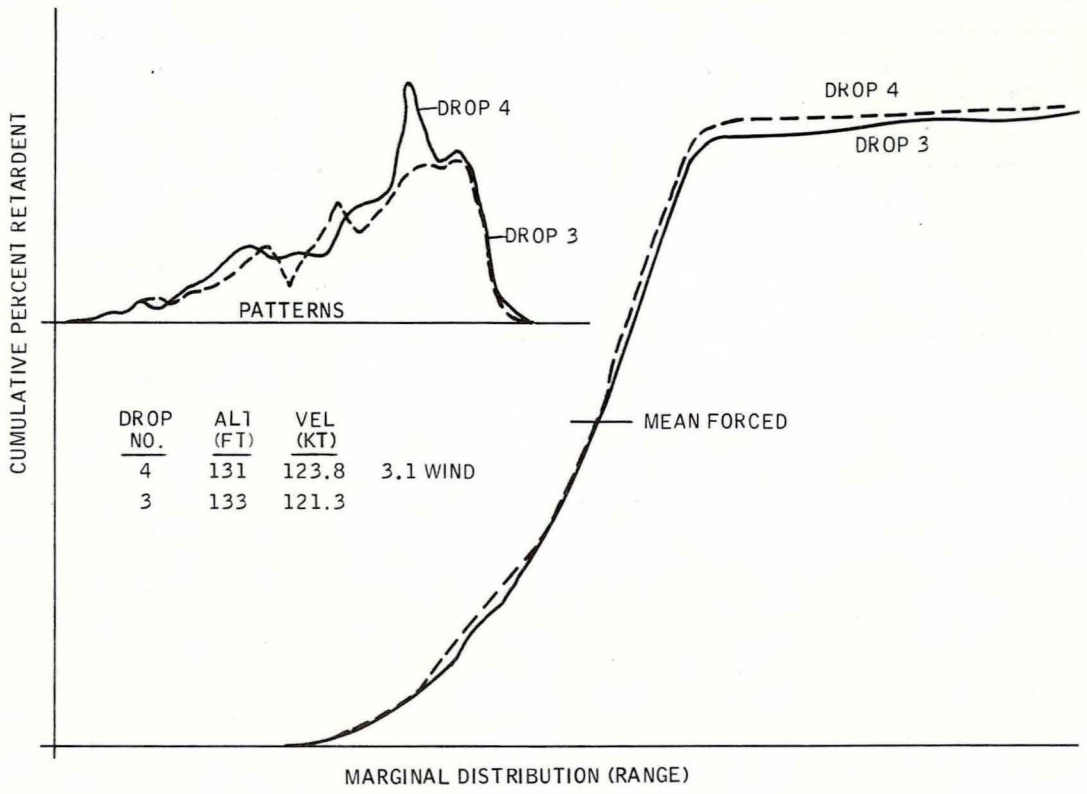

Figure 51. Comparison of Two Replicate Drops - 3/4-Door, Rate 6, Phos-Chek

Table 4. Replicate Drops (Center Tank)

Set	Drop Number	Drop Height (feet)	Velocity (knots)	Travel* Distance (ft)	Wind	
					Speed (mph)	Direction
Low-Speed	154	339	131	685	2.0	47R
	163	335	130	570	3.4	170R
High-Speed	131	329	180	580	.1	72R
	159	334	183	790	5.2	87R
	161	367	186	730	.1	56L

Table 5. Pattern Statistics

Set	Number	Average Coverage (gpc)	Weibul Parameters		90% Length (ft)	Pattern Area at 1 gpc (ft^2)	Crossrange (ft)
Low-Speed	154	1.739	1.29	1.50	351	15080	29.9
	163	1.332	1.80	1.03	406	15905	26.4
High-Speed	131	1.047	1.99	0.82	518	15560	39.4
	159	0.978	1.36	0.78	405	8200	57.9
	161	1.046	2.50	0.78	429	158700	34.5

Fourier Analysis

The Fourier Analysis was first applied to pattern analyses during the High-Altitude Retardant Delivery Program (Reference 1) in an attempt to determine if the pattern frequency data could be traced to perturbations in flow rate or to the instability modes in the break-up process. A further extension of this method of linear

*Travel distance was determined by the Forest Service from analysis of drop films. It is essentially the distance from point of release (indicated by a flash-bulb on the aircraft) to the end of the major concentrations in the ground pattern.

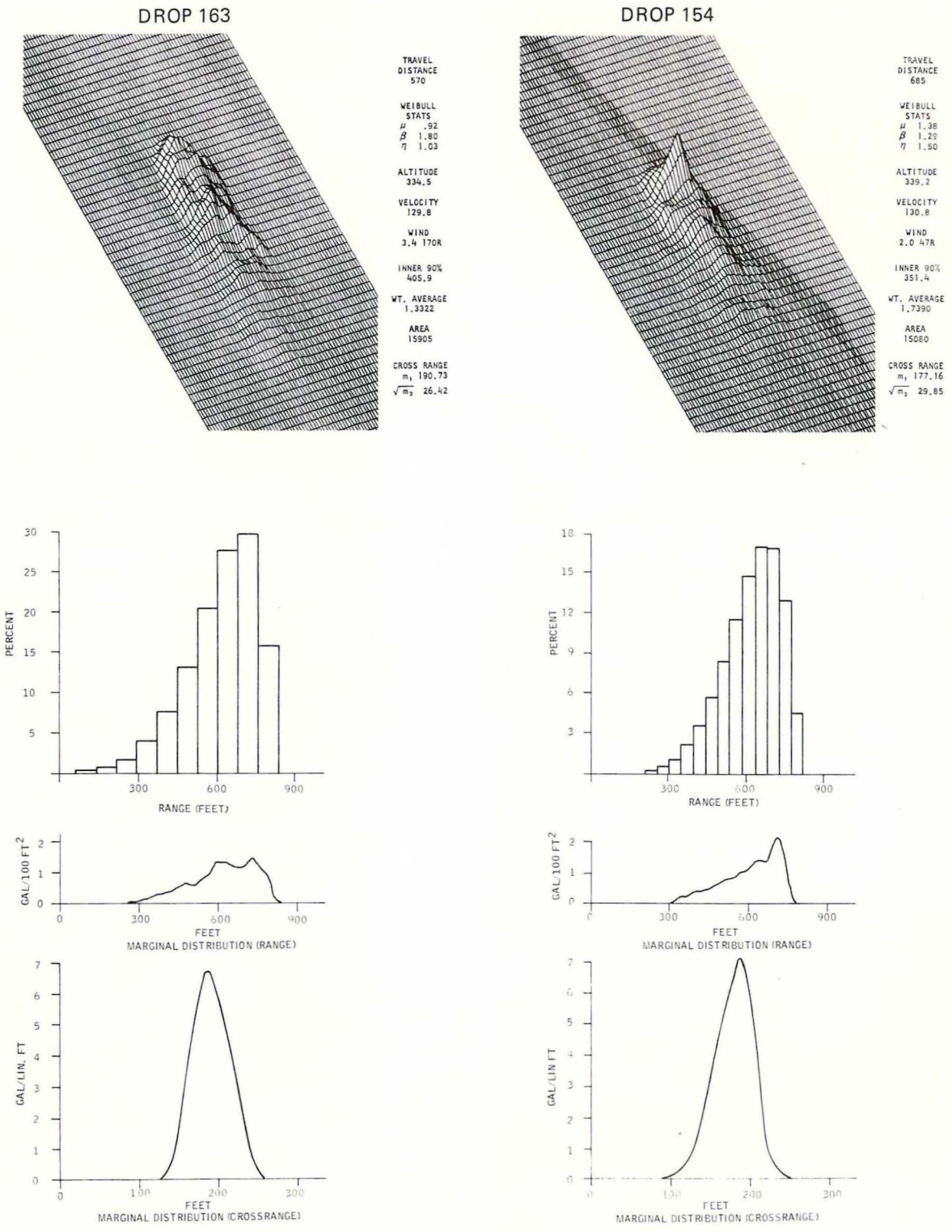

Figure 52. Replicate Analysis - Low-Speed Group

DROP 131

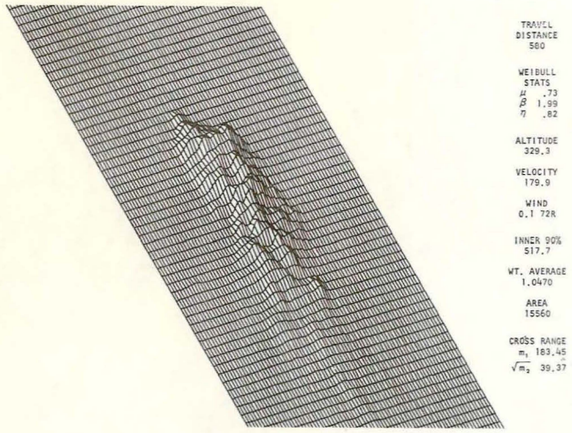

TRAVEL DISTANCE 580

WEIBULL STATS
μ .73
β 1.99
η .82

ALTITUDE 329.3

VELOCITY 179.9

WIND 0.1 72R

INNER 90% 517.7

WT. AVERAGE 1.0470

AREA 15560

CROSS RANGE
m_1 183.45
$\sqrt{m_2}$ 39.37

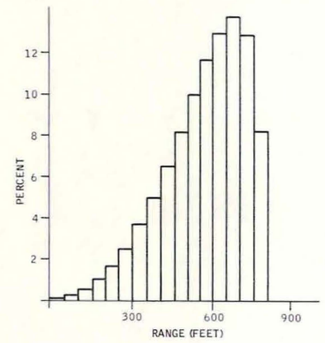

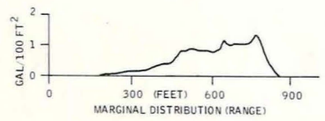

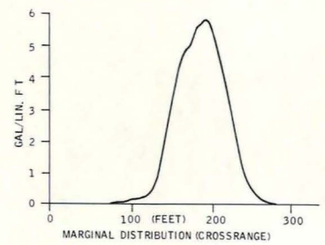

DROP 159

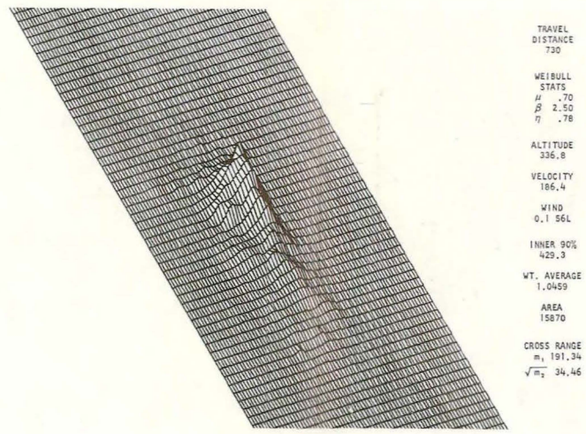

TRAVEL DISTANCE 730

WEIBULL STATS
μ .70
β 2.50
η .78

ALTITUDE 336.8

VELOCITY 186.4

WIND 0.1 56L

INNER 90% 429.3

WT. AVERAGE 1.0459

AREA 15870

CROSS RANGE
m_1 191.34
$\sqrt{m_2}$ 34.46

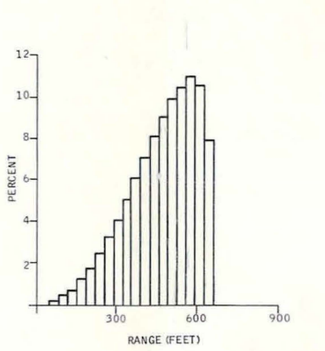

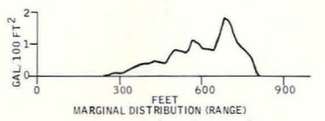

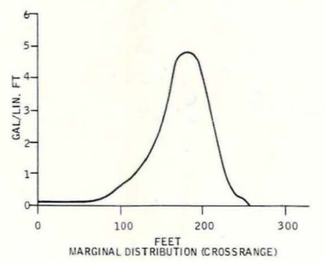

DROP 161

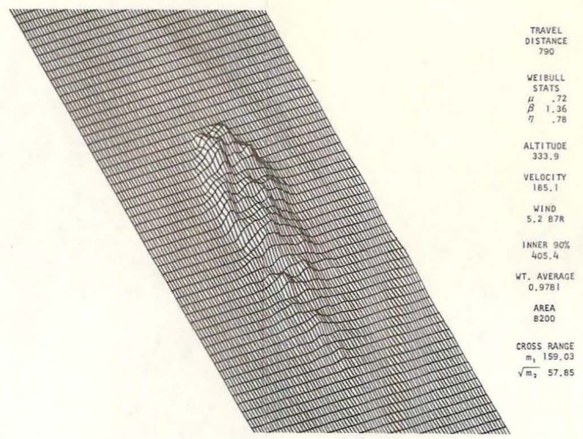

TRAVEL DISTANCE 790

WEIBULL STATS
μ .72
β 1.36
η .78

ALTITUDE 333.9

VELOCITY 185.1

WIND 5.2 87R

INNER 90% 405.4

WT. AVERAGE 0.9781

AREA 8200

CROSS RANGE
m_1 159.03
$\sqrt{m_2}$ 57.85

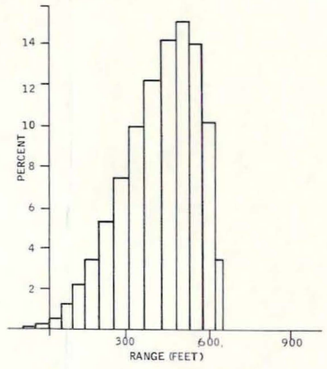

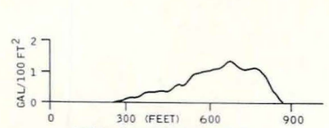

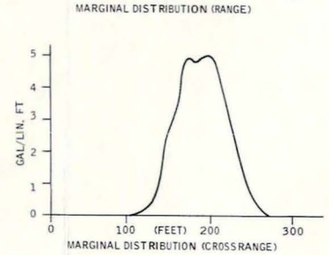

Figure 53. Replicate Analysis - High-Speed Group

analysis had long been hypothesized but not evaluated in terms of the simulation process. In this process, the transfer function between flow rate and pattern could be calculated and applied to generate a flow rate from ground pattern or a ground pattern from flow rate. This hypothesis appeared to offer an alternative technique of generating expected values as well as a method of exploring the differences in the transform caused by such parameters as configuration; i. e., parameters of the transform could serve as the metric for further analysis, thus lumping the process between retardant release and ground impact into a single abstract system.

Historically, all of the pattern simulations have been based on the numerical calculation of a convolution. This process involves the superposition of the response of small portions of the system input. For the pattern model, the flow out of the tank is input signal, and this is broken up into small discrete quantities which are operated on by a system operator or transfer function. For example, in the PATSIM model the solution of the following differential equation is used as a transfer function.

$$\frac{dQi}{dt} = \frac{K_1}{Q_i V_{A/C}} \quad e^{K_2 t}$$

where Q is the quantity in the i^{th} packet and K_1 and K_2 are empirical constants.

This convolution operation can be expressed in the following form:

let
- $f_1(x)$ be the flow function out of the tank in a fixed coordinate system
- $f_2(x)$ be the transfer function between the release and ground coordinates
- $f_3(x)$ be the pattern range marginal distribution; then

$$f_3(x) = \int_{-oo}^{oo} f_1(x)\, f_2(x-\tau)\, d\tau$$

In the case of the retardant breakup, the function $f_2(x)$ is unknown, and it describes the system breakup.

In linear system theory, it is shown that convolution operation can be carried out by Fourier transforms. This technique has become practical with the computer, in particular with the Fast Fourier Transform programs. The convolution operation leads to the above integral quation which has to be approximated numerically or determined by use of the transform methods discussed in the following paragraphs.

The Fourier integral can be used to represent an arbitrary function f (t) valid for every t:

$$f(t) = \frac{1}{2} \int_{-\infty}^{\infty} F(\omega)\, e^{i\omega t}\, dt$$

The quantity F (ω) given by

$$F(\omega) = \int_{-\infty}^{\infty} f(t)\, e^{-i\omega t}\, dt$$

is known as the Fourier integral or the Fourier transform of f (t). The function F (ω) is complex:

$$F(\omega) = R(\omega) + iX(\omega) = A(\omega)\, e^{iQ(\omega)}$$

where

A (ω) is the Fourier spectrum of f (t)

A^2 (ω) is its energy spectrum

Q (ω) is its phase angle

The Fast Fourier transform algorithm takes the data (e.g., flow or pattern) and converts into a frequency domain representation. This frequency domain representation in the retardant application is a computational artifice as will be seen. The data points are transformed into complex number data pairs that represent a collection of spatial sinusoids. These sinusoids have a frequency, an amplitude, and a phase angle.

The Fourier representation of the flow and pattern data can be used to solve this integral equation for the transfer function. This follows from the two representations of a linear process:

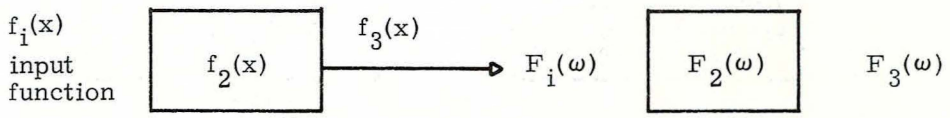

$$g(t) = \int_{-oo}^{oo} f(t)\, h(x-\tau)\, d \qquad F_3(\omega) = F_2(\omega) \times F_1(\omega)$$

Time Domain — Frequency Domain

In the breakup process the variable out of the tank is gallons per foot and oo is the pattern range marginal. By Fourier methods we have a linear spatial frequency representation of the two events, i.e., the pattern and the flow. In the frequency domain, we can obtain a representation of the transfer function as the ratio of two quantities for which data exists:

$$F_2(\omega) = \frac{F_3(\omega)}{F_1(\omega)} \quad \text{or} \quad \frac{\text{frequency function of pattern}}{\text{frequency function of flow}}$$

In essence all of the processes between the flow out of the tank and the ground distribution are included in $F_2(\omega)$. Both data sets have some measurement noise, so we are not working with theoretical data.

To recover the transfer function of the process in a common spatial coordinate system, the inverse transformation of $F_2(\omega)$ has to be made. This then produces a spatial breakup function that could be applied to the flow function to produce a pattern by the convolution integral.

The steps in this process are shown in Figure 54.

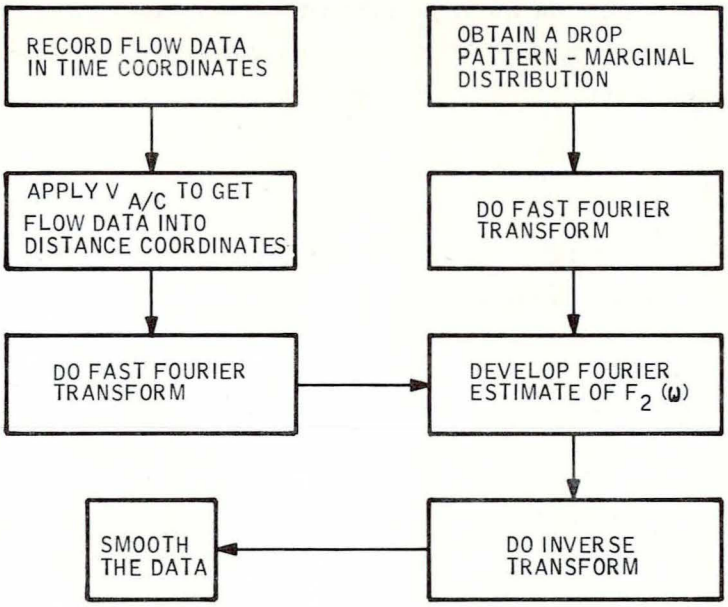
RECORD FLOW DATA IN TIME COORDINATES
APPLY V A/C TO GET FLOW DATA INTO DISTANCE COORDINATES
DO FAST FOURIER TRANSFORM
SMOOTH THE DATA
OBTAIN A DROP PATTERN - MARGINAL DISTRIBUTION
DO FAST FOURIER TRANSFORM
DEVELOP FOURIER ESTIMATE OF F2 (ω)
DO INVERSE TRANSFORM

Figure 54. Steps in the Fourier Simulation

Figure 55 shows the transfer functions for six drops of the configuration matrix. These functions plotted in the frequency domain represent the ratio between the Fourier transforms of the flow rate and the Fourier transforms of the pattern. They are thus directly computed differences between the flow-rate-implied coverage and the actual coverage in terms of gain. The data on these functions was noisy, requiring considerable smoothing to yield the plots shown in the figure. They were smoothed with a three-point moving-average filter. Note that, to relate pattern and flow rate, a starting time must be assumed. This delay between pattern and flow must be at least as long as the time to evacuate the tank, which was used as the assumed offset. Although this time is itself ambiguous in terms of the analysis, the following points can be made.

First, the patterns have gains in the frequency domain (fine structure) that do not appear related to flow rate. Second, gains from essentially identical flow rates differ radically as a function of velocity. Third, the possibility of using a limited set of transforms to generate expected values appears remote. As a result, this possibility of generating expected values was abandoned.

Despite the failure of the Fourier application to yield an analysis scheme for bulk processing, it is useful to speculate on the information contained in the transfer functions.

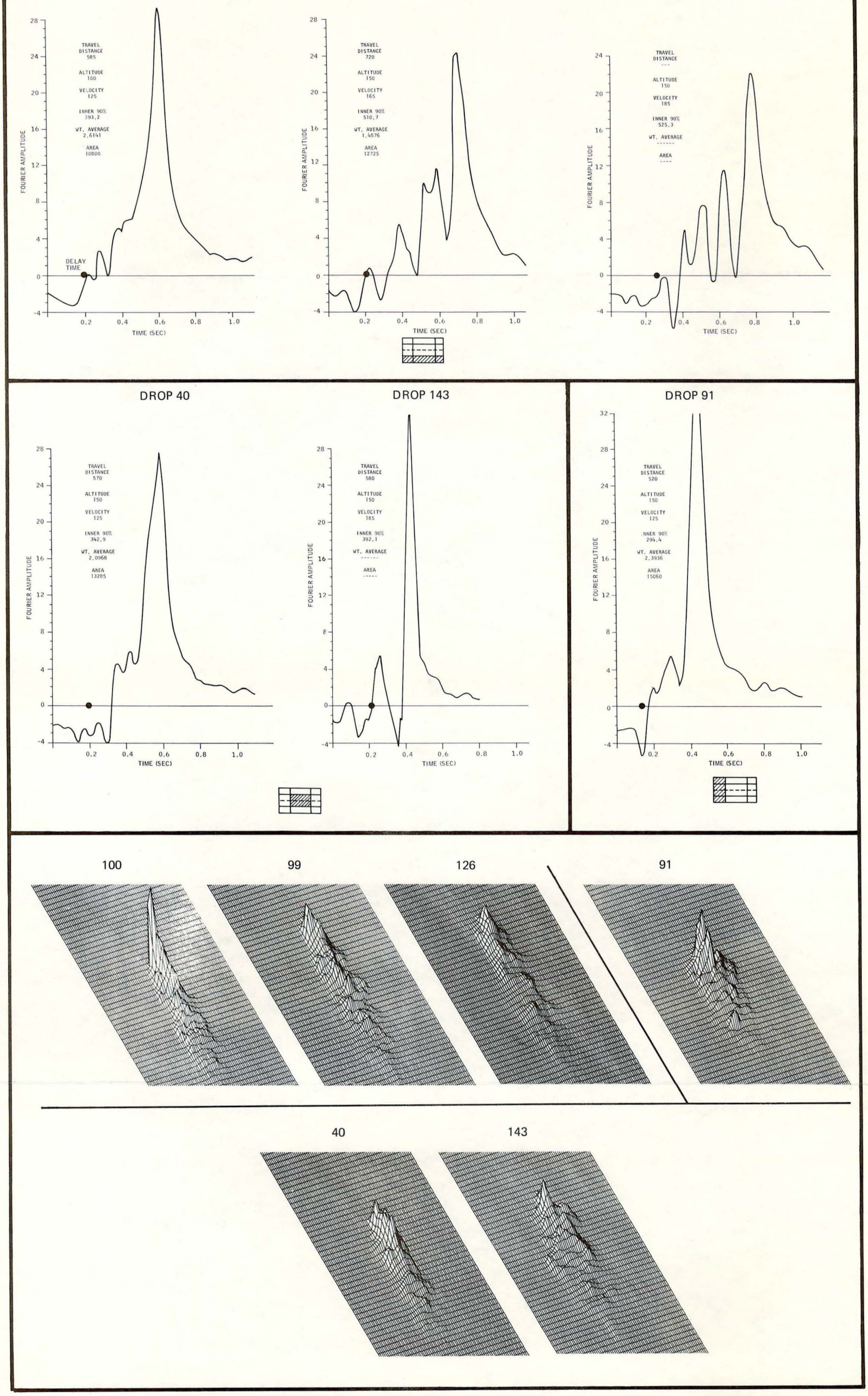

Figure 55. Fourier Transfer Functions for Selected Configuration Drops

The low-velocity drops exhibit a single band of gain, becoming generally narrower as the length of the fluid column facing the airstream is reduced. With increased velocity, the single event appears to separate into a series of semidiscrete events, which may be related to curtain phenomena observed in retardant drops as a form of discontinuous chaffing of bulk retardant through the flight. If so, it is not surprising that the view used in the simulation as a continuous process of retardant spread over the trajectory distance fails to match the peaks and valleys of the actual patterns.

Distributional Studies

If pattern characteristics are to be measured parametrically without the aid of a simulation to generate an expected value, it is necessary to identify the class of distribution to which they belong. Previous studies had shown that most pattern-range distributions could be reasonably fit within the Weibul distribution fully defined by three parameters, Nu, Mu, and Beta, where Mu could legitimately be ignored, leaving essentially a two-parameter descriptor. This model, which was the original basis for the experiment, was in fact used in the subsequent analysis. It does, however, apply to a three-dimensional abstraction of the pattern that obscures the important practical parameter of pattern length. Further, since the initial studies using the Weibul, it was discovered that the crossrange distribution was legitimately defined by a normal distribution. This contention is readily confirmed by the ETAGS data. Thus, the width, and consequently area, aspects of the pattern are well controlled if the range conditionals can be categorized.

Visual examination of the range distributions suggests that they are Beta or Gamma distributions in nature. Both are multiparameter distributions. Subsequent analysis showed that most patterns, the flow rate, and the simulation distributed pattern are reasonable Beta distributions. This explains in part the reasonably good predictive capability of the simulation, despite the lack of correspondence in the fine structure. A useful feature of the Beta distribution is that it is virtually defined by a single metric, i.e., the 90th centile length. For further discussion of this metric see Reference 4.

The studies on these distributed forms are summarized in the following paragraphs.

Retardant ground patterns are complex, three-dimensional distributions as evident in Figure 44. This means that their geometrical description, suitable for analysis, requires the use of many interrelated dimensions. The complexity of these dimensions makes analysis difficult. As a result, there is a need to simplify the problem in a way that allows inspection or measurement of differences between them.

The first simplification is to define the pattern as two separate distributions; one along the flight path and another normal to the flight path (see Figure 56). These are called marginal distributions taken in range and crossrange.

The second simplification, a significant one, is to eliminate quantity and retardant from the pattern by normalizing the values, i.e., expressing the quantity as a percent of the total retardant in the pattern. This abstraction is important to understanding the phenomena of retardant delivery and, most significantly, to modeling it. As with any abstraction, certain relevant values are lost – the normalized distribution contains no information on width or length at a specific coverage level (the information is recoverable by multiplying the percentage by the quantity in the pattern). From a modeling standpoint, this procedure enables us to determine, for example, whether quantity changes the way in which the retardant is distributed or simply the level in the distribution.

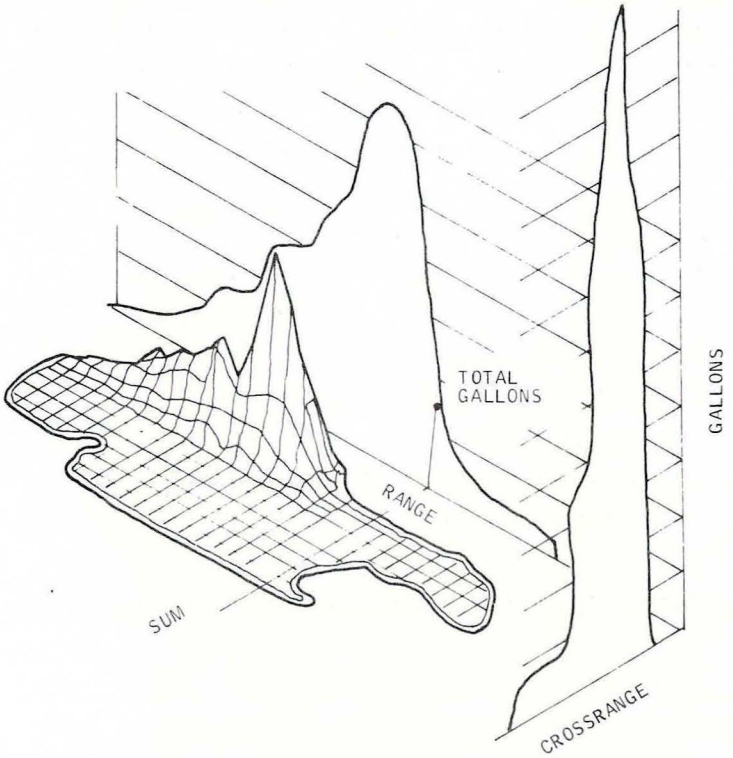

Figure 56.
Marginal Distribution
Definition

The analysis problem is greatly simplified if these distributions can be approximated by one of the standard statistical forms; i.e., can we generate a reasonable approximation to the form as a model for analysis. In crossrange, previous studies (High Altitude Delivery Program) have shown a good fit to the common normal distribution, or "bell" cruve. This distribution is the basis of most statistics and mathematically well defined. The correspondence or "goodness of fit" to this distribution was confirmed by analyzing the extreme conditions resulting from the ETAGS drops. The nature of the pattern is not strongly dictated by the crossrange development. It changes gradually with altitude at a rate dictated by the retardant type or rheology. The form and dimensions are not substantially affected by aircraft velocity, quantity or retardant or exit geometry. There appear to be minor variations with tank width and skew introduced by slow-opening doors. The crossrange is of interest in determining mixing from separated tanks. In other words, major determinants of a retardant pattern derive from the way the fluid is spread along the aircraft flight path. Little in tank design can be done to control pattern width.

The range marginal distribution is far more difficult to define in a way suitable for analysis. Work, herein described, shows that range distributions are in general good fits to the Beta distribution, a specific form within the set of Gamma distributions. A discussion of the Beta distribution is presented later in this section. Those have, like the patterns, the general shape shown below.

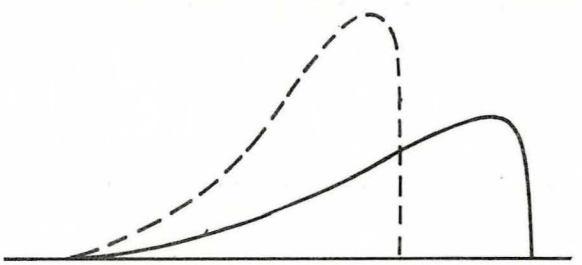

This means that a smooth curve mathematically defined by the Beta function can be fit to approximate a pattern marginal distribution. A useful property of the Beta function is that it is almost completely defined when we know its length. Under this modeling hypothesis, the pattern length taken from the 5th to 95th percentile virtually defines the distribution.

It should be noted that the integral or area under the curve which is a normalized quantity remains the same with the shape constrained by other values of the Beta function. As a result, longer distributions have lower peak values than short ones. Thus the pattern-length value used in our analysis is a measure of the

distribution. It is not necessarily a measure of the specific line length at any coverage level until the amount of retardant in the pattern is re-introduced. For example, the length and form of the distribution remain substantially unchanged regardless of the aircraft drop height. The amount available is however decreased by lateral spread and retardant evaporation to produce lesser line lengths at a specific value.

Conclusions in the subsequent sections are based on distribution of the retardant rather than coverage levels. The values to be preserved are length and uniformity. It is a separate issue to assure delivery of sufficient quantity to effectively treat fire fuels.

Weibul Analysis -- The Weibul distribution model (Figure 57) is based on gallons distributed by area, and is defined by η, the gallons per hundred square feet average of the pattern distributed in the Weibul fashion, and β, a form factor that estimates the uniformity of the distribution – a high Beta indicates that coverage extremes differ little from the average value, η. A low Beta indicates that the coverage is highly variable; thus a pattern nearing its terminal condition, fully broken and spread, exhibits a high Beta (2 or better). A pattern whose breakup process is incomplete exhibits a low Beta (1 or less).

This distribution has two parameters, β for the shape and η as the scale parameter. The Weibul cumulative distribution is given by

$$F(x;\beta,\eta) = 1 - \exp\left[-\frac{x}{\eta}\right]^{\beta}$$

To interpret this concept of the Weibul to the pattern, consider four example cases as shown in Table 6.

This table shows the importance of scale parameter η in evaluating a pattern as a characteristic number; 63% of the pattern will be concentrated at 2 gpc or lower. The Beta parameter indicates the spread of concentration of the distributions about the η value. A large value of β will increase the amount concentrated about the η.

Mathematically, the Weibull distribution (ref 5) is the cumulative probability distribution

$$F(x^{j}\ \beta,\ \eta) = 1 - \exp\left[-\frac{X^{\beta}}{\eta}\right]$$

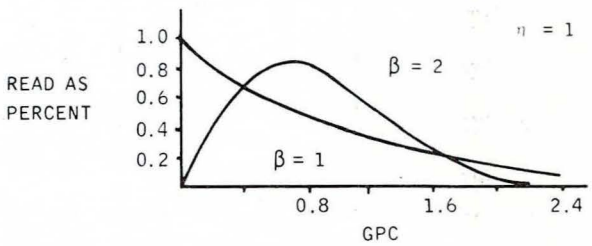

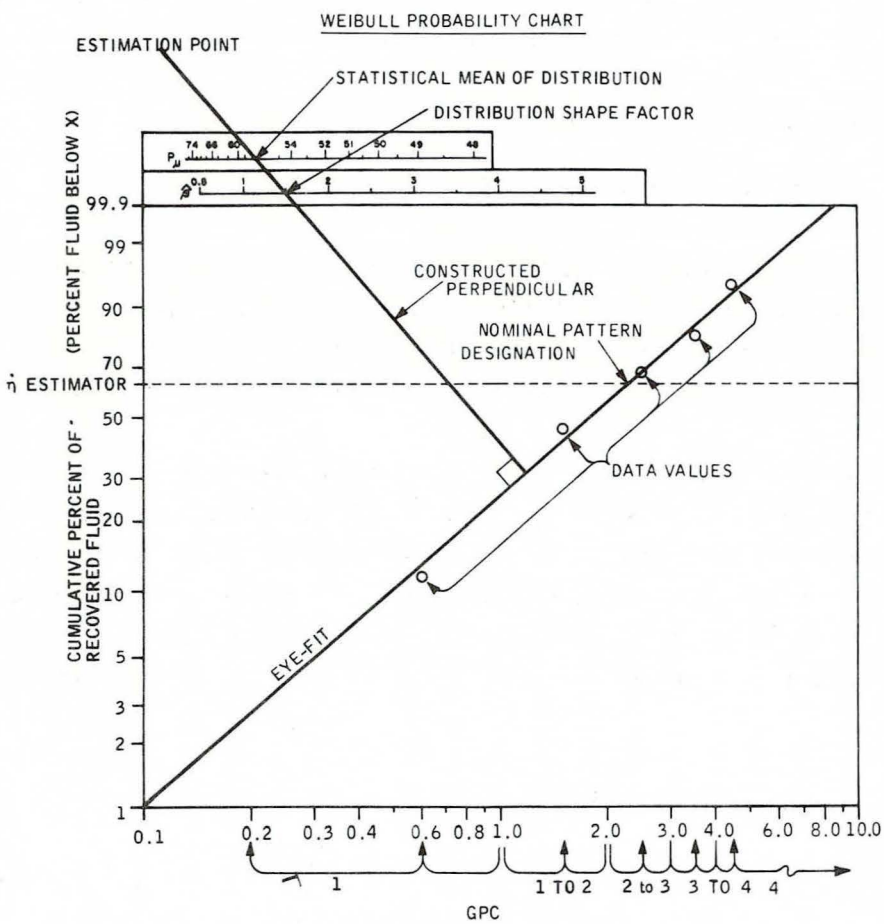

Figure 57. Weibul Distribution Model as Applied to Retardant Pattern Analysis

Table 6. Examples of Weibull Analysis (Pattern Concentration)

Coverage Level	$\eta = 1, \quad \beta = 1$	$\eta = 2, \quad \beta = 1$	$\eta = 1, \quad \beta = 2$	$\eta = 2, \quad \beta = 2$
1gpc	37%	61%	37%	78%
1-2gpc	26%	23%	36.3%	40%
2-3gpc	7%	16%	1.7%	28%
4-5gpc	1.2%	5%	-	1.7%

The data from the Flow Rate Study Matrix on Phos-Chek were used to study the effect of altitude and exit time on the two parameters of the Weibull:

$$\beta = 0.9684 + 0.05788 \text{ time} + 0.00235 \text{ height}$$

$$\eta = 2.6777 - 0.29425 \text{ time} - 0.00411 \text{ height}$$

These relationships show Weibull parameters can be used to characterize the breakup process in terms of the delivery conditions. Increasing the altitude of delivery concentrates the distribution by the increase in the Beta parameter, whereas the η parameter is decreased. Decreasing the exit time increases η.

If one considers the breakup process as a transient, then one can identify the two Weibull parameters with this event; η as a function of altitude will have the shape of a negative exponential which will have an assymtotic value. This value is the fully developed breakup. Correspondingly, the Beta value would increase, indicating more uniformity in distribution. In the low-altitude case the value β is small. This implies a higher average level of the pattern with a lot more variety in coverage.

This can be summarized as follows:

High η, low β = large variety of coverage at a high average level — incomplete breakup process

Low η, high β = limited variety of coverage at a low average level — complete breakup process

Although these statistics are useful in evaluating the parameters they obscure certain important and practical pattern characteristics, specifically the length of line; i.e., there are multiple pattern-length solutions to the same Weibull distribution. Consequently, it is desirable to provide finer resolution to the length issue.

Crossrange Distribution -- The current simulation views the crossrange expansion of the pattern as a normal distribution. A check on pattern data on 12 drops shows little reason to reject this hypothesis. This aspect of performance was checked in an initial flow-rate matrix by graphing the distributions on semilog paper (Figure 58). It was rechecked against extreme patterns observed in the remainder of drops (Figure 59). In all cases they were reasonably represented by straight lines. They do indicate the altitude dependency contained in the simulation. There is also a suggestion that they may be configuration dependent.

Applying the matrix analysis technique initially anticipated to evaluate the effects of altitude, door rate, and door area, the simulation errors were found not to be at a significant level, in χ^2 test. The effect of rate, however, was considerably larger than the error effects of altitude or area. The coupled effects of door rate and altitude also approached significance levels.

Examination of the crossrange distributions (Figure 60) shows an apparent skew due to deflection of the fluid mass by the door when the door rate is very slow. The effect on total pattern is nonetheless negligible. Although the potential use of these data was to refine the simulation crossrange development rules, the effect is confounded by issues relating to the range distribution.

Significantly, the simulation appears to handle the crossrange adequately.

Furthermore, since the crossrange is definable as a distributed form, the analysis problem can be simplified to assess the lengthwise distribution.

Beta Distribution of the Range Marginal -- The Pearson system of distributions, as described in Reference 6 for example, includes most of the common density functions. These density functions are the solutions of the differential equation

$$\frac{dy}{dx} = \frac{y(x+a)}{b_o+b_1x+b_2x^2}, \text{ where a, } b_o, b_1, \text{ and } b_2$$

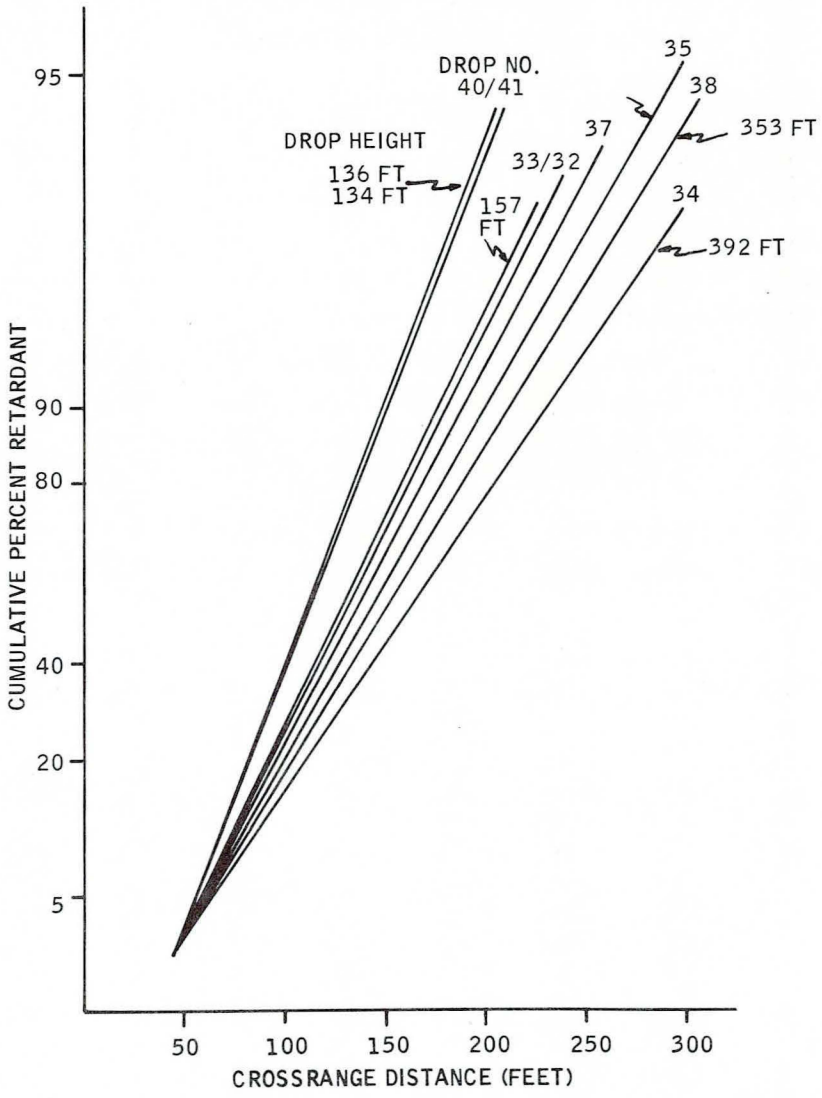

Figure 58. Tests for Normal Distribution of Crossrange Patterns

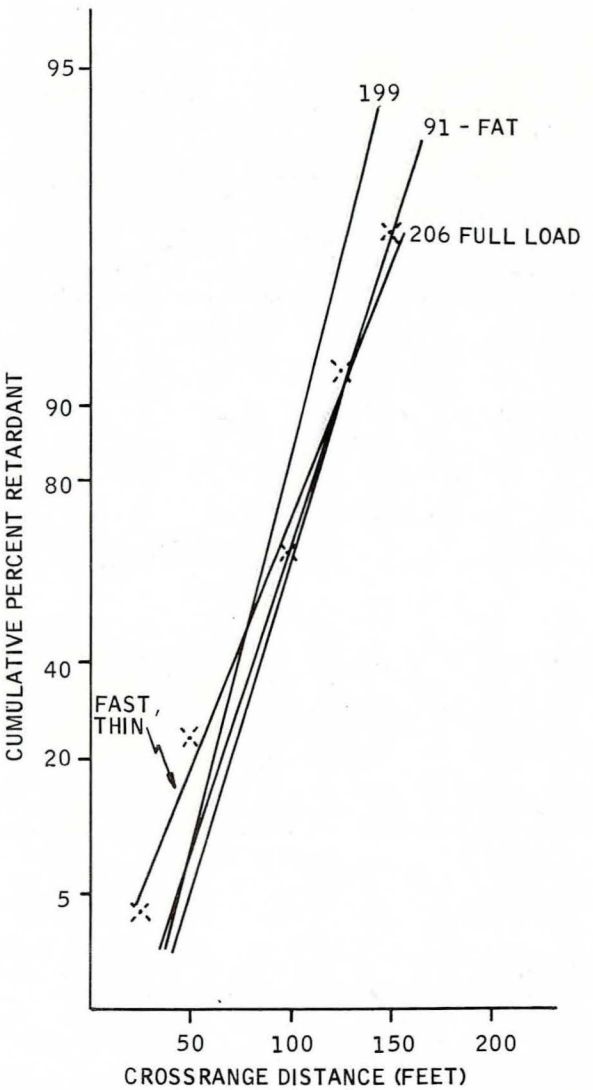

Figure 59. Confirmation of Normal Distributions in Extreme Patterns

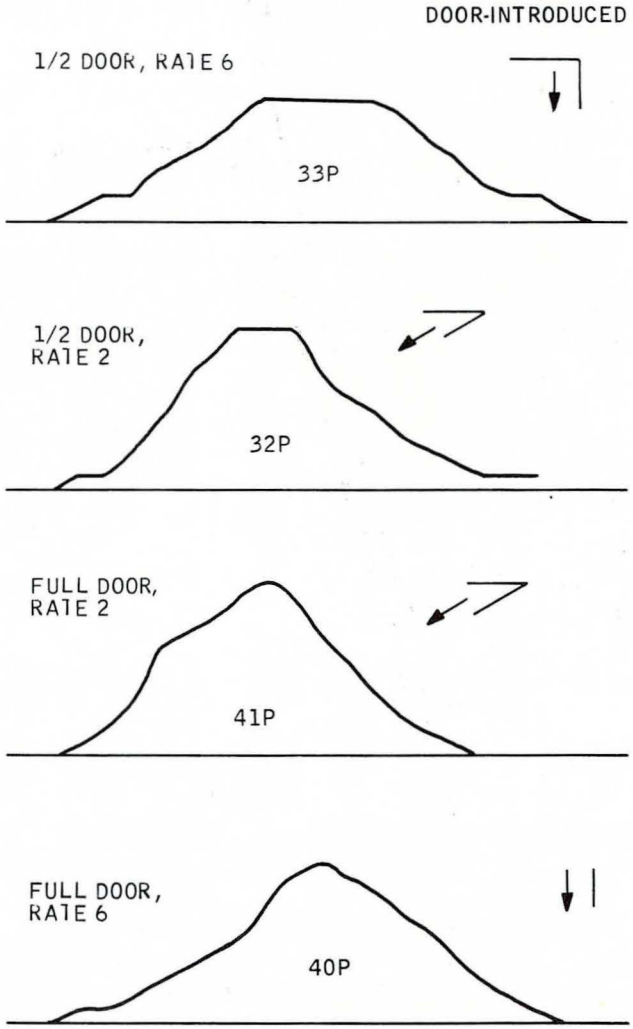

Figure 60. Crossrange Marginals of Selected Drops

are parameters. The type of curve depends on $K = b_1^2/4b_o b_2$, which can be related to the first four moments of the distribution. This expression for K in terms of the moments, i.e., u_1, u_2, u_3, and u_4 is

$$K = \frac{\beta_1 (\beta_2+3)^2}{4(4\beta_2^2 - 3\beta_1)(2\beta_2 - 3\beta_1 - 6)} \quad \text{where}$$

$$\beta_1 = \frac{u_3^2}{u_2^2} \quad \text{and} \quad = \beta_2 = \frac{u_4}{u_2^2}$$

The pattern range marginal data can be used to estimate sample moments values that can be substituted into the expression for K. This assumes that sample moments are reasonable estimations of the population moments. When this substitution is made the numerical value of $K < 0$ corresponds to a Beta distribution.

The Beta distribution is a two parameter (a, b) density defined on the interval (0, 1) by

$$f(x) = \frac{1}{\beta(p, q)} \quad x^{p-1} \quad (1-x)^{q-1}, \text{ where}$$

$\beta(p, q)$ is Beta function $\int_o^1 x^{p-1}(1-x)^{p-1}dx.$

The Beta function is related to the Gamma function by

$$\beta(p, q) = \frac{\Gamma(p)\,\Gamma(q)}{\Gamma(p+q)}, \quad \text{where } \Gamma(p) = \int_o^{\infty} x^{p-1}e^{-x}dx.$$

For integral values of p and q, the Beta function can be expressed in terms of the factorial

$$\beta(p, q) = \frac{(p-1)!\,(q-1)!}{(p+q-2)!}$$

The first two moments of the Beta distribution are:

$$\mu_1 = \frac{p}{p-q}$$

$$\mu_2 = \frac{q}{(p+q)^2(p+q+1)}$$

To relate the sample moments to the Beta distribution, the following equations apply.

$$y = y_o \left(\frac{1+x}{a_1}\right)^{m_1} \left(\frac{1-x}{a_2}\right)^{m_2} \qquad -a_1 \le x \le a_2$$

with the origin at the mode.

$$y_o = \frac{a_1^{m_1} a_2^{m_2}}{(a_1+a_2)^{m_1+m_2+1}} \qquad \frac{\Gamma(m_1+m_2+2)}{\Gamma(m_1+1)\,\Gamma(m_2+1)}$$

$$m_1+m_2+2 = r = \frac{6(\beta_2 - \beta_1 - 1)}{6 + 3\beta_1 - 2\beta_2}$$

$$(m_1+1)(m_2+1) = \epsilon = r^2 \Big/ \left(\frac{4+\beta_1}{4}\left(\frac{(r+2)^2}{r+1}\right)\right)$$

$$(a_1+a_2)^2 = \frac{\mu_2 (r+1) r^2}{\epsilon} = \text{Z}$$

$$\frac{m_1}{a_1} = \frac{m_2}{a_2}$$

$$\text{Mode} = \mu_1 - \frac{1}{2} \cdot \frac{\mu_3}{\mu_2} \cdot \frac{r+2}{r+2}$$

After the first four moments and the β coefficients have been calculated, substitution in equations for r, ϵ, and Z are performed. Two solutions for m_2 can be obtained from

$$m_2^2 - (r-2)\, m_2 + (\epsilon - r+1) = 0, \text{ and for each}$$

$$m_1 = (r-2) - m_2.$$

With these values of m_1 and m_2, a_2 is

$$a_2 = \text{Z}^{1/2} \Big/ \frac{(m_1+1)}{m_2}, \text{ and}$$

$$a_1 = \mathbb{Z}^{1/2} - a_2.$$

The cumulative distribution can be obtained by

$$p(\leq x) = \frac{1}{\beta(p_1 q)} \int_0^x t^{p-1} (1-t)^{q-1} dt,$$

where $p = m_1 + 1$, and $q = m_2 + 1$

Table 7 contains the calculations to estimate the density function.

As a check on the application of the Beta distribution Figures 61 and 62 compare the sample cumulative distribution using the Beta and the sample distribution. One aspect of the Beta distribution that is extremely useful in data analysis is that the distribution is reasonably well defined by the inner 90% length according to Catherine Thompson (Reference 4). Thus, insofar as the patterns are true Beta distributions as they appear to be, this single metric can legitimately be employed in data analysis. It was subsequently selected as the primary item for linear regression analysis of the test matrices. Table 8 contains the comparison of predicted and actual length statistics using Catherine Thompson's tables and sample estimators with the real values.

Modified PATSIM

The use of PATSIM to provide expected values for application to a χ^2 technique of data analysis became impractical when it was discovered that exit configuration had a profound effect on the distributed values of the patterns. Unfortunately, exit geometry is a pervasive variable in that by holding gallonage constant, and varying other aspects of the drop changes the exit geometry even when it was not the variable under examination, i.e., in head height and restricted door matrices. One potential means of recovering the preplanned analysis technique was to introduce a simple modification to PATSIM that would include in some reasonable manner the input of exit geometry. The obvious modification would relate the two empirical constants K_1 and K_2 to some geometrical characteristic such as length, width, frontal area or length-to-width ratio. Unfortunately, it was found that K_1 and K_2 could not in themselves produce the dynamic range required to accommodate the observed data. Although several other approaches to modifying

Table 7. Calculations for Beta Distribution

Drop No.	Mean	2nd Moment	3rd Moment	4th Moment	β_1	β_2	r	ϵ	z
154	620.5	12426.86	-1038496.3	5.17947×10^8	0.5625	3.35	10.86076	19.78788	8.78607×10^5
163	622.79	19172.50	-2567239.9	1.467384×10^9	0.9409	3.99	14.58953	26.10883	2.43673×10^6
131	575	23845	-2.95×10^6	1.841×10^9	0.64195	3.23756	6.5992	7.8303	1007791
161	401	18325	-1.683×10^6	1.056×10^9	0.46046	3.14378	9.23362	15.732	1016329
159	468	16507	-1.469×10^6	7.769×10^8	0.47946	2.8513	4.7336	4.53704	468805

Drop No.	r-2	ϵ-r+1	m_2	m_2'	m_1	m_1'	$\frac{m_1}{m_2}$	$\frac{m_1'}{m_2'}$
154	8.86076	9.92712	7.545	1.3157	1.31576	7.545	0.17438	5.7346
163	12.5995	12.5093	11.5130	1.08654	1.08654	11.5130	0.09438	10.5960
131	4.5992	2.2311	4.0480	0.5512	0.5512	4.048	7.1362	7.3498
161	7.2336	7.4984	5.9796	1.2540	1.2540	5.9796	2.2097	4.7684
159	2.7386	0.7984	2.4069	0.33172	0.3317	2.4069	0.1378	7.2558

Drop No.	$\left(1+\frac{m_1}{m_2}\right)^{-1}$	$\left(1-\frac{m_1}{m_2}\right)^{-1}$	q_2	q_2'	q_1	q_1'	r+2	$1/2\ \frac{r+2}{r-2}$	Mode
154	0.8515	0.1485	798.15	139.2	139.2	798.14	12.86076	0.7257	681.146
163	0.91376	0.08623	1426.38	134.61	134.61	1426.38	16.5895	0.6583	710.94
131	0.8801	0.1198	883.6	120.3	120.3	883.7	8.5992	0.9349	698.7
161	0.8267	0.1734	833.4	174.8	174.8	83.4	11.2336	0.7765	472.3
159	0.8789	0.1211	601.8	82.9	82.9	601.8	6.7386	1.2303	577.5

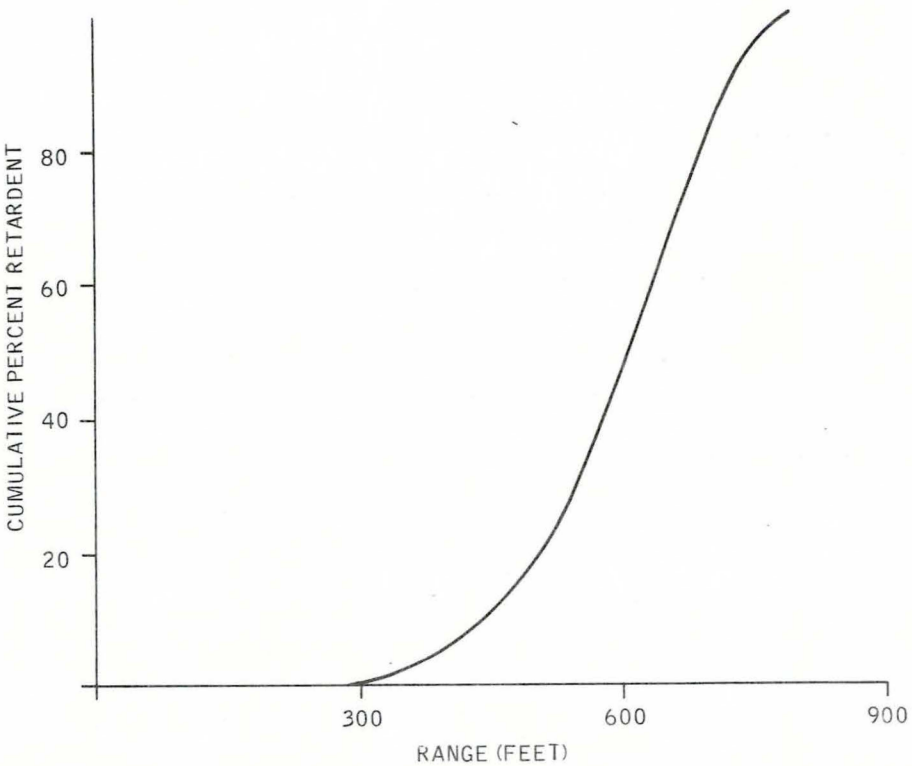

Figure 61. Cumulative Marginal Distribution Using Beta

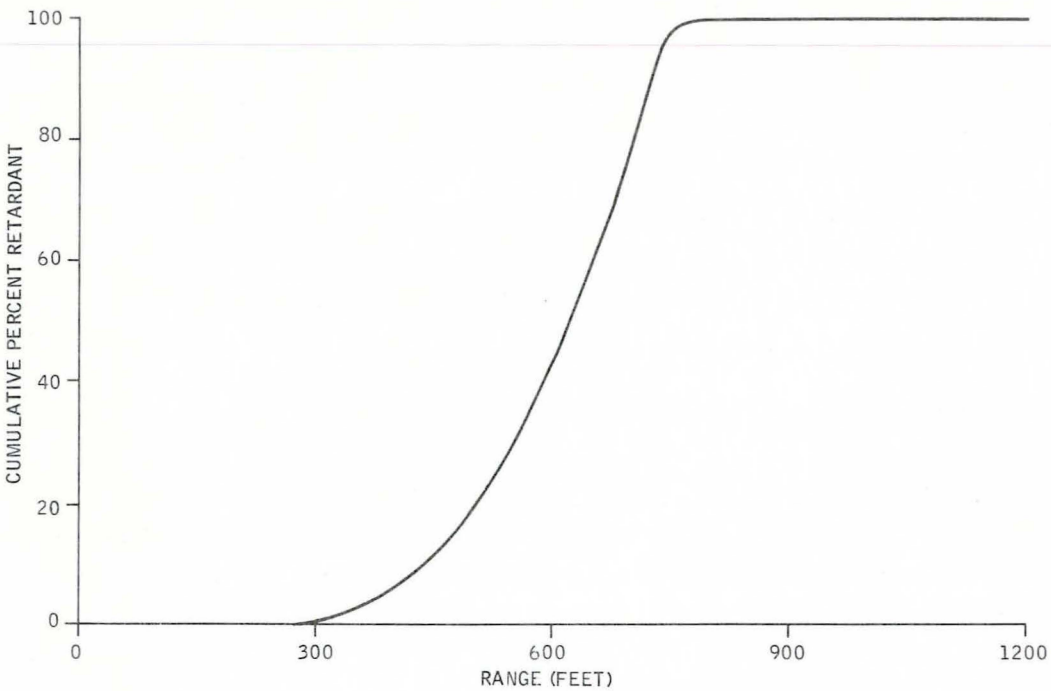

Figure 62. Sample Distribution of Actual Drop

Table 8. Inner 90% Pattern Length Comparison

Drop 131	σ = 154.4
UL =	(1.29) (Xp-μ) / σ = 1.29 = 774
LL =	(Xp-μ) / σ = 1.91 = 280
	Range = 494 Actual = 517.7
Drop 161	σ = 135.4
UL =	(Xp-μ) / σ = 1.36 = 585
LL =	(X-μ) / σ = 1.88 = 146.5
	Range = 438.5 Actual = 429
Drop 159	σ = 128.5
UL =	131(X-μ)2 = 1.31 = 636.3
LL =	(X-μ)(σ) = 1.91 = 222.6
	Predicted = 413.7 Actual = 405.4

the simulation were examined, none could provide the ad hoc confidence required to serve as an expected value generator. As a result, the expected value technique for parameter analysis was abandoned in favor of regression models.

This subsection describes analyses and discussions on:

- The indicated error in the simulation due to exit geometry
- Sensitivity of PATSIM to K_1 and K_2
- Alternative recovery models.

Effect of Velocity and Configuration on Range Marginals -- Experiments on configuration (i.e., the aerodynamic aspect of the fluid mass) were introduced in the ETAGS test to answer key questions in tank design involving the best methods of partitioning a tank system. No previous data had provided a dynamic range of geometries under controlled conditions. The effect of this characteristic has been hypothesized based on physical understanding of the breakup process, although no

evidence of its effect had been noted in prior analysis. It was thought that the geometry influenced pattern placement – distance traveled downrange – rather than the distribution itself. As a result, the configuration test matrix was subject to initial analysis.

Figures 63 and 64 show the range marginals and distance from release to impact for the simple configuration delivering 460 gallons in a long, moderate, and wide configuration.

It appears from the marginal distributions that the distributions resemble the tanks from which they emerged (Figure 65) and that the differences are amplified by velocity.

Figure 66 shows the range marginals for three drops of Phos-Chek at comparable velocities as compared with the simulation. Note that since flow rates were essentially identical, the simulation predicts the same performance for all three drops. The simulation represents a reasonable approximation to moderate and short tanks, but differs considerably from the performance of the long, thin tank at 124 knots. To further explore this correspondence, a study was conducted to assess the ability of the simulation to generate patterns comparable to real patterns over the range of configurations and velocities.

Two yardsticks were employed, first the length of the range marginal from 2% to 98% of the distribution, and second, the length of the pattern from 2% to 50% of the distribution. The length is essentially Catherine Thompson's 95th centile lines used to eliminate ambiguities in the tail off sections of the marginal curves. Figure 67 shows the organization of the data with respect to Phos-Chek drops with the long thin tanks.

For the flow rate under investigation, the simulation generates a distribution estimate of:

Half range (ft) = 2.5 velocity (knots) - 23.7

Full range (ft) = 3.57 velocity (knots) - 5.6

Whereas, moderate tanks dumping water and Phos-Chek produce:

Half range (ft) = 2.3 velocity (knots) - 21

Full range (ft) = 4.3 velocity (knots) - 182

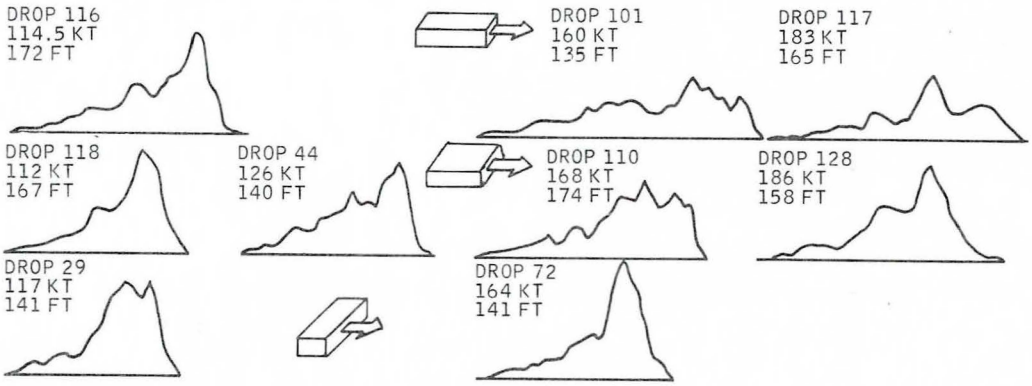

Figure 63. Range Marginals and Distance from Release to Impact - Water

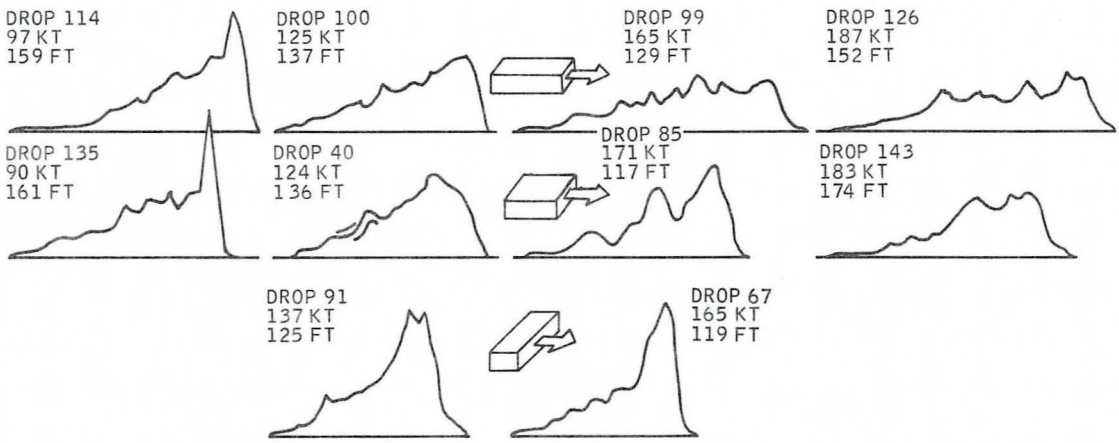

Figure 64. Range Marginals and Distance from Release to Impact - Phos-Chek

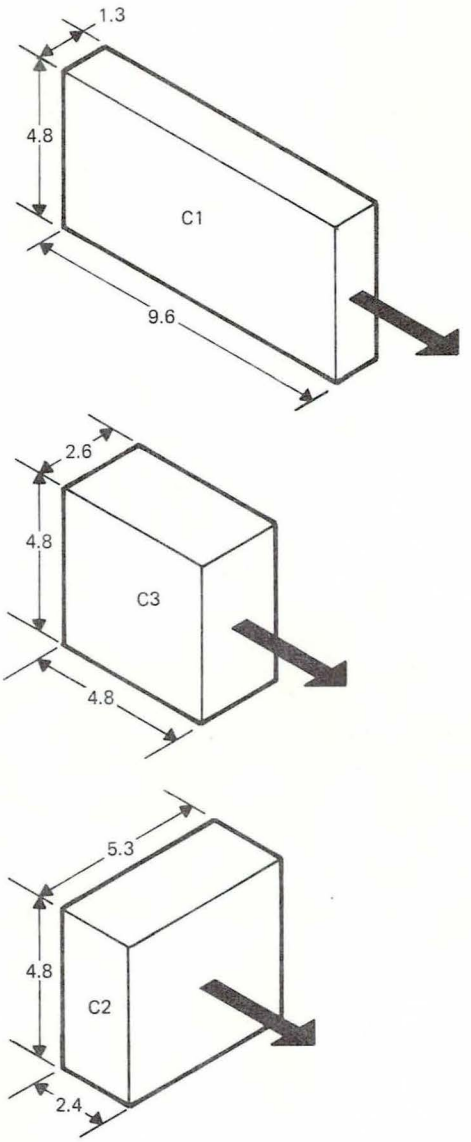

Figure 65. Tank Configuration Geometries

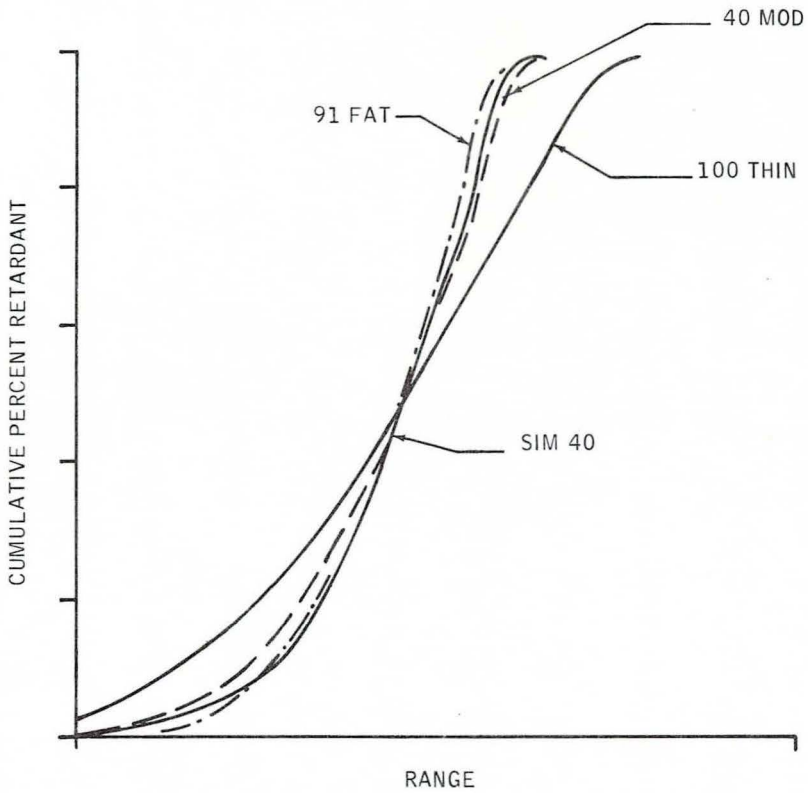

Figure 66. Range Marginals for Phos-Chek Drops of Three Configurations ("means" forced)

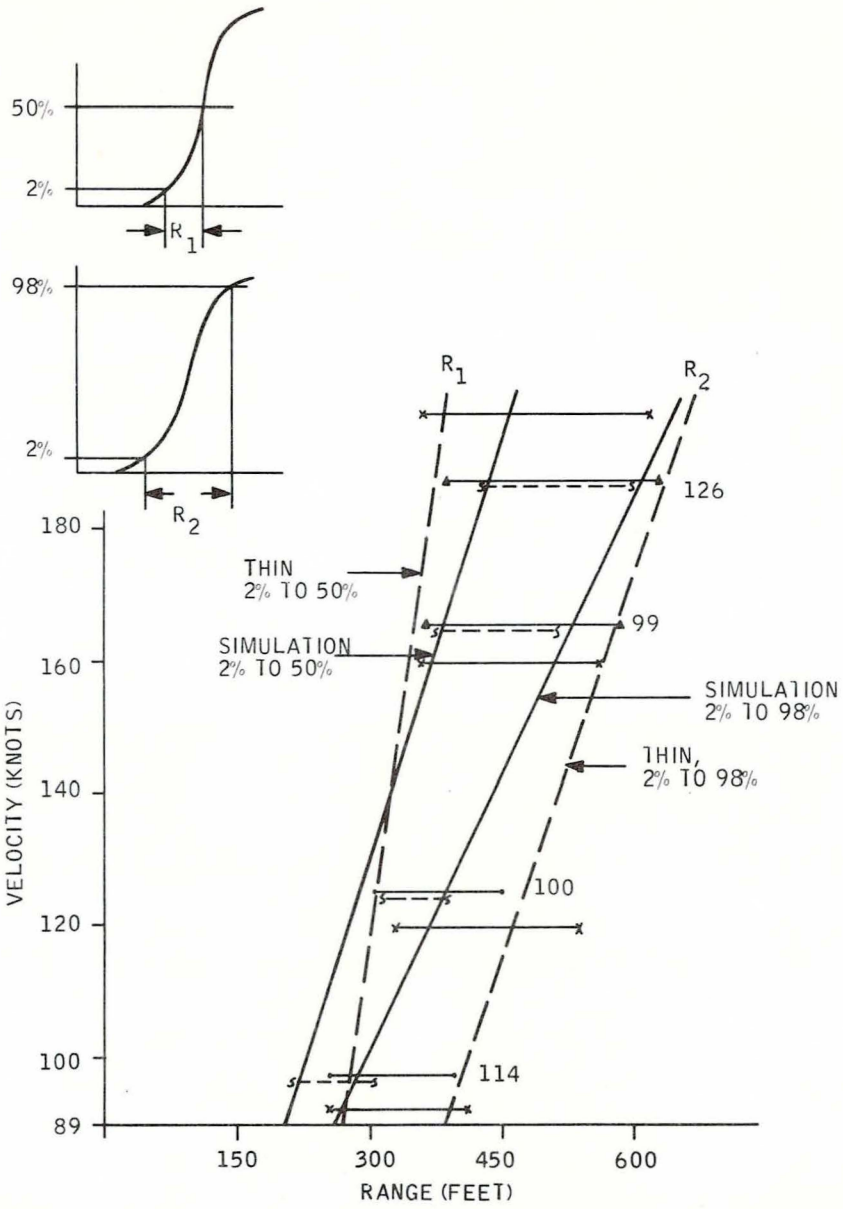

Figure 67. Pattern Length Parameters as a Function of Velocity for All Phos-Chek Drops of Tank Configuration C1

These reults are unambiguous and show a reasonable correspondence – i.e., the variability of both parameters with velocity are similar. The thin tank performance is more difficult to evaluate, primarily due to two water drops that appear anomolous. Figure 68 shows C1 water drops compared with the previous data on Phos-Chek. The variability of water data was not entirely unanticipated. Phos-Chek data yielded:

Half range (ft) = 1.45 velocity (knots) + 129

Full range (ft) = 2.5 velocity (knots) + 169

Note, however, that if the two high-velocity water drops are ignored, the following regression is generated:

1/2 length (ft) = 2y knots + 113

Full length (ft) = 4y knots + 33.2

which is close in slope to the simulation and its Phos-Chek neighbors.

Data on the third configuration were too sparse to allow similar evaluation, but negative slopes are implied by the data set.

As a result of this study, it was concluded that the PATSIM simulation, though adequate for generating expected values for moderate length-to-width tanks (on the order of 2 to 1); provided increasing errors as the tank departed from the basic configuration and that these errors were increased by release velocity. This led directly to an assessment of techniques to accommodate configuration in the model.

Adjustment of K_1 and K_2 -- It is impractical to generate the expected value analysis with a value generator that is itself being developed. It was thought, however, that the basic confidence in the model might be maintained if one or both of the emperical constants in the convolution generator could be related to a configuration parameter. Before exploring this relationship, it was necessary to determine how sensitive the simulation was to the two constants. The convolution generator is

$$\frac{dQi}{dt} = \frac{K_1 e K_2 t}{Qi Va/e}$$

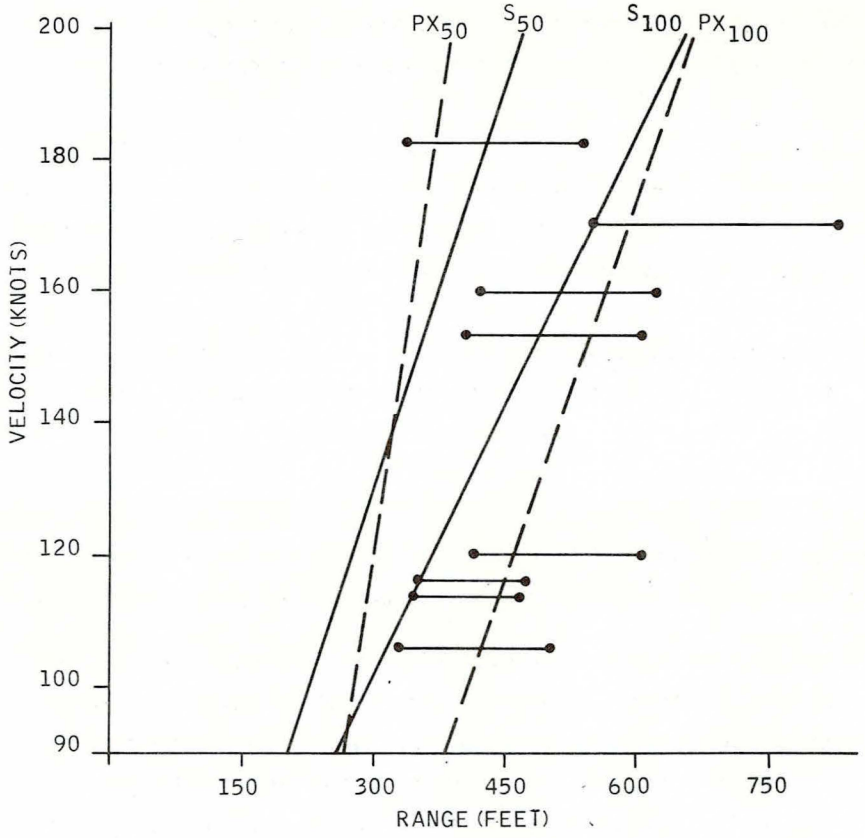

Figure 68. Tank Configuration C1 Water Drops Compared with Phos-Chek (PX) and Simulation (S) Drops

A series of simulation runs was made to examine the ability of K_1 and K_2 to modify the 90% length of the pattern. Table 9 presents matrices of lengths generated by K_1 and K_2 combinations. From these combinations the best-fit constants were selected for the six drops used in the Fourier analysis set as shown in Table 10.

It appears from these data that K_1 and K_2 do not have the dynamic range to accommodate all the lengths observed, and further, that they are not organized in a manner to yield direct correlation with geometric parameters.

Alternative Models -- The alternatives to operating on the two constants, while retaining confidence in the existing model, were also examined as a means to preserving the expected value form of analysis. Specifically, these were aimed at redefining quantitative parameters in the convolution equation.

The quantity Qi is an incremental volume that has as its dimensions the length of the tank, its width, and a height constrained by the velocity efflux over the incremental time period. By consequence, it contains the product of length and width.

The most likely determinant of fluid flight is length due to several arguments. Aerodynamically, the ballistic coefficient is defined as $\frac{W}{C_D A}$ where W is the weight and A the frontal area. For the fluid, the W/A or sectional density is simply length times density. In addition, when viewed as an acceleration dominated system, length x density yields the unit force opposed by the dynamic pressure. Width enters the picture either as a concept of total pressure, difficult to envision in a fluid with limited surface forces, or, more subtly, as the dimension of the fluid in which the aerodynamic and hydraulic forces are reacted.

At this time, limited experiments were attempted to view the basic equation as a differential of length with respect to time. Although these experiments showed some promise, they did not preserve the existing model and were abandoned.

In the net, the simulation is an adequate predictor on the average, but not capable of the accuracy required for expected value analysis. This plan of evaluation was subsequently abandoned in favor of regression-type operations.

Table 9. Matrices of Lengths Generated by K_1 and K_2 Combinations

125-Knot Drop Speed

K_2 \ K_1	2.25	2.50	2.75	3.00	3.25	3.5	3.75	4.0
8	468	432	399	375	352	334	316	301
10	466	429	398	373	352	334	317	300
12	463	426	396	374	350	330	316	300
14	461	424	395	370	345	331	315	303

165-Knot Drop Speed

K_2 \ K_1	2.25	2.50	2.75	3.00	3.25	3.50	3.75	4.0
8	626	578	558	499	468	444	423	403
10	623	577	530	496	468	442	420	403
12	617	577	530	495	466	442	422	402
14	618	558	528	493	465	441	418	401

Table 10. PATSIM Comparisons

Item	Drop Velocity (knots)			Tank Configuration
	125	165	185	
Drop Number	100	99	126	
Inner 90%	392	511	525	
K_1	2.75	2.75	2.75	C1
K_2	14	8	14	
Drop Number	40		143	
Inner 90%	343		419	
K_1	3.25		3.75	C3
K_2	14		14	
Drop Number	91			
Inner 90%	234			
K_1	4.0			C2
K_2	8.0			

SECTION VII
MATRIX ANALYSIS

The ETAGS experiments were structured to determine significant tank and delivery parameters based on regression analysis of differences between PATSIM program predicted and actual pattern characteristics. However, factors such as tank configuration and aircraft velocity were found to have a significant effect on pattern characteristics, and these either were not considered by PATSIM or were not adequately represented in the simulation. This required that the analysis strategy be changed to accommodate information gained outside the PATSIM model.

This section covers the matrix analysis outlined in blocks 4, 9, and 10 of Figure 38.

MEASURES OF PATTERN PERFORMANCE

Length of Inner 90% of Pattern

The most substantial changes in a pattern due to aircraft and tank variables occur in the range distribution – the way in which retardant is distributed on the ground along the flight path. This distribution is also the most useful to practical fire fighting in that it ultimately determines the length of line at a given concentration level. When line lengths at a specific coverage level are used in analysis some difficulties are introduced, since small variations in the actual drop, altitude, or even unexplained variation (noise) cause considerable variability in the measured line length. Prior discussions have shown that the Beta-like distributions of most patterns are reasonably defined by their length measured between the 5th and 95th centile of the distribution. This value is stable when used as a metric, and, although it does not relate directly to line length, it allows us to assert the effect or change caused by a parametric variable on the pattern distribution.

This concept can be illustrated by assuming that patterns can be approximated by a triangular distribution (in lieu of the more complex Beta). The 90% length rule eliminates the somewhat anomolous low-level tails that extend fore and aft of the useful concentrations:

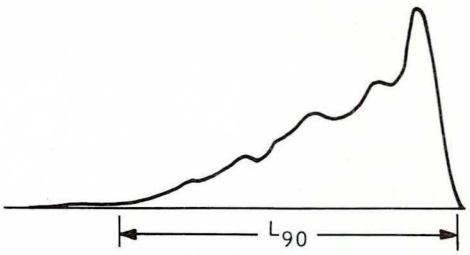

The Beta and simplified triangular approximations appear as follows:

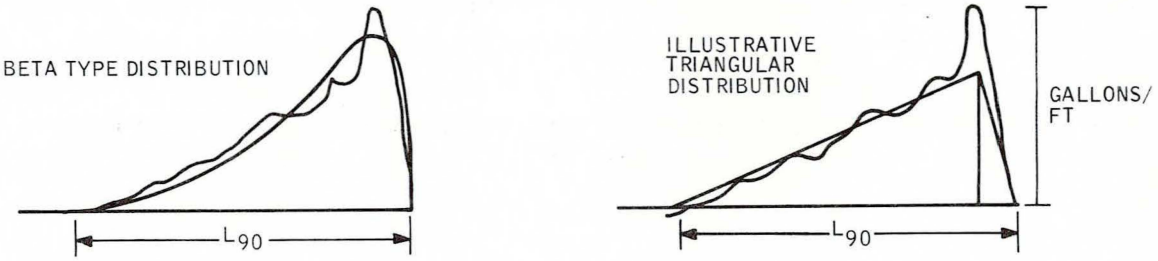

The triangular distribution does not acknowledge the difference between extreme patterns, and, in consequence, there are a number of equivalent triangles. The right triangular representation with an appropriate scale factor thus represents an approximation of the line length of various coverage levels:

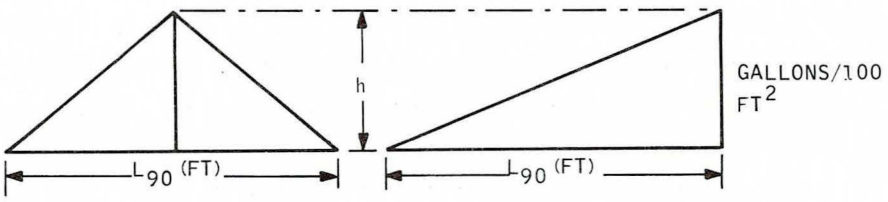

This concept assumes that there is a triangular approximation to the concentration length data generated for each drop. Inspection suggests that such an approximation exists. The triangular distribution assumption is useful (and will be employed) for illustrative purposes. The exact scaling of the height to concentration is not at issue since it would involve complex modeling. Furthermore, the Beta approximation is a better description of the process if such modeling were to be attempted. The transform scaling from the Beta parameter yields curves more of the form seen in the concentration/length curves. The recognition of the Beta-like nature of pattern distributions and the ability to reasonably define the distribution by its 90% length make this value a useful metric for use in analysis:

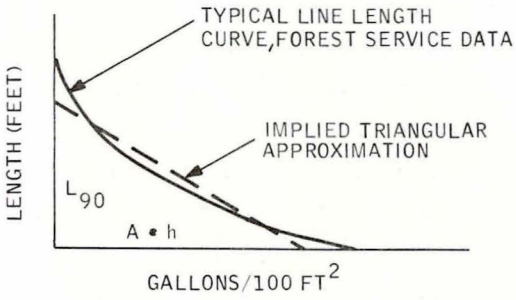

Area Above 1 gpc

Another measure of the pattern is the area greater than 1 gpc. This value provides a gross area measure in conjunction with the length to provide estimates of the meaningful part of the patterns. Attempts to associate a length and width measurement, using the standard deviation of the crossrange marginal, to estimate the average coverage were made. Such a relationship was not found.

Weighted Average Concentration

This measure led to the explicit calculation of the average concentration level in the pattern, estimated by

$$m = \frac{\Sigma ai \cdot ci}{\text{Total Area}}$$

where ai is the area at concentration level ci.

This measure gave a single estimator for the patterns to make comparisons in a linear statistical model.

Three-Dimensional Pattern Concentration Plots

Three-dimensional plots of the retardant concentration pattern for each drop were made using computer plotting techniques. To exploit the visual representation of the data, charts using these three-dimensional plots and patterned after the experimental layout have been constructed. These charts afford further visualization of the experiments. Effects of configuration, aircraft velocity, and drop altitude show in a clear manner.

One or more measures for each drop pattern have been listed on the charts. These include pattern length, area, average level of coverage, and distance traveled by the retardant from release to impact. Changes in the patterns are sensitive to changes in combinations of flow rate, frontal area of the bulk pattern, length of the fluid column opposing the airstream, aircraft velocity, and drop height. It is important to remember in interpreting the experiments that the retardant drop pattern is the result of the ground plane intercepting a transient or developing process. Inherently this generates a "noisy" signal to analyze, and a certain amount of variability can be expected to occur even under identical drop conditions.

Interpretive Graphics for Inner 90% Pattern Length

For all matrices, sketches of data associated with the inner 90% lengths of patterns were made to assist in analyzing these data. In many cases these sketches point out a trend when taken in combination with other analysis efforts. The inner 90% length statistic has been emphasized during the data analysis since it has been determined to be a significant descriptor of the distribution of retardant within the pattern. The inner 90% pattern length should not necessarily be interpreted in terms of length of pattern to specific coverage levels.

Linear Regression Statistics

Standard linear statistical analysis models have been used in the evaluation of each test matrix. Separate analyses for Phos-Chek and water drops were made. Regression analysis statistics for the inner 90% pattern length and other pattern measures are recorded in these tables. Linear regression equations, written as a function of the independent variables under investigation, are shown; 90% confidence interval values for the coefficients of these equations have been calculated. These values have been determined using the Student's (t-) distribution. To test for the significance of the regression coefficients, the F-ratio test was applied.

F-Ratio Test for Significance -- The F-ratio was calculated to determine the goodness of fit of the coefficients of the linear regression equation. The F-ratio is calculated by

$$\text{F-ratio} = \frac{\text{regression variance estimate}}{\text{remainder variance estimate}}$$

This calculated value is then compared with entries contained in standard F-distribution tables for the appropriate number of degrees of freedom associated with the numerator and denominator. These tables are for various levels of significance. If the calculated value is greater than the table entry, then the probability that the independent variables of the experiment are not correlated is less than the level of significance. The linear regression equation is the best estimator of the dependence of the variables, and the t-test confidence interval coefficients provide an estimate of the possible variance of the linear regression equation. It is possible to have a large F-ratio value, which strongly suggests the independent variables are correlated, and yet have large confidence interval coefficients. These large coefficients would suggest that the linear regression equation, although it is the best available estimator of variable dependence, may not be a particularly good estimator, even though the F-ratio indicates very strongly that the variables are correlated.

t-Test Confidence Interval Coefficients -- Confidence intervals about the coefficients of the linear regression equations have been calculated. These intervals are based on the Student's test (or t-test). The band values shown in the tables of this section are for a 90% confidence level. The linear regression coefficients and confidence band values in these tables are interpreted as follows: There is a 90% probability that the true linear coefficients lie within the indicated interval about that coefficient.

FLOW RATE (TIME OUT OF TANK) STUDIES (TEST MATRIX 1)

The objective of this set of experiments was to determine the effect of flow rate on pattern characteristics. The same tank was used for all drops in this series. Flow rate was varied by changing both the tank exit area and the door opening rate. The primary metric of concern associated with these two parameters is the total time to empty the tank. Water and Phos-Chek drops at 125 knots were made at both 150- and 300-foot drop heights.

Results of these tests establish a strong correlation between time out of tank and pattern length. Most of this length increase is due simply to the increased aircraft travel during the evacuation period, i.e., aircraft-induced spread. The retardant mass itself travels less distance as a function of flow rate or configuration – not resolved in this matrix. Significant increases in pattern length

can be achieved by increasing time out of tank. The Phos-Chek linear regression equation for inner 90% pattern length as a function of release altitude H and time out of tank t is:

$$y = 0.31445H + 79t + 246.5.$$

Thus, for example, for a fixed drop height, increasing the retardant time out of tank from 1 to 2 seconds will have the effect of increasing the pattern length by about 79 x 1 = 79 feet.

The F-ratio test of the regression analysis established a high level of significance.

Three-dimensional plots of the retardant concentration in the drops of this test series are shown in Figures 69 and 70. Clearly, increased time out of tank increases pattern length.

In Figure 71 both the linear regression lines and data points are shown for Phos-Chek. Again, the dependence of pattern length on time out of tank can be seen.

Statistics from the linear regression analysis are given in Tables 11, 12, and 13.

TANK CONFIGURATION STUDIES (TEST MATRIX 2)

The objective of this test series was to determine the effect of tank configuration on pattern characteristics. Six different tank configurations were tested as sketched at the top of Figures 72 and 73. A constant head height was maintained for each of the tested configurations. Water and Phos-Chek drops were made from both 150 and 300 feet at drop speeds of both 125 and 160 knots. A near-constant time out of tank was maintained for all drops, thereby diminishing the effect of this factor on pattern length.

In general, long, narrow tanks yield longer patterns than square tanks or short, fat tanks. This effect is more pronounced at 160 knots than at 125 knots (which is consistent with test results achieved during the drop speed test series).

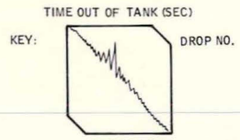

150-FOOT DRO

2.4 | 2.2 | 1.4 | 1.25 | 1.16 | .78 | .98 | .61

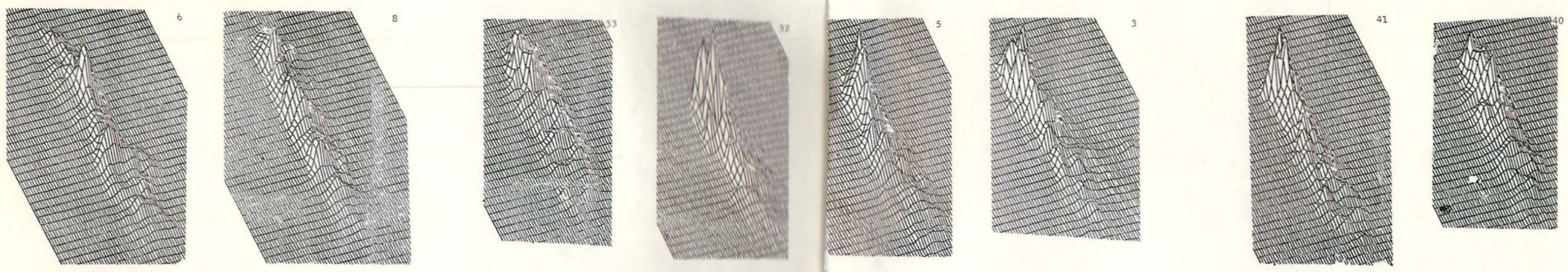

300-FOOT DR

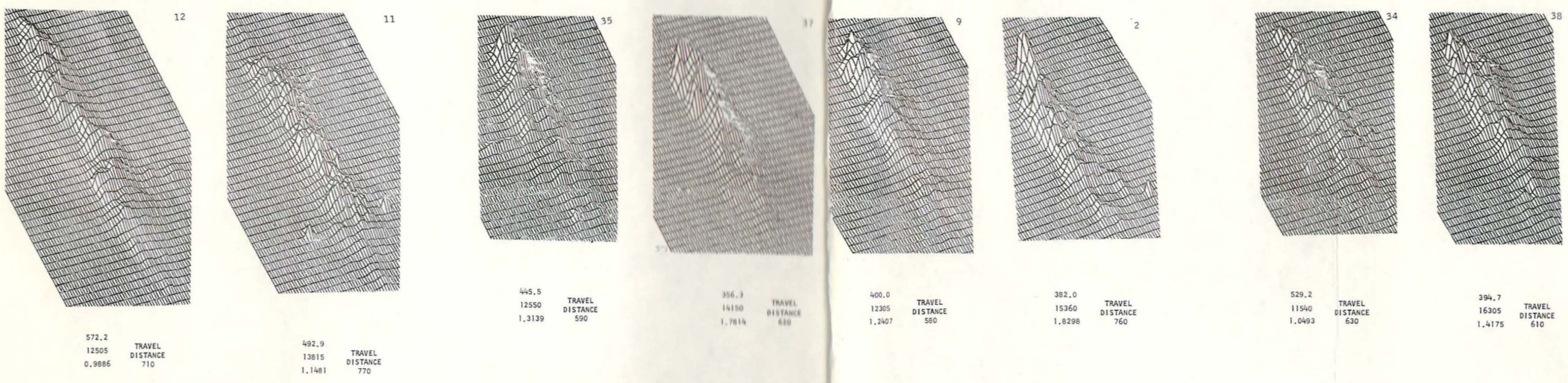

Figure 69. Three-Dimensional Retardant Concentration from Flow Rate Studys-Chek

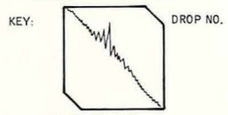

150-FOOT DROP HEIGHT

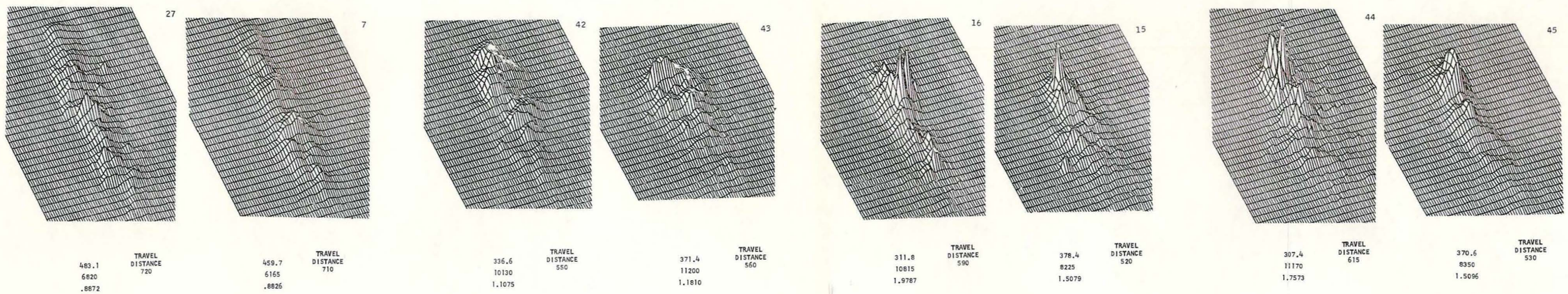

300-FOOT DROP HEIGHT

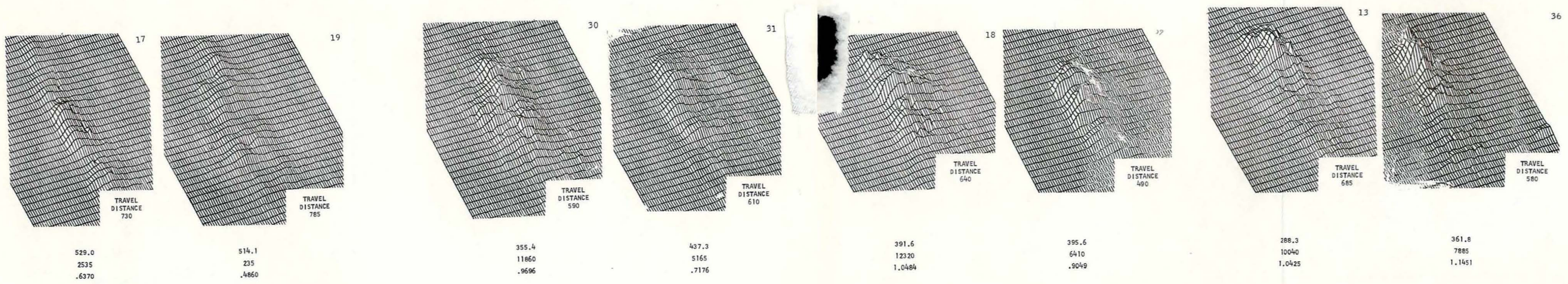

Figure 70. Three-Dimensional Plots of Retardant Concentration from Flow Rate Study - Water

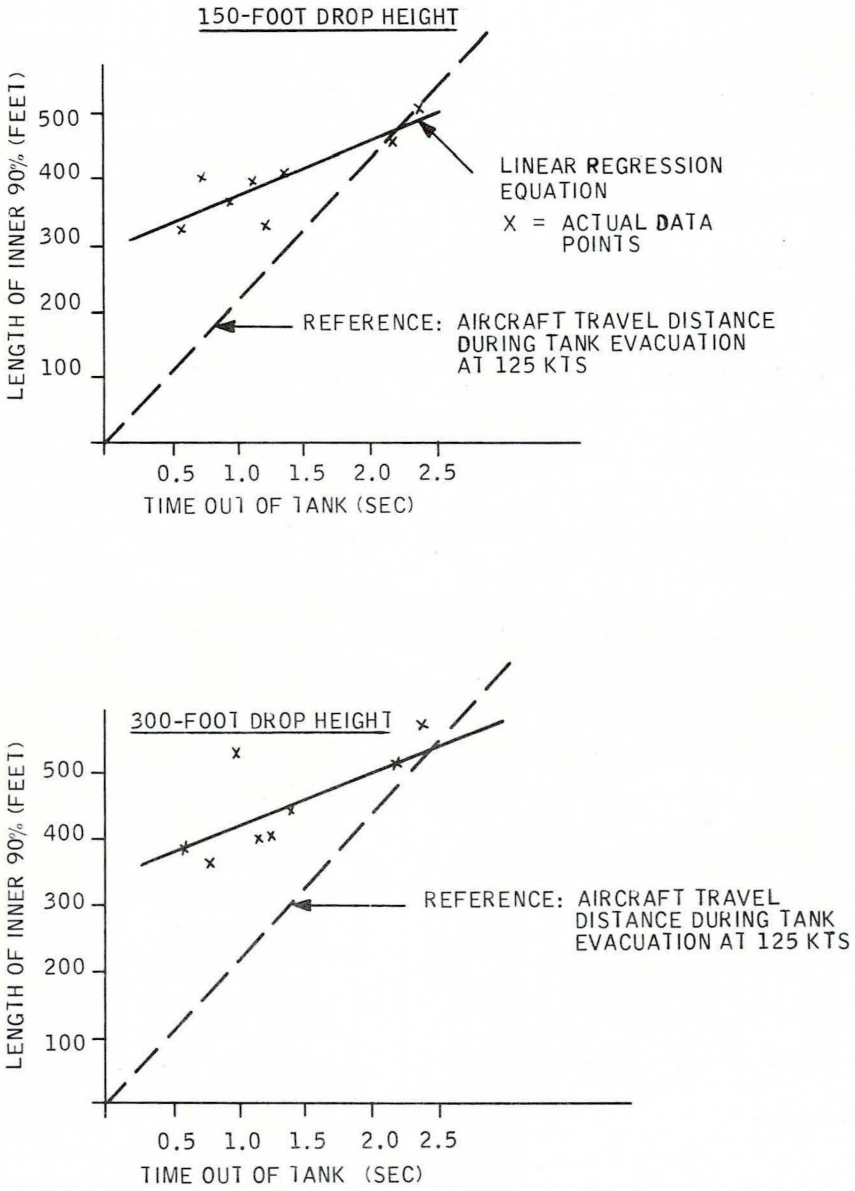

Figure 71. Flow Rate Study Results for Phos-Chek Drops at 150 and 300 Feet

Table 11. Linear Regression Analysis Data - Test Matrix 1, Weighted Average

Phos-Chek

Linear Regression Equation: $y - 1.733 = -0.00516 (H - 225) - .4237 (t - 1.348)$

Degrees of Freedom:

Regression:	2
Remainder:	13
Total:	15

90% Confidence Band Values for Linear Regression Coefficients

Altitude:	-0.00516 ± 0.00558
Time:	-0.4237 ± 0.2633

F Ratio for 2, 13 Degrees of Freedom: 13.45

Water

Linear Regression Equation: $y - 1.110 = -0.003217 (H - 225) - 0.4464 (t - 1.348)$

Degrees of Freedom:

Regression:	2
Remainder:	13
Total:	15

90% Confidence Band Values for Linear Regression Coefficients

Altitude:	-0.003217 ± 0.001609
Time:	-0.4464 ± 0.1220

F Ratio for 2, 13 Degrees of Freedom: 37.98

Table 12. Linear Regression Analysis Data - Test Matrix 1, Area

Phos-Chek

Linear Regression Equation: $y - 13222 = 4.588 (H - 225) - 632.5 (t - 1.348)$

Degrees of Freedom:

Regression:	2
Remainder:	13
Total:	15

90% Confidence Band Values for Linear Regression Coefficients

Altitude:	4.588 ± 14.772
Time:	-632.5 ± 1119

F Ratio for 2, 13 Degrees of Freedom: .9119

Water

Linear Regression Equation: $y - 8083 = -13.69 (H - 225) - 4172 (t - 1.348)$

Degrees of Freedom:

Regression:	2
Remainder:	13
Total:	15

90% Confidence Band Values for Linear Regression Coefficients

Altitude:	-13.69 ± 20.70
Time:	4172 ± 1569

F Ratio for 2, 13 Degrees of Freedom: 12.96

Table 13. Linear Regression Analysis Data - Test Matrix 1, Length of Inner 90%

Phos-Chek

Linear Regression Equation: $y - 423.2 = 0.31225 (H - 225) + 78.99 (t - 1.348)$

Degrees of Freedom:

Regression:	2
Remainder:	13
Total:	15

90% Confidence Band for Linear Regression Coefficients

Altitude:	0.31225 ± 0.4672	; (0.31225 ± 0.4672)
Time:	78.99 ± 35.40	; (43.59, 114.39)

F Ratio for 2, 13 Degrees of Freedom: 9.711

Water

Linear Regression Equation: $y - 393.3 = 0.2118 (H - 225) + 105.8 (t - 1.348)$

Degrees of Freedom:

Regression:	2
Remainder:	13
Total:	15

90% Confidence Band Values for Linear Regression Coefficients

Altitude:	0.2118 ± 0.2803	; (-0.068, 0.492)
Time:	105.8 ± 21.2	; (84.6, 127.0)

F Ratio for 2, 13 Degrees of Freedom: 41.36

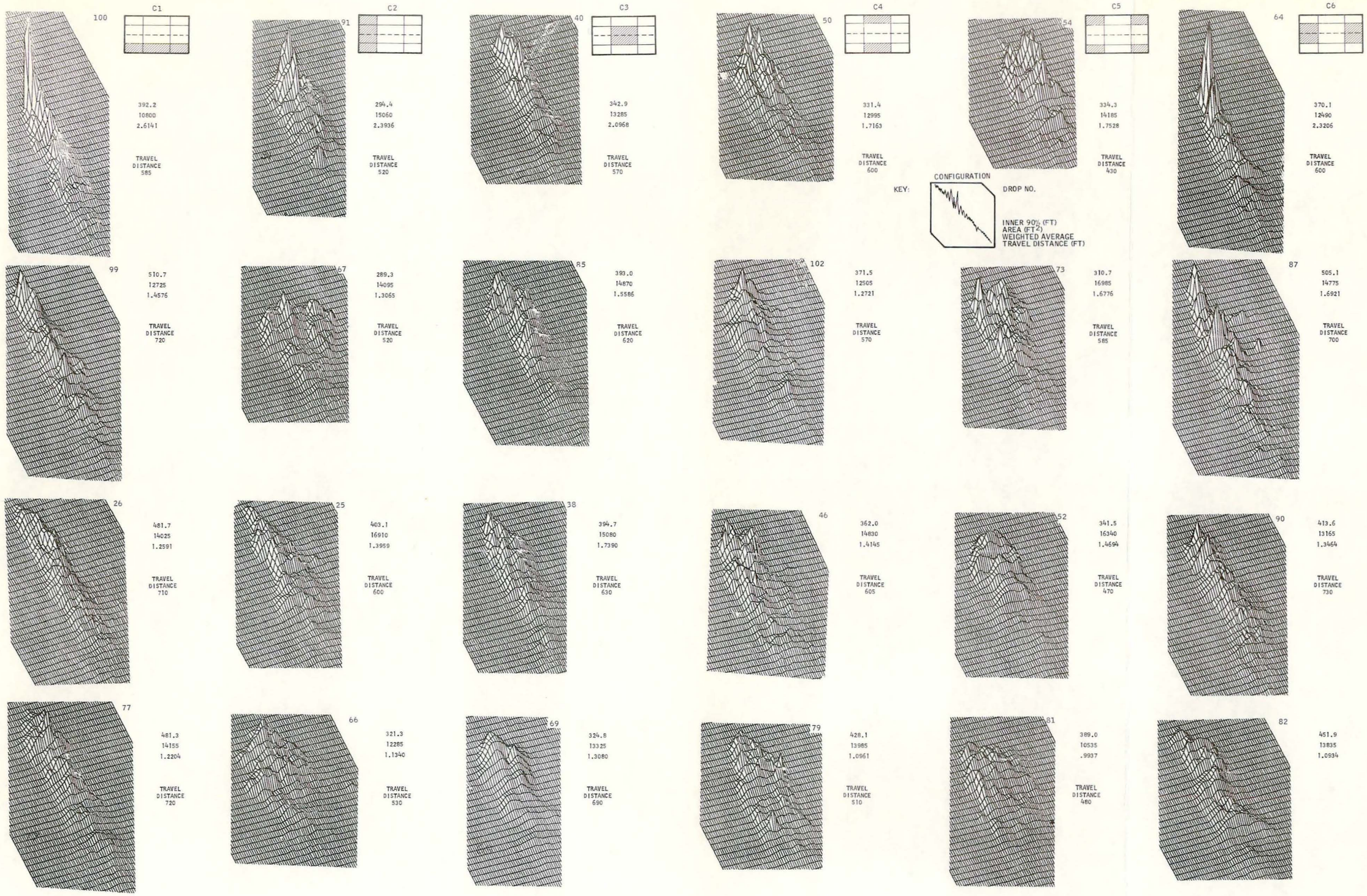

Figure 72. Three-Dimensional Plots of Retardant Concentrations from Tank Configuration Studies - Phos-Chek

CONFIGURATION STUDY

(500)

125 KNOTS

150 FT.

160 KNOTS

KEY:

CONFIGURATION

DROP NO.

INNER 90% (FT)
AREA (FT^2)
WEIGHTED AVERAGE
TRAVEL DISTANCE (FT)

300 FT.

125 KNOTS

160 KNOTS

INNER 90%
AREA
WT. AVERAGE

	C1	C2	C3	C4	C5	C6
125 KNOTS, 150 FT.	21 373.2 12030 1.7721 TRAVEL DISTANCE 535	29 267.2 11595 1.9801 TRAVEL DISTANCE 460	44 307.4 11170 1.7573 TRAVEL DISTANCE 530	104 302.4 10105 1.0766 TRAVEL DISTANCE 510	53 323.1 10930 1.0445 TRAVEL DISTANCE 635	63 444.9 9170 1.9538 TRAVEL DISTANCE 575
160 KNOTS, 150 FT.	101 371.5 9545 2.0834 TRAVEL DISTANCE 710	92 317.1 12420 1.3869 TRAVEL DISTANCE 540	89 TRAVEL DISTANCE 610	103 331.4 10005 1.0500 TRAVEL DISTANCE 590	74 243.3 13520 1.6380 TRAVEL DISTANCE 610	86 365.3 10185 1.5537
125 KNOTS, 300 FT.	23 494.7 10720 .9331 TRAVEL DISTANCE 600	24 423.9 12745 1.1143 TRAVEL DISTANCE 455	39 288.3 10040 1.0425 TRAVEL DISTANCE 580	47 381.4 6950 .8012 TRAVEL DISTANCE 620	62 343.4 13235 1.0378 TRAVEL DISTANCE 470	49 361.2 7530 .9060 TRAVEL DISTANCE 750
160 KNOTS, 300 FT.	78 481.3 3420 .6697 TRAVEL DISTANCE 650	68 316.3 5595 .7862 TRAVEL DISTANCE 660	70 326.9 7120 .8783 TRAVEL DISTANCE 620	80 461.3 3150 .6808 TRAVEL DISTANCE 480	84 313.1 4675 .7902 TRAVEL DISTANCE 630	83 422.8 5975 .8076 TRAVEL DISTANCE 700

Figure 73. Three-Dimensional Plots of Retardant Concentrations from Tank Configuration Studies - Water

The three-dimensional plots of this test series are shown in Figures 72 and 73. Examination of these plots reveals a trend toward configuration geometry preservation in the pattern geometry.

Figures 74 through 77 show pattern-length data for this test series. Figures 76 and 77 display the trend of increased length with increasing tank length-to-width ratio (L/W). In Figure 77 there appears to be anomalies in this trend. However, it is believed these anomalies are due to the increased variability of pattern characteristics achieved with water drops as compared with Phos-Chek drops.

Figure 78 shows least-square fits of the L/W provided by configurations C1, C2 and C3. It is noted here, however, that these predictive equations did not work well for predicting inner 90% line lengths achieved with the 920-gallon load size configuration tests (Test Matrix 3).

In Figure 78, note that the difference between the regression lines at 160 knots are similar with respect to altitude and can probably be grouped. Length 90% = 26.4 L/W + 301. By contrast the differences at 125 knots of about 100 feet would tend to indicate some incompletion of breakup at 150 foot drop heights. If we assume that the length constant for the 125-knot case is appropriately that established at the higher altitude, the slope can probably be averaged, yielding: length 90% = 12.3 L/W + 394.

If we remove the range due to aircraft travel during the release increment, the two sets of data could be compared directly. This is 178 feet at 160 knots and 140 feet at 125 knots.

$$L_{(160)} = 26.4\ L/W + 123$$

$$L_{(125)} = 12.3\ L/W + 254$$

When regressions are done as a factor of length (Figure 79), we obtain a somewhat better predictor of pattern performance when compared with results from other matrices. But contrast regressions as a function of width alone do not yield reasonable predictions for other matrix uses. It appears, therefore, that length is a more significant parameter than width.

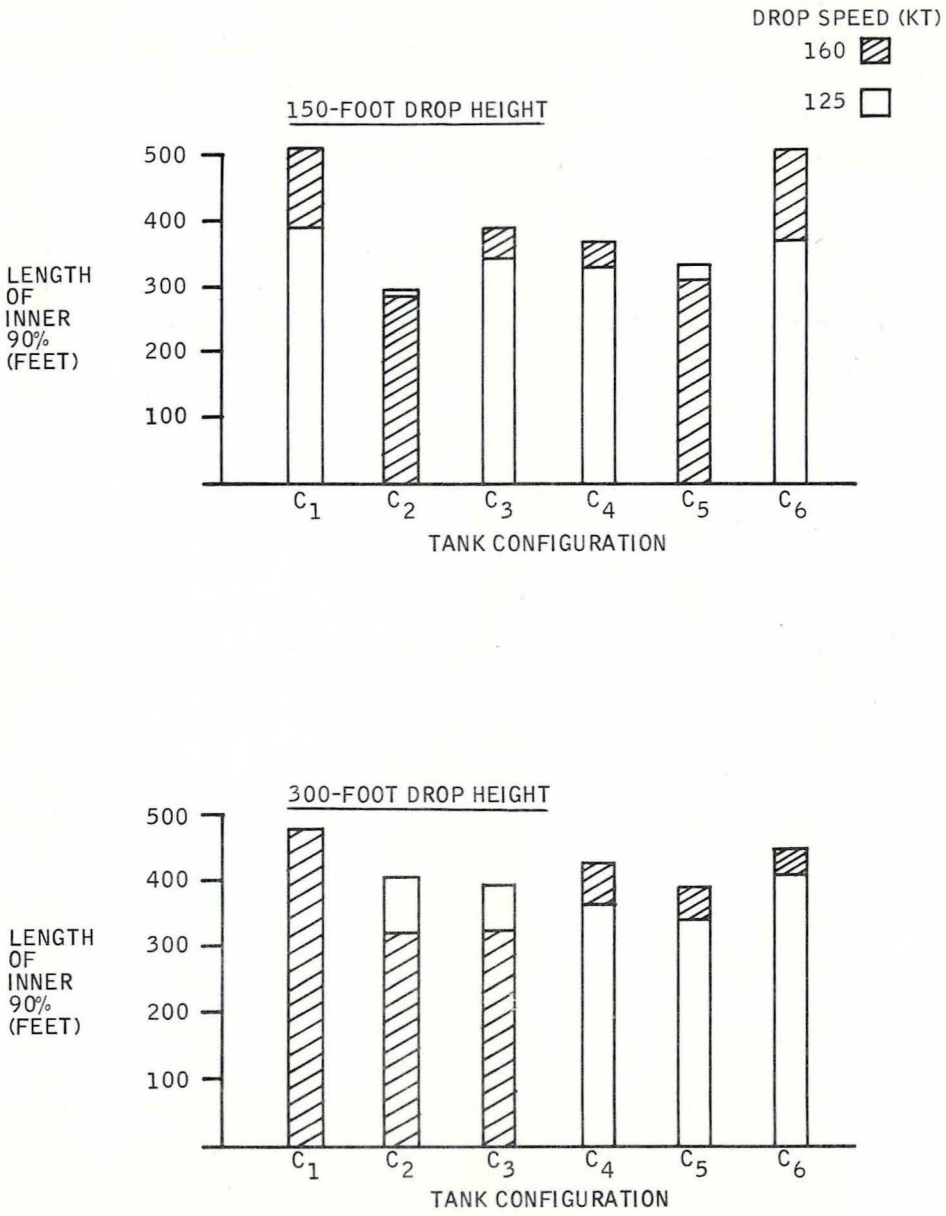

Figure 74. Pattern Length versus Tank Configuration at Two Drop Heights and Two Drop Speeds - Phos-Chek

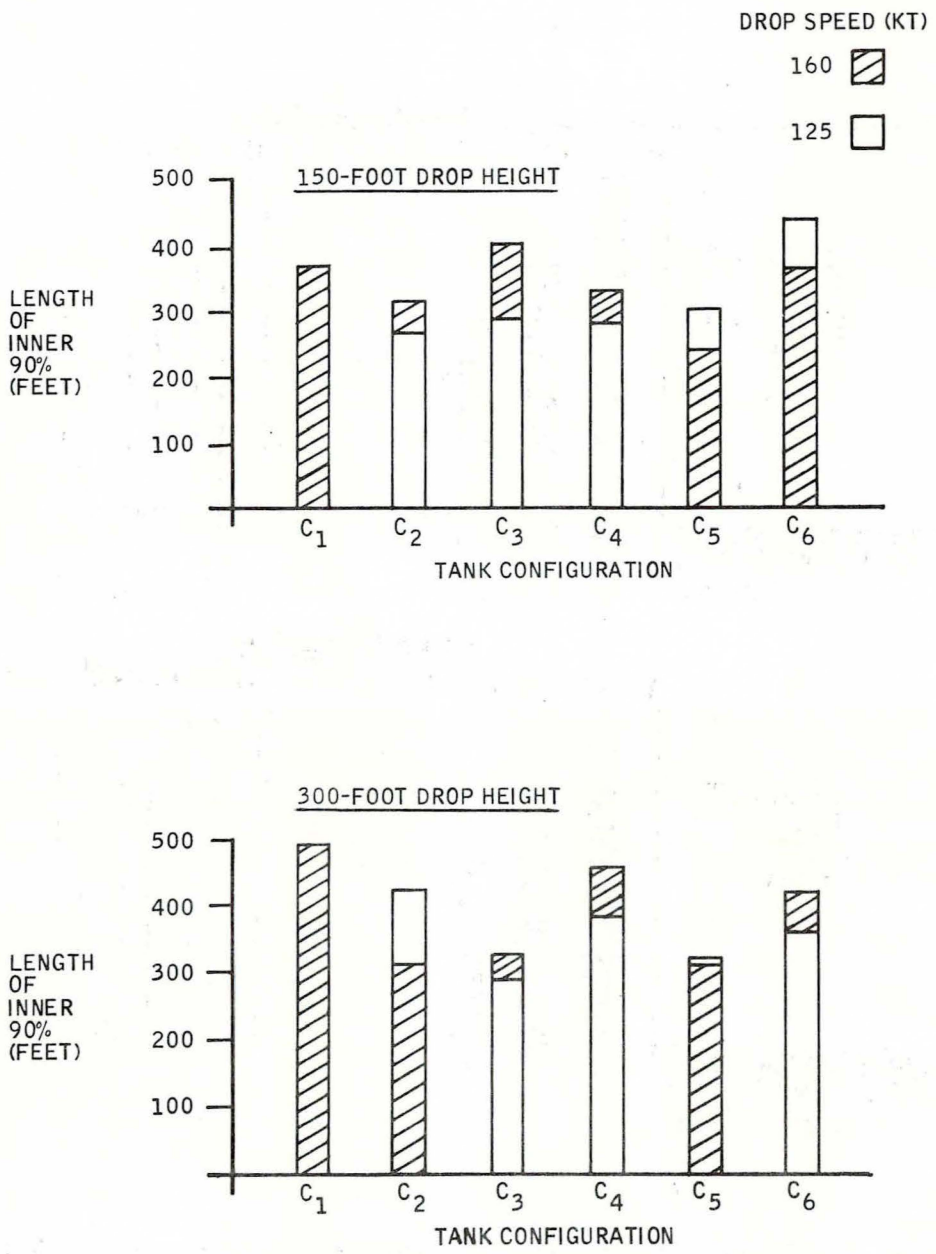

Figure 75. Pattern Length versus Tank Configuration at Two Drop Heights and Two Drop Speeds - Water

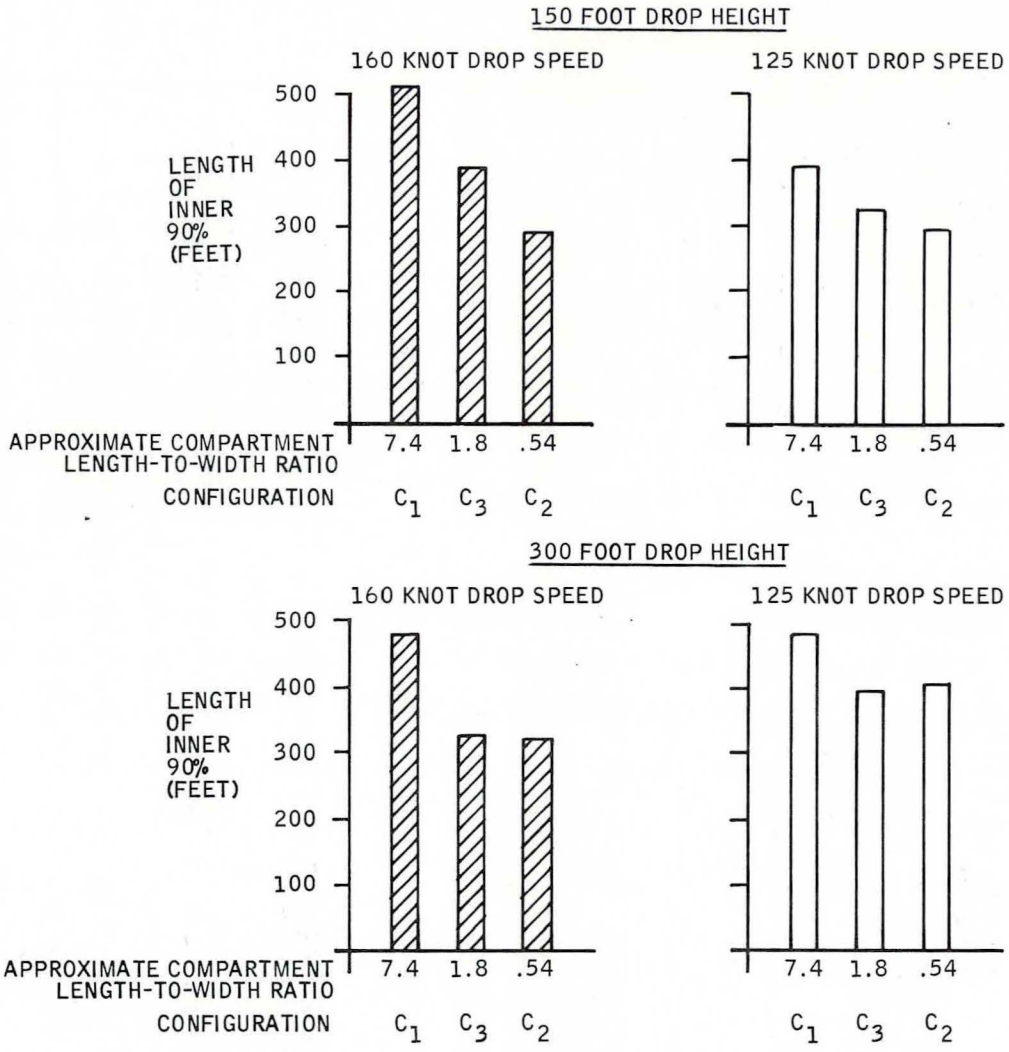

Figure 76. Pattern Length versus Compartment Length-to-Width Ratio for Two Drop Heights and Two Drop Speeds - Phos-Chek

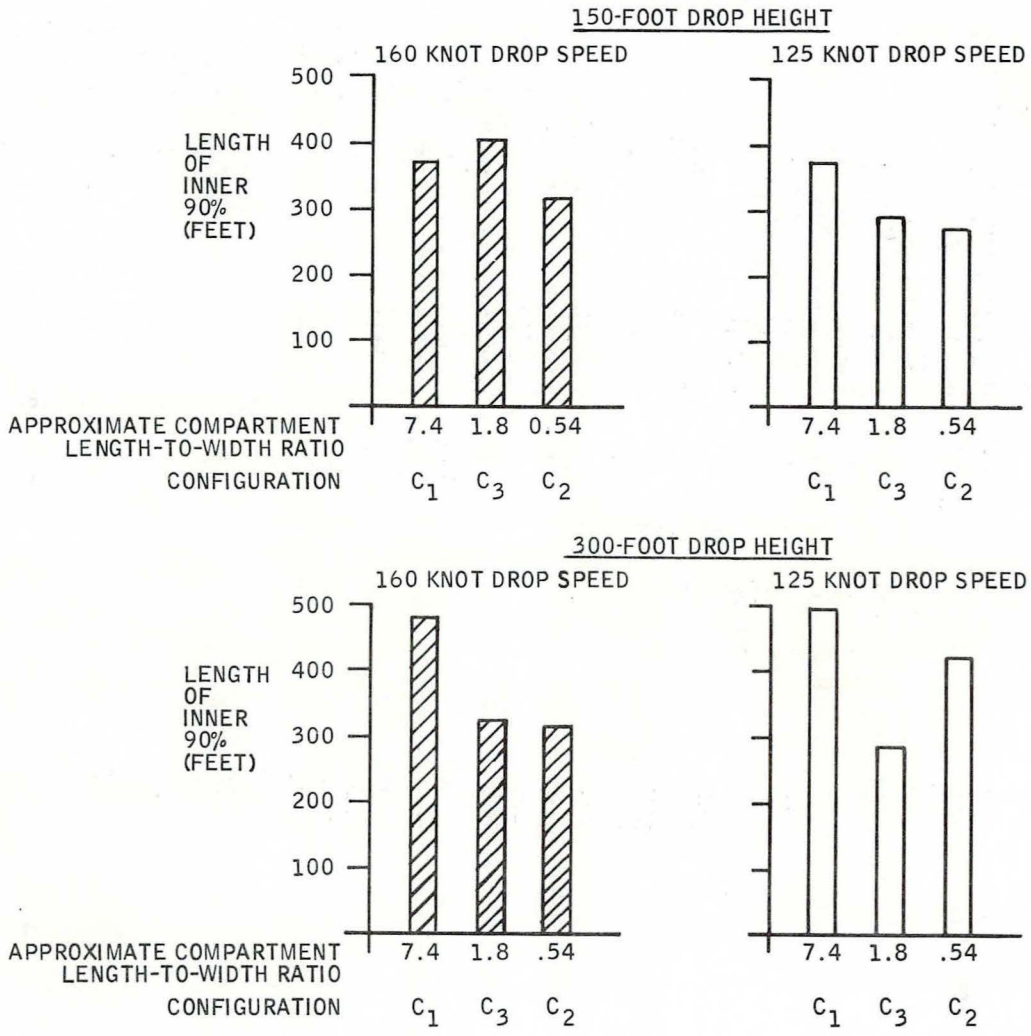

Figure 77. Pattern Length versus Compartment Length-to-Width Ratio for Two Drop Heights and Two Drop Speeds - Water

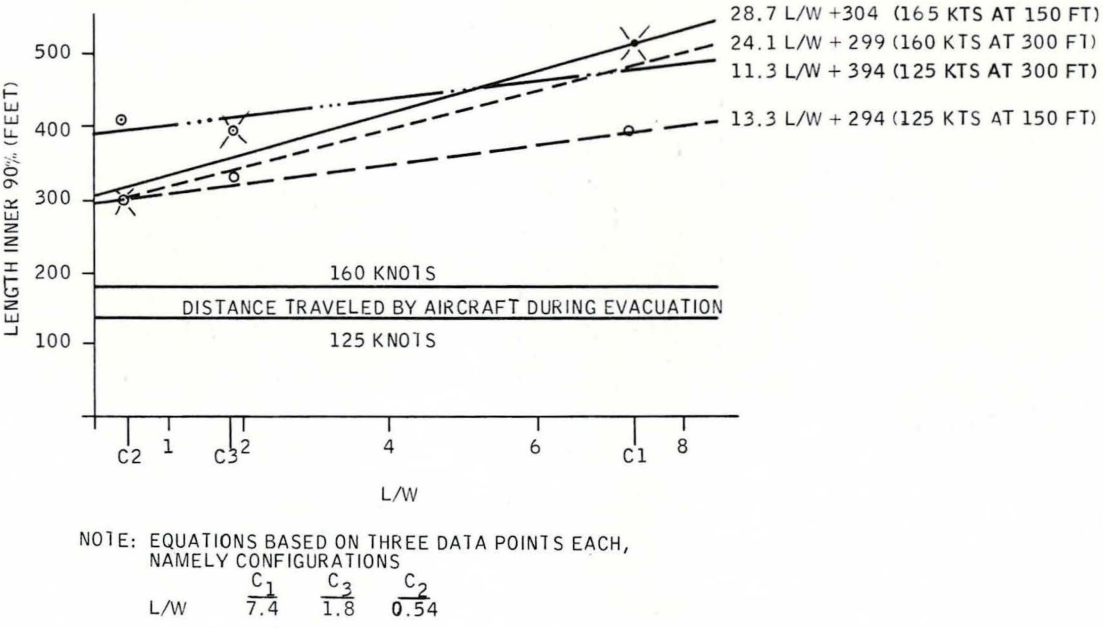

NOTE: EQUATIONS BASED ON THREE DATA POINTS EACH, NAMELY CONFIGURATIONS

	C_1	C_3	C_2
L/W	7.4	1.8	0.54

Figure 78. Least-Squares Fit of Length of Inner 90% as a Function of Compartment Length-to-Width Ratio

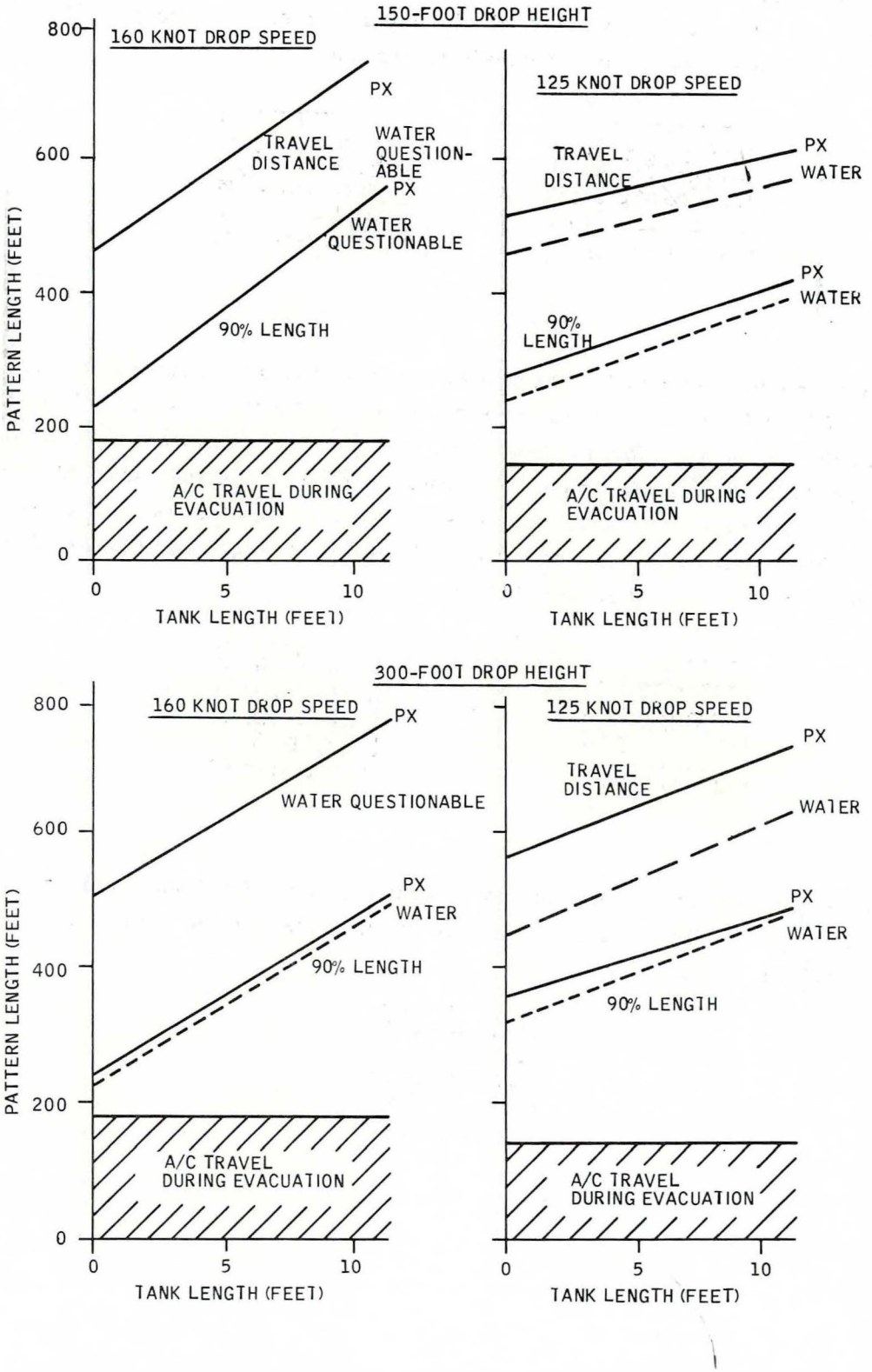

Figure 79. Pattern Length as a Function of Compartment Length

An anomoly observed in this test series is the length achieved by configuration C6. From an L/W standpoint of the filled compartments, this configuration is similar to C3 except for a forward-to-aft separation:

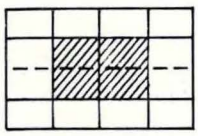

CONFIGURATION C3

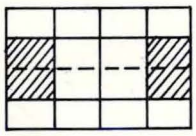

CONFIGURATION C6

However the length achieved with C6 in all cases was greater than that achieved with C3 (L/W = 2) and in many cases was near that achieved with C1 (L/W = 8). No plausible explanation for this phenomenon has been determined. Configuration C4 where the lateral compartment separation from an L/W standpoint of the filled compartments is the same as C3 did not exhibit such anomolous performance. From a 150-foot altitude, C3 tended to yield greater length, while from a 300 foot altitude C4 tended to yield greater length.

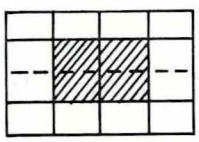

CONFIGURATION C3

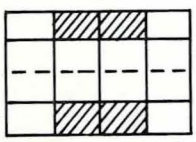

CONFIGURATION C4

In comparison with other configurations, configuration C5 did not exhibit good line-building capability. This can also be visually observed in the three-dimensional plots of the patterns.

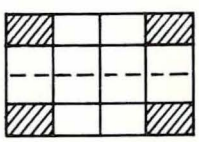

CONFIGURATION C5

920-GALLON LOAD SIZE CONFIGURATION (TEST MATRIX 3)

The objective of this test series was to assess the effect of a higher gallonage configuration on pattern characteristics. Configurations C7, C8, C9 and C10, were tested with various door rates. Sketches of these configurations are included on Figures 80 and 81. Most test drops were from a 300-foot altitude. Both Phos-Chek and water drops were made.

Results from these tests are mixed insofar as identifying a preferred configuration for achieving pattern length. Three-dimensional plots of the test drops are shown in Figures 80 and 81. With configuration C7, which has a larger L/W than the other configurations tested in this series, Phos-Chek achieved longer patterns than the others tested, as can be seen in Figure 82. However, this trend was not preserved with water, as can be seen in Figure 83. As was the case with a 460-gallon load size, the forward-to-aft configuration represented by configuration C10 exhibited good line-building capabilities with both Phos-Chek and water. As with the 460-gallon case, no physical explanation of this phenomenon has been found.

Examination of the three-dimensional plots indicates that configuration geometry is somewhat preserved in pattern geometry.

When the results are viewed in total, there is an indication that a large tank size (920 gallons) dominates or masks pattern characteristics attributable to other tank parameters.

It is noted that a relatively small number of drops were made during this test series.

Statistics from the regression analysis are given in Table 14.

HEAD HEIGHT EXPERIMENT (TEST MATRIX 4)

The objective of this test series was to determine the effect of head height on pattern characteristics. Head heights of 2/3, 1/2 and 1/4 were tested in this series. For each head height, a constant quantity (460 gallons) of retardant was dropped. The constant quantity was maintained by varying tank configuration. The configurations tested and three-dimensional plots of this test series are shown in Figures 84 and 85.

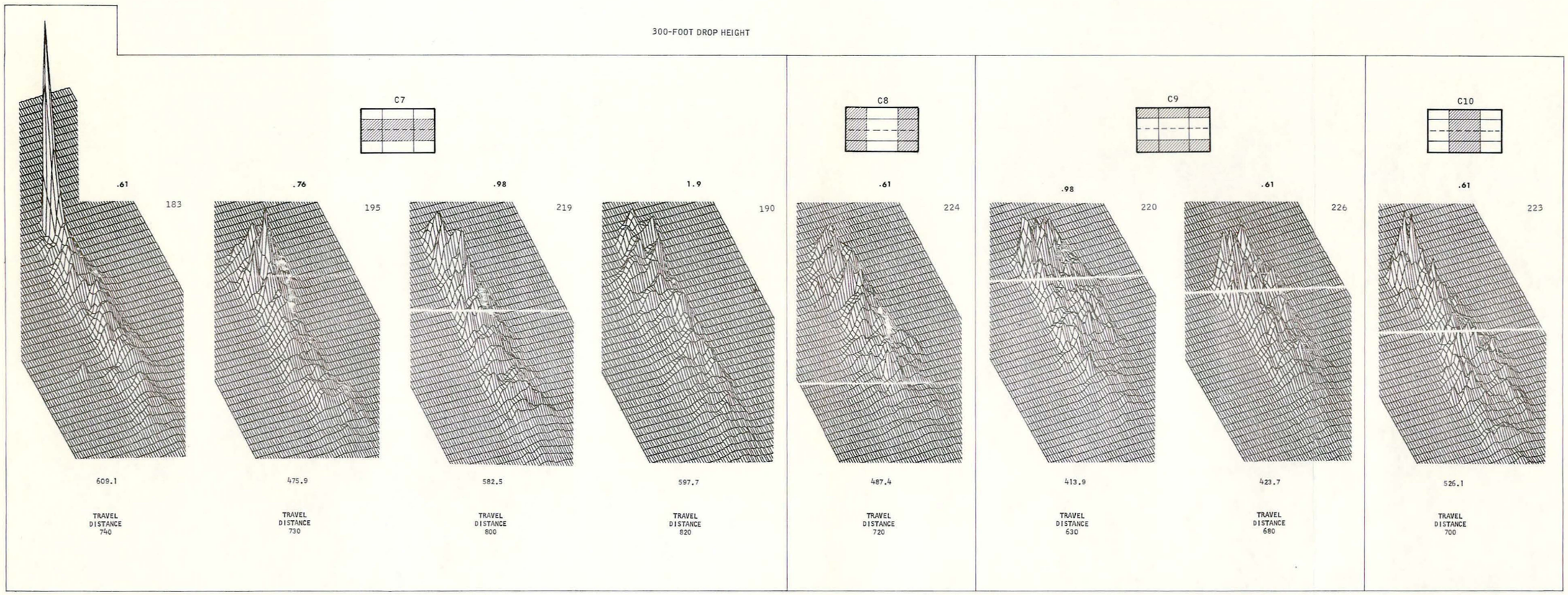

Figure 80. Three-Dimensional Plots of Retardant Concentration from 920-gallon Load Size Studies, 300-foot Drop Height - Phos-Chek

300-FOOT DROP HEIGHT

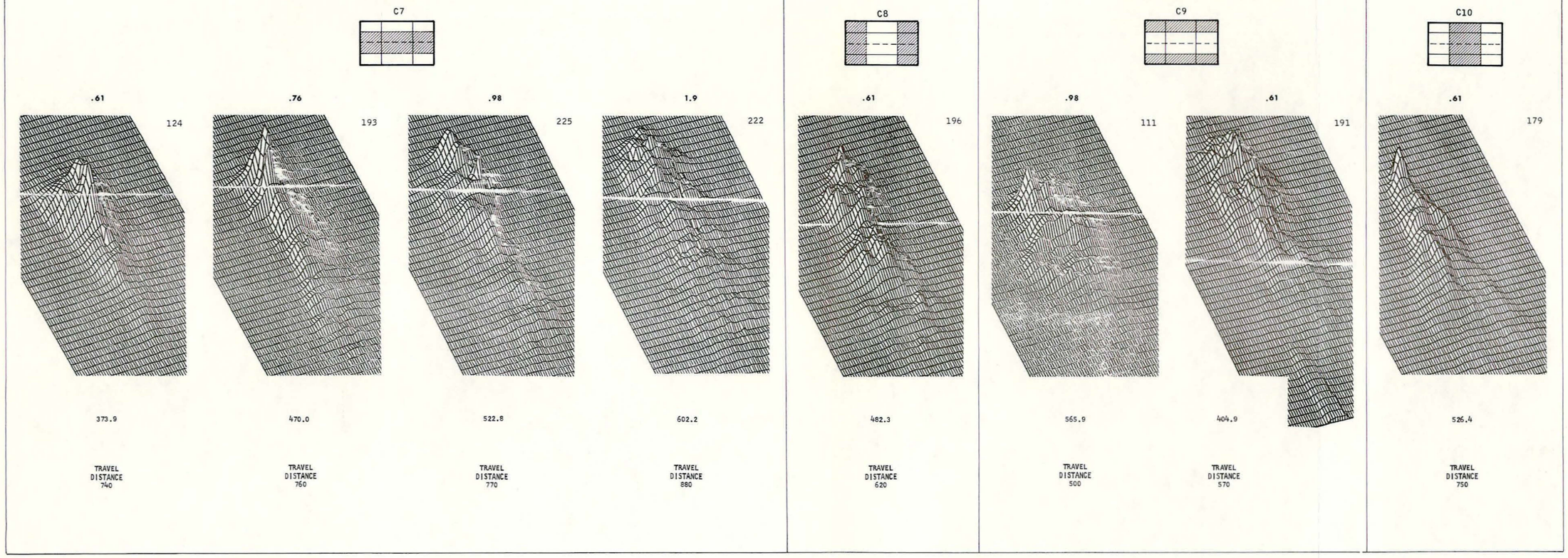

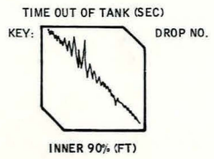

Figure 81. Three-Dimensional Plots of Retardant Concentration from 920-gallon Load Size Studies, 300-foot Drop Height - Water

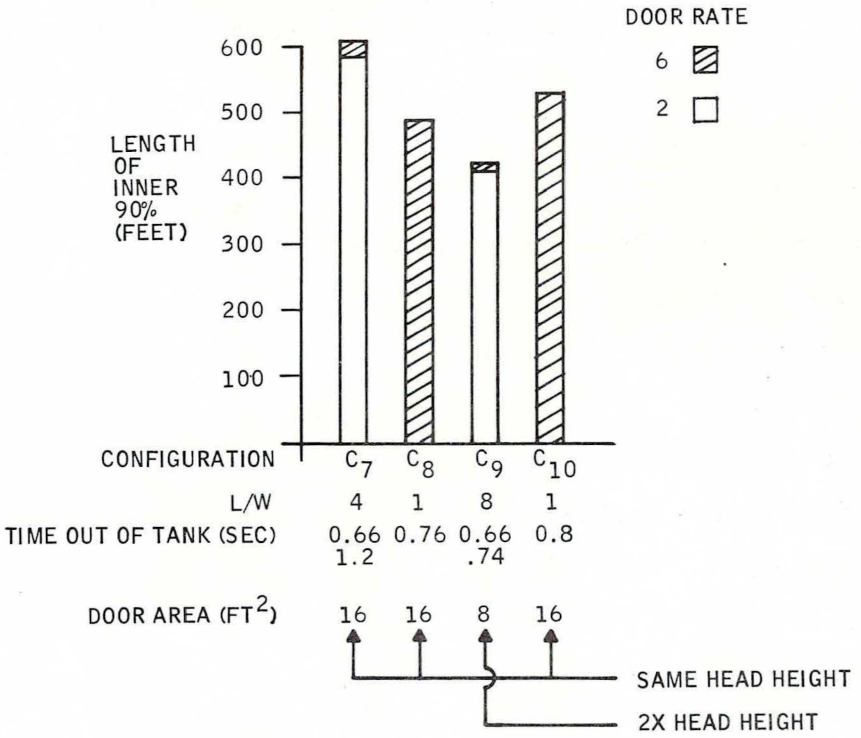

Figure 82. Pattern Length versus Tank Configuration (920-gallon load) at 300-foot Drop Height and Two Door Rates - Phos-Chek

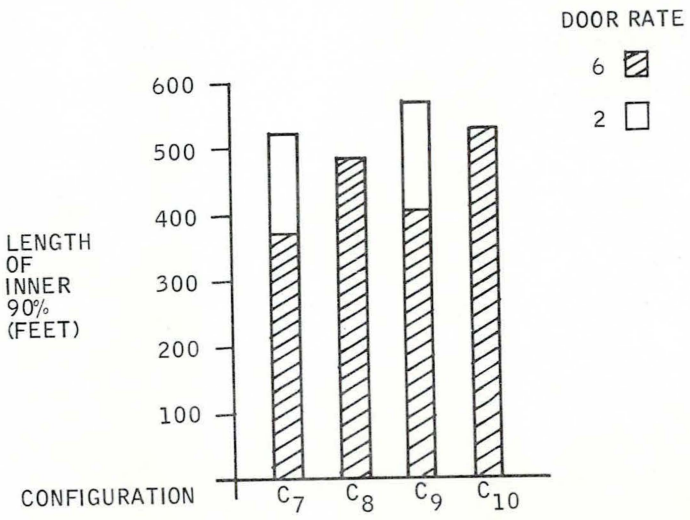

Figure 83. Pattern Length versus Tank Configuration (920-gallon load) at 300-Foot Drop Height and Two Door Rates - Water

Table 14. Linear Regression Analysis Data - Test Matrix 3, Length of Inner 90%

Phos-Chek

Linear Regression Equation: Y - 566.3 = 32.8 (t - 1.06)

Degrees of Freedom:

Regression:	2
Remainder:	1
Total:	3

90% T Confidence Band Values for Linear Regression Coefficients

Altitude:	-
Time:	32.8 ± 635.2

F Ratio for 2, 1 Degrees of Freedom: 0.053

Water

Linear Regression Equation: y - 492.2 = 149.2 (t - 1.06)

Degrees of Freedom:

Regression:	2
Remainder:	1
Total:	3

90% T Confidence Band Values for Linear Regression Coefficients

Altitude:	-
Time:	149.2 ± 452.7

F Ratio for 2, 1 Degrees of Freedom: 21.6

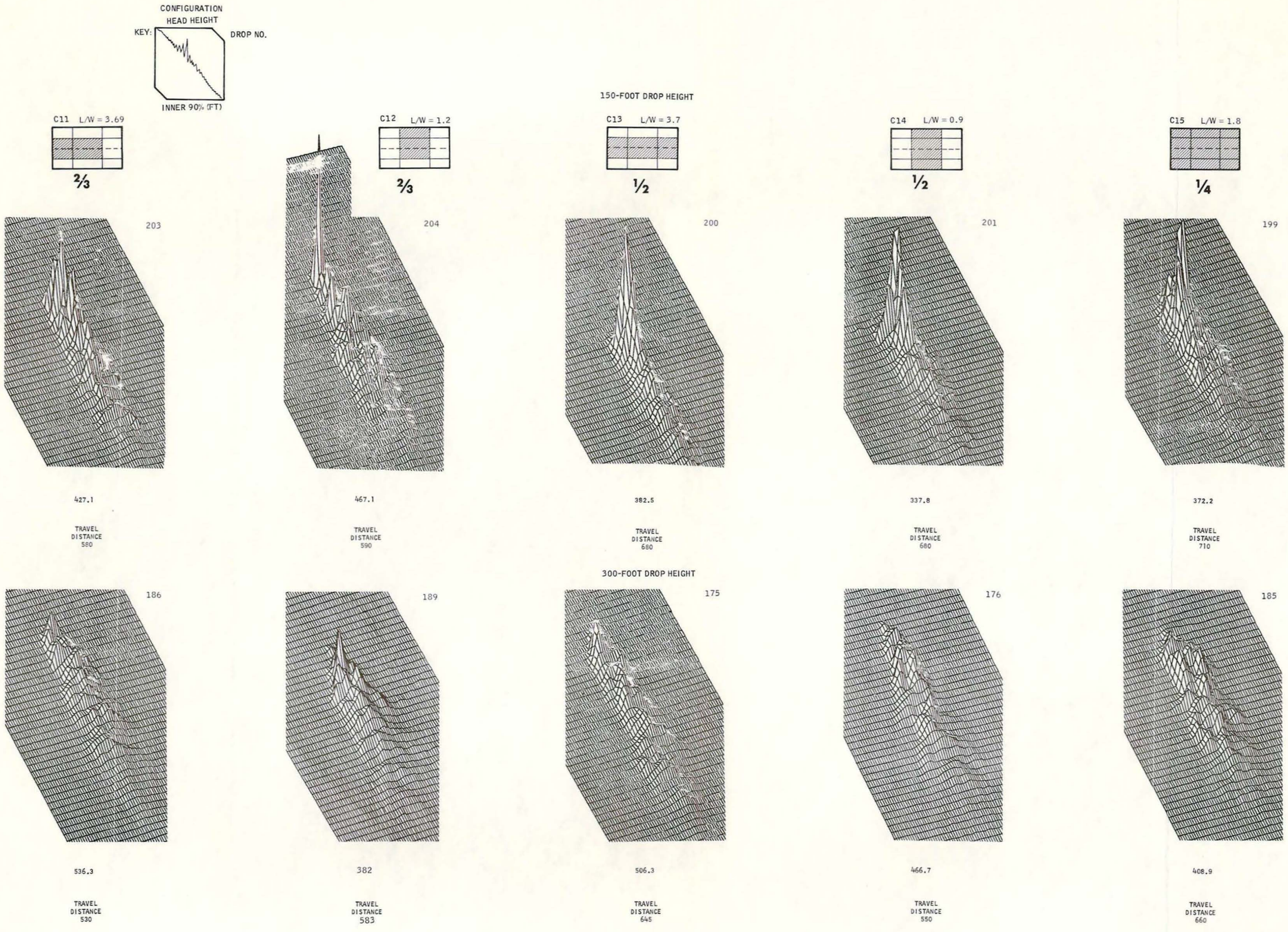

Figure 84. Three-Dimensional Plots of Retardant Concentration from Head-Height Experiment - Phos-Chek

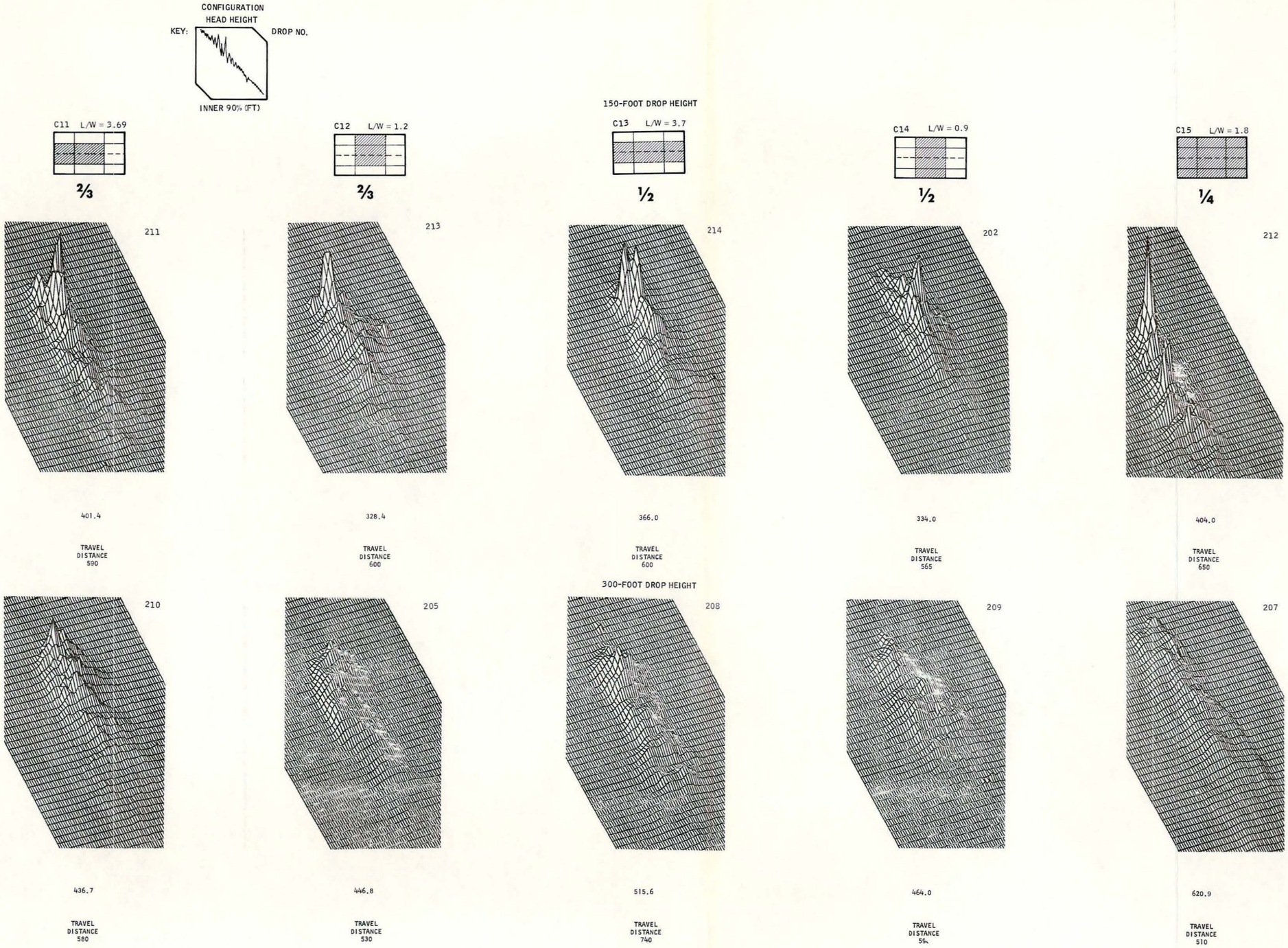

Figure 85. Three-Dimensional Plots of Retardant Concentration from Head-Height Experiment - Water

A result of this test series is that, with Phos-Chek a decreasing pattern length occurs with decreasing head height. This trend is not evident in the water drops, and, in fact, the opposite occurs. It was thought the trend with Phos-Chek might have been due to decreased time out of tank. However, an examination of the times established that, from a length-of-line viewpoint, these times were nearly constant (0.54 - 0.68 second). When line length as a function of time was calculated, using the predictive equations developed from Test Matrix 1, and compared with the data and associated predictive equations from this test series the data in Figure 86 resulted. Within the constraints of the two particular data sets forming the basis of this comparison, head height had a more important effect than time out of tank. However, it is again pointed out that the times out of tank were nearly constant, and that this trend was not present with the water tests. Test results for water are shown in Figure 87.

Another factor examined as part of this experiment was the possible effect of configuration on the results of this test series and in particular the L/W of the tank. Results of this examination are shown in Figure 88.

The predictive equation based on L/W from Test Matrix 2 is not a good predictor of the results achieved during the head height test series. As with the configuration test results, water drops from low altitude tend to fall within the retardant set. At higher altitudes, water drops become significantly longer.

Predictions based on tank length alone, show a generally better correspondence to the set, as shown in Figure 89. One drop with configuration C12 appears abnormal with respect to the remainder of the set.

Statistics from the linear regression analysis conducted on Test Matrix 4 are given in Table 15. A higher level of significance was obtained with the water tests than with the Phos-Chek tests.

LOAD SIZE TEST SERIES (TEST MATRIX 5)

The objective of this test series was to determine the effect of load size on pattern characteristics. Drops ranging from 230 gallons to 1840 gallons were made for both water and Phos-Chek. Drops were made from both 150 and 300 feet. The configurations used for the test drops are shown in Figures 90 and 91. All drops were made at 125 knots.

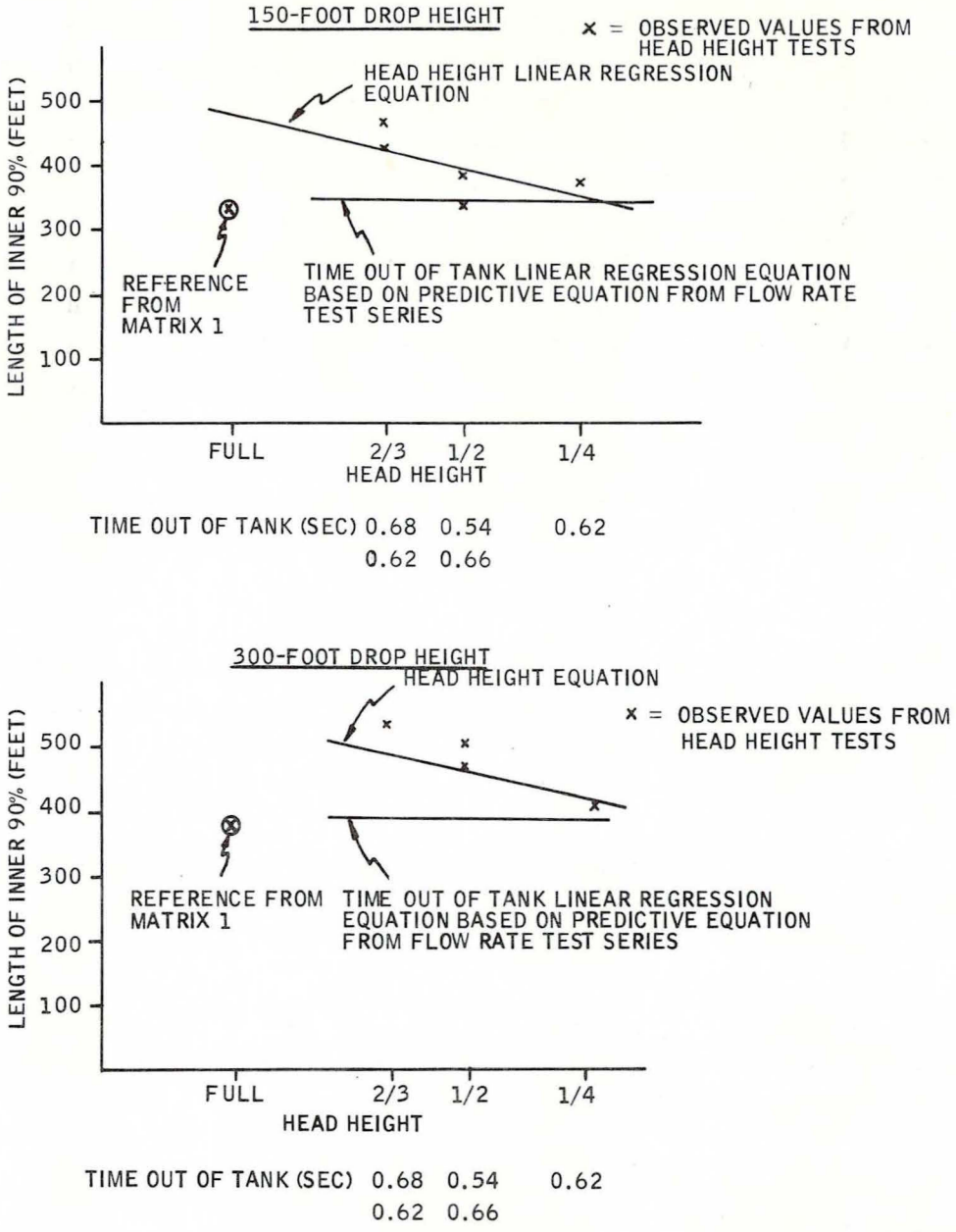

Figure 86. Pattern Length versus Head Height and Time-Out-of Tank - Phos-Chek

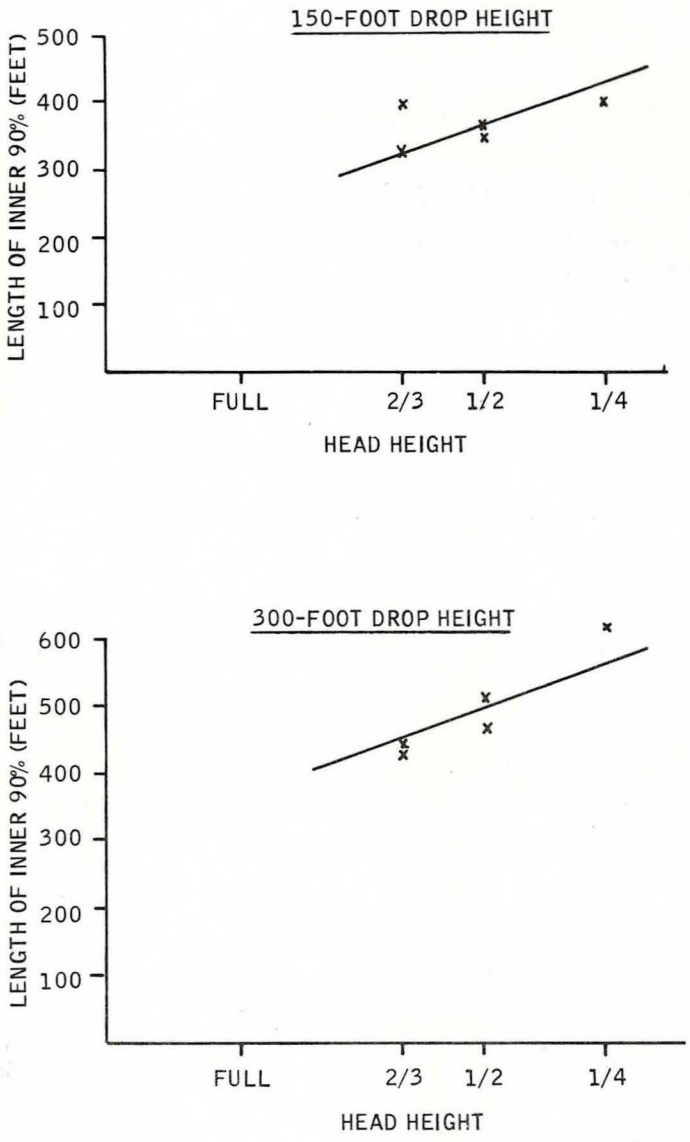

Figure 87. Pattern Length versus Head Height and Time-Out-of Tank - Water

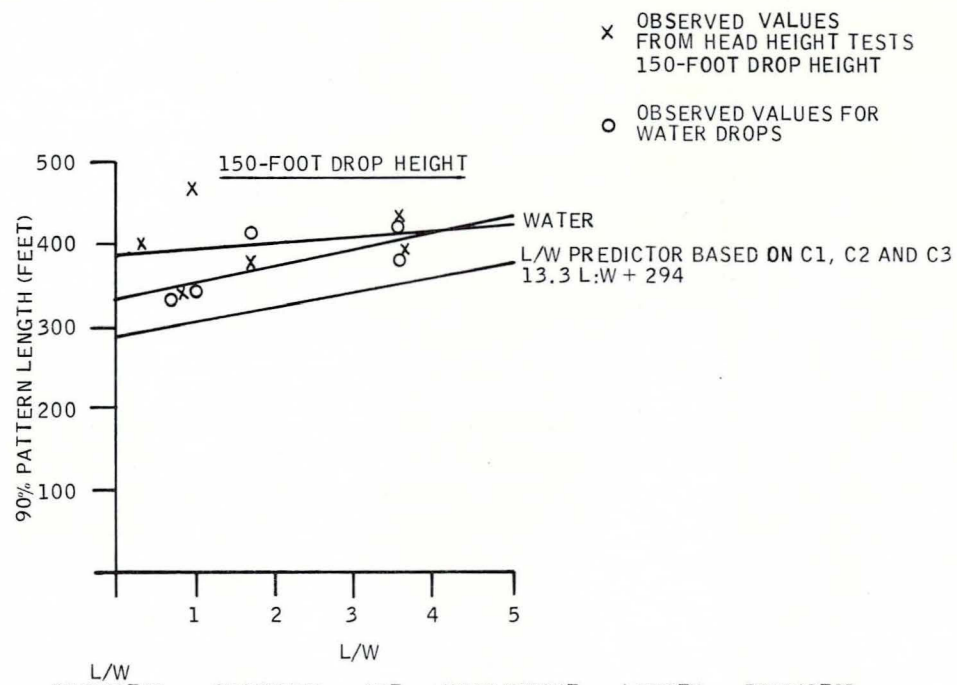

CONFIG	L/W	L/W PREDICTOR	OBSERVED	ΔFT	HEAD HEIGHT	LENGTH	PREDICTOR
C11	3.69	343	427.1	84	2/3	364	63
C12	1.2	309	467.1	157	2/3	331	136
C13	3.7	343	382.5	39	1/2	394	-12
C14	0.9	305	337.8	32	1/2	331	7
C15	1.8	318	372.2	54	1/4	394	-22

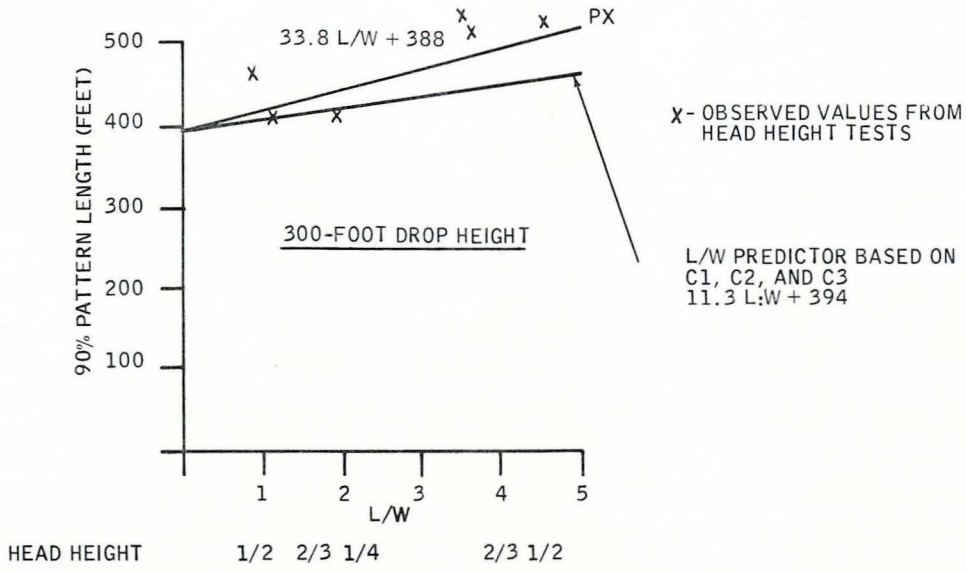

Figure 88. Effects of Tank Length-to-Width Ratio on Head Height Experiment

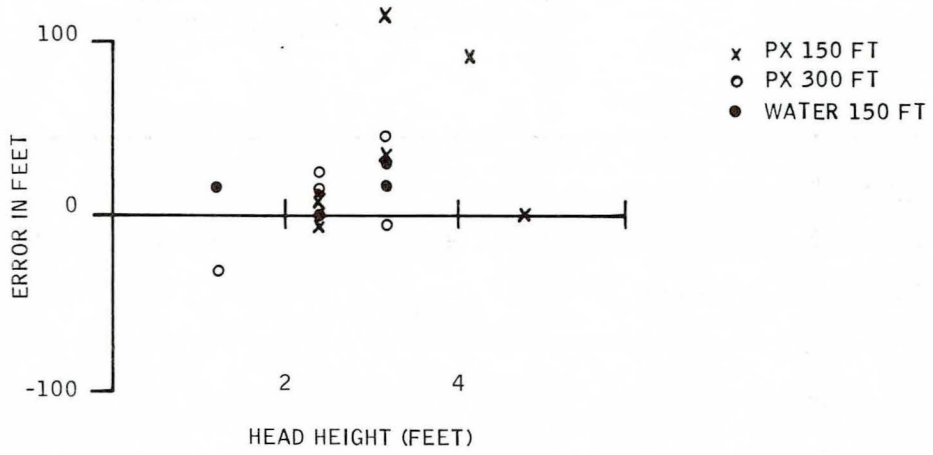

Figure 89. Error from Use of Length as a Predictor of 90% Pattern Length

The results of this test series indicate that significantly increasing the size of the drop, for example from 460 gallons to 920 gallons, provides only modest increases in the pattern length. For example, the linear regression equation for Phos-Chek line length as a function of drop height and lead size is y - 0.3082 Q + 313.8, which implies that increasing the drop size from 460 gallons to 920 gallons would only increase the pattern length by about 0.1302 X 460 feet = 60 feet. This indicates that quantity has a limited effect on the distributed length of the pattern, with a consequent sizeable effect on the distributed levels.

The three-dimensional plots for this test series are shown in Figures 90 and 91. In figure 92, the results of the test drops for Phos-Chek are graphically displayed.

Regression analysis statistics are provided in Table 16. A high level of significance is indicated for the regressions based on the F-ratio test.

AIRSPEED TEST SERIES (TEST MATRIX 6)

The objective of this test series was to evaluate the effect of aircraft drop speed on pattern characteristics. A constant quantity (460 gallons) was dropped from configurations C1 and C3 at velocities ranging from 100 to 180 knots. Drops were made from altitudes of 150 and 300 feet.

Table 15. Linear Regression Analysis Data - Test Matrix 4, Length of Inner 90%

Phos-Chek

Linear Regression Equation: $Y - 431.0 = 0.449 (H - 225) + 166.6 (H_{head} - 0.517)$

Degrees of Freedom:

Regression:	2
Remainder:	7
Total:	9

90% Confidence Band Values for Linear Regression Coefficients

Altitude:	0.449 ± 0.610
Time:	166.6 ± 199.2

F Ratio for 2, 7 Degrees of Freedom: 3.63

Water

Linear Regression Equation: $Y - 431.8 = 0.867 (H - 225) - 254.2 (H_{head} - 0.517)$

Degrees of Freedom:

Regression:	2
Remainder:	7
Total:	9

90% Confidence Band Values for Linear Regression Coefficients

Altitude:	0.867 ± 0.531
Time:	-254.2 ± 173.3

F Ratio for 2, 7 Degrees of Freedom: 15.44

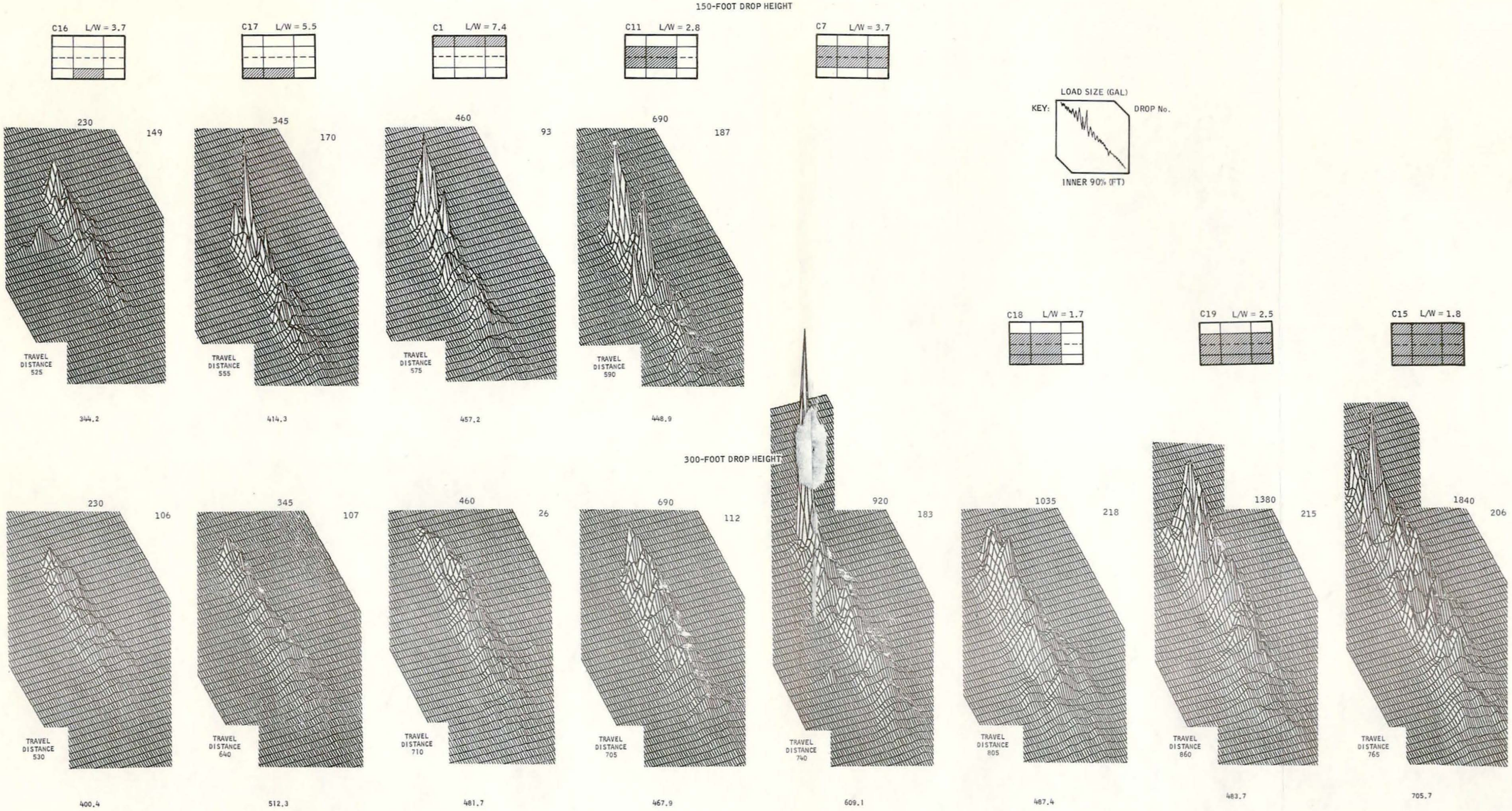

Figure 90. Three Dimensional Plots of Retardant Concentration from Load-Size Test Series - Phos-Chek

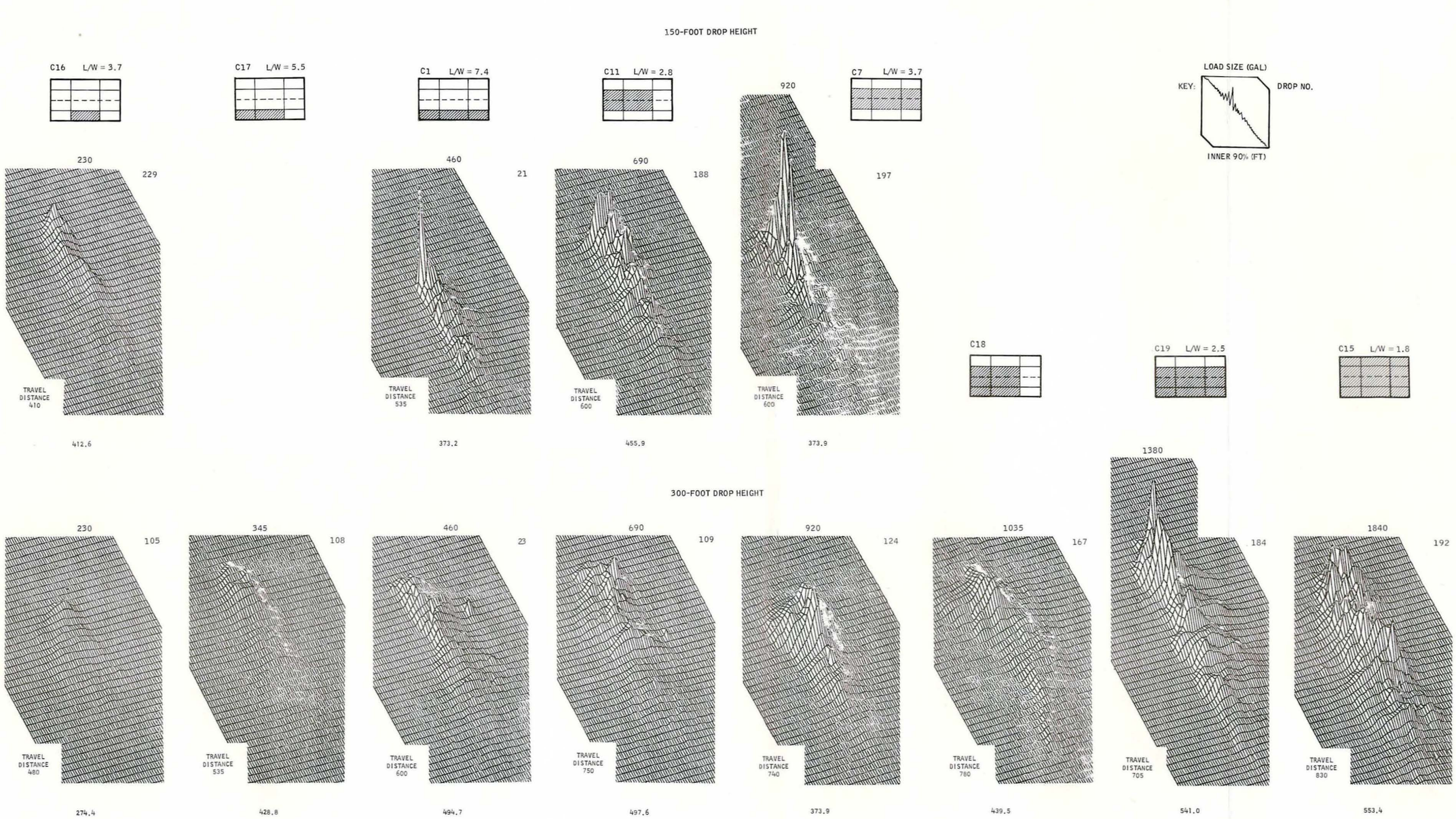

Figure 91. Three-Dimensional Plots of Retardant Concentration from Load-Size Test Series - Water

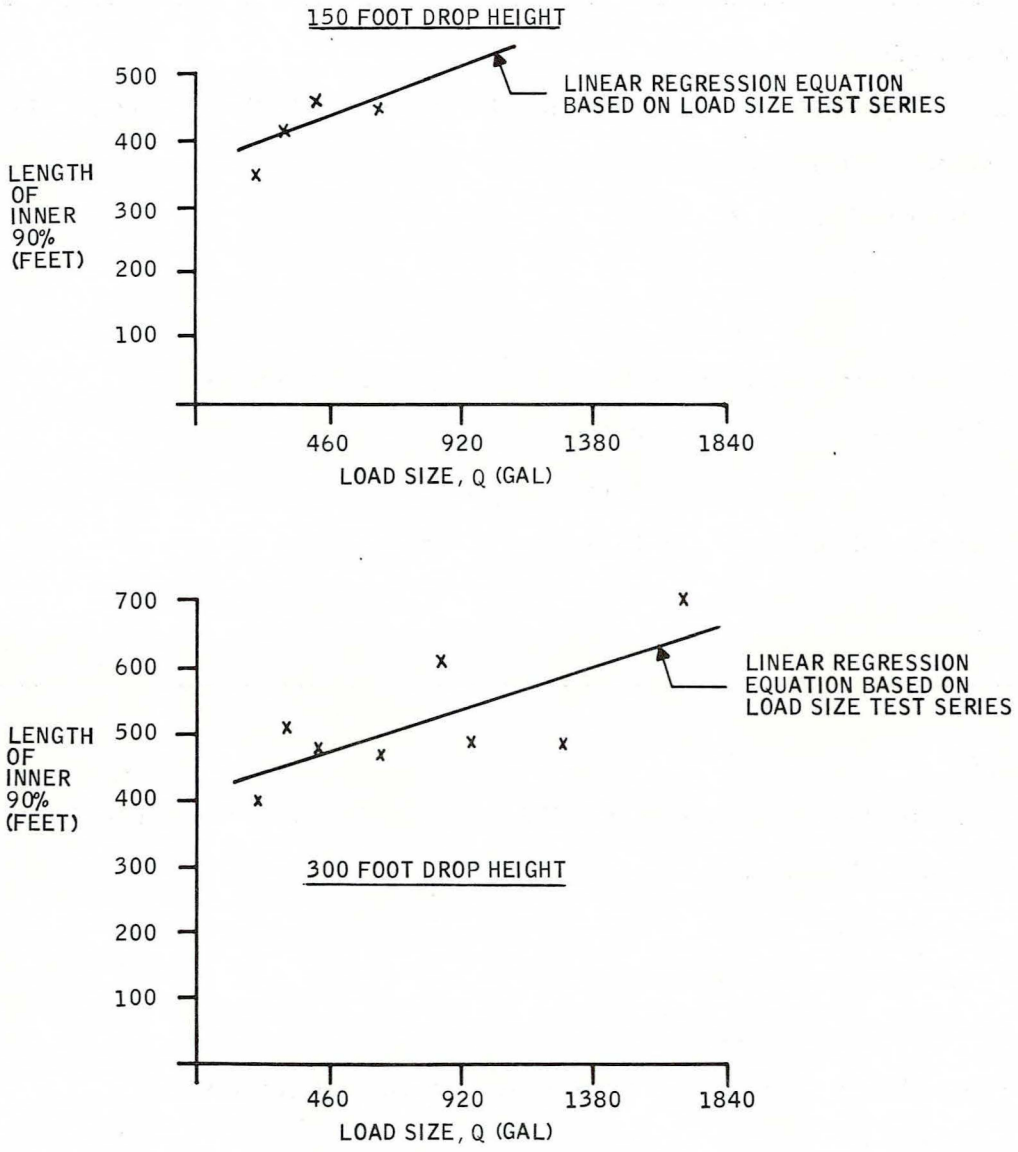

Figure 92. Pattern Length versus Load Size for Two Drop Heights - Phos-Chek

Table 16. Linear Regression Analysis Data - Test Matrix 5, Length of Inner 90%

Phos-Chek

Linear Regression Equation: $Y = 484.4 = 0.308 (H - 250) + 0.130 (G - 718.8)$

Degrees of Freedom:

Regression:	2
Remainder:	9
Total:	11

90% Confidence Band Values for Linear Regression Coefficients

Altitude:	0.308 ± 0.803
Time:	0.130 ± 0.075

F Ratio for 2, 9 Degrees of Freedom: 8.85

Water

Linear Regression Equation: $Y - 428.5 = 0.156 (H - 242.3) + 0.101 (G - 734.2)$

Degrees of Freedom:

Regression:	2
Remainder:	10
Total:	12

90% Confidence Band Values for Linear Regression Coefficients

Altitude:	0.156 ± 0.774
Time:	0.101 ± 0.076

F Ratio for 2, 10 Degrees of Freedom: 4.03

Results of the airspeed test series indicate that significant increases in pattern length are achieved with increases in drop speed. This trend can be observed in the three-dimensional plots for this test series shown in Figures 93 and 94. Examination of these plots also establishes that much higher peak concentrations are achieved with low drop speeds than with high drop speeds. Conversely high drop speeds result in more uniform pattern retardant concentrations. Phos-Chek and water inner 90% pattern length data are graphed in Figures 95 through 98.

It can again be observed in this test series that configuration C1, which has a larger L/W than configuration C3, for the most part yielded longer patterns than C3.

Regression analysis statistics for this test series are given in Tables 17 and 18. High levels of significance are indicated for the regression analysis by the F-ratio test.

ADDITIONAL DOOR RATE STUDIES (TEST MATRIX 7)

The primary objective of this test series was to evaluate tank doors as a method of controlling flow rates. This test series also provides additional data on the effect of time out of tank and configuration. Configurations C1 and C3 were tested at drop altitudes of 150 and 300 feet. Door rates 1, 2, 3, 4, and 6 were tested with configuration C3. Door rates 2, 4, and 6 were tested with configuration C1.

Three-dimensional plots of the test series are shown in Figures 99 and 100. Phos-Chek results are shown in Figures 101 and 102. Results of the test series clearly indicates that flow rate and retardant time out of tank, and hence pattern length, can be controlled by varying the door rate. For example, the ranges of lengths shown in Figure 101 span about the same range as that shown in Figure 71 of Test Matrix 1. This latter series also examined door exit area.

Pairwise comparison of C1 and C3 corresponding data points again supports the contention that long, narrow tanks contribute more to pattern length than do more square-type tanks. The following tabular data illustrates this:

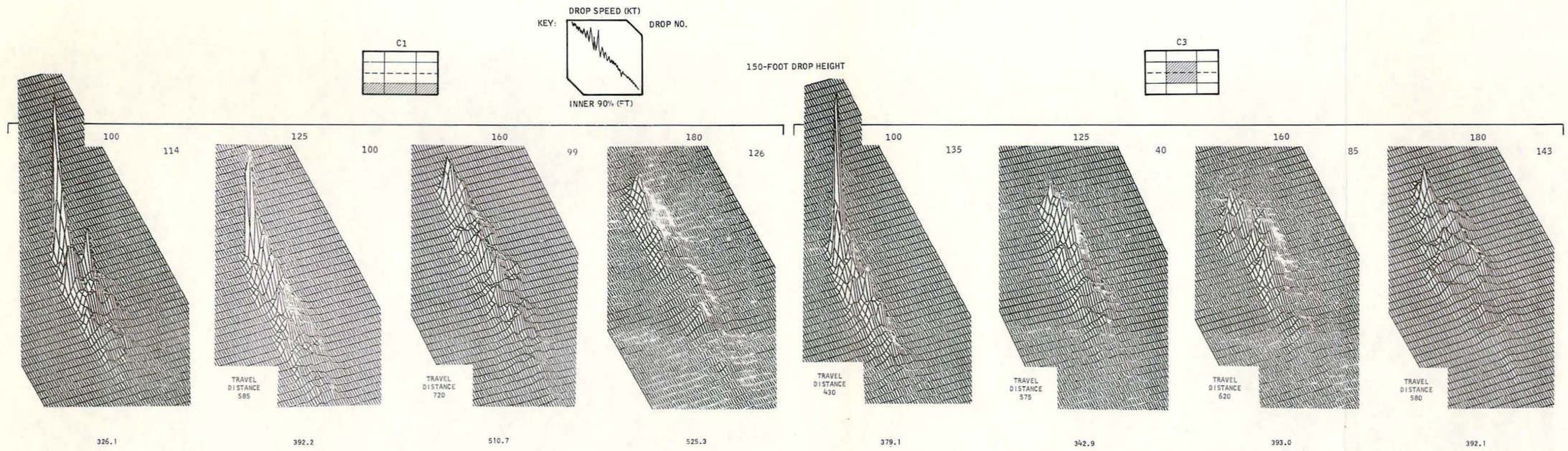

Figure 93. Three-Dimensional Plots of Retardant Concentration from Airspeed Test Series - Phos-Chek

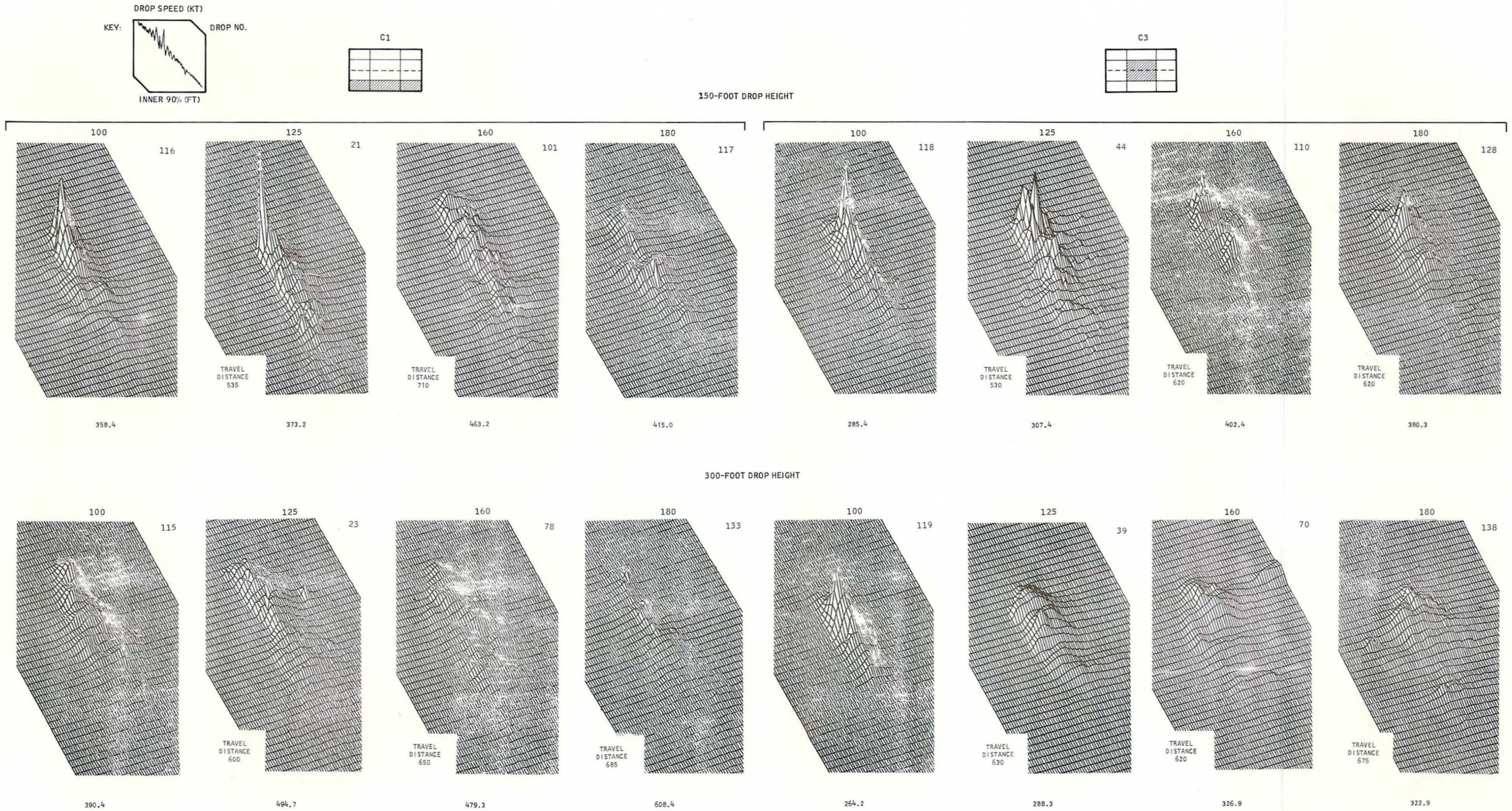

Figure 94. Three-Dimensional Plots of Retardant Concentration from Airspeed Test Series - Water

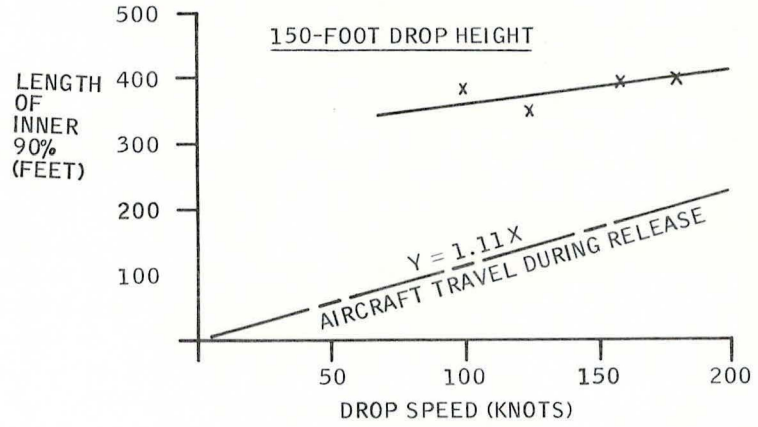

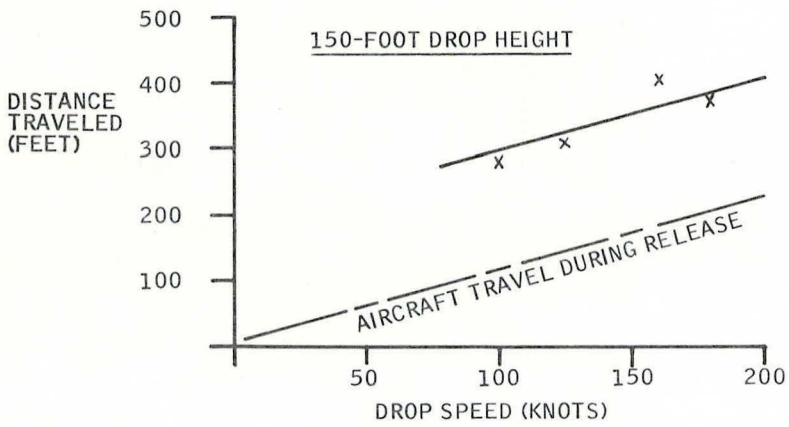

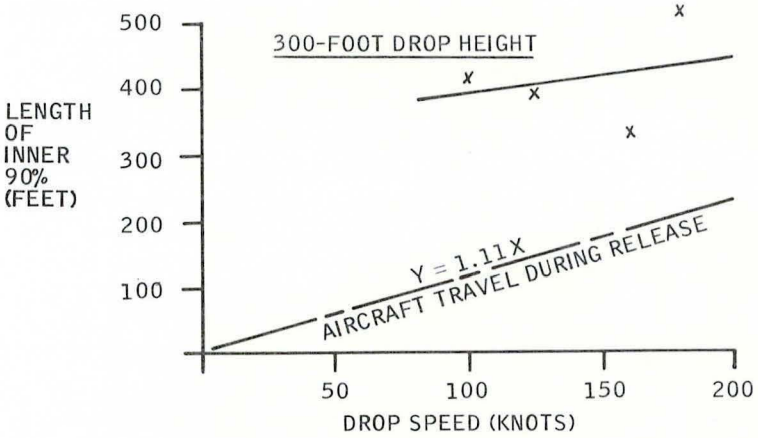

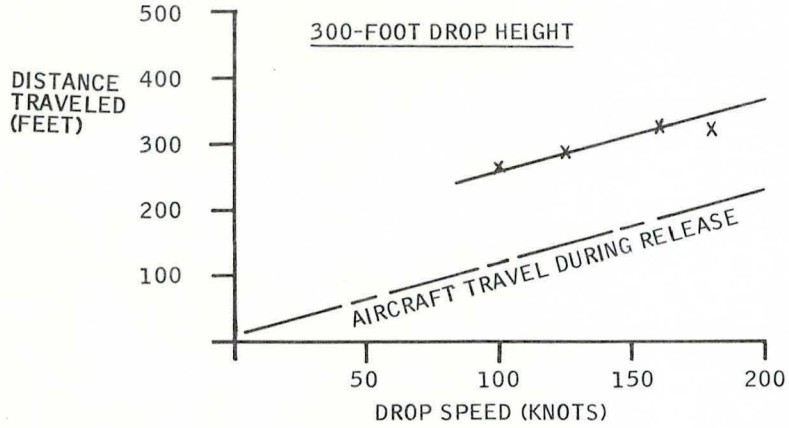

Figure 95. Pattern Length versus Drop Speed for Two Drop Heights - Configuration C3, Phos-Chek

Figure 96. Pattern Length versus Drop Speed for Two Drop Heights - Configuration C3, Water

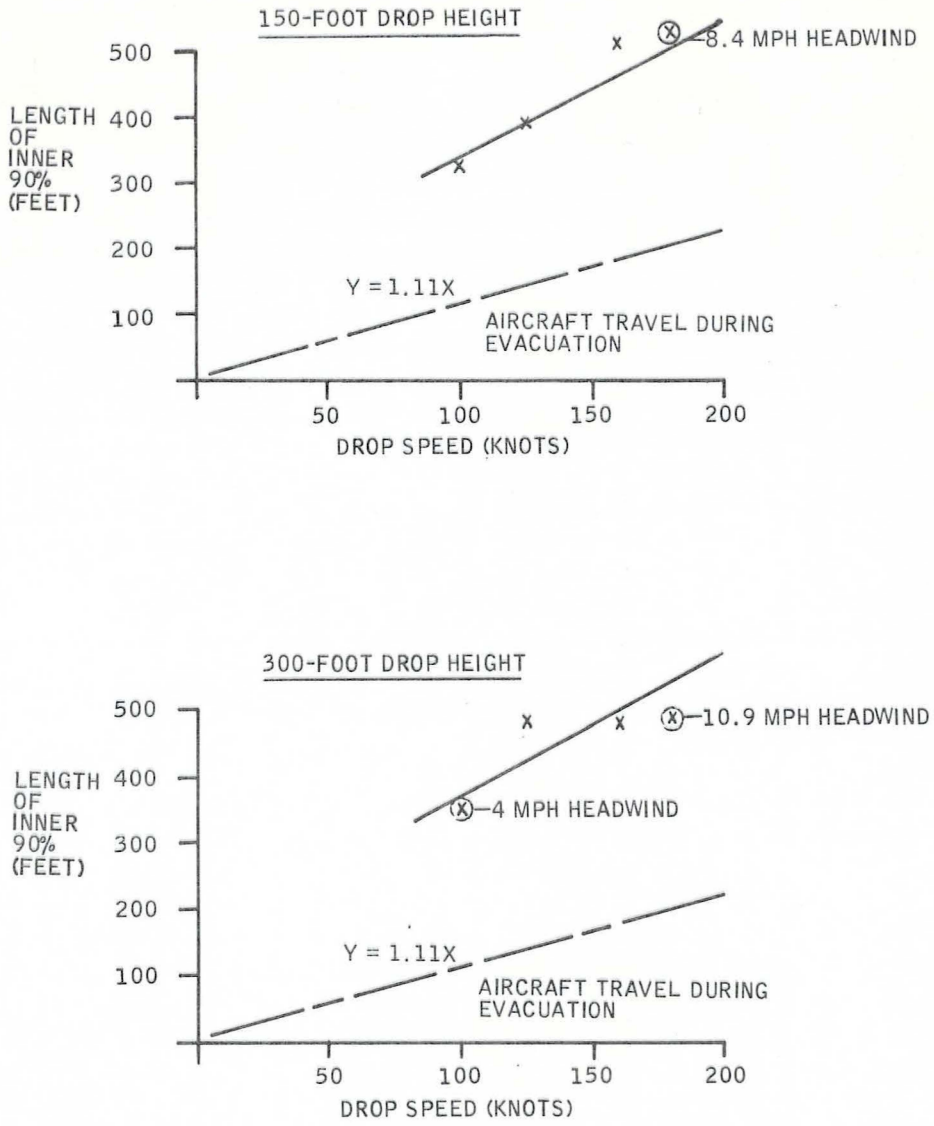

Figure 97. Pattern Length versus Drop Speed for Two Drop Heights - Configuration C1, Phos-Chek

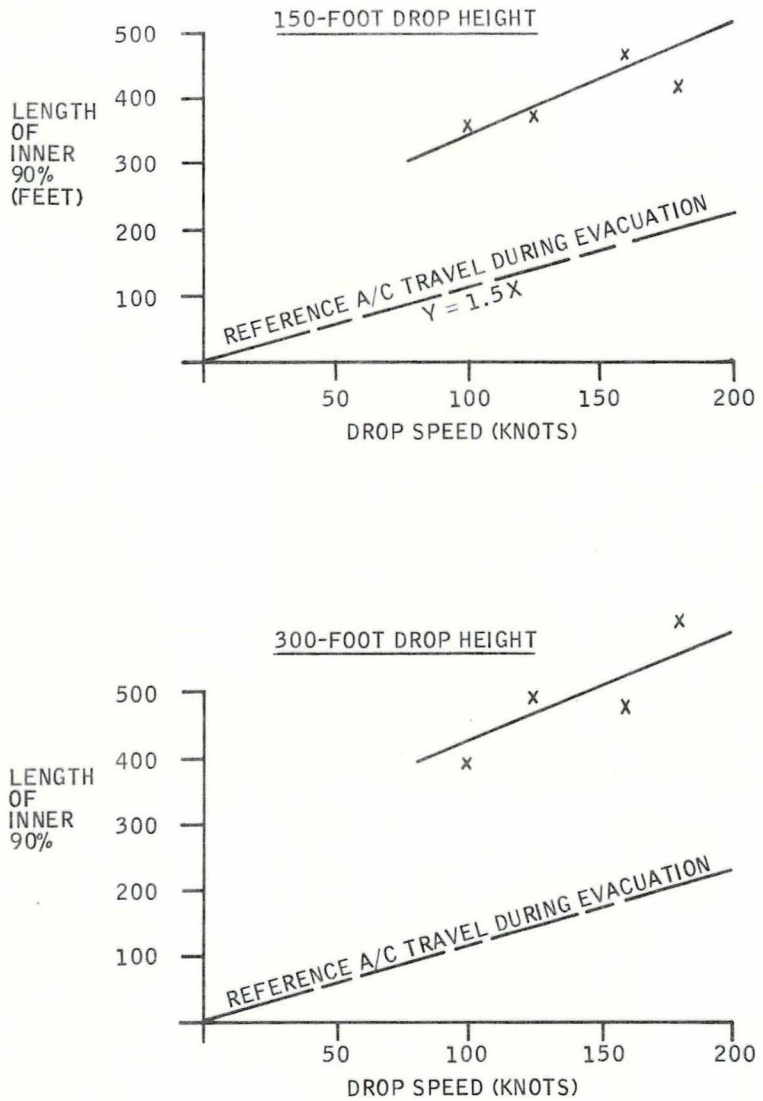

Figure 98. Pattern Length versus Drop Speed for Two Drop Heights - Configuration C1, Water

Table 17. Linear Regression Analysis Data - Test Matrix 6, Length of Inner 90%, Configuration C1

Phos-Chek

Linear Regression Equation: $y - 448.1 = 0.127 (H - 225) + 2.147 (V - 141.25)$

Degrees of Freedom:

Regression:	2
Remainder:	5
Total:	7

90% Confidence Band for Linear Regression Coefficients

Altitude:	0.127 ± 0.496
Velocity:	$2.147 \pm .834$

F Ratio for 2, 5 Degrees of Freedom: 13.76

Water

Linear Regression Equation: $y - 447.8 = 0.605 (H - 225) + 1.615 (V - 141.25)$

Degrees of Freedom:

Regression:	2
Remainder:	5
Total:	7

90% Confidence Band Values for Linear Regression Coefficients

Altitude:	0.605 ± 0.639
Velocity:	1.615 ± 1.070

F Ratio for 2, 5 Degrees of Freedom: 8.47

Table 18. Linear Regression Analysis Data - Test Matrix 6, Length of Inner 90%, Configuration C3

Phos-Chek

Linear Regression Equation: $y - 394.9 = 0.242 (H - 225) + 0.519 (V - 141.25)$

Degrees of Freedom:

Regression:	2
Remainder:	5
Total:	7

90% Confidence Band Values for Linear Regression Coefficients

Altitude:	0.242 ± 0.841
Velocity:	0.519 ± 1.408

F Ratio for 2, 5 Degrees of Freedom: 0.629

Water

Linear Regression Equation: $y - 322.2 = 0.289 (H - 225) + 1.122 (V - 141.25)$

Degrees of Freedom:

Regression:	2
Remainder:	5
Total:	7

90% Confidence Band Values for Linear Regression Coefficients

Altitude:	-0.289 ± 0.310
Velocity:	1.122 ± 0.520

F Ratio for 2, 5 Degrees of Freedom: 1.31

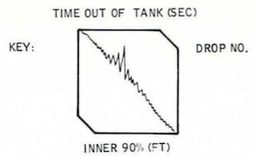

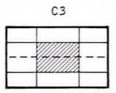

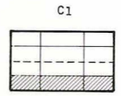

150-FOOT DROP HEIGHT

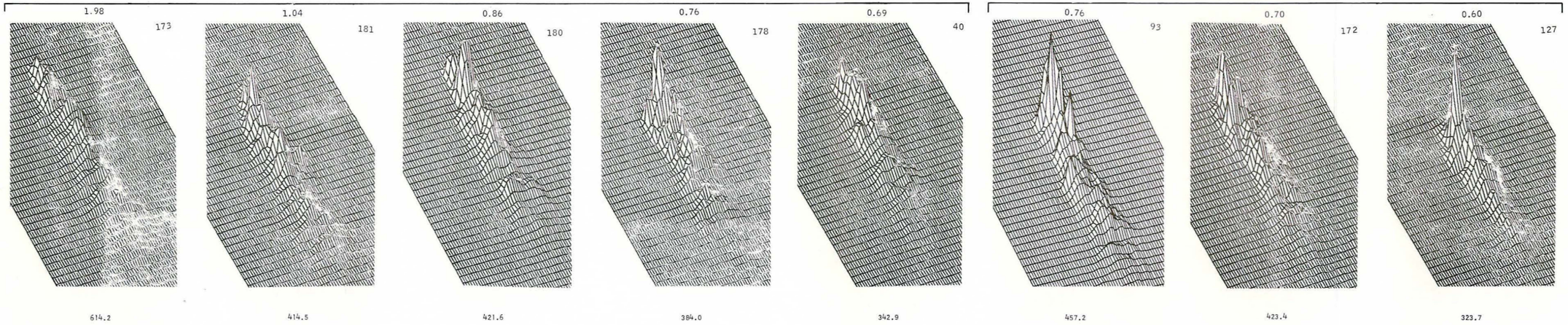

300-FOOT DROP HEIGHT

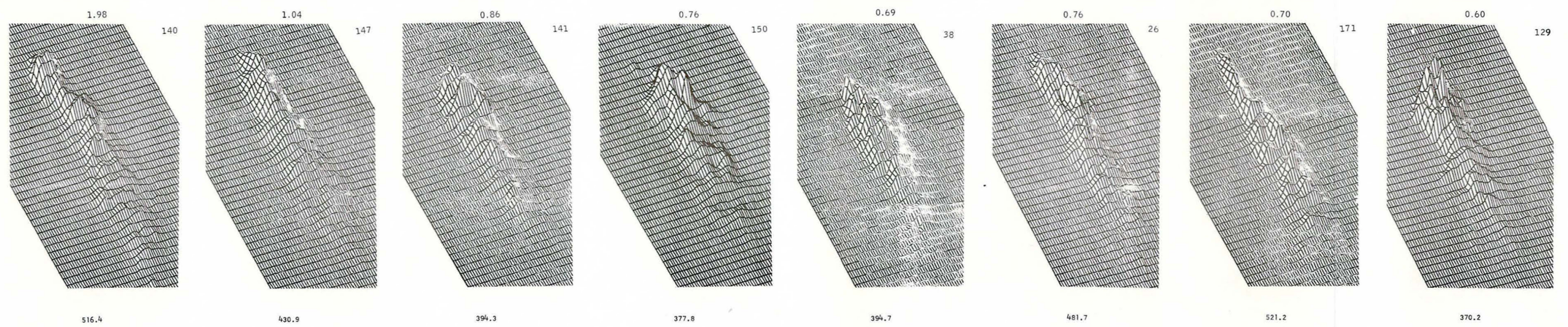

L/W = 1.7

Figure 99. Three-Dimensional Plots of Retardant Concentration from Additional Door Rate Studies - Phos-Chek

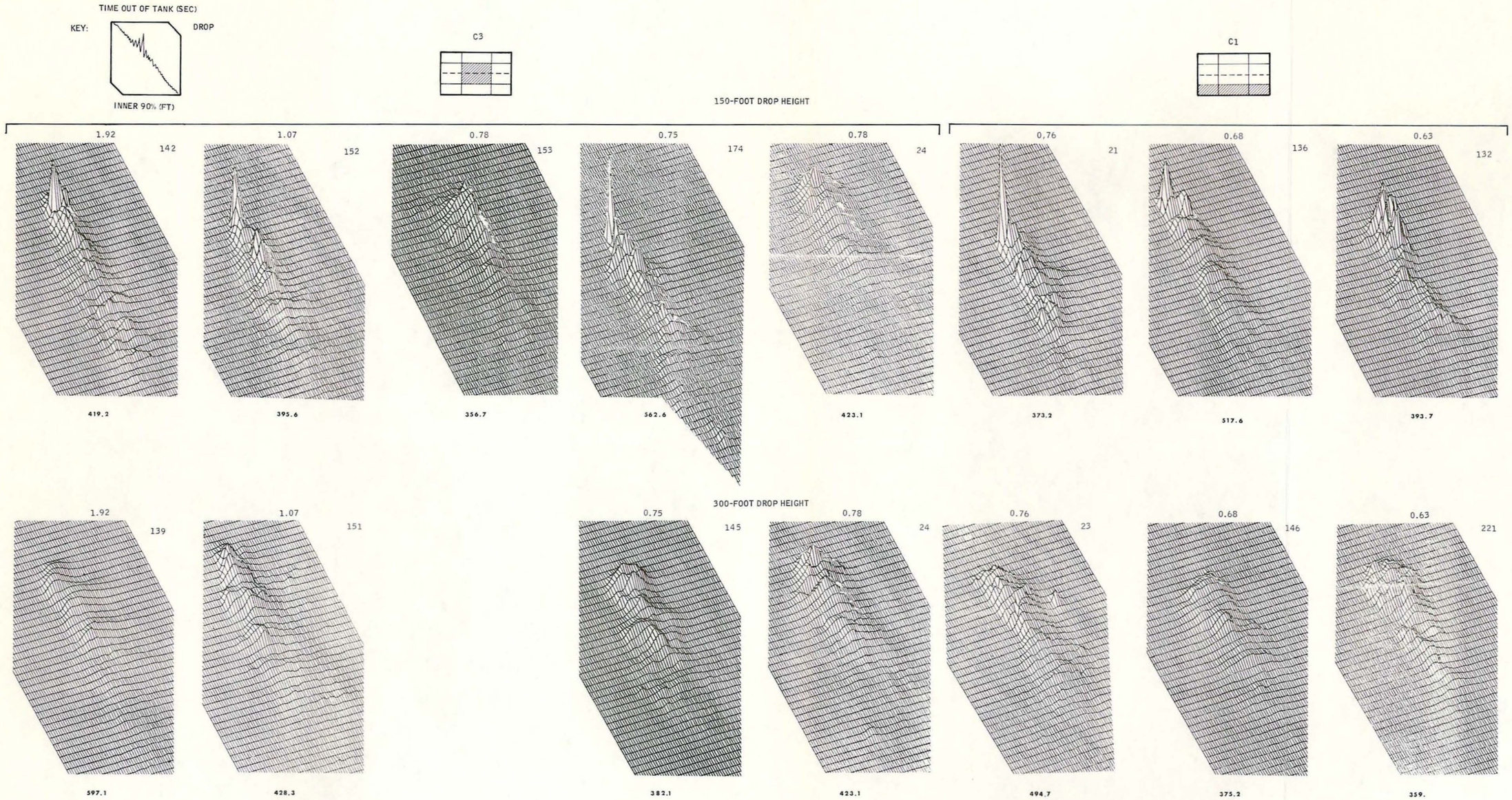

Figure 100. Three-Dimensional Plots of Retardant Concentration from Additional Door Rate Studies - Water

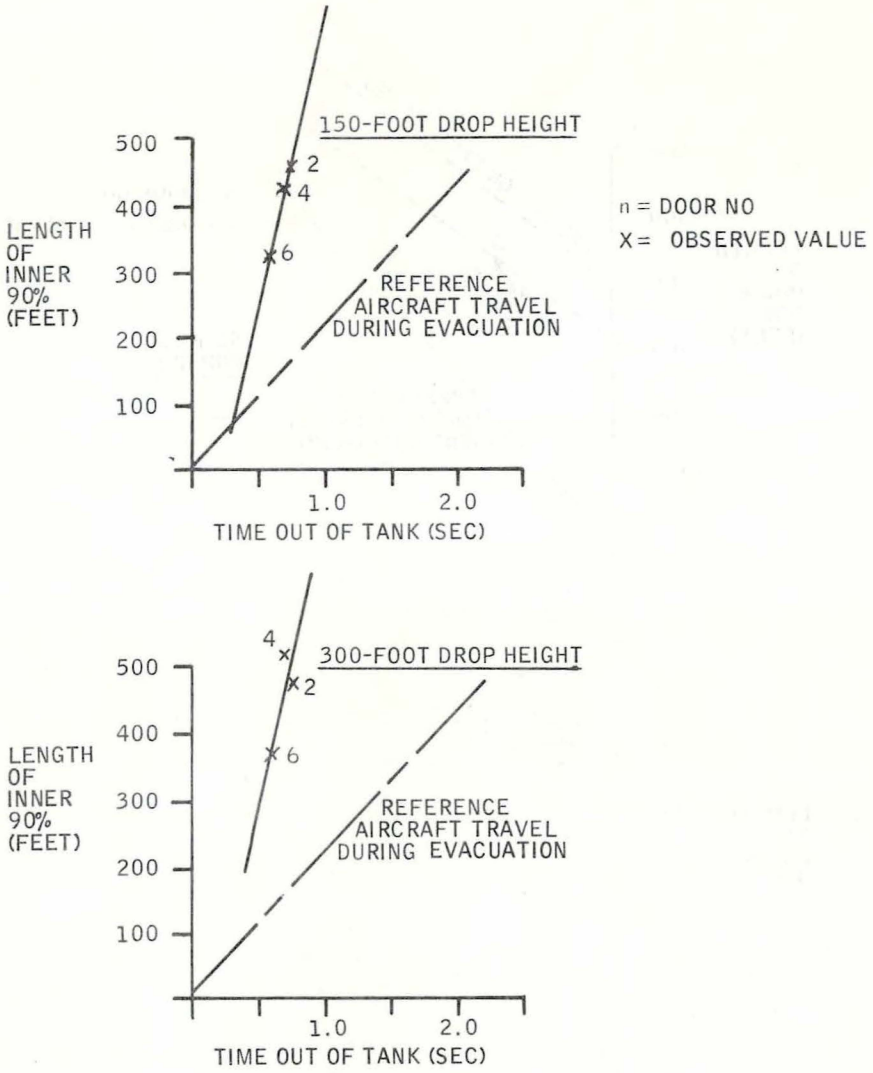

Figure 101. Pattern Length versus Time Out of Tank for Configuration C1 and Two Drop Heights - Phos-Chek

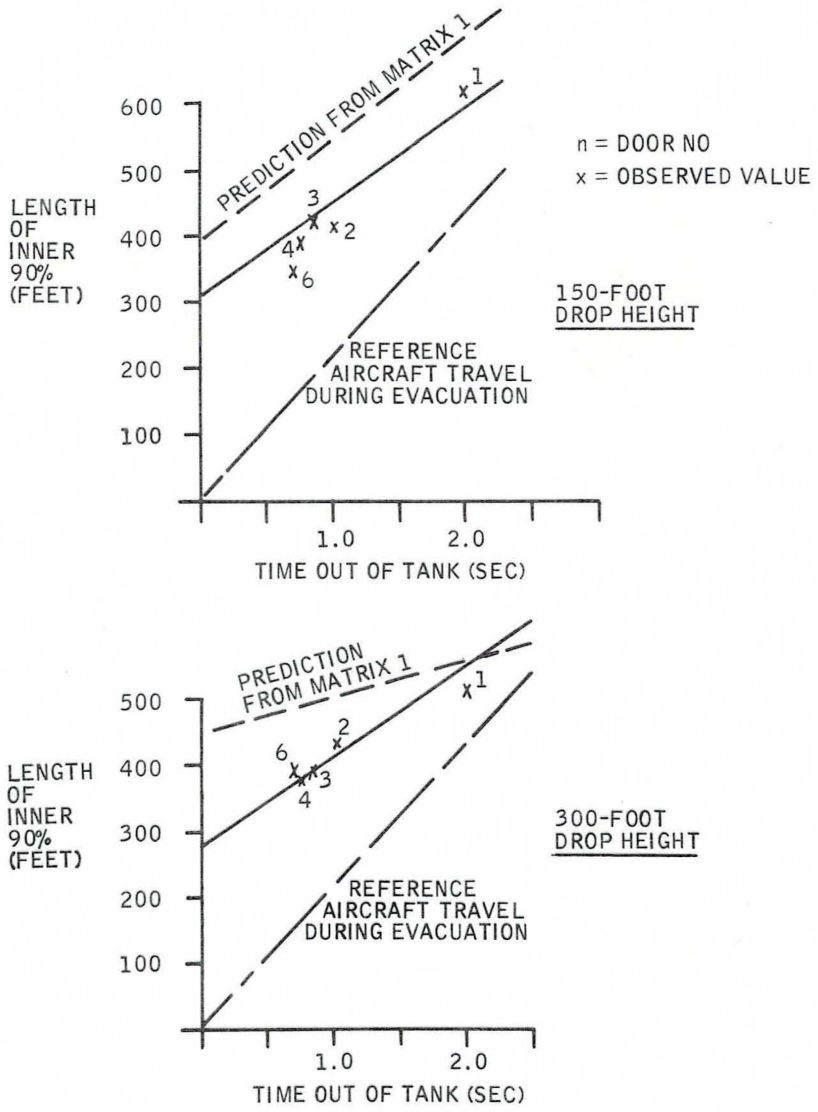

Figure 102. Pattern Length versus Time Out of Tank for Configuration C3 and Two Drop Heights - Phos-Chek

Inner 90% Pattern Length (feet)

150-Foot Drop Height				300-Foot Drop Height		
Door Rate				Door Rate		
2	4	6		2	4	6
			Configuration C 3			
414	384	343		430	378	395
			Configuration C 1			
457	423	324		482	521	370

Regression analysis statistics for this test series are given in Tables 19 and 20. A high level of significance for the regression analysis of Phos-Chek results is indicated by the F-ratio test. A high level of significance is not indicated by the F-ratio test for the water results.

RETARDANT DOWNRANGE DISTANCE TRAVELED

Retardant drops were examined to determine tank and delivery parameter effects on the downrange retardant travel. The results of this examination are shown in Figures 103 through 109. Regression analysis statistics are provided in Tables 21 through 25. Of the parameters examined, time out of tank and load size have the most significant effect on distance traveled. The F-ratio test for the regressions associated with these two parameters indicated a high level of significance. The regression analyses conducted on the other parameters examined did not indicate a high level of significance. However, the data points for the airspeed test series seemed to separate into two dinstinct groupings – one group for low-speed drops and one group for high-speed drops. No physical explanation of this phenomenon could be determined. It is noted that, if this apparent phenomenon is real, this would have an effect on the significance of the regression analysis of this data set.

It is interesting to observe the similarity between the configuration-influenced distance traveled in Figure 103 and those for the configuration-influenced inner 90% length shown in Figure 73.

Table 19. Linear Regression Analysis Data - Test Matrix 7, Length of Inner 90%, Configuration C3

Phos-Chek

Linear Regression Equation: $y - 439.1 = 0.217 (H - 225) + 137.6 (t - 1.066)$

Degrees of Freedom:

Regression:	2
Remainder:	7
Total:	9

90% Confidence Band Values for Linear Regression Coefficients

Altitude:	-0.217 ± 0.628
Time:	$137.6 + 65.5$

F Ratio for 2, 7 Degrees of Freedom: 8.86

Water

Linear Regression Equation: $y - 435.1 = 0.0465 (H - 225) + 69.1 (t - 1.03)$

Degrees of Freedom:

Regression:	2
Remainder:	7
Total:	9

90% Confidence Band Values for Linear Regression Coefficients

Altitude:	-0.0465 ± 1.0162
Time:	69.1 ± 102.2

F Ratio for 2, 7 Degrees of Freedom: .873

Table 20. Linear Regression Analysis Data - Test Matrix 7, Length of Inner 90%, Configuration C1

Phos-Chek

Linear Regression Equation: $y - 429.6 = 0.297 (H - 225) + 878.8 (t - 0.693)$

Degrees of Freedom:

Regression:	2
Remainder:	3
Total:	5

% Confidence Band Values for Linear Regression Coefficients

Altitude:	0.250	0.297 ± 0.73
Time:	320.6	878.8 ± 754.4

F Ratio for 2, 3 Degrees of Freedom: 4.90

Water

Linear Regression Equation: $y - 419.0 = -0.122 (H - 225) + 206.5 (t - .77)$

Degrees of Freedom:

Regression:	2
Remainder:	3
Total:	5

% Confidence Band Values for Linear Regression Coefficients

Altitude:	0.436	-0.122 ± 1.273
Time:	265.2	206.5 ± 624.0

F Ratio for 2, 3 Degrees of Freedom: 0.342

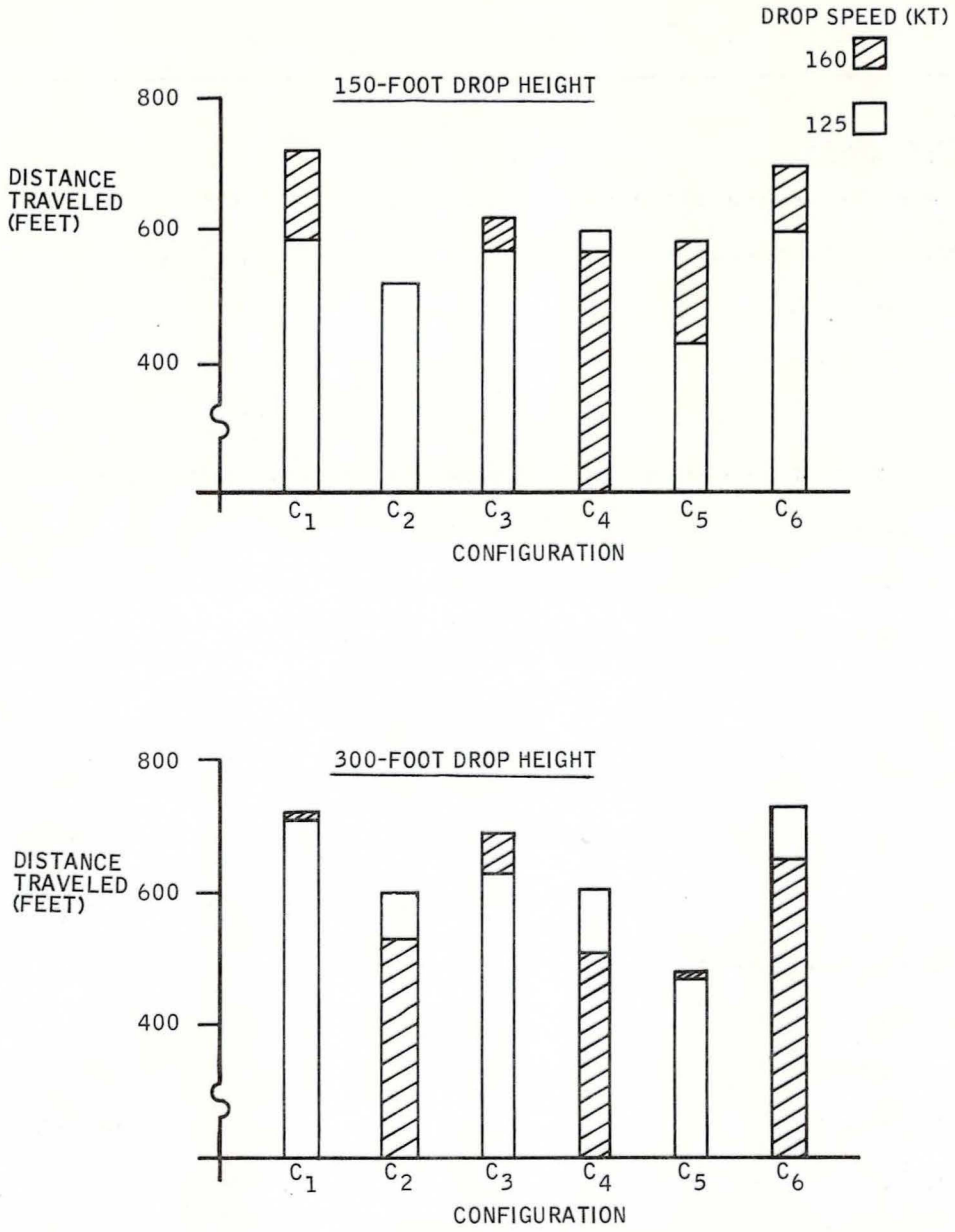

Figure 103. Retardant Downrange Distance Traveled versus Tank Configuration for Two Drop Heights and Two Drop Speeds - Phos-Chek

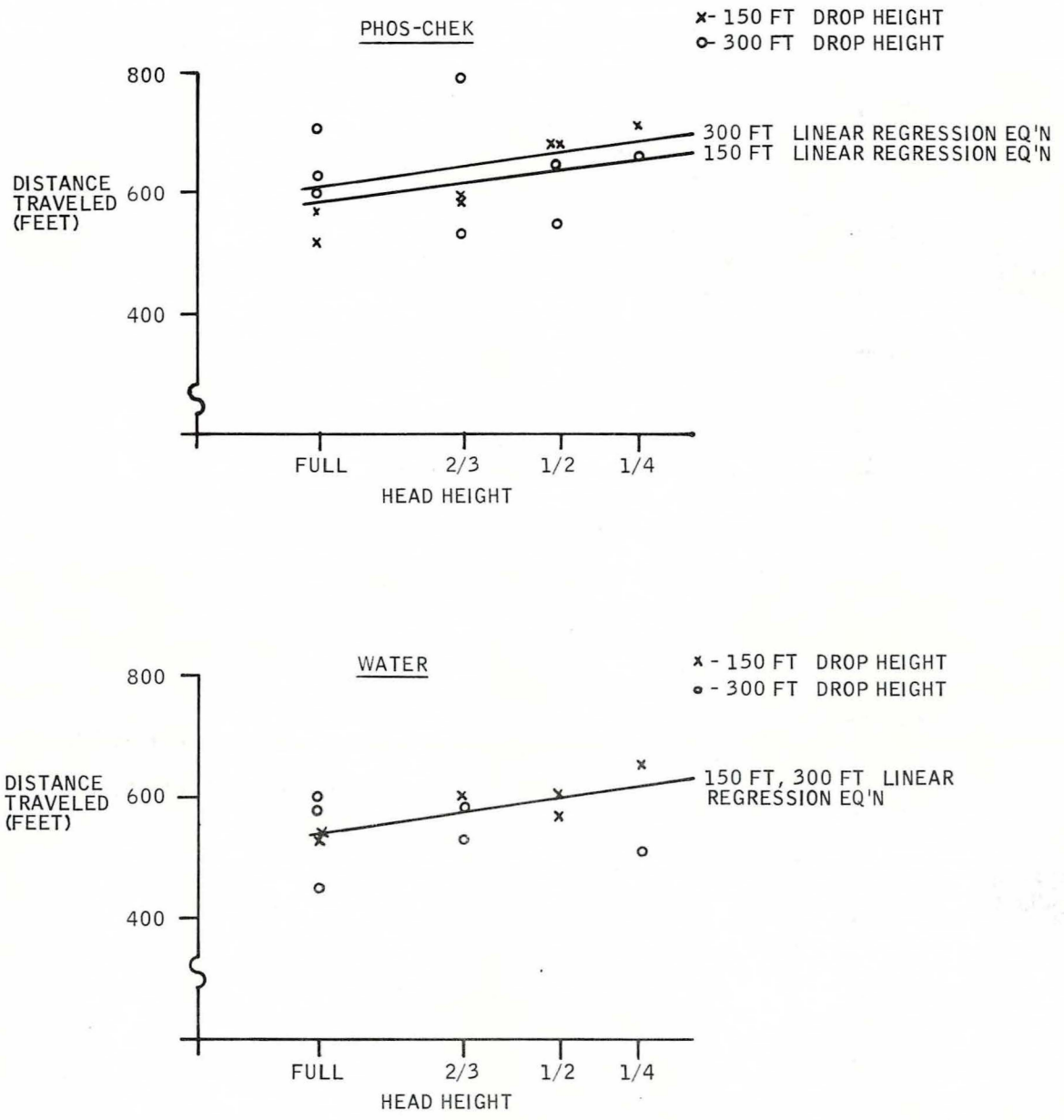

Figure 104. Retardant Downrange Distance Traveled versus Head Height at Two Drop Heights - Phos-Chek and Water

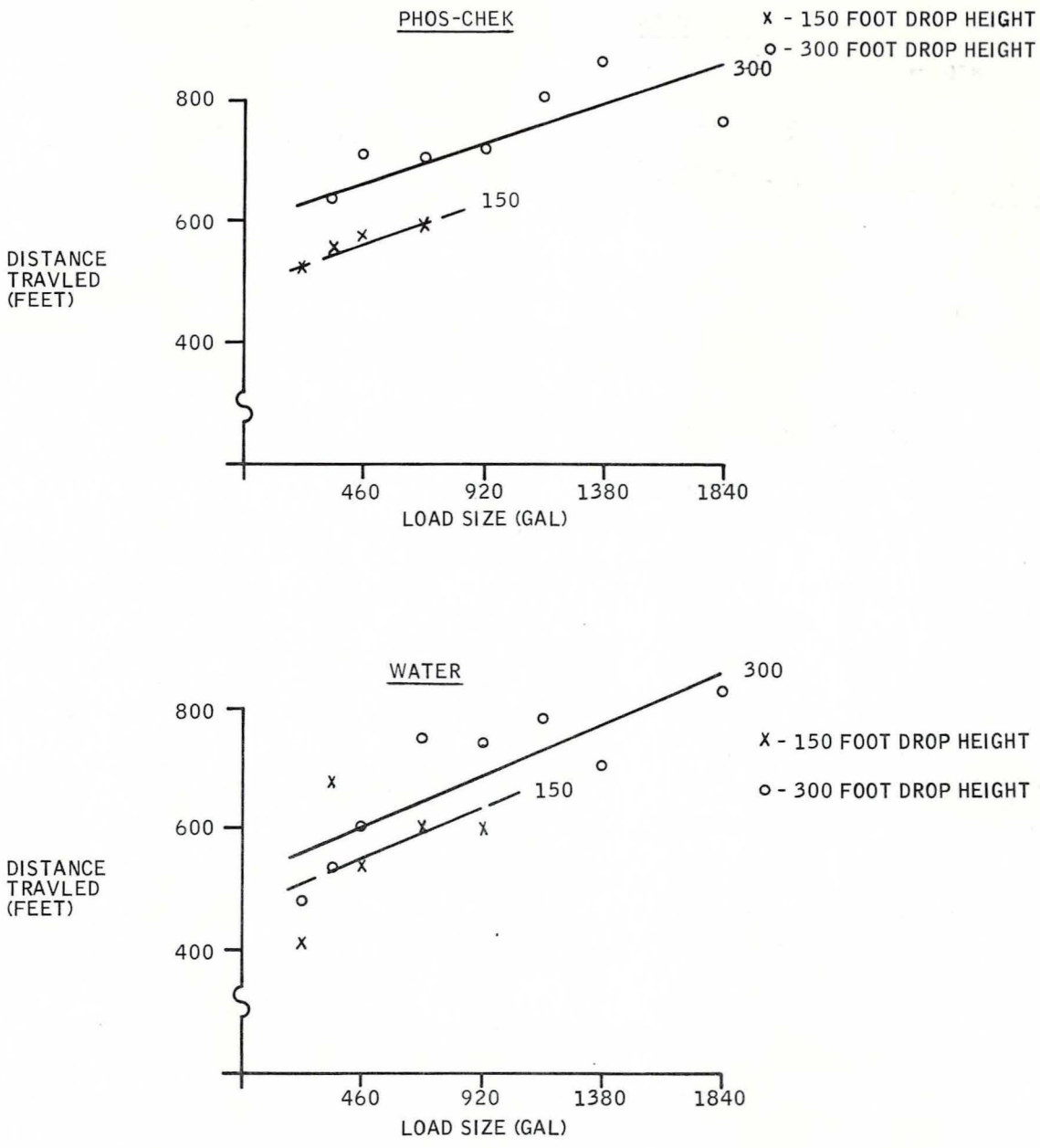

Figure 105. Retardant Downrange Distance Traveled versus Load Size at Two Drop Heights - Phos-Chek and Water

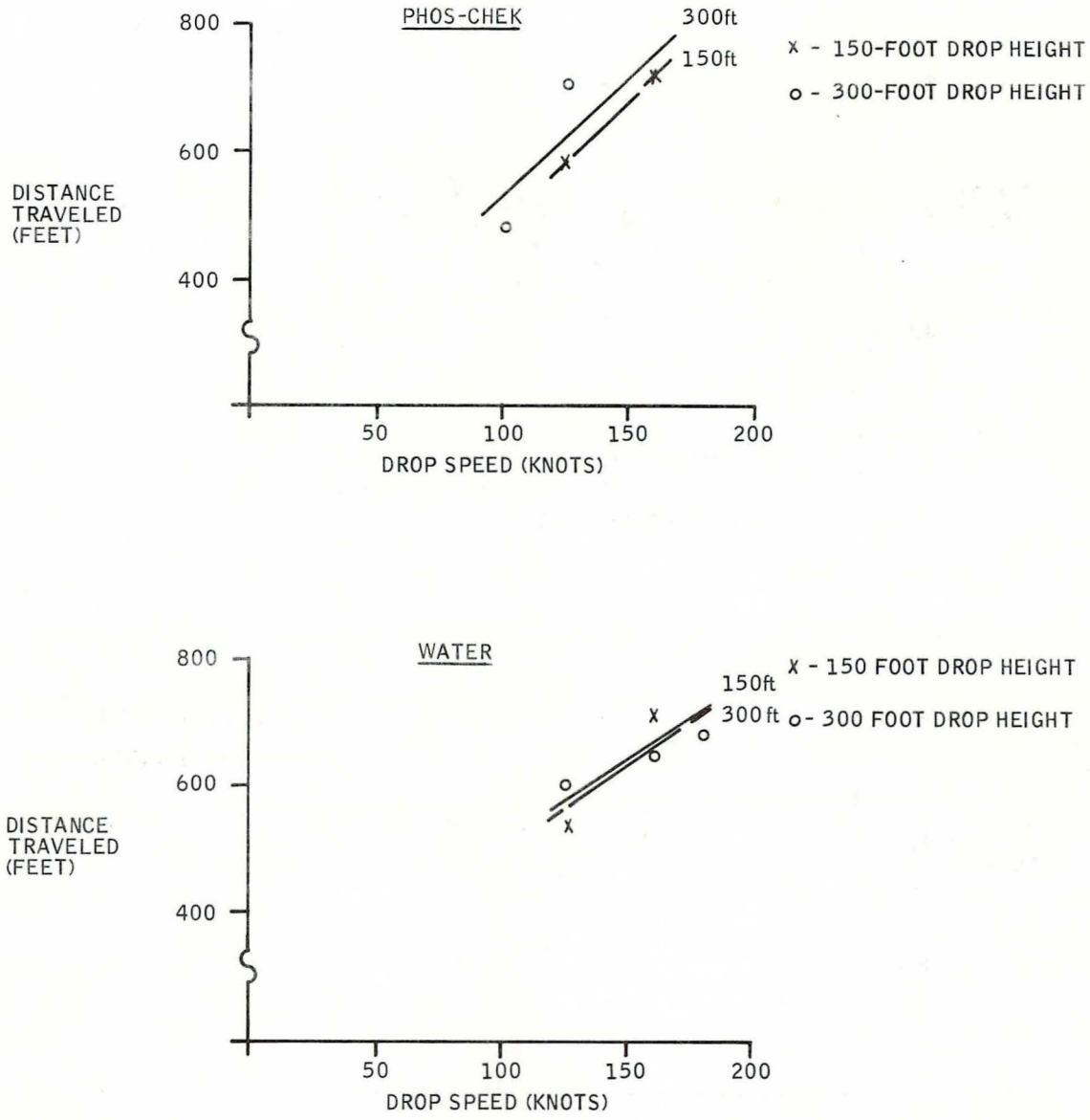

Figure 106. Retardant Downrange Distance Traveled versus Drop Speed for Two Drop Heights - Configuration C1, Phos-Chek and Water

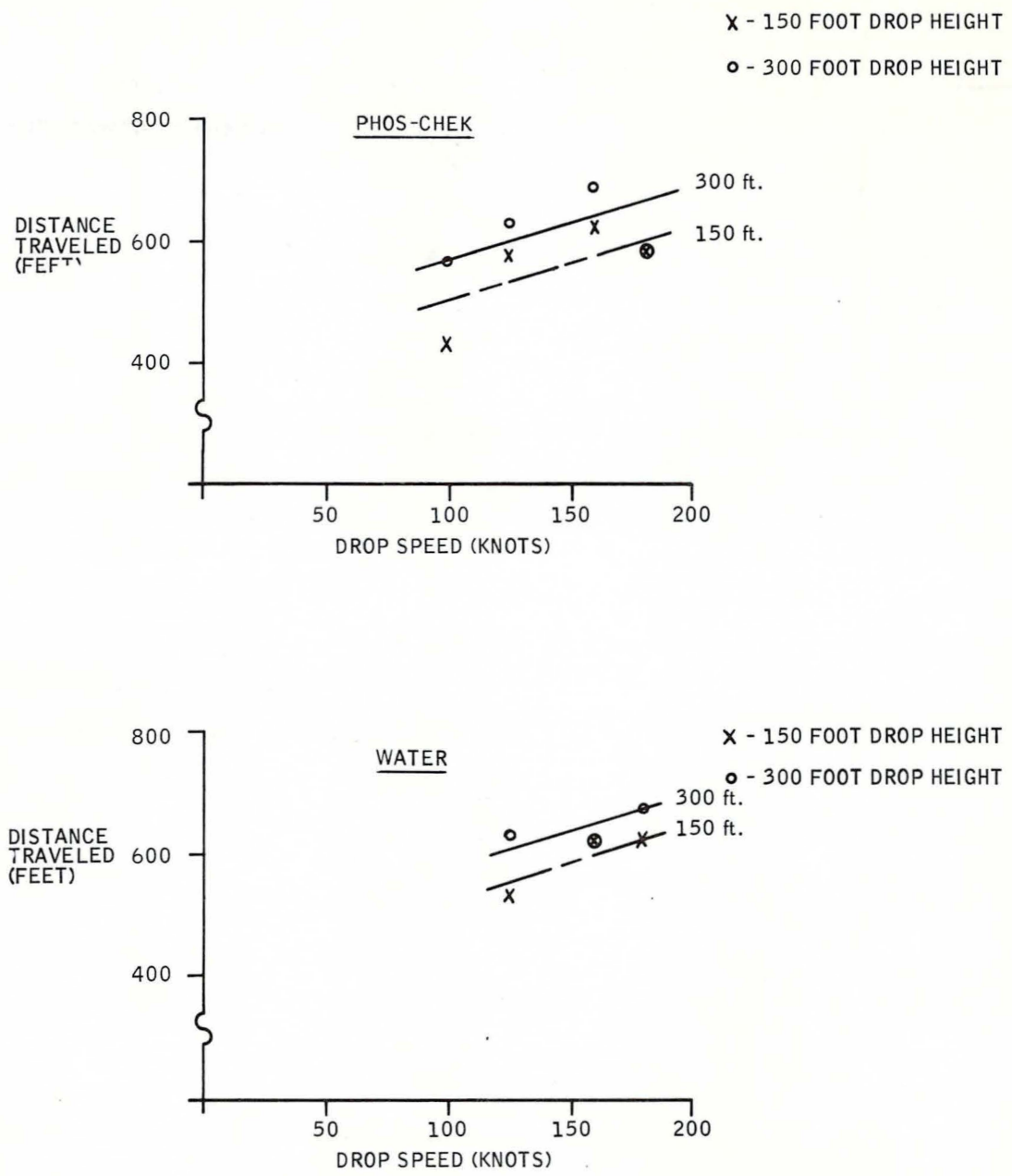

Figure 107. Retardant Downrange Distance Traveled versus Drop Speed for Two Drop Heights - Configuration C3, Phos-Chek and Water

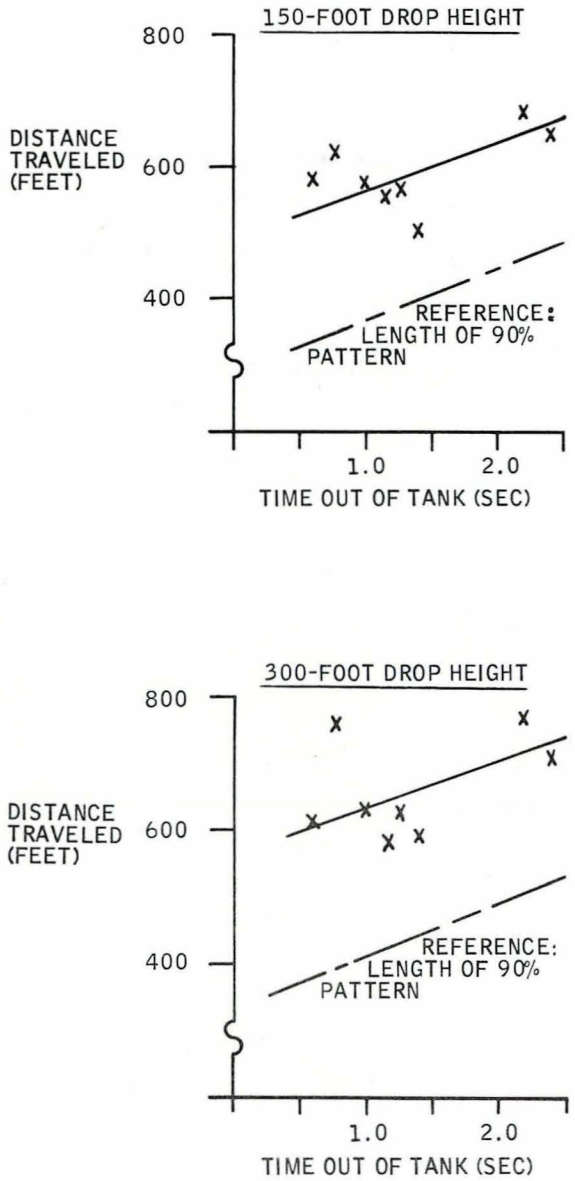

Figure 108. Retardant Downrange Distance Traveled versus Time Out of Tank for Two Drop Heights - Phos-Chek

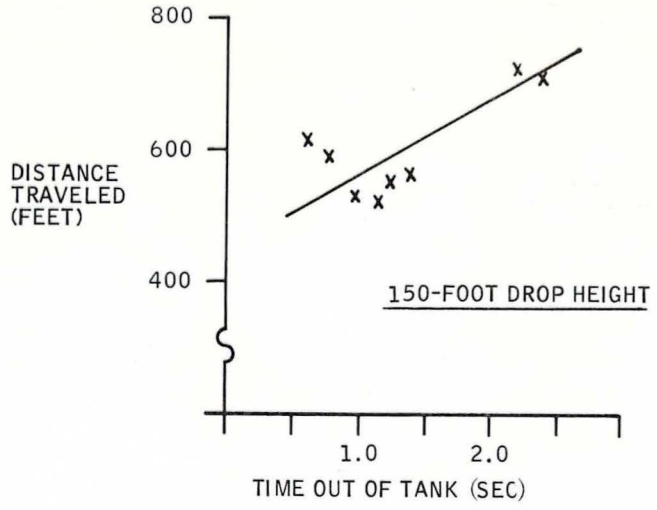

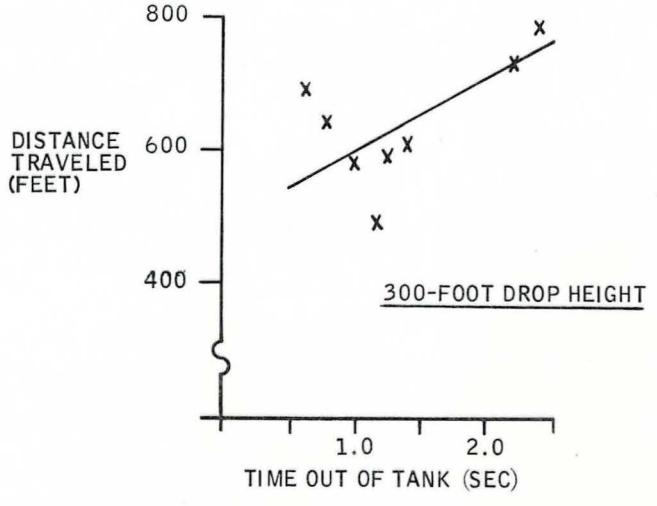

Figure 109. Retardant Downrange Distance Traveled versus Time Out of Tank for Two Drop Heights - Water

Table 21. Linear Regression Analysis Data - Test Matrix 1, Distance Traveled

Phos-Chek

Linear Regression Equation: D - 624.7 = 0.454 (H - 225) + 72.2 (t - 1.3475)

Degrees of Freedom:

Regression:	2
Remainder:	13
Total:	15

90% Confidence Band for Linear Regression Coefficients

Altitude:	0.454 ± 0.493
Time:	72.2 ± 37.5

F Ratio for 2, 13 Degrees of Freedom: 9.407

Water

Linear Regression Equation: D - 619.1 = 0.2625 (H - 225) + 112.1 (t - 1.3475)

Degrees of Freedom:

Regression:	2
Remainder:	13
Total:	15

90% Confidence Band Values for Linear Regression Coefficients

Altitude:	0.161	0.2625 ± 0.470
Time:	20.15	112.1 ± 35.7

F Ratio for 2, 13 Degrees of Freedom: 16.79

Table 22. Linear Regression Analysis Data - Test Matrix 4, Distance Traveled

Phos-Chek

Linear Regression Equation: $D - 626.9 = 0.167 (H - 225) - 94.7 (H_{HEAD} - 0.698)$

Degrees of Freedom:

Regression:	2
Remainder:	13
Total:	15

90% Confidence Band Values for Linear Regression Coefficients

Altitude:		0.167 ± 0.718
Time:	70.2	94.7 ± 124.3

F Ratio for 2, 13 Degrees of Freedom: 1.14

Water

Linear Regression Equation: $D - 572.8 = .00417 (H - 225) - 104.2 (H_{HEAD} - .698)$

Degrees of Freedom:

Regression:	2
Remainder:	13
Total:	15

90% Confidence Band Values for Linear Regression Coefficients

Altitude:	0.225	0.00417 ± 0.657
Time:	64.1	104.2 ± 113.5

F Ratio for 2, 13 Degrees of Freedom: 1.322

Table 23. Linear Regression Analysis Data - Test Matrix 5, Distance Traveled

Phos-Chek

Linear Regression Equation: D - 666.7 = 0.647 (H - 225) + 0.142 (Q - 718.75)

Degrees of Freedom:

Regression:	2
Remainder:	9
Total:	11

90% Confidence Band Values for Linear Regression Coefficients

Altitude:		0.647 ± 0.756
Time:	.0384	0.142 ± 0.070

F Ratio for 2, 9 Degrees of Freedom: 16.91

Water

Linear Regression Equation: D - 633.8 = 0.344 (H - 242.3) + 0.185 (Q - 734.2)

Degrees of Freedom:

Regression:	2
Remainder:	9
Total:	11

90% Confidence Band Values for Linear Regression Coefficients

Altitude:	0.328	0.344 ± 0.958
Time:	0.0518	0.185 ± 0.095

F Ratio for , Degrees of Freedom: 9.45

Table 24. Linear Regression Analysis Data - Test Matrix 6, Distance Traveled Configuration C3

Phos-Chek

Linear Regression Equation: $D - 583.8 = 0.433 (H - 225) + 1.164 (V - 141.25)$

Degrees of Freedom:

Regression:	2
Remainder:	5
Total:	7

90% Confidence Band Values for Linear Regression Coefficients

Altitude:	0.433 ± 0.870
Time:	1.164 ± 1.459

F Ratio for 2, 5 Degress of Freedom: 2.34

Water

Linear Regression Equation: $D - 615.8 = 0.344 (H - 225) + 1.218 (V - 155)$

Degress of Freedom:

Regression:	2
Remainder	3
Total:	5

90% Confidence Band Values for Linear Regression Coefficients

Altitude:	0.344 ± 1.004
Time:	1.218 ± 1.226

F Ratio for 2, 3 Degrees of Freedom: 5.12

Table 25. Linear Regression Analysis Data - Test Matrix 6, Distance Traveled, Configuration C1

Phos-Chek

Linear Regression Equation: $D - 643.0 = 0.252 (H - 240) + 3.786 (V - 134)$

Degrees of Freedom:

Regression:	2
Remainder:	2
Total:	4

90% Confidence Band for Linear Regression Coefficients

Altitude:	0.252 ± 1.392
Time:	3.786 ± 11.055

F Ratio for 2, 2 Degrees of Freedom: 3.14

Water

Linear Regression Equation: $D - 636 = -0.0595 (H - 240) + 2.514 (V - 150)$

Degress of Freedom:

Regression:	2
Remainder:	2
Total:	4

90% Confidence Band for Linear Regression Coefficients

Altitude:	-0.0595 ± 0.952
Time:	2.514 ± 3.230

F Ratio for 2, 2 Degress of Freedom: 2.70

SECTION VIII
DATA ANALYSIS SUMMARY

This section summarizes the analysis of flight data, difficulties encountered in executing the planned analysis technique, and the rationale for ultimately selecting a metric for regression analysis through the matrices of the tests. In the process of analysis, critical characteristics of pattern formation were developed. The metric selected is the length of the pattern covered by 90% of the retardant. This value reasonably defines the major distribution along the flight path. Increases in pattern length are normally associated with a general and proportional reduction in concentration. Nonetheless, the data show that tank characteristics can be selected to maximize the length and uniformity of the distribution and that quantity can be added to bring coverage density to acceptable levels almost independently. Definitions used in this summary are shown in Figure 110. The source of the regressions employed may be found in Section VII, Matrix Analysis. The effects of key factors involved in this data analysis are discussed below.

AIRCRAFT-INDUCED SPREAD

Aircraft velocity induces a spread in the range direction corresponding to the distance traveled during tank evacuation. In the baseline test series (125 knots at $\approx$0.66-second evacuation), this produces about 140 feet or roughly 28 to 50 percent of the total pattern length depending on other parameters.

TIME OUT OF TANK

Time out of tank was examined in Matrix 1 and Matrix 7 on a 460-gallon load. These were interlocking in that flow control in Matrix 1 utilized both door restrictions and door rate, whereas, Matrix 7 utilized only door rate. In evaluating the mechanism of pattern development, it is useful to eliminate the length due to aircraft-induced spread. This yields a measure of the distribution's development due to fluid flight prior to breakup. When this is done, regressions from Matrix 1 and the portions of Matrix 7 dealing with the C3 configuration are:

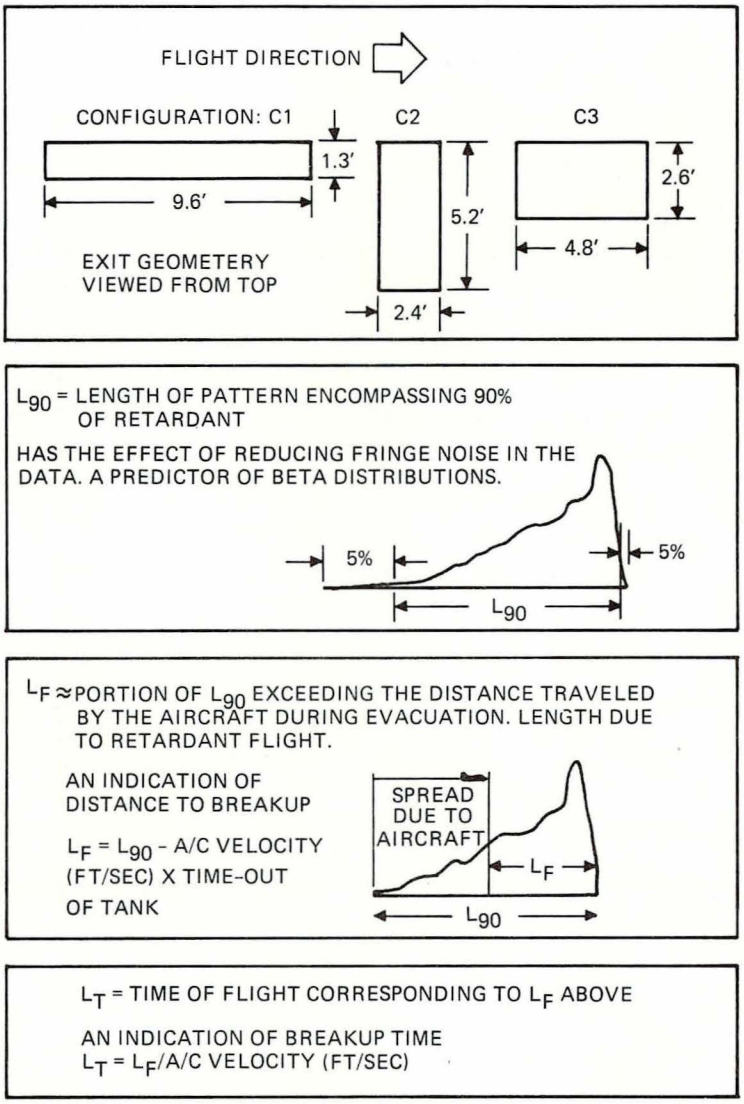
FLIGHT DIRECTION
CONFIGURATION: C1
C2
C3
1.3'
9.6'
5.2'
2.6'
4.8'
2.4'
EXIT GEOMETERY
VIEWED FROM TOP
L_{90} = LENGTH OF PATTERN ENCOMPASSING 90% OF RETARDANT
HAS THE EFFECT OF REDUCING FRINGE NOISE IN THE DATA. A PREDICTOR OF BETA DISTRIBUTIONS.
5%
5%
L_{90}
$L_F \approx$ PORTION OF L_{90} EXCEEDING THE DISTANCE TRAVELED BY THE AIRCRAFT DURING EVACUATION. LENGTH DUE TO RETARDANT FLIGHT.
AN INDICATION OF DISTANCE TO BREAKUP
$L_F = L_{90}$ - A/C VELOCITY (FT/SEC) X TIME-OUT OF TANK
SPREAD DUE TO AIRCRAFT
L_F
L_{90}
L_T = TIME OF FLIGHT CORRESPONDING TO L_F ABOVE
AN INDICATION OF BREAKUP TIME
$L_T = L_F$/A/C VELOCITY (FT/SEC)

Figure 110. Definitions, Parameters and Factors Pertaining to Data Analysis Summary

		$L_F = L_{90} - 211t$	$L_T = L_F / 211$ ft/sec
Phos-Chek	Mat 7	$L_F = -73t + 309$ or in time of flight	$L_T = -.34t + 1.46$
	Mat 1	$L_F = -132t + 293$	$L_T = -.62t + 1.39$
Water	Mat 7	$L_F = -141t + 441$	$L_T = -.67t + 2.09$
	Mat 1	$L_F = -105t + 234$	$L_T = -.29t + 1.11$

Note: The dimensions of the coefficients are velocity (ft/sec). These data show that breakup occurs faster as the time out of tank increases, or as flow rate decreases. This is fully compatible with prior views on the importance of flow rate. This feature is fundamental in PATSIM and is incorporated in Forest Service rules of thumb for estimating allowable drop heights to preserve ground safety.

When rewritten in a form $\frac{1}{T}$ which is proportional to flow rate, the equations for L_F become

Phos-Chek	Matrix 7	$L_F = 146\frac{1}{T} + 90$
	Matrix 1	$L_F = 264\frac{1}{T} - 103$
Water	Matrix 7	$L_F = 282\frac{1}{T} + 18$
	Matrix 1	$L_F = 210\frac{1}{T} - 81$

EXIT GEOMETRY

Information on exit geometry was obtained primarily from Matrix 2, with supplementary data obtained from most of the remaining matrices. The effect of tank exit geometry on patterns is most difficult to resolve because it may involve any of several parameters, including length, width, length-to-width ratio (L/W), or area (the latter is also a flow rate variable). Regressions were generated for L/W, and for length and width singularly. In this test L/W was constant. All three regressions were then tested as predictors against results from the Head Height Study where the product of L and W was varied. Prior distributions based on the predictors show tank length to be the dominant characteristic:

	Mean Error	Variance	Standard Deviation	Standard Error
Predicted by tank length (L)	14.8	2343	48	16
Predicted by L/W	48.5	1217	36	12
Preicted by W	18	7420	86	28

Regressions in terms of tank length are:

		Phos-Chek	Water
125 kt	150 ft	$L_{90} = 13L + 269$	$L_{90} = 14L + 234$
	300 ft	$L_{90} = 12L + 359$	$L_{90} = 15L + 334$
160 kt	150 ft	$L_{90} = 30L + 230$	$L_{90} = 54L + 334$
	300 ft	$L_{90} = 24L + 243$	$L_{90} = 24L + 239$

Note that these regressions are remarkably stable. With the exception of water at low altitude and 160 knots, the remaining sets of equations are closely paired. This is particularly important in that it lends statistical weight to the trends observed. There is about 100 feet of difference between the high- and low-altitude drops at 125 knots, suggesting that from low altitude, the retardant pattern is still extending when it hits the ground. This does not appear true at 160 knots, where breakup appears to be complete.

When normalized to exclude aircraft-induced spread the equations become:

		Phos-Chek	Water
125 kt	150 ft	$L_F = 13L + 129$	$L_F = 14L + 94$
	300 ft	$L_F = 12L + 219$	$L_F = 15L + 194$
160 kt	150 ft	$L_F = 30L + 52$	$L_F = 54L + 156$
	300 ft	$L_F = 24L + 65$	$L_F = 24L + 61$
125 kt	150 ft	$L_T = 0.06L + 0.61$	$L_T = 0.07L + 0.44$
	300 ft	$L_T = 0.06L + 1.03$	$L_T = 0.07L + 0.92$
160 kt	150 ft	$L_T = 0.17L + 0.29$	$L_T = 0.30L + 0.87$
	300 ft	$L_T = 0.13L + 0.36$	$L_T = 0.13L + 0.34$

There is little basis to assert a difference in performance between water and Phos-Chek as a function of tank length. Length would normally be associated with fluid density to yield a fluid pressure with respect to the airstream. Phos-Chek is about 107% the density of water and, as such, it not clearly resolvable in this experiment. This value is on the order of the difference between length coefficients for Phos-Chek and water in the 125-knot groups.

AIRCRAFT VELOCITY

Aircraft velocity, in addition to influencing the induced spread, imparts inertial force to the retardant and a resulting resistance or drag. These influences are both positive (aircraft-induced spread and inertial forces) and negative (drag). The regressions normalized to 150 feet are:

	Phos-Chek	Water
Configuration C1	$L_{90} = 2.147\ V_{kt} + 135$	$L_{90} = 1.615\ V_{kt} + 174$
Configuration C3	$L_{90} = 0.519\ V_{kt} + 303$	$L_{90} = 1.122\ V_{kt} + 185$

Correcting from knots to feet per second, these equations may be rewritten:

	Phos-Chek	Water
Configuration C1	$L_{90} = 1.27\ V_{fps} + 135$	$L_{90} = 0.956\ V_{fps} + 174$
Configuration C3	$L_{90} = 0.307\ V_{fps} + 303$	$L_{90} = 0.66\ V_{fps} + 185$

To eliminate the aircraft-induced spread, we subtract 0.66 V, yielding a new set of equations showing the effect of velocity on travel from release to breakup:

	Phos-Chek	Water
C1	$L_F = 0.61\ V_{fps} + 135$	$L_F = 0.25\ V_{fps} + 174$
C3	$L_F = -0.35\ V_{fps} + 303$	$L_F = 0\ V_{fps} + 185$

The coefficient of velocity has the dimensions of time. When the release time is subtracted, as above, the data suggest that velocity has minor or even negative effect on breakup of the baseline configuration. The higher the velocity, the quicker the breakup occurs. This would be the expected effect from prior studies. The velocity effect in any case is essentially linear, not reflective of velocity squared as is dynamic pressure. Flight time (or, indeed, length values) can also be derived from Phos-Chek data on configuration. This manipulation yields:

C1 $L_F = 2.62\ V + 145$

C3 $L_F = 0\ V + 190$

This basically supports the velocity independence of the shorter C3 tank (4.8 feet) in breakup time.

Because velocity effects are important in association with configuration, additional analysis was applied to the airspeed matrix. There is a great deal of data in the matrix taken under wind conditions which might be recovered. Unfortunately wind acts in two distinct ways on the pattern. First and most important to modeling, it introduces a difference between ground and airspeed. An existing tailwind would result in our making a drop at higher ground speed since the desired speed is determined using the airspeed indicator. A data point of 190 kts (ground speed) might be comparable to a 180 kts drop with a 10 knot tailwind in terms of the air velocity tending to break the retardant mass. Drift, i.e., wind effects on retardant droplets, is the second effect. It would be expected to introduce a 10 kt forward shift of the pattern with respect to the ground. These factors result in a pattern distortion that cannot be simply resolved. To test the recoverability of wind data, the 180-knot nominal, 300 foot set of Phos-Chek drops from Configuration C3 was examined. This set has six elements due to the rheology experiment matrix (Matrix 8).

Drop No.	L_{90}	V_{kt} (ground speed)	Wind Speed (ft/sec) and Direction	V_{kt} (airspeed)
131	518	180	0	180
156	540	179	-9.5	174
157	428	188	-4.6	185
158	465	187	-3.8	183
159	398	183	-0.4	183
161	428	186	0	161

Note that a local regression in terms of corrected airspeed yields a strong negative slope. Regression of pattern length to resolved wind speed exhibits a poor (0.53) correlation coefficient. As a result, the expanded sets yields little to resolve the velocity as a configuration issue.

RETARDANT QUANTITY

The quantity of retardant is viewed in most current statistics with flow rate as a fundamental of breakup time. In the context of this experiment (Matrix 5), quantity and flow rate are directly related since the time out of the tank was held constant.

Regressions on quantity normalized to a 150-foot drop height are:

Phos-Chek	$L_{90} = 0.130g + 360$	$L_F = 0.130g + 220$	$L_T = 0.0006g + 1.7$
Water	$L_{90} = 0.101g + 340$	$L_F = 0.101g + 200$	$L_T = 0.0004g + 1.6$

Note that gallons divided by length yields the available gallons to make up the pattern distribution:

$$\text{Gallons/ft (Phos-Chek)} = \frac{1}{0.13 + 360/g}$$

$$\text{Gallons/ft (water)} = \frac{1}{0.10 + 340/g}$$

This implication is shown graphically in Figure 111. The data show that the rate of length increase is slow compared to the rate of quantity buildup, and this is important in providing control over retardant densities or coverage levels within the pattern.

A side note on the quantity regression is that the dimensions of the coefficient are of the form (cubic feet/gallons) (area). Like length, they are in the form of a fluid pressure. Rewriting the equations in terms of cubic feet yields:

Phos-Chek $L_{90} = 0.972\ Q + 360$

Water $L_{90} = 0.755\ Q + 340$

The door areas implied of 1.03 ft^2 (Phos-Chek) and 1.32 ft^2 (water) are not however clearly related to physical properties of the tank.

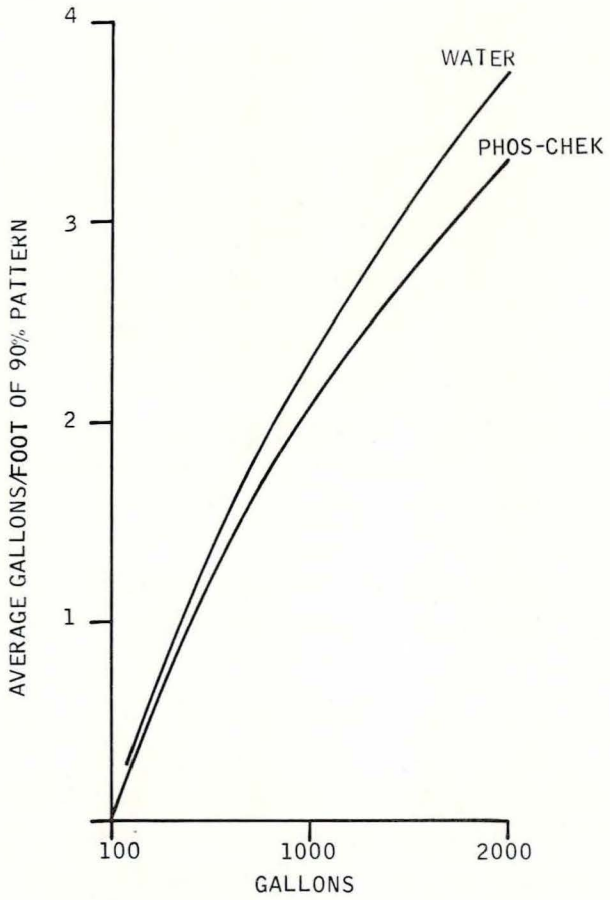

Figure 111.
Rate of Pattern Length Increase
versus Quantity Buildup

TANK SEPARATION

There are two types of tank separations that must be considered in modeling retardant breakup and in tank design. Separation of drops usually occurs to preserve center of gravity stability of the aircraft or the retardant loading scheme, but its effect on pattern performance can be considerable. The first class of separation is fore-to-aft separation along the flight path. Previous studies have lead to the presumption that such drops are essentially additive; i. e., they perform approximately as if they were dropped in a concise volume. This does not appear to be the case.

In the configuration matrix, Configuration C3, a concise volume, was compared with Configuration C6, the same volume separated into two compartments along the flight path. Results were that the separated volumes generally produced longer patterns:

		L_{90} at 125 kt			L_{90} at 160 kt		
		C3	Δft	C6	C3	Δft	C6
Phos-Chek	150 ft	343	27	370	393	112	505
	300 ft	395	19	414	325	127	452
Water	150 ft	307	138	445	405	-40	365
	300 ft	288	73	361	327	96	423

This difference was not the case in 920-gallon drops. Nonetheless there was striking evidence of the reason for this performance in a series of colorometric tests conducted to examine mixing between fluid in different tank compartments. Paint pigment was mixed with the water in various compartments. Later color samples were taken from recovery cups in the pattern. In addition, high-speed color film coverage of the drop was taken from the ground.

These tests clearly show that the front fluid in the tank forms the rear of the pattern. In other words, it is first to break or erode and consequently forms the back of the pattern. The rear quantities are last to loose forward velocity, and they form the front of the pattern. The fluid order in the tank is reversed in the pattern. This is shown in Figure 112. Unfortunately the three colors did not yield a very precise resolution. The yellow was substantially dominated by the red.

A more striking example occurred in the drop from separated tanks. Here films clearly showed the virtually complete breakup of red fluid from the front compartments followed by emergence of the blue fluid from the rear. The pattern (Figure 113) appears almost as the pattern added from sequenced drops, i. e., with a delay between 460-gallon releases. One hypothesis to describe the process may be offered. Both fluid volumes are released over the same time frame. In the airstream only the frontal fluid is subjected to dynamic pressures until it breaks up. The trailing fluid mass flies in the wake of the forward fluid and is not substantially affected by the dynamic air forces. The difference in range in this case would be expected to equal the range due to length from configurational analyses. These conditions are:

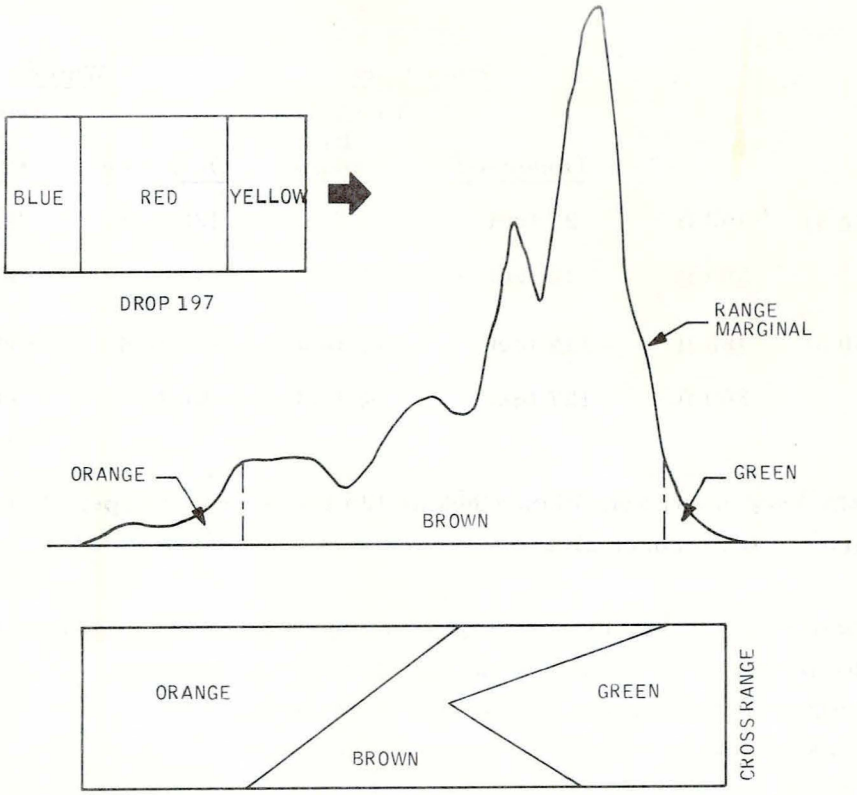

Figure 112. Mixing of Fluid from Various Tank Compartments - 160-foot Drop Height

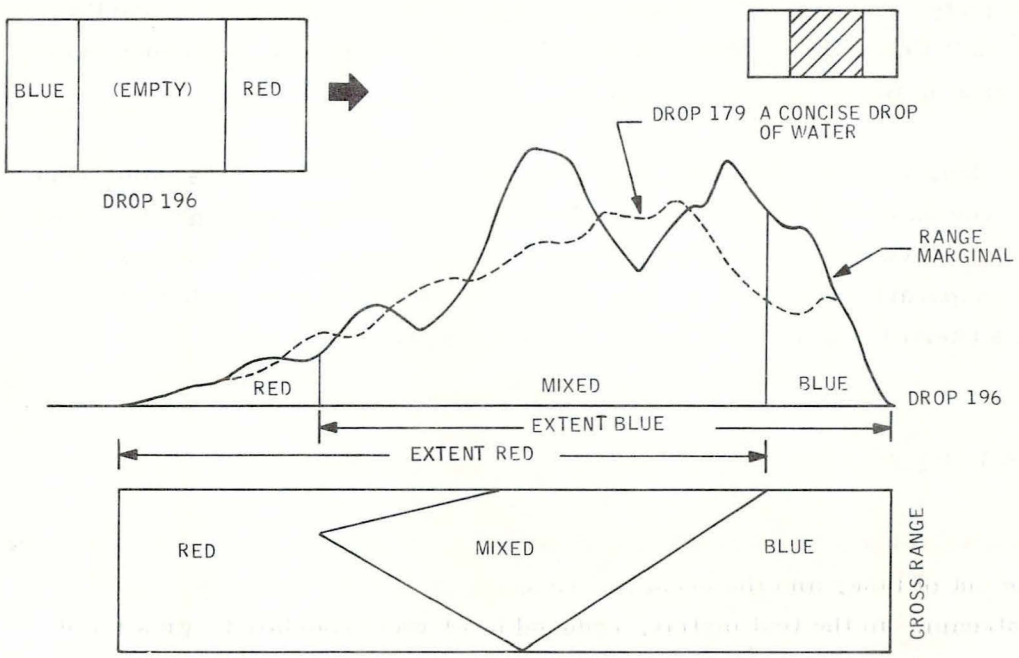

Figure 113. Pattern Formation from Tanks Separated Along the Flight Path - 300-foot Drop Height

		Phos-Chek		Water	
		Observed	Predicted by Length	Observed	Predicted by Length
125 kt	150 ft	27 feet	31 feet	138 feet	34 feet
	300 ft	19 feet	29 feet	73 feet	36 feet
160 kt	150 ft	112 feet	72 feet	-40 feet	130 feet
	300 ft	127 feet	58 feet	96 feet	58 feet

Although the least noisy set, Phos-Chek at 125 knots, would appear to be supportive, the data are far from conclusive.

The nature of this performance is of great interest in modeling pattern formation, but it is not particularly significant in its effect on field results. Patterns generated by fore-to-aft separation covered similar areas with average coverage levels comparable to those generated by concise drops.

The second form of separation is lateral separation of tanks across the flight path. Figure 114 shows mixing from outboard tanks. This mixing appears relatively complete. This contention appears to be supported by results from Matrix 2 where the separated and concise volumes appear to produce very similar patterns in terms of length.

Note that, although laterally separated tanks generate about the same length patterns as their concise counterparts, they do exhibit a tendency to a lower average coverage level. This tendency is supported by observations that a distinct separation can develop in laterally separated drops from low-flow-rate tanks (Aero Union B-17 trail drops, for example).

HEAD-HEIGHT

The conditions of downloading have the effect of reducing the head height, the time out of tank, and the cross-sectional area of retardant opposing the airstream. In the test matrix, reduced head was associated with a fixed quantity, the reduction in time out of tank was not significant (on the order of 15 feet of range or less). Flow rates and configuration do, however, change.

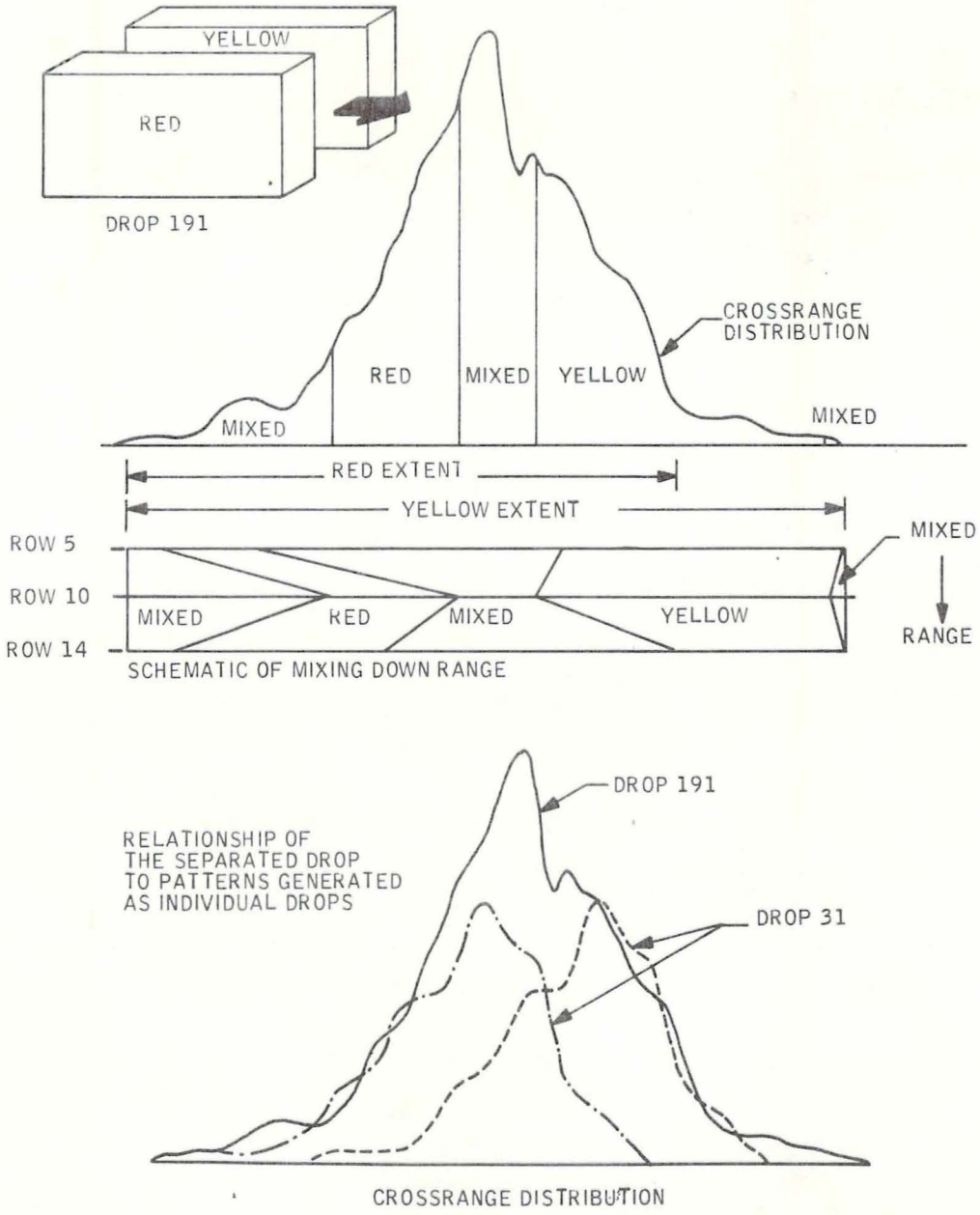

Figure 114. Mixing of Fluid from Laterally Separated Tanks

Generally, however, tank length was the best predictor of performance. Pattern length was, if anything, inversely proportional to flow rate, and the data in general failed to rationalize on any predictor.

COMPARISON OF MATRIX RESULTS

The following predictors estimate performance of the baseline drop – 460 gallons of Phos-Chek released from a compartment 4.8 feet tall, 4.8 feet long, and 2.6 feet wide, dropped at 150 feet from an aircraft traveling at 125 knots:

		L_{90}	Average (gallons/ft)	Determined (ft)	%	Indeterminate (ft)
Time out of tank	Matrix 7	400	1.03	91	22	309
	Matrix 1	345	1.20	52	15	293
Average		372	1.11	71.5	19	301
Tank Length	Matrix 2	331	1.24	62	19	269
A/C Velocity	Matrix 6	367	0.96	64	17	303
Load Size	Matrix 5	420	0.98	60	14	360
Observed		343	1.21			

Each parameter presumes to account for from 15 to 20 percent of the observed performance when examined individually. They are in order of importance time out of tank (flow rate), tank length (configuration) aircraft velocity, and load size. When the values associated with aircraft-induced spread are eliminated, the parametric influence on additional fluid flight are considerably different:

		L_{90} (ft)	Determined (ft)	%	
Time out of tank	Matrix 7	311	221	71	
	Matrix 1	206	-87	42	
Average		258	+67	26	
Tank Length		191	62	32	
A/C Velocity		285	-18	6	Note: would be higher for other Phos-Chek regressions
Quantity		280	60	21	
Observed		203			

In the baseline case, velocity-related effects are minimal when the time of delivery is eliminated – note, however, that the regression on the baseline configuration for velocity has the lowest velocity coefficients of the set. In this case the parameters account for substantially greater percentages of the total prediction.

A second way to view the data is the effect of parametric variations in the distributed amount of retardant; i.e., with a fixed volume of retardant, the average gallons per foot is essentially a function of the distribution length. Figure 115 shows the effect of test parameters on pattern concentrations. It indicates that

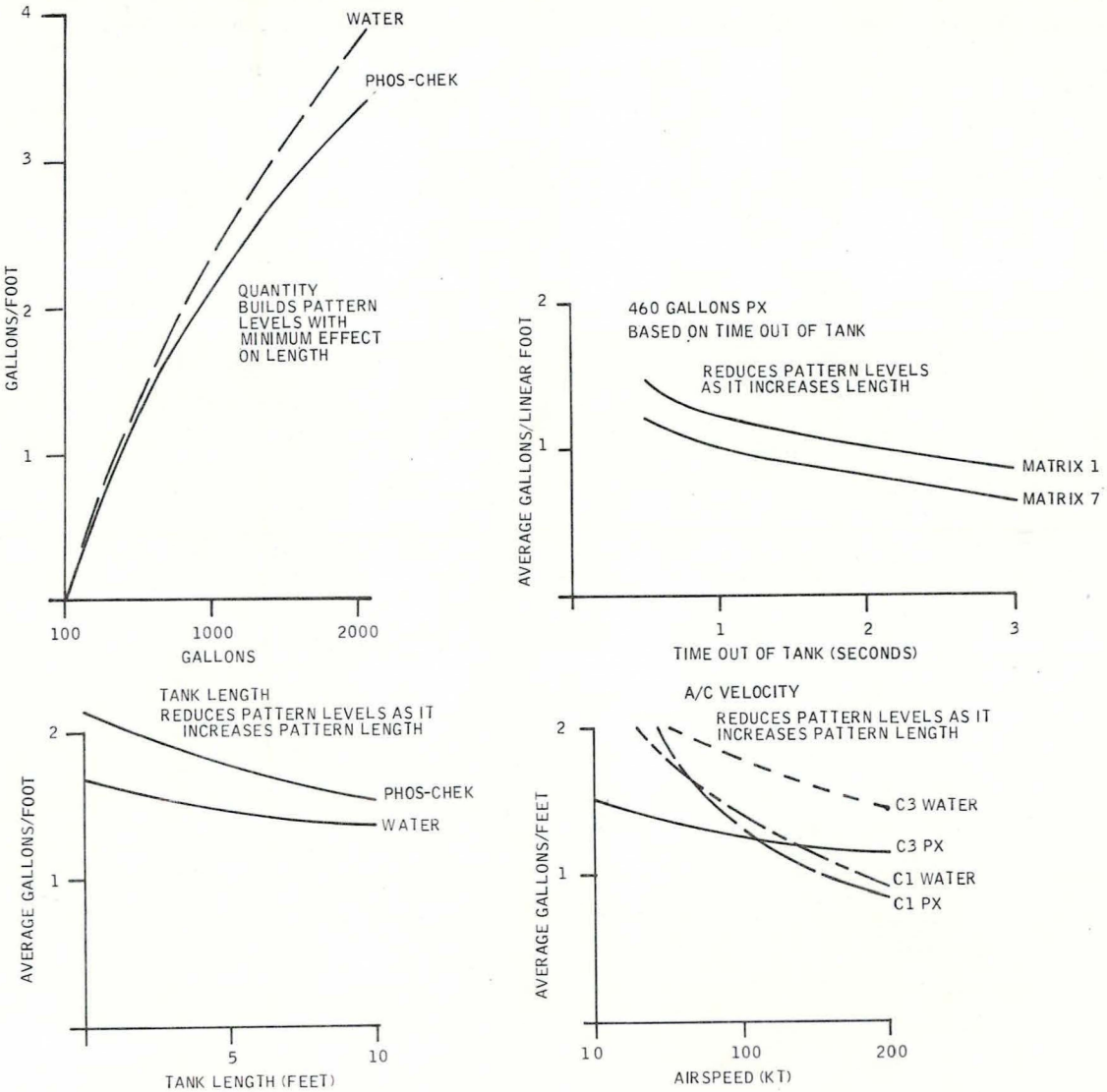

Figure 115. Sensitivity of Baseline Pattern to Test Parameters in Terms of Pattern Length Divided by Available Retardant

length is generally increased by velocity, tank length, and flow rate at the expense of the concentration level of the pattern. The level can be built by increasing quantity with a minimal effect on pattern length (note that actual gallons per linear foot values are substantially less than predicted by this simple approximation).

The above analysis presumes the pattern to be approximated by a Beta distribution. Not all patterns are well defined by this distributed form. The departures come typically at high velocity or at very low flow rates. Both patterns tend to more uniform distributions and consequently uniform though typically at low coverage levels. A similar trend toward uniformity has been observed as the pattern decays over large drop heights. Roughly three forms of distribution appear to occur as shown in Figure 116.

Form C is most desirable if the level can be maintained adequate for coverage. There is little advantage in Form B and it should be avoided.

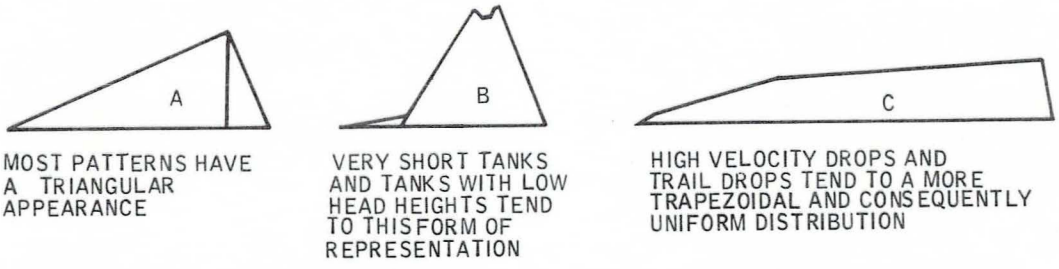
A
B
C
MOST PATTERNS HAVE A TRIANGULAR APPEARANCE
VERY SHORT TANKS AND TANKS WITH LOW HEAD HEIGHTS TEND TO THIS FORM OF REPRESENTATION
HIGH VELOCITY DROPS AND TRAIL DROPS TEND TO A MORE TRAPEZOIDAL AND CONSEQUENTLY UNIFORM DISTRIBUTION

Figure 116. Forms of Retardant Distribution

SECTION IX
CONCLUSIONS AND RECOMMENDATIONS

The results of the ETAGS tests and subsequent analyses showed certain deficiencies in the ability of the PATSIM program to account for all aspects of tank performaces. In particular, the convolution operator that transforms a flow rate distribution to a ground distribution does not have:

- The dynamic range to accommodate all aircraft velocities
- The ability to include the exit geometry of the fluid

Although the program does produce a reasonable predictor under most conditions, a more physically based model is desirable to relate ground pattern performance more decisively to tank design. On the basis of the new understanding of performance effects, some aspects of a new model can be outlined.

The following model elements are presented not as a unified or operable program, but as a point of departure for future simulation attempts and to assist in the subjective understanding of delivery phenomena as it may apply to tank design.

MODEL ELEMENTS

Any new model must relate two substantially independent conditions: (1) flow rate, shown to establish the basic shape of the downrange distribution, and (2) exit geometry or aerodynamic configuration that, in association with aircraft velocity, determines the way the flow rate distribution is transformed to the ground. It would also be desirable to include the mechanism of breakup which contributes variations to the basic patterns. Such models would be useful in assessing the relationship of controllable factors to the variability and repeatability of the ensuing events.

Flow Rate

The first element to consider is flow rate. It concerns the way the fluid in the tank is translated into the airstream.

The 4.8-foot-high fast-fall ETAGS tank with a fast door evacuates at a free-fall rate of about 0.81gt. As a result, the top surface falls as a function of time as shown in Figure 117. Although fluid falling within the tank is retrained, after it drops below the tank walls it will fall at a rate determined by gravity, 32 ft/sec^2. As a result, the bottom surface will fall faster than the top surface. This velocity gradient is a function of the fall rate in the tank and the time to evacuation (for the ETAGS example, 4 ft/sec). This produces an apparent elongation in the fluid mass (Figure 118) that can be seen in most photographs; i.e., the evacuated fluid appears taller than the aircraft tank.

Since the elongated mass has the same volume that it had in the tank (less some breakup products), the vertical expansion must be accommodated by a reduction in length and width. In the absence of other forces, as in a helicopter drop, the shape of the fluid on emergence would appear as in Figure 119.

If this process of elongation were to progress without frontal forces, it ultimately would cause the fluid column to break in tension, just as the slow stream from a faucet degenerates into droplets (Figure 120). The velocity gradient, and the tension failures it promotes, contribute to the growth of instabilities on the frontal surface under the influence of the airstream.

The velocity gradient imparted to the fluid mass by tank evacuation continues to contribute to the breakup process. As the time out of the tank increases with increases in head height or flow rate restriction, it becomes more and more predominant in influencing the formation of the pattern. The problem remains to relate this process to the more dramatic force structure operating on the front surface of the mass in aircraft delivery.

When retardant is delivered from fixed-wing aircraft, dynamic pressures on the frontal surface dominate the breakup process. A series of high-speed photographs from the ETAGS test series shows the release and flight of the fluid-mass resulting from a water drop. This film taken with sunlight backlighting the drop has the effect of x-raying the drop and separating the intact fluid (a dark mass) from the early products of breakup. The film clearly illustrates the vertical elongation of the fluid-mass. The width appears constant or slightly expanding. Effects on tank length are occluded by the mass itself. It is likely the shape change to accommodate the vertical expansion from the velocity gradient is a foreshortening of the length of the fluid column facing the airstream. Under these conditions, the shape of the mass on full exit from the tank is approximately that shown in Figure 121.

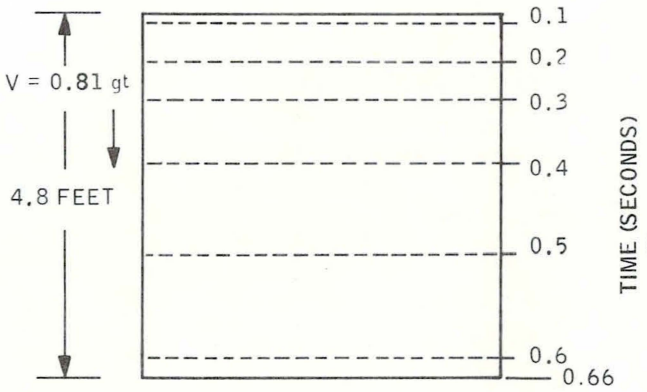

Figure 117. Location of Fluid Head During Tank Evacuation

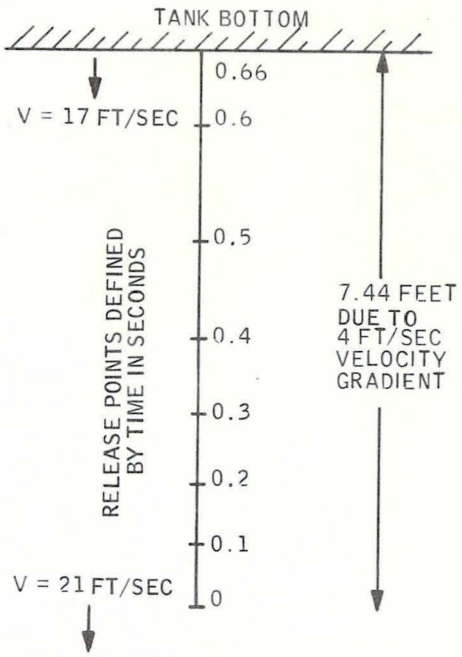

Figure 118. Fluid Elongation at Tank Evacuation

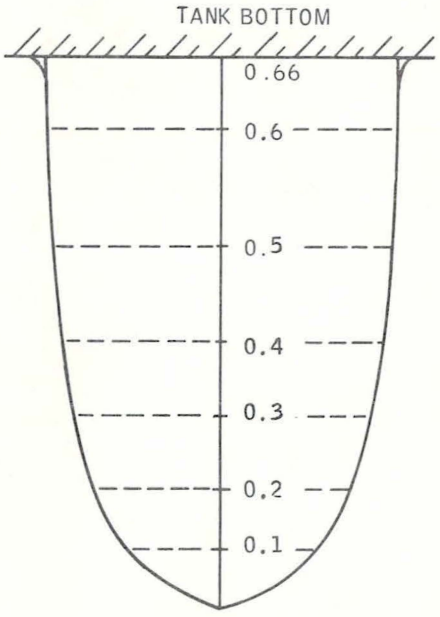

Figure 119. Example of How Fluid Column Reforms to Maintain Equal Volume while Increasing in Length

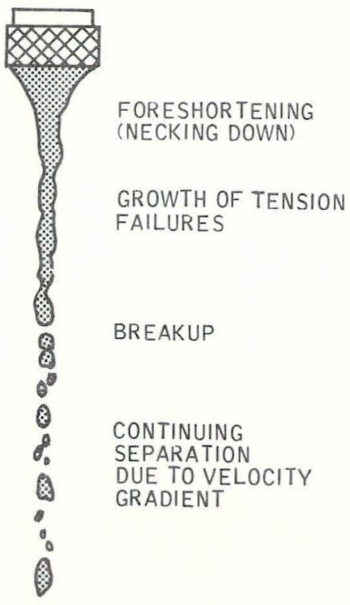

Figure 120. Faucet Example

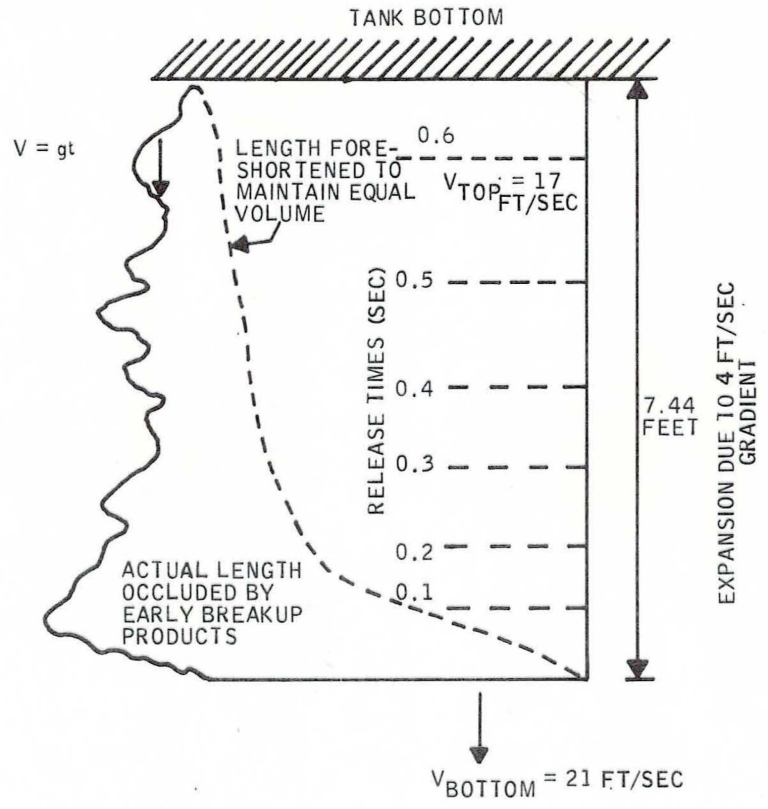

Figure 121. Approximate Shape of Fluid Mass on Full Exit from Tank

This model suggests that the vertical elongation of the fluid-mass is a function of time out of tank. The length of the fixed-volume column at tank evacuation is determined by the distance the first emerging fluid will have fallen under gravity at the time the last fluid increment leaves the tank. This vertical elongation in the absence of other breakup is a free-fall curve (Figure 122).

With a fixed volume, this elongation must be accommodated by a proportional area reduction. If the length-to-width ratio remains constant, this results in an apparent length reduction which is proportional to the root of the ratio between the initial fluid height (head) and the elongated height (Figure 123). This can be related to the ETAGS configurations as shown in Figure 124. If we assign cataclysmic breakup to the conditions when the dynamic frontal pressure equals the fluid column pressure opposing it, the breakup limits for two retardants at two velocities can be estimated as shown in Figure 124. The 4.8-foot, head ETAGS tank in the Matrix 1 configuration is 4.8 feet long in exit geometry. In this case the elongation to catastrophic failure would occur at about 2.6 seconds evacuation time for water and about 3 seconds for Phos-Chek. Average time out of tank producing zero flight for Matrix 7 and Matrix 1 tests were 2.68 and 3.3 seconds for Phos-Chek and water respectively.

Tank Configuration

If a fluid column is released into air with a forward velocity, V, it is resisted by the dynamic pressure, Q. The fluid is decelerated by the ratio of the dynamic pressure and the fluid pressure, pL (density x length) to:

$$a = \frac{Qpsi\ G}{pL}$$

If the fluid column were a solid it would be slowed at this acceleration rate by frontal (and skin) drag. But an unrestrained fluid has no strength in compression. Consequently, the column will collapse, displacing fluid laterally (or vertically) from the front. The rear surface will move forward virtually unslowed while drag energy is dissipated laterally. The situation is analagous to the stream from a hose splashing against a soft, receding wall. It is shown schematically in Figure 125.

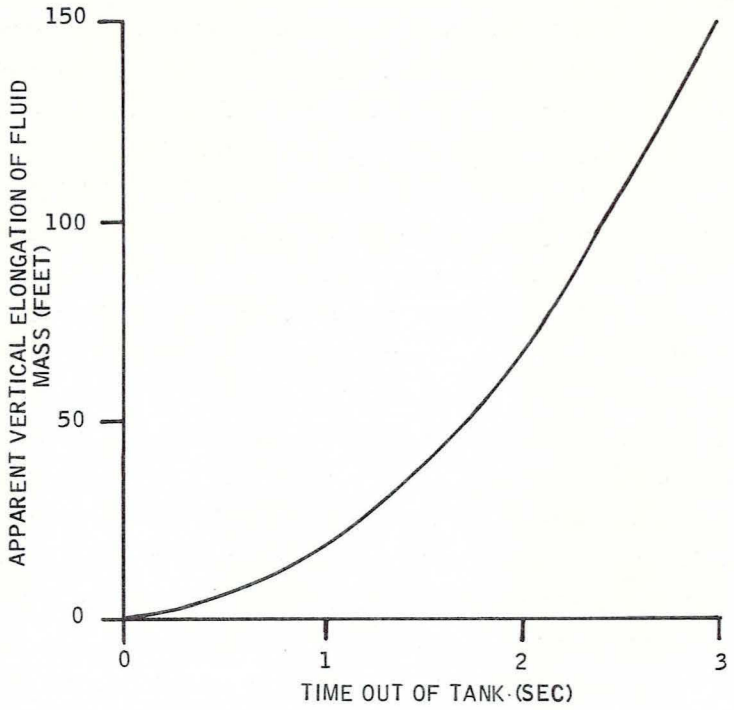

Figure 122. Vertical Fluid Elongation Due to Flow Rate and its Effect on Breakup

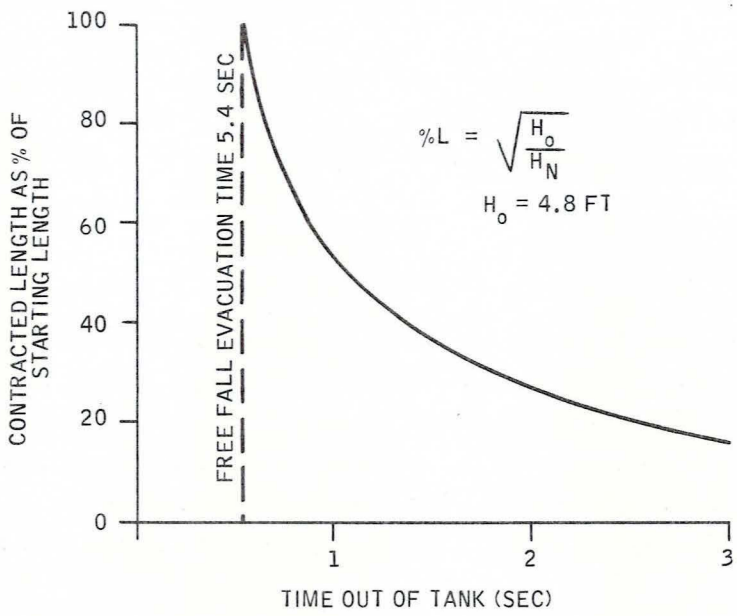

Figure 123. Fluid Contraction as a Function of Time Out of Tank

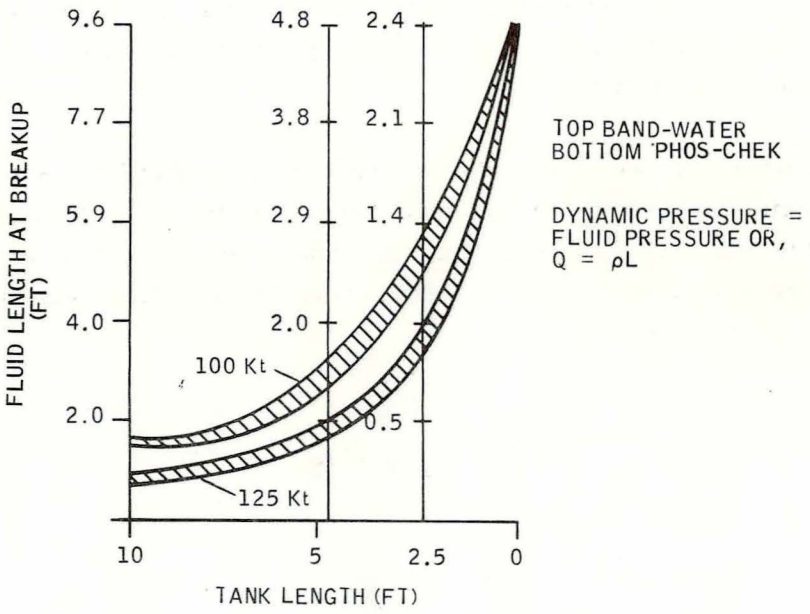

Figure 124. Theoretical Breakup Length

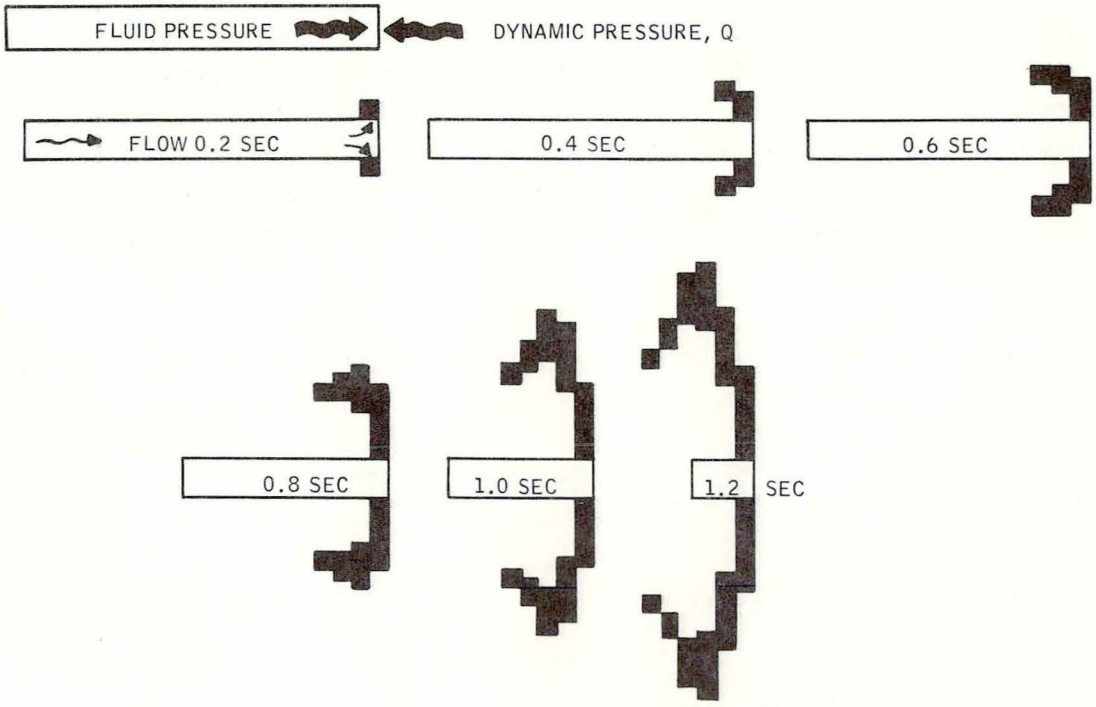

Figure 125. Approximate Model for Fluid Column Breakup

Under this hypothesis a 5-foot-long column of fluid in a 200-ft/sec airstream will collapse in about 1.3 seconds 260 feet downrange from its release point and about 27 feet below the aircraft.

This mechanism of breakup, based on acceleration, is intuitively satisfying in that it projects a process similar to that observed in the colorometric test series; i.e., the fluid mass inverts itself from the front in forming the pattern. It is also appropriate in describing the observed flow shown in films emanating laterally from a vertical parting line:

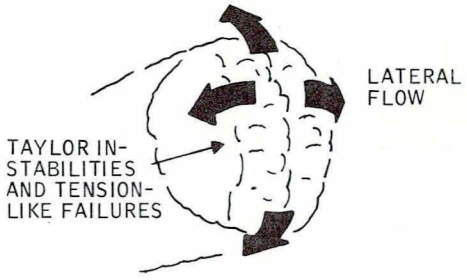

Unfortunately, the data analysis shows that flight to breakup is not nearly so strong a function of length as this hypothesis would suggest. The effect of tank length facing the airstream generated on this basis alone yields little correspondence to the actual data, as shown in Figure 122. If the length decay rule is superimposed on the velocity gradient, the curve crossing through the regressions can be generated by approximate techniques (Figure 126). Basically, the forward velocity of the rear-most fluid is viewed as the sum of two velocities: velocity due to vertical velocity gradient plus velocity due to horizontal deceleration. This has the effect of reducing the significance of length on the projected breakup times.

A second point of comparison is the implied performance over the velocity range as shown by the following matrix analysis:

	Phos-Chek	Water	Model
C_1 breakup distance range function of velocity	$0.61\ V_{fps}$	$0.29\ V_{fps}$	$0.33\ V_{fps}$
C_3 breakup distance range function of velocity	$-0.35\ V_{fps}$	$0\ V_{fps}$	$-0.05\ V_{fps}$
C_2 breakup distance range function	N/A	N/A	$-0.21\ V_{fps}$

This suggests reasonably consistent model response to analytical values.

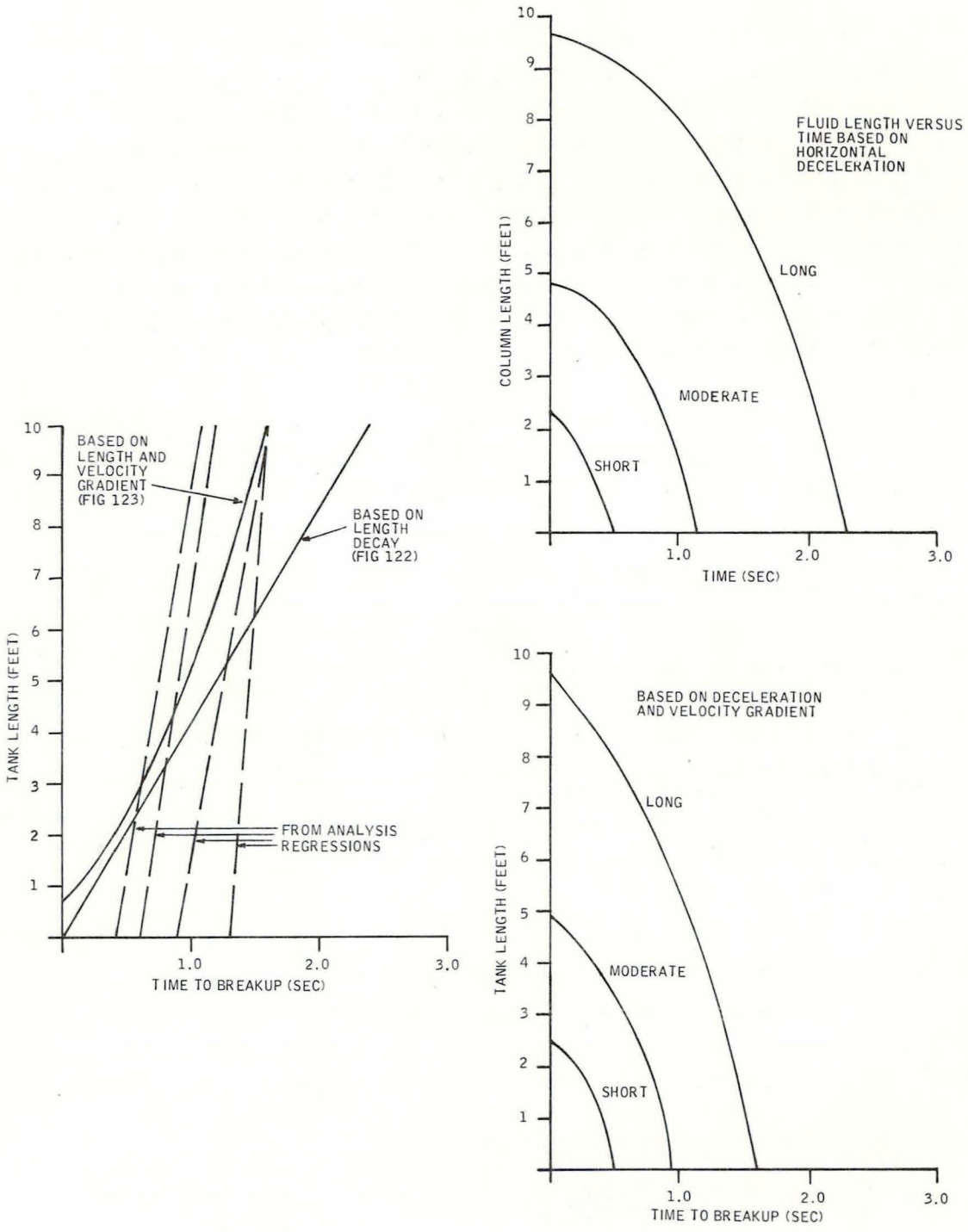

Figure 126. Fluid Breakup as a Function of Time and Tank Configuration

APPROXIMATE EFFECTS OF THE PROPOSITIONS ON PATTERN FORMATION

The pattern implications of this modeling hypothesis can be estimated by construction methods as a check on its ability to predict the form of the patterns. First, construct a tank divided into volume increments of fixed time interval (Figure 127(a)). Start length decay of each column on its emergence from the tank as in Figure 127(b), using the length decay rule of Figure 124. Although the model suggests that the actual foreshortening occurs in the rear, the loss occurs at the front. This frontal loss convention is used here to relate estimated patterns to fluid locations in the tank. The released quantity in each 0.1-second increment can then be accumulated in a 20-foot cell on a range distribution. This process yields the patterns of Figure 128.

The patterns thus generated bear reasonable likenesses to the actual pattern distributions in the configuration study matrix. Although the model is not precise, it appears to relate configuration and flow rate factors in a manner that adds to the comprehension of tank contributions to ground patterns.

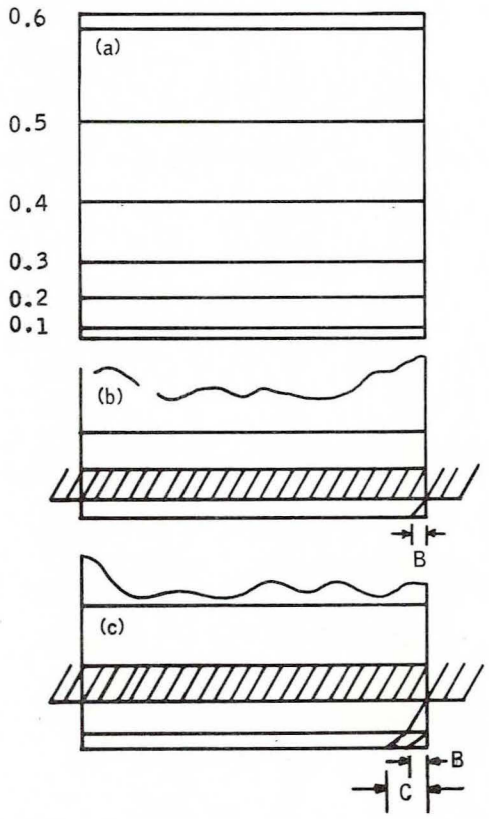

Figure 127. Sequence of Tank Evacuation

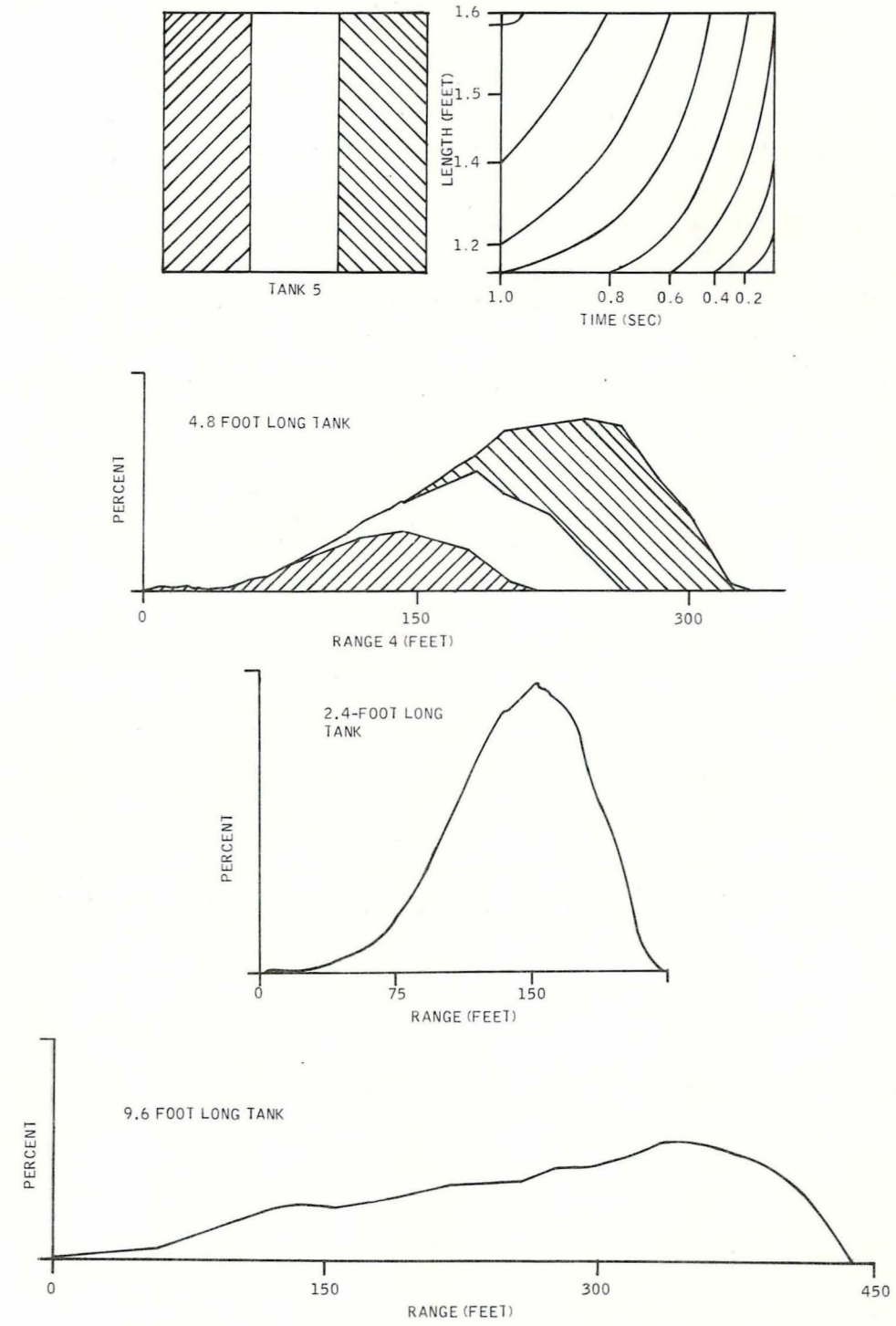

Figure 128. Pattern Formations Generated Using an Approximate Model

REFERENCES

1. Swanson, D. H., Luedecke, A. D., Helvig, T. N., and Parduhn, F. J., "Development of User Guidelines for Selected Retardant Aircraft," Final Report, Contract 26-3332, 15 February 1975, Honeywell Inc., Government and Aeronautical Products Division, Hopkins, Minnesota 55343.

2. MacPhearson, J. I., "A Theoretical Model for the Prediction of the Distribution of Water Released from a Water Bomber," Aeronautical Report LR-480, National Research Council of Canada, Ottawa, March, 1967.

3. Swanson, D. H., Luedecke, A. D., Helvig, T. N., and Parduhn, F. J., "Development of User Guidelines for Selected Retardant Aircraft," Supplement to Final Report, Contract 26-3332, April 1977, Honeywell Inc., Defense Systems Division, Hopkins, Minnesota 55343.

4. Thompson, Catherine M., Biometrika 32, 151-181. (Reprinted in E. S. Pearson and Hartley 1954, T. 16, pp 142-155; Vianelli 1959, Pro. 211, pp 661-674)

5. Nelson, L. S., "Weibul Probability Paper," Industrial Quality Control, March 1967.

6. Pearson, K., Tables of the Incomplete Beta Function, London (Biometrika Office), 1934.

INERTIAL LOADING CONDITIONS

- **COND A**

  n_x = -3.0 g's (FORWARD)

  n_z = -1.0 g's (DOWN)

- **COND B**

  n_y = ±1.5 g's (LATERAL)

  n_z = -1.0 g's (DOWN)

- **COND C**

  n_z = 1.0 g's (UP)

- **COND D**

  n_z = -3.0 g's (DOWN)

INTERNAL PRESSURE LOADING CONDITIONS

(CENTER COMPARTMENT ONLY)

- **COND E**

  P = 3.0 PSI (FULL CENTER COMPARTMENT)

  n_z = -1.0 g's (DOWN)

- **COND F**

  P = 5.4 PSI (EMPTY CENTER COMPARTMENT)

  n_z = -1.0 g's (DOWN)

NOTES:

- COND A-F ARE LIMIT LOADING CONDITIONS
- THE ULTIMATE FACTOR OF SAFETY FOR THE INERTIAL LOADS IS 1.5
- THE ULTIMATE FACTOR OF SAFETY FOR THE PRESSURE LOADS IS 2.0
- COND A-F ARE CONSIDERED INDEPENDENTLY

CALC	GRJ	11-25-74	REVISED	DATE
CHECK				
APR				
APR				

STRUCTURAL DESIGN CRITERIA

AEROSPACE & DEFENSE GROUP
GOVERNMENT & AERONAUTICAL PRODUCTS DIVISION

EWA No	TYPE No	PAGE 3

HT-51 REV 11/71

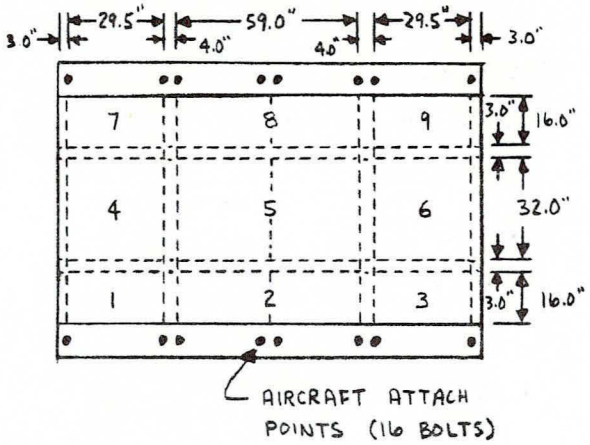

WEIGHT DISTRIBUTION

EMPTY TANK	=	2,500 LBS
RETARDANT	=	20,000
TOTAL WT	=	22,500 LBS

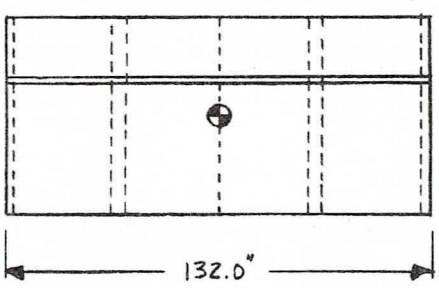

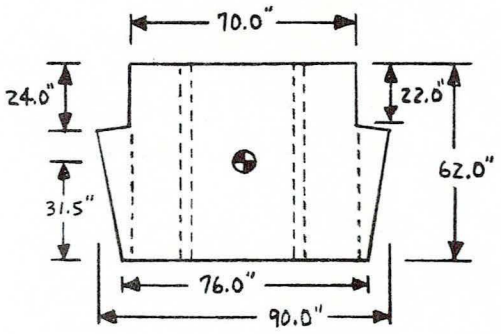

CALCULATE RETARDANT WEIGHT FOR VARIOUS COMPARTMENTS

RETARDANT DENSITY = 10 LBS/GAL = .0433 LBS/IN^3
RETARDANT DEPTH = 61.2 INCHES

WT = VOLUME × DENSITY

$WT_1 = WT_3 = WT_7 = WT_9 = 16.0 \times 29.5 \times 61.2 \times .0433 = 1250$ LBS

$WT_2 = WT_8 = 16.0 \times 59.0 \times 61.2 \times .0433 = 2500$ LBS

$WT_4 = WT_6 = 32.0 \times 29.5 \times 61.2 \times .0433 = 2500$ LBS

$WT_5 = 32.0 \times 59.0 \times 61.2 \times .0433 = 5000$ LBS

$\Sigma WT = 4 \times 1250 + 2 \times 2500 + 2 \times 2500 + 5000 = 20{,}000$ LBS

CALC	GRJ	11-26-74	REVISED	DATE
CHECK				
APR				
APR				

GEOMETRY AND WEIGHT DISTRIBUTION

AEROSPACE & DEFENSE GROUP
GOVERNMENT & AERONAUTICAL PRODUCTS DIVISION

EWA No	TYPE No	PAGE 4

HT-51 REV 11/71

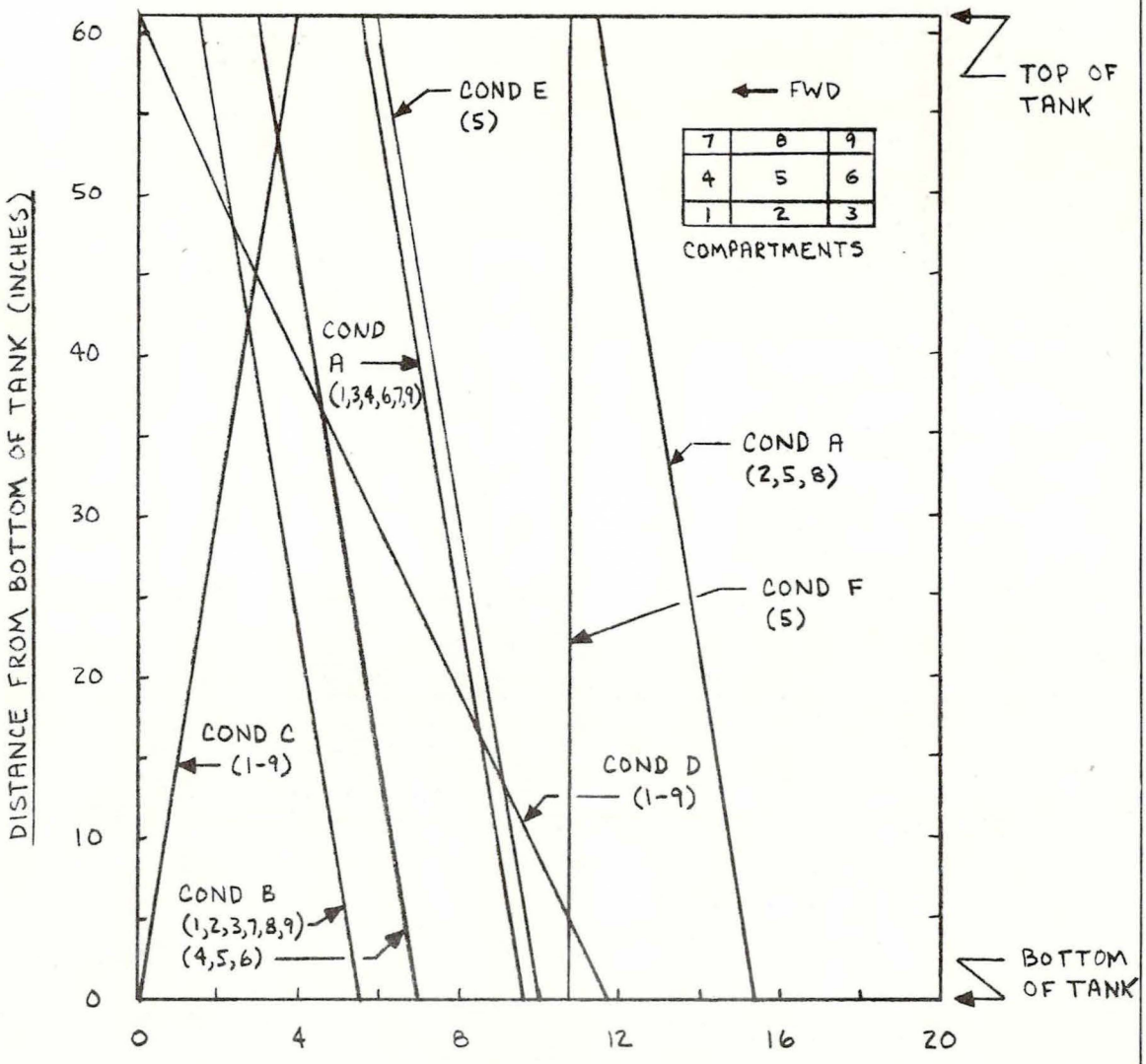

NOTES: • SEE PAGES 3 & 4 FOR LOADING CONDITIONS & WEIGHTS

• NUMBERS IN ( ) REFER TO COMPARTMENTS IN WHICH THE PRESSURES OCCUR

CALC	GRJ	11-25-74	REVISED	DATE
CHECK				
APR				
APR				

ULTIMATE DESIGN PRESSURES

AEROSPACE & DEFENSE GROUP
GOVERNMENT & AERONAUTICAL PRODUCTS DIVISION

EWA No	TYPE No	PAGE 5

HT-51 REV 11/71

NOTE: THE MAX NORMAL PRESSURES OCCUR FOR LOADING CONDITION A, AND THEY ACT ON THE FORWARD WALL OF COMPARTMENTS 2, 5 & 8. (SEE P. 5)

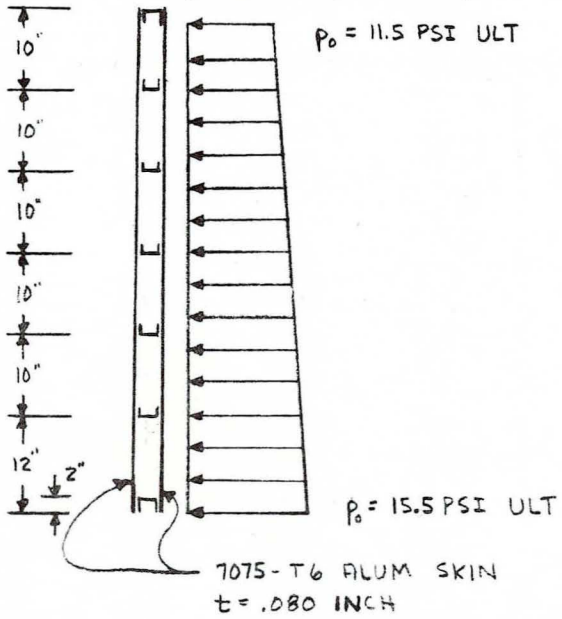

MATERIAL:

7075-T6 ALUM

F_u = 75,000 PSI

LOWER SPAN IS CRITICAL BECAUSE OF HIGHER PRESSURE (P_o = 15.5 PSI)

ULT BENDING MOMENT, M_p, FOR UNIT STRIP OF SKIN

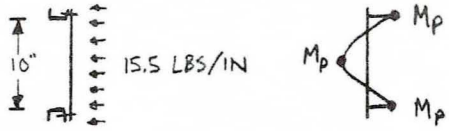

$M_p = \frac{1}{16}\omega l^2 = \frac{1}{16}(15.5)(10)^2$

M_p = 96.9 IN-LBS ULT ✓

ULT BENDING STRESS

$f_b = \frac{4M_p}{t^2} = \frac{4 \times 96.9}{(.08)^2}$

f_b = 60,563 PSI ULT ✓

$M.S. = \frac{75,000}{60,563} - 1$

→ M.S. = +.24 ✓

NOTE: CHANNEL ANALYSIS IS SHOWN ON PP. 9-11.

CALC	GRJ	1-8-75	REVISED	DATE
CHECK				
APR				
APR				

SIDEWALL SKIN ANALYSIS FOR MAX NORMAL PRESSURE (COND A)

AEROSPACE & DEFENSE GROUP
GOVERNMENT & AERONAUTICAL PRODUCTS DIVISION

EWA No	TYPE No	PAGE 6

HT-51 REV 11/71

AVE ULT PRESSURE, P_o, ON 20" SPAN { COND A / SEE P. 5 }

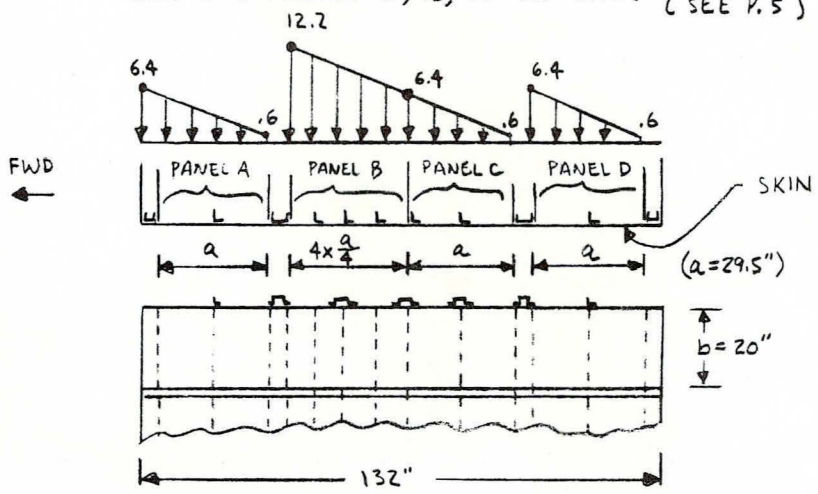

SKIN MATERIAL:
7075-T6 ALUM
$F_u = 75{,}000$ PSI

SKIN THICKNESS
$t = .080"$

ULTIMATE PRESSURE CAPACITY, P_{ULT}, FOR PANELS A, C, & D

$$P_{ULT} = \frac{\beta F_u t^2}{ab}$$ { ROARK - P. 243 / UNIFORM PRESSURE WITH FIXED EDGES }

$$\frac{b}{a} = \frac{20}{29.5} = .68 \Rightarrow \beta = 8.4$$

$$P_{ULT} = \frac{8.4 \times 75{,}000 \times .080^2}{29.5 \times 20}$$

$P_{ULT} = 6.8$ PSI

$$M.S. = \frac{\bar{P}_o}{P_{ULT}} - 1$$

$$M.S. = \frac{6.8}{3.5} - 1$$

→ $M.S. = +.94$

NOTE: THE M.S. IS COMPUTED FOR THE AVERAGE STRESS, $\bar{P}_o = 3.5$ PSI, ON PANELS A, C, & D. ALSO, THE EFFECT OF THE VERTICAL ANGLE WILL INCREASE THE STRENGTH.

ULTIMATE BENDING STRESS FOR PANEL B

ASSUME SKIN "BEAMS" PRESSURE TO VERTICAL ANGLES (SPAN = $\ell = \frac{a}{4} = 7.38"$)

$$M = \frac{1}{16} w \ell^2 = \frac{1}{16}(12.2)(7.38)^2$$

$M = 41.5$ IN-LBS ULT

$$f_b = \frac{4M}{t^2} = \frac{4 \times 41.5}{(.08)^2}$$

$f_b = 25{,}938$ PSI ULT

NOTE: ANALYSIS OF VERTICAL ANGLES SHOWN ON P. 12.

$$M.S. = \frac{75{,}000}{25{,}938} - 1$$

→ $M.S. = +1.89$

CALC	GRJ	1-9-75	REVISED	DATE
CHECK				
APR				
APR				

UPPER EXTERNAL SKIN ANALYSIS FOR MAX NORMAL PRESSURE (COND A)

AEROSPACE & DEFENSE GROUP
GOVERNMENT & AERONAUTICAL PRODUCTS DIVISION

EWA No	TYPE No	PAGE 7

HT-51 REV 11/71

ULT PRESSURES, P_o, ON TOP SKIN

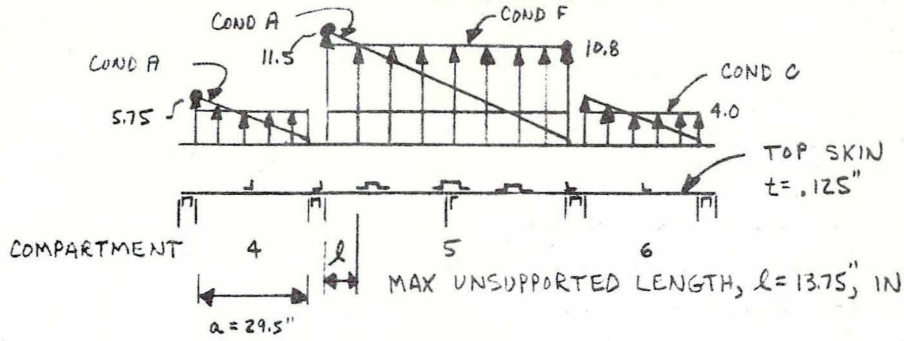

MAX UNSUPPORTED LENGTH, $\ell = 13.75"$, IN COMPARTMENT 5

WIDTH OF COMPARTMENTS, $b = 32"$

MATERIAL:
7075-T6 ALUM
F_u = 75,000 PSI

ULTIMATE PRESSURE CAPACITY, P_{ULT}, FOR TOP SKIN ON COMPARTMENTS 4 & 6

$$P_{ULT} = \frac{B F_u t^2}{ab}$$ { ROARK - P.243 UNIFORM PRESSURE WITH FIXED EDGES }

$$\frac{a}{b} = \frac{29.5}{32} = .92 \Rightarrow B = 6.0$$

$$P_{ULT} = \frac{6.0 \times 75{,}000 \times .125^2}{29.5 \times 32}$$

P_{ULT} = 7.45 PSI ✓

$$M.S. = \frac{7.45}{4.0} - 1$$

→ M.S. = +.86 ✓

NOTE: M.S. IS BASED ON COND C - P_o = 4.0 PSI

ULTIMATE BENDING STRESS FOR TOP SKIN ON COMPARTMENT 5

ASSUME SKIN "BEAMS" PRESSURE TO HORIZONTAL ⌐¬ SECTIONS

$$M = \frac{1}{16} w \ell^2 = \frac{1}{16}(11.5)(13.75)^2$$ (SPAN = ℓ = 13.75")

M = 135.9 IN-LBS ULT ✓

$$f_b = \frac{4M}{t^2} = \frac{4 \times 135.9}{.125^2}$$

$$M.S. = \frac{75{,}000}{34{,}790} - 1$$

f_b = 34,790 PSI ULT ✓

→ M.S. = +1.16 ✓

NOTES: ANALYSIS OF HORIZONTAL ⌐¬ SECTIONS SHOWN ON P. 12.

CUTOUTS IN TOP SKIN MUST BE REINFORCED TO DEVELOP FULL STRENGTH OF SKIN.

CALC	GRJ	1-9-75	REVISED	DATE
CHECK				
APR				
APR				

TOP SKIN ANALYSIS FOR MAX NORMAL PRESSURE (COND A, C, & F)

AEROSPACE & DEFENSE GROUP
GOVERNMENT & AERONAUTICAL PRODUCTS DIVISION

EWA No	TYPE No	PAGE 8

HT-51 REV 11/71

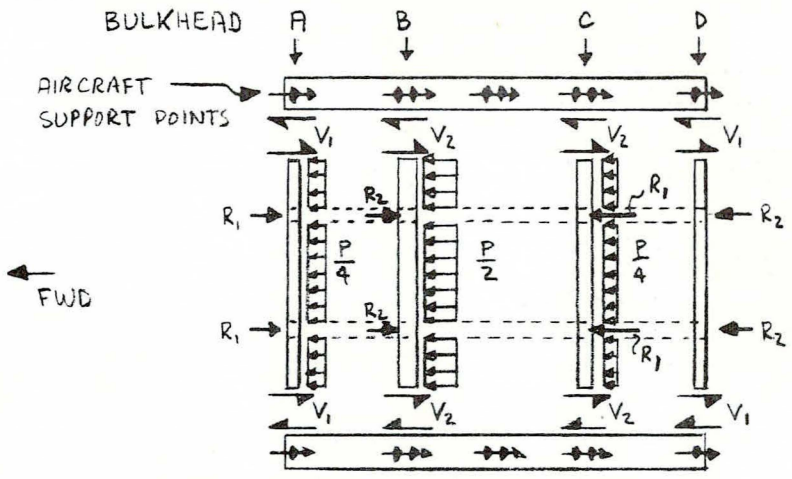

P = TOTAL ULT LOAD IN FORWARD DIRECTION

$P = 1.5 \times 3.0\ g's \times 22{,}500$ LBS

$P = 101{,}250$ LBS ULT ✓

$V_1 = \frac{P}{12}$

$V_1 = 8438$ LBS ULT ✓

$V_2 = 2V_1 = \frac{P}{6}$

$V_2 = 16{,}875$ LBS ULT ✓

$R_1 = \frac{P}{24}$

$R_1 = 4219$ LBS ULT ✓

$R_2 = \frac{P}{12}$

$R_2 = 8438$ LBS ULT ✓

NOTE:

THE ABOVE LOADS DO NOT INCLUDE THE EFFECTS OF THE VERTICAL LOADS DUE TO $n_z = 1.0$ g DOWN. THIS EFFECT IS SMALL, HOWEVER, AND WILL NOT SIGNIFICANTLY AFFECT THE RESULTS.

ULTIMATE BENDING MOMENTS FOR BULKHEADS (IN-KIPS)

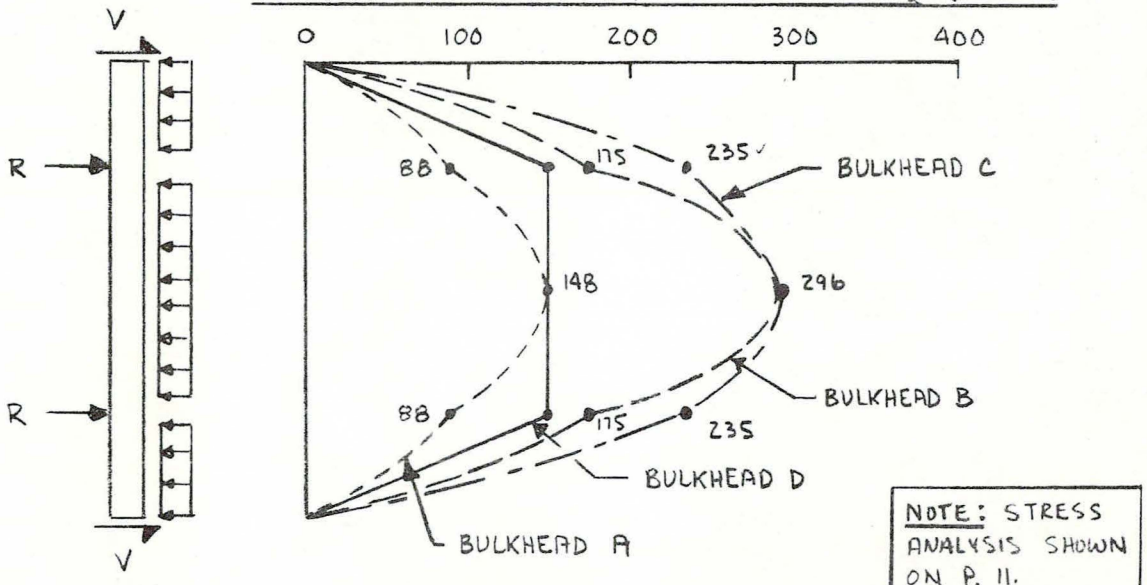

NOTE: STRESS ANALYSIS SHOWN ON P. 11.

CALC	GRJ	12-15-74	REVISED	DATE
CHECK				
APR				
APR				

INTERNAL CHANNEL LOADS FOR COND A

AEROSPACE & DEFENSE GROUP
GOVERNMENT & AERONAUTICAL PRODUCTS DIVISION

EWA No	TYPE No	PAGE 9

HT-51 REV 11/71

ULT PRESSURES, P_o, ON TOP SKIN

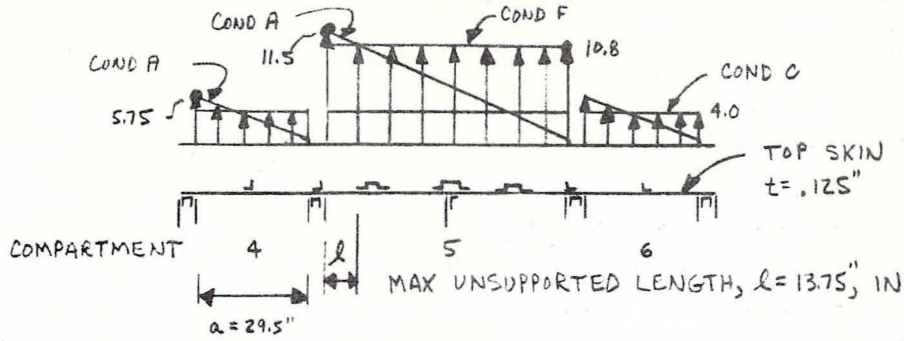

MAX UNSUPPORTED LENGTH, $\ell = 13.75"$, IN COMPARTMENT 5

WIDTH OF COMPARTMENTS, $b = 32"$

MATERIAL:
7075-T6 ALUM
F_u = 75,000 PSI

ULTIMATE PRESSURE CAPACITY, P_{ULT}, FOR TOP SKIN ON COMPARTMENTS 4 & 6

$$P_{ULT} = \frac{B F_u t^2}{ab}$$ { ROARK - P.243 UNIFORM PRESSURE WITH FIXED EDGES }

$$\frac{a}{b} = \frac{29.5}{32} = .92 \Rightarrow B = 6.0$$

$$P_{ULT} = \frac{6.0 \times 75{,}000 \times .125^2}{29.5 \times 32}$$

P_{ULT} = 7.45 PSI ✓

$$M.S. = \frac{7.45}{4.0} - 1$$

→ M.S. = +.86 ✓

NOTE: M.S. IS BASED ON COND C - P_o = 4.0 PSI

ULTIMATE BENDING STRESS FOR TOP SKIN ON COMPARTMENT 5

ASSUME SKIN "BEAMS" PRESSURE TO HORIZONTAL ⌐¬ SECTIONS

$$M = \frac{1}{16} w \ell^2 = \frac{1}{16}(11.5)(13.75)^2$$ (SPAN = ℓ = 13.75")

M = 135.9 IN-LBS ULT ✓

$$f_b = \frac{4M}{t^2} = \frac{4 \times 135.9}{.125^2}$$

$$M.S. = \frac{75{,}000}{34{,}790} - 1$$

f_b = 34,790 PSI ULT ✓

→ M.S. = +1.16 ✓

NOTES: ANALYSIS OF HORIZONTAL ⌐¬ SECTIONS SHOWN ON P. 12.

CUTOUTS IN TOP SKIN MUST BE REINFORCED TO DEVELOP FULL STRENGTH OF SKIN.

CALC	GRJ	1-9-75	REVISED	DATE
CHECK				
APR				
APR				

TOP SKIN ANALYSIS FOR MAX NORMAL PRESSURE (COND A, C, & F)

AEROSPACE & DEFENSE GROUP
GOVERNMENT & AERONAUTICAL PRODUCTS DIVISION

EWA No	TYPE No	PAGE 8

HT-51 REV 11/71

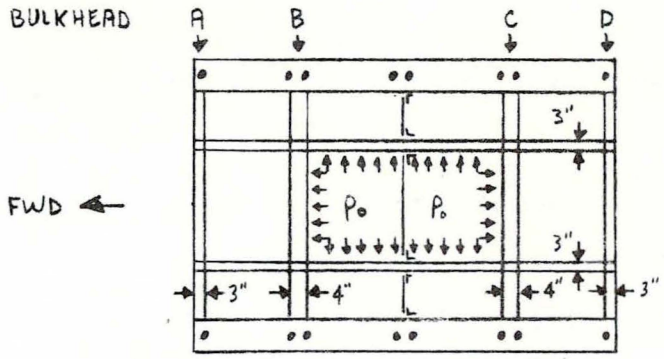

P_o = 10.8 PSI ULT
COND F (SEE P. 5)

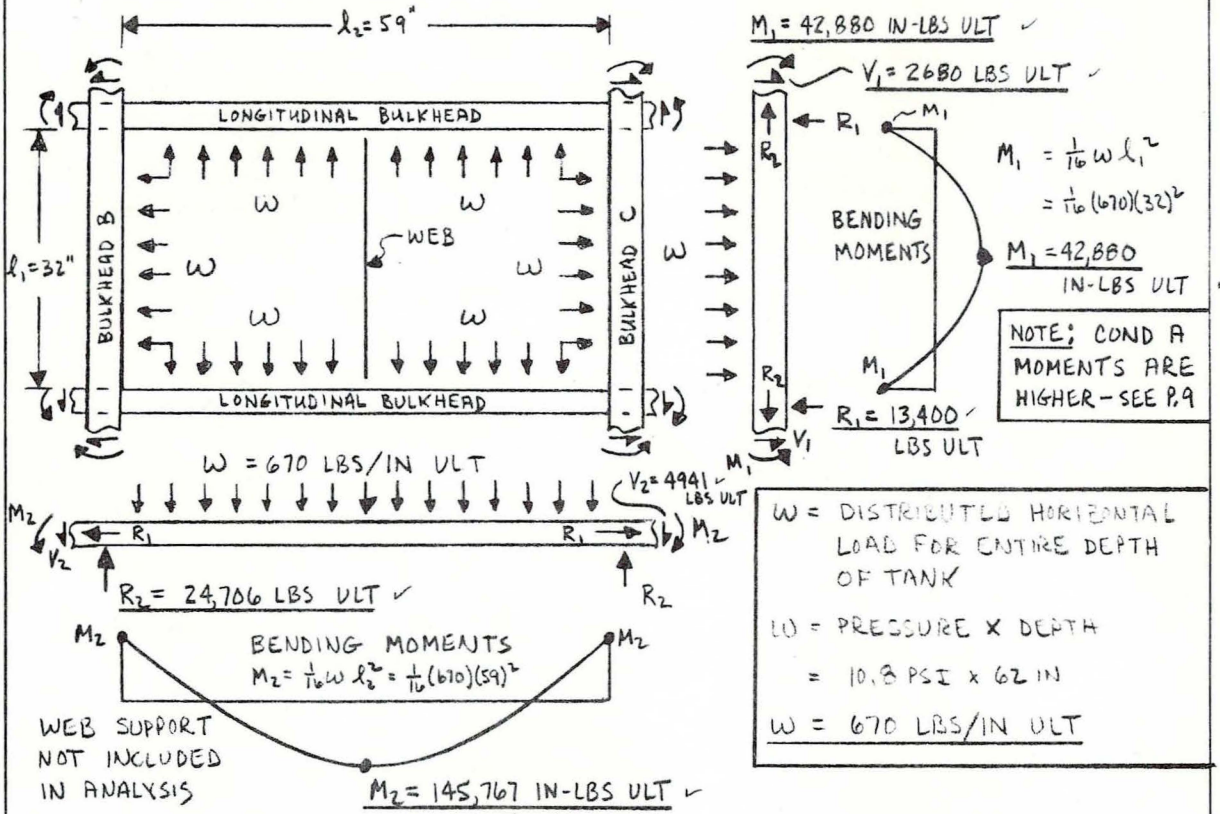

NOTE; COND A MOMENTS ARE HIGHER – SEE P.9

w = DISTRIBUTED HORIZONTAL LOAD FOR ENTIRE DEPTH OF TANK

w = PRESSURE x DEPTH
= 10.8 PSI x 62 IN
w = 670 LBS/IN ULT

NOTE: THE LONGITUDINAL BULKHEAD HAS A 3" DEPTH AND A CROSS-SECTION SIMILAR TO THE FORWARD AND AFT BULKHEADS (A & D) SHOWN ON P. 9. THE MAX BENDING MOMENT IN THE LONGITUDINAL BULKHEAD (M=145,767) IS SLIGHTLY LESS THAN IN THE THE FORWARD AND AFT BULKHEADS (M=148,000). SEE P. 9.

CALC	GRJ	1-10-75	REVISED	DATE
CHECK				
APR				
APR				

INTERNAL CHANNEL LOADS FOR COND F

AEROSPACE & DEFENSE GROUP
GOVERNMENT & AERONAUTICAL PRODUCTS DIVISION

EWA No	TYPE No	PAGE 10

HT-51 REV 11/71

RIVET ANALYSIS FOR COND A LOADS

RIVET ANALYSIS FOR COND F LOADS IS SHOWN ON P. 11

LOADS SHOWN ARE FOR A SINGLE CHANNEL. THEY ARE 1/6 OF THE TOTAL LOADS SHOWN ON P. 9.

AD/5 RIVETS ($D=\frac{5}{32}$")
SHEAR STRENGTH = 596 LBS

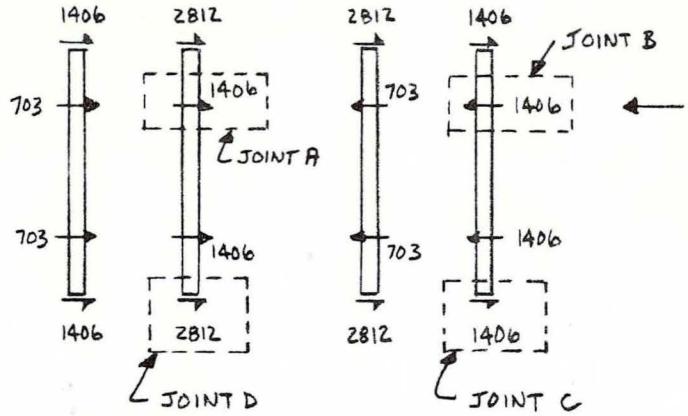

$$M.S._1 = \frac{\text{ALLOWABLE LOAD}}{\text{ACTUAL LOAD}} - 1$$

JOINT A

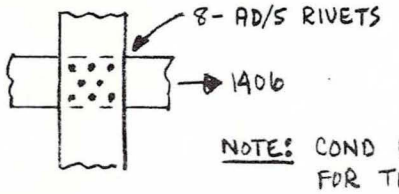

$$M.S._1 = \frac{8 \times 596}{1406} - 1 \longrightarrow M.S._1 = +2.4$$ ✓

NOTE: COND F LOADS ARE MORE CRITICAL FOR THIS JOINT. SEE P. 11

JOINT B

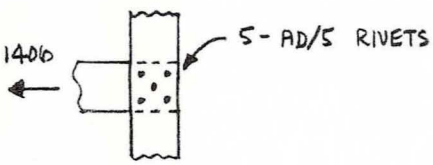

$$M.S._1 = \frac{5 \times 596}{1406} - 1 \longrightarrow M.S._1 = +1.12$$ ✓

JOINT C

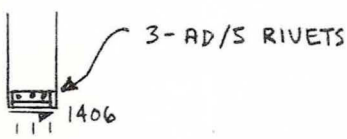

$$M.S._1 = \frac{3 \times 596}{1406} - 1 \longrightarrow M.S._1 = +.27$$ ✓

JOINT D

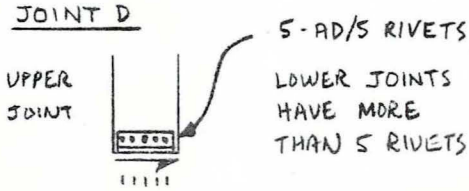

$$M.S._1 = \frac{5 \times 596}{2812} - 1 \longrightarrow M.S._1 = +.06$$ ✓

CALC	GRJ	1-28-75	REVISED	DATE
CHECK				
APR				
APR				

STRESS ANALYSIS FOR INTERNAL CHANNELS

AEROSPACE & DEFENSE GROUP
GOVERNMENT & AERONAUTICAL PRODUCTS DIVISION

EWA No	TYPE No	PAGE 12

HT-51 REV 11/71

P = ULT DOWNWARD INERTIAL RETARDANT FORCE

P = 1.5 x 3.0 g's x 20,000 LBS

P = 90,000 LBS ULT

APPLIED LOADS ON TANK WITH DOORS REMOVED

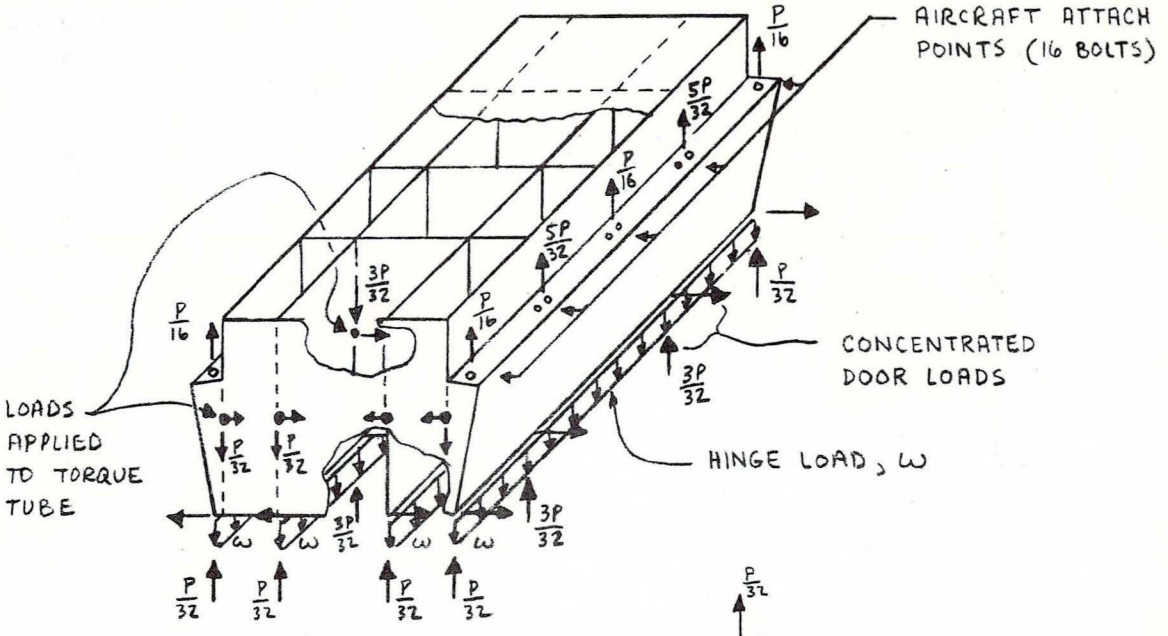

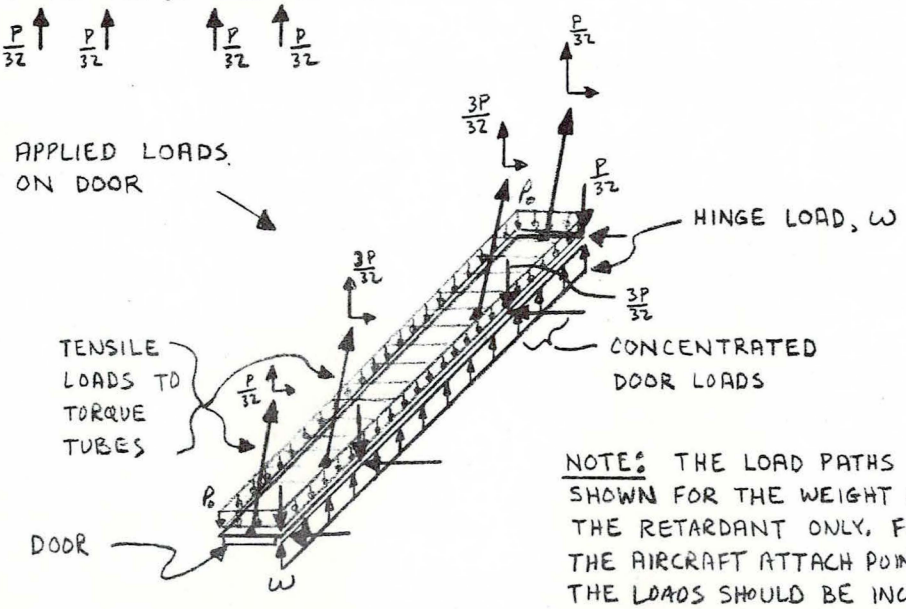

NOTE: THE LOAD PATHS ARE SHOWN FOR THE WEIGHT OF THE RETARDANT ONLY. FOR THE AIRCRAFT ATTACH POINTS, THE LOADS SHOULD BE INCREASED TO ACCOUNT FOR STRUCTURE WEIGHT.

CALC	GRJ	1-20-75	REVISED	DATE
CHECK				
APR				
APR				

LOAD PATHS FOR COND D

AEROSPACE & DEFENSE GROUP
GOVERNMENT & AERONAUTICAL PRODUCTS DIVISION

EWA No	TYPE No	PAGE 14

HT-51 REV 11/71

DOOR SUPPORT

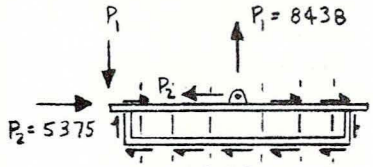

INTERMEDIATE SUPPORT SEE P. 15

$q = 1038$ {INCLUDES BOTH SIDES OF SUPPORT 1.5×692}

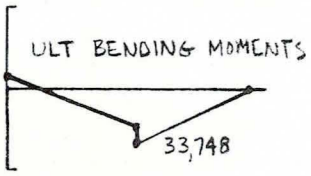

WEB ATTACHED TO SKIN WITH 6 - $\frac{1}{4}$" BOLTS

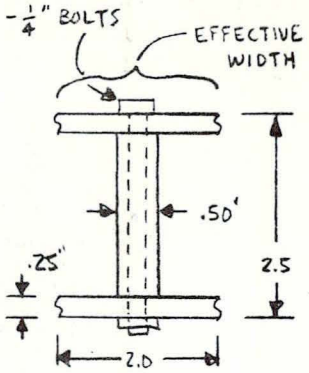

$I = I_{WEB} + 2A_{FLANGE}\left(\frac{d-t}{2}\right)^2$

$= \frac{.5}{12}(2)^3 + 2(1.25\times2.0)(1.125)^2$

$I = 1.60\ IN^4$ ✓

BENDING STRESS

$f_b = \frac{Mc}{I} = \frac{33,748\times1.25}{1.6}$

$f_b = 26,366$ PSI ULT ✓

$M.S. = \frac{43,000}{26,366} - 1$

$M.S. = +.63$ ✓

SHEAR STRESS IN BOLTS {MS9490-38, $F_s = 75,000$ PSI}

$12P_s = qs$ → P_s = SHEAR IN BOLT; s = DISTANCE AT WHICH SHEAR FLOW ACTS

$P_s = \frac{1038}{12}(2\times14.45 + 2\times2.25)$

$P_s = 2889$ LBS ULT ✓

$f_s = P_s/A_s = 2889/(\pi.125^2)$ (SHEAR STRESS)

$f_s = 58,854$ PSI ULT ✓

$M.S. = \frac{75,000}{58,854} - 1$

$M.S. = +.27$ ✓

LUG ANALYSIS

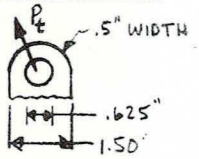

$P_t = \sqrt{P_1^2 + P_2^2} = \sqrt{8438^2 + 5375^2}$

$P_t = 10,005$ LBS ULT

TENSILE STRESS AT HOLE IN LUG

$f_t = \frac{P_t}{A} = \frac{10,005}{.5(1.5-.625)}$

$f_t = 22,869$ PSI ULT ✓

$M.S. = \frac{43,000}{22,869} - 1$

$M.S. = +.88$ ✓

CALC	GRJ	1-28-75	REVISED	DATE
CHECK				
APR				
APR				

DOOR ANALYSIS (CONT)

AEROSPACE & DEFENSE GROUP
GOVERNMENT & AERONAUTICAL PRODUCTS DIVISION

EWA No	TYPE No	PAGE 16

HT-51 REV 11/71

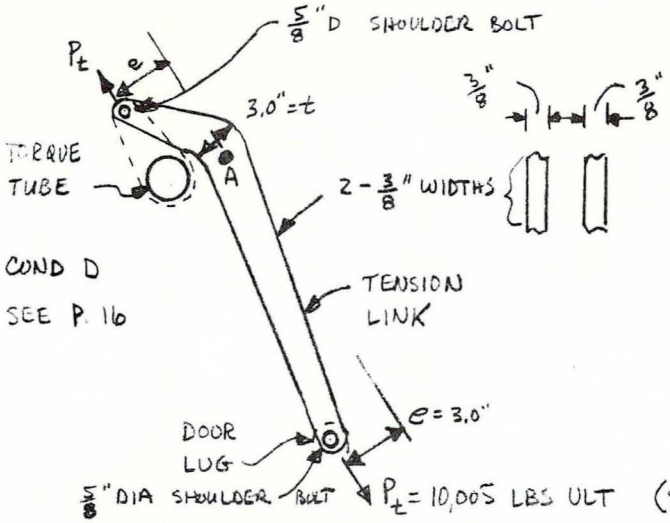

MATERIAL:

LINK 6061-T6 ALUM
F_u = 43,000 PSI

BOLT F_s = 75,000 PSI

FIND STRESS IN LINK AT "A"

$$f_t = \frac{6M}{bt^2} + \frac{P_t}{bt} = \frac{6 \times (10{,}005 \times 3")}{(2 \times \frac{3}{8}) \times (3.0)^2} + \frac{10{,}005}{(2 \times \frac{3}{8}) \times (3.0)}$$

$$= 26{,}680 + 4447$$

f_t = 31,127 PSI ULT ✓

$$M.S. = \frac{43{,}000}{31{,}127} - 1$$

M.S. = +.38 ✓

SHEAR STRESS IN SHOULDER BOLTS

$f_s = P_t / A_s = 10{,}005 / (2\pi \cdot .3125^2)$ (DOUBLE SHEAR)

f_s = 16,306 PSI ULT ✓

$$M.S. = \frac{75{,}000}{16{,}306} - 1$$

M.S. = +3.6 ✓

CALC	GRJ	1-29 75	REVISED	DATE
CHECK				
APR				
APR				

TENSION LINK ANALYSIS

AEROSPACE & DEFENSE GROUP
GOVERNMENT & AERONAUTICAL PRODUCTS DIVISION

EWA No	TYPE No	PAGE 18

HT-51 REV 11/71

FORWARD & AFT BULKHEADS

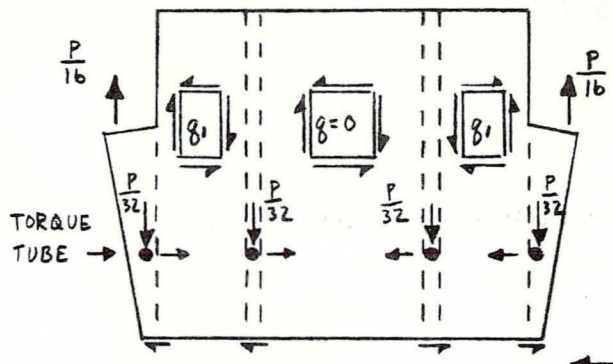

DOORS REMOVED

P = 90,000 LBS ULT

SEE P. 14

NOTE: THE LOADS SHOWN ARE FOR THE RETARDANT ONLY. FOR THE STRESS ANALYSIS OF THE ATTACH POINTS, THE LOADS WILL BE INCREASED TO ACCOUNT FOR THE STRUCTURE WEIGHT.

THE HINGE LOADS (SEE P. 14) ARE "BEAMED" TO THE BULKHEADS AND THEY CANCEL OUT THE VERTICAL CONCENTRATED DOOR LOADS (SEE P. 14)

$q_1 = \left(\frac{P}{32}\right) / \text{TOTAL DEPTH} = \frac{90{,}000}{32 \times 60}$

$q_1 = 47$ LBS/IN ULT

INTERMEDIATE BULKHEADS

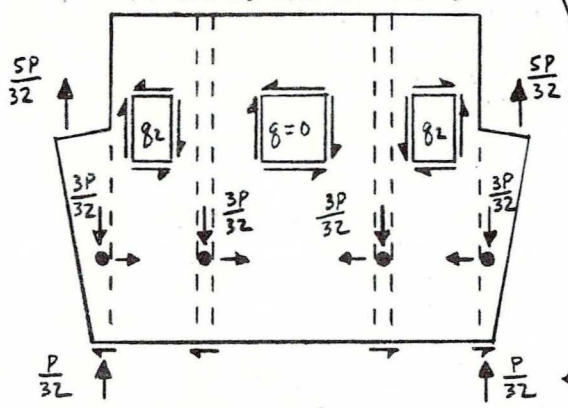

IT IS ASSUMED THE CENTER PARTITION DOES NOT DISTRIBUTE ANY OF THE INTERNAL HINGE LOADS TO THE SUPPORTS, SO THE CONCENTRATED DOOR LOADS ARE COMPLETELY CANCELED. A PORTION OF THE EXTERNAL HINGE LOADS IS TRANSFERRED DIRECTLY TO THE CENTER SUPPORTS (ATTACH POINTS), SO THE CONCENTRATED DOOR LOADS ARE NOT COMPLETELY CANCELED.

$q_2 = \frac{3P}{32} / \text{TOTAL DEPTH} = \frac{3 \times 90{,}000}{32 \times 60}$

$q_2 = 141$ LBS/IN ULT

CENTER PARTITION

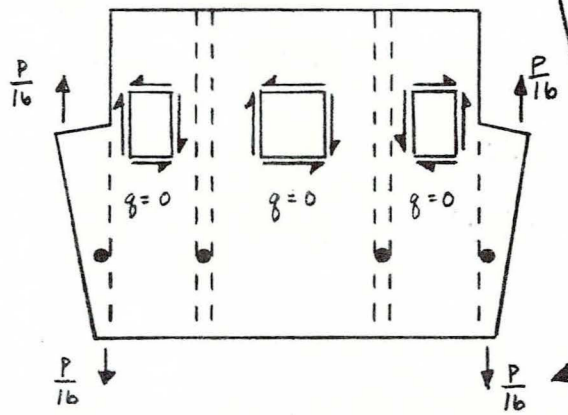

A PORTION OF THE EXTERNAL HINGE LOADS IS TRANSFERRED DIRECTLY TO THE SUPPORT.

THE PARTITION CARRIES NO SHEAR.

CALC	GRJ	1-25-75	REVISED	DATE
CHECK				
APR				
APR				

BULKHEAD LOADS FOR COND D

AEROSPACE & DEFENSE GROUP
GOVERNMENT & AERONAUTICAL PRODUCTS DIVISION

EWA No	TYPE No	PAGE 20

HT-51 REV 11/71

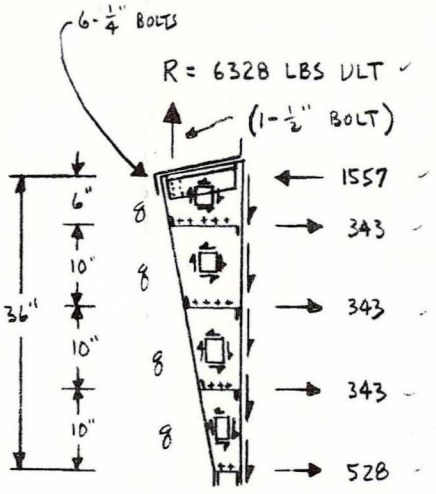

FROM P. 14, R IS GIVEN FOR THE WEIGHT OF THE RETARDANT ONLY. TO INCLUDE THE WEIGHT OF THE STRUCTURE, IT MUST BE INCREASED BY 12.5%

$$R = 1.125\,\frac{P}{16} = 1.125\,\frac{90{,}000}{16}$$

$$\underline{R = 6328 \text{ LBS ULT}} \quad ✓$$

EQUAL SHEAR FLOW, q, IN ALL PANELS

$$q = \frac{R}{L} = \frac{6328}{36}$$

$$\underline{q = 176 \text{ LBS/IN ULT}} \quad ✓$$

OUTER SKIN ON FWD & AFT BULKHEADS IS CONTINUOUS. THEREFORE, THE HORIZONTAL LOADS ARE SIMPLY TRANSFERRED INTO THE OUTER SKIN.

OUTER SKIN ⇒ 6061-T6 ALUM, $t = .063"$, $F_{CRIT} = \frac{\pi^2 k_s E}{12(1-\nu^2)}\left(\frac{t}{b}\right)^2$

$$= \frac{\pi^2 10(10^3)}{12(1-.3^2)}\left(\frac{.063}{10}\right)^2$$

$$\underline{F_{CRIT} = 3587 \text{ PSI}} \quad ✓$$

FIND SHEAR STRESS DUE TO SHEAR FLOW

$$f_s = q/t = 176/.063$$

$$\underline{f_s = 2794 \text{ PSI ULT}} \quad ✓$$

$$M.S. = \frac{3587}{2794} - 1$$

$$\underline{M.S. = +.28} \quad ✓$$

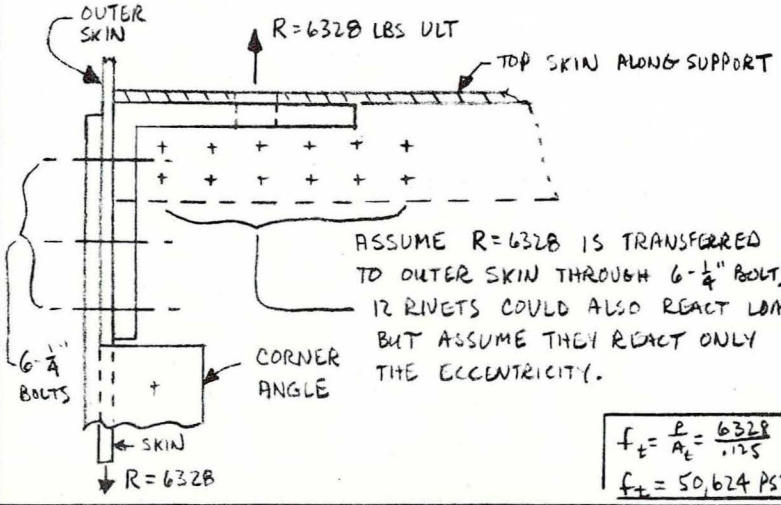
OUTER SKIN
R = 6328 LBS ULT
TOP SKIN ALONG SUPPORT
ASSUME R = 6328 IS TRANSFERRED TO OUTER SKIN THROUGH 6-¼" BOLTS. 12 RIVETS COULD ALSO REACT LOAD, BUT ASSUME THEY REACT ONLY THE ECCENTRICITY.
6-¼" BOLTS
CORNER ANGLE
SKIN
R = 6328

BEARING STRESS IN OUTER SKIN

6061-T6 ⇒ $F_{bru} = 90{,}000$ PSI

$$f_{br} = \frac{R}{A_{br}} = \frac{6328}{6\times.25\times.063} = \underline{66{,}963 \text{ PSI ULT}} \quad ✓$$

$$M.S. = \frac{90{,}000}{66{,}963} - 1 \Rightarrow \underline{M.S. = +.34} \quad ✓$$

SHEAR STRESS IN 6-¼" BOLTS

$$f_s = \frac{R}{A_s} = \frac{6328}{6\pi(.125)^2} = \underline{21{,}485 \text{ PSI ULT}}$$

$$M.S. = \frac{75{,}000}{21{,}485} - 1 \Rightarrow \underline{M.S. = +2.5}$$

TENSILE STRESS IN ½" ATTACH BOLT

$F_u = 160{,}000$ PSI

$$f_t = \frac{f}{A_t} = \frac{6328}{.125}$$

$$\underline{f_t = 50{,}624 \text{ PSI ULT}}$$

$$M.S. = \frac{160{,}000}{50{,}624} - 1$$

$$\underline{M.S. = +2.1} \quad ✓$$

CALC	GRJ	1-30-75	REVISED	DATE
CHECK				
APR				
APR				

ANALYSIS OF ATTACH POINTS AT END BULKHEADS FOR COND D

AEROSPACE & DEFENSE GROUP
GOVERNMENT & AERONAUTICAL PRODUCTS DIVISION

EWA No	TYPE No	PAGE 22

HT-51 REV 11/71

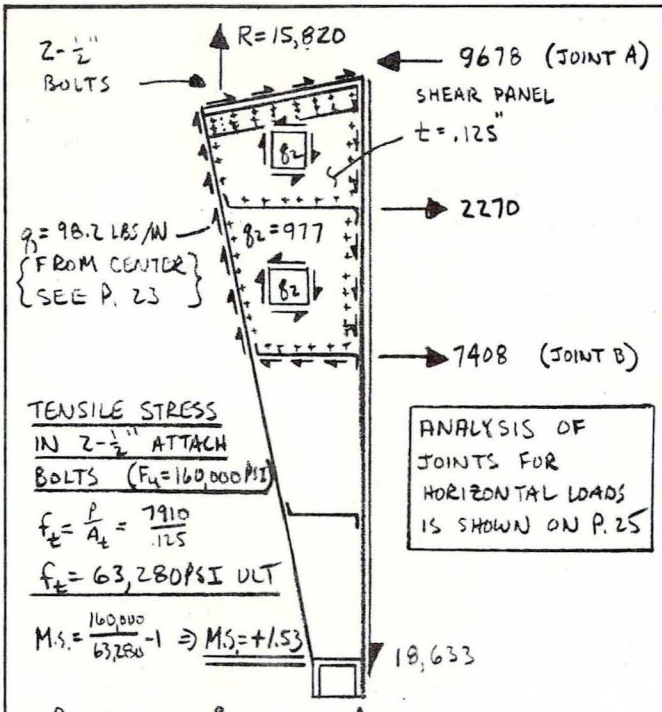

TENSILE STRESS IN 2-1/2" ATTACH BOLTS (F_{tu}=160,000 PSI)

$f_t = \frac{P}{A_t} = \frac{7910}{.125}$

f_t = 63,280 PSI ULT

$M.S. = \frac{160,000}{63,280} - 1 \Rightarrow M.S. = +1.53$

ANALYSIS OF JOINTS FOR HORIZONTAL LOADS IS SHOWN ON P. 25

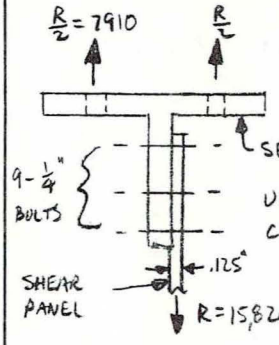

SEE P. 23 FOR GEOMETRY

ULT STRENGTH OF "T" CLIP = P_u = 22,500 LBS (P.23)

$M.S. = \frac{22,500}{15,820} - 1$

$M.S. = +.42$

SHEAR IN 9-1/4" BOLTS (F_s = 75,000 PSI)

$f_s = \frac{P}{A_s} = \frac{15,820}{9\pi(.125)^2}$ $\quad M.S. = \frac{75,000}{35,809} - 1$

f_s = 35,809 PSI ULT → $M.S. = +1.09$

BEARING IN SHEAR PANEL (F_{bru} = 90,000 PSI)

$f_{bru} = \frac{P}{A_{br}} = \frac{15,820}{9 \times .25 \times .025}$ $\quad M.S. = \frac{90,000}{56,249} - 1$

f_{bru} = 56,249 PSI ULT → $M.S. = +.59$

$R = 1.125 \times \frac{5}{32}(90,000)$ (SEE PP. 14, 20 & 22)

R = 15,820 LBS ULT

FIND SHEAR FLOW, q_2

$q_2 = \frac{15,820}{18"} + q = 879 + 98.2$

q_2 = 977 LBS/IN ULT

STRESS IN SHEAR PANEL (6061-T6)

$F_{CRIT} = \frac{\pi^2 k_s E}{12(1-\nu^2)}\left(\frac{t}{b}\right)^2 = \frac{\pi^2 10(10^3)}{12(1-.3^2)}\left(\frac{.125}{10}\right)^2$

F_{CRIT} = 14,122 PSI

$f_s = \frac{q_2}{t} = \frac{977}{.125}$ $\quad M.S. = \frac{14,122}{7816} - 1$

f_s = 7816 PSI ULT → $M.S. = +.81$

CHECK FASTENERS AROUND SHEAR PANEL

1/4" BOLTS @ 1.0" SPACING ⇒ 977 #/BOLT

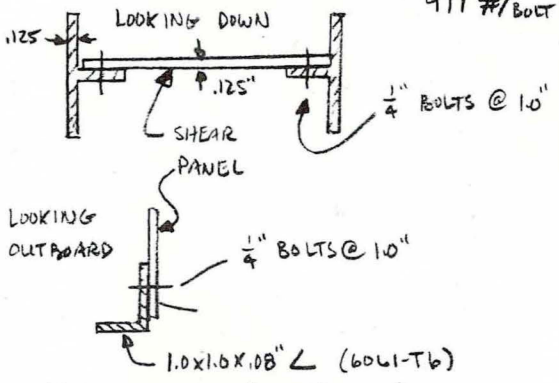

SHEAR IN BOLTS (F_s = 75,000 PSI)

$f_s = \frac{P}{A_s} = \frac{977}{\pi(.125)^2}$ $\quad M.S. = \frac{75,000}{19,903} - 1$

f_s = 19,903 PSI ULT → $M.S. = +2.8$

BEARING IN ANGLE (F_{bru} = 90,000 PSI)

$f_{bru} = \frac{P}{A_{br}} = \frac{977}{.25 \times .08}$ $\quad M.S. = \frac{90,000}{48,850} - 1$

f_{bru} = 48,850 PSI ULT → $M.S. = +.84$

CALC	GRJ	1-30-75	REVISED	DATE
CHECK				
APR				
APR				

ANALYSIS OF ATTACH POINTS AT INTERMEDIATE BULKHEADS FOR COND D

AEROSPACE & DEFENSE GROUP
GOVERNMENT & AERONAUTICAL PRODUCTS DIVISION

EWA No	TYPE No	PAGE 24

HT-51 REV 11/71

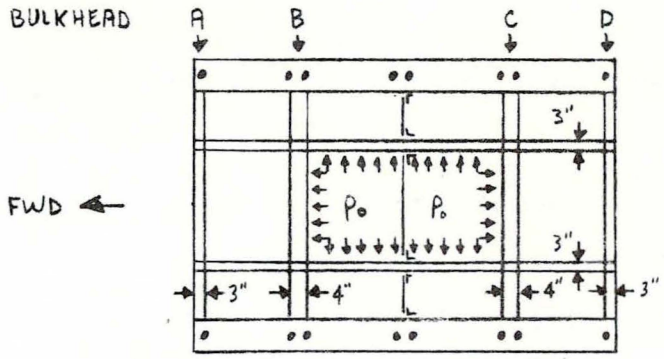

P_o = 10.8 PSI ULT
COND F (SEE P. 5)

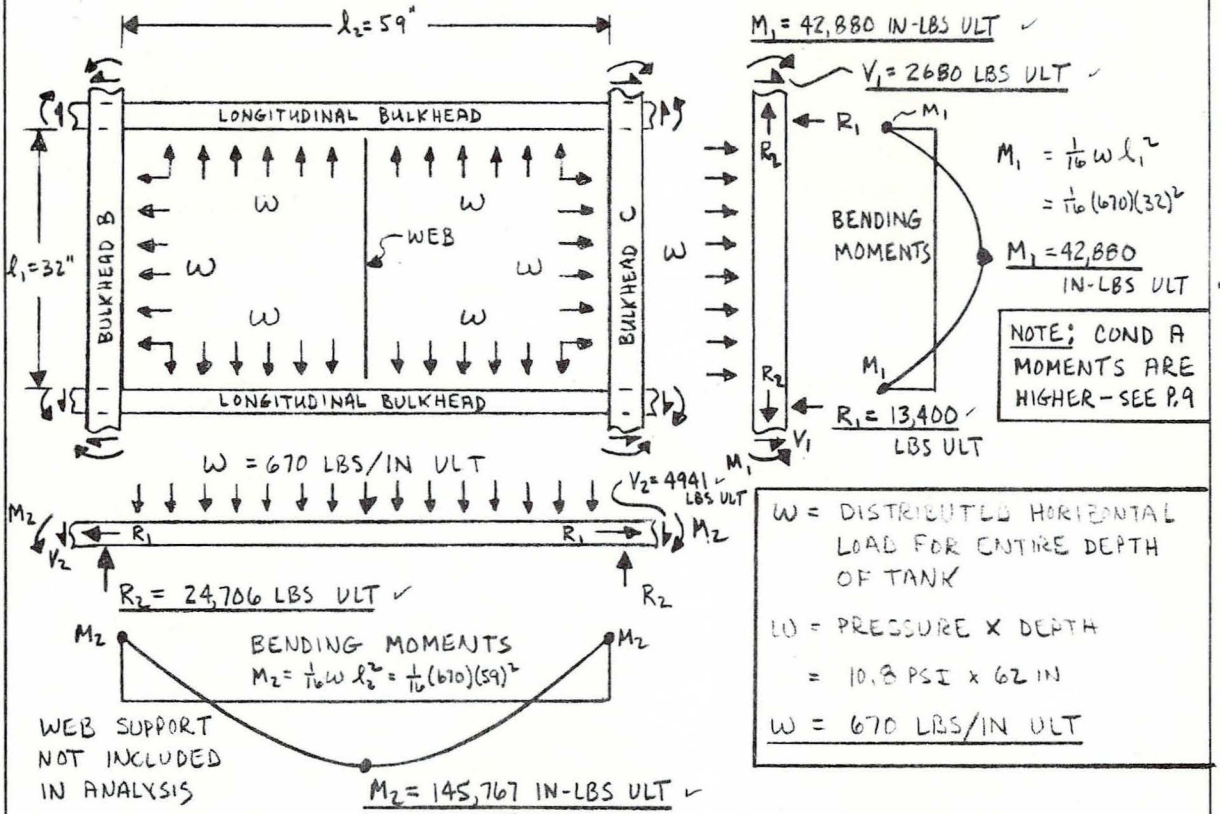

NOTE; COND A MOMENTS ARE HIGHER – SEE P.9

w = DISTRIBUTED HORIZONTAL LOAD FOR ENTIRE DEPTH OF TANK

w = PRESSURE x DEPTH
= 10.8 PSI x 62 IN
w = 670 LBS/IN ULT

NOTE: THE LONGITUDINAL BULKHEAD HAS A 3" DEPTH AND A CROSS-SECTION SIMILAR TO THE FORWARD AND AFT BULKHEADS (A & D) SHOWN ON P. 9. THE MAX BENDING MOMENT IN THE LONGITUDINAL BULKHEAD (M=145,767) IS SLIGHTLY LESS THAN IN THE THE FORWARD AND AFT BULKHEADS (M=148,000). SEE P. 9.

CALC	GRJ	1-10-75	REVISED	DATE
CHECK				
APR				
APR				

INTERNAL CHANNEL LOADS FOR COND F

AEROSPACE & DEFENSE GROUP
GOVERNMENT & AERONAUTICAL PRODUCTS DIVISION

EWA No	TYPE No	PAGE 10

HT-51 REV 11/71

ANALYSIS OF 3" CHANNELS FOR FWD & AFT BULKHEADS, AND LONGITUDINAL BULKHEADS (SEE PP 9 & 10)

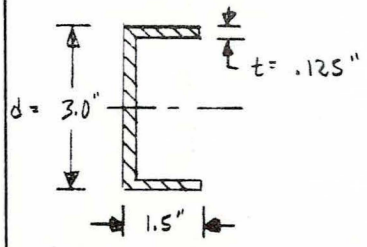

$$I = I_{WEB} + 2A_{FLANGE}\left(\frac{d-t}{2}\right)^2$$

$$= \frac{.125}{12}(3.0)^3 + 2(.125 \times 1.375)\left(\frac{3.0-.125}{2}\right)^2$$

$$I = .99 \text{ IN}^4$$

MATERIAL:

6061-T6 ALUM
F_u = 43,000 PSI

RIVETS - AD/5 ($D = \frac{5}{32}$")
SHEAR STRENGTH = 596 LBS

THE BULKHEADS ARE DIVIDED INTO 6 EQUAL SPANS (SEE P. 6). EACH CHANNEL MUST THEREFORE SUPPORT 1/6 OF THE TOTAL MOMENTS SHOWN ON PP. 9 & 10. THE MAX ULT MOMENT FOR THE 3" CHANNELS IS THEREFORE $\frac{1}{6} \times 148{,}000 = 24{,}667$ IN-LBS ULT. (COND A - P. 9)

BENDING STRESS - IGNOR EFFECT OF SKIN

$$f_b = \frac{Mc}{I} = \frac{24{,}667 \times 1.5}{.99}$$

f_b = 37,374 PSI ULT ✓

$$M.S._1 = \frac{43{,}000}{37{,}374} - 1$$

$M.S._1 = +.15$ ✓

ANALYSIS OF 4" CHANNELS FOR INTERMEDIATE BULKHEADS, B & C. (COND A - P. 9)

THE CRITICAL BENDING STRESS OCCURS WHERE BULKHEAD C CROSSES THE LONGITUDINAL BULKHEAD. EVEN THOUGH THE NET MOMENT AT THE INTERSECTION (M = 235,000) IS LESS THAN THE MOMENT AT MIDSPAN (M = 296,000), THE BENDING STRESS IS CRITICAL AT THE INTERSECTION BECAUSE THE SKIN IS NOT EFFECTIVE IN BENDING AT THIS POINT. MOMENT PER CHANNEL = $\frac{1}{6} \times 235{,}000 = 39{,}167$ IN-LBS ULT.

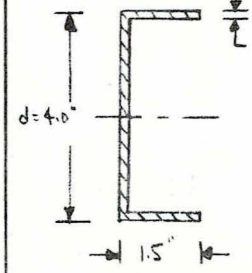

$$I = I_{WEB} + 2A_{FLANGE}\left(\frac{d-t}{2}\right)^2$$

$$= \frac{.125}{12}(4.0)^3 + 2(.125 \times 1.375)\left(\frac{4.0-.125}{2}\right)^2$$

$$I = 1.96 \text{ IN}^4$$

BENDING STRESS

$$f_b = \frac{Mc}{I} = \frac{39{,}167 \times 2.0}{1.96}$$

f_b = 39,966 PSI ULT ✓

$$M.S._1 = \frac{43{,}000}{39{,}966} - 1$$

$M.S._1 = +.08$ ✓

RIVET ANALYSIS (8 RIVETS)

LOADS FROM P. 10

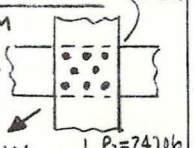

LOADS ARE FOR TOTAL DEPTH OF TANK - USE $\frac{1}{6}\bar{R} = 4684$ FOR EACH INTERSECTION

$$M.S._1 = \frac{8 \times 596}{4684} - 1$$

$M.S._1 = +.02$ ✓

CALC	GRJ	1-13-74	REVISED	DATE
CHECK				
APR				
APR				

STRESS ANALYSIS FOR INTERNAL CHANNELS

AEROSPACE & DEFENSE GROUP
GOVERNMENT & AERONAUTICAL PRODUCTS DIVISION

EWA No	TYPE No	PAGE 11

HT-51 REV 11/71

RIVET ANALYSIS FOR COND A LOADS

RIVET ANALYSIS FOR COND F LOADS IS SHOWN ON P. 11

LOADS SHOWN ARE FOR A SINGLE CHANNEL. THEY ARE 1/6 OF THE TOTAL LOADS SHOWN ON P. 9.

AD/5 RIVETS ($D=\frac{5}{32}$")
SHEAR STRENGTH = 596 LBS

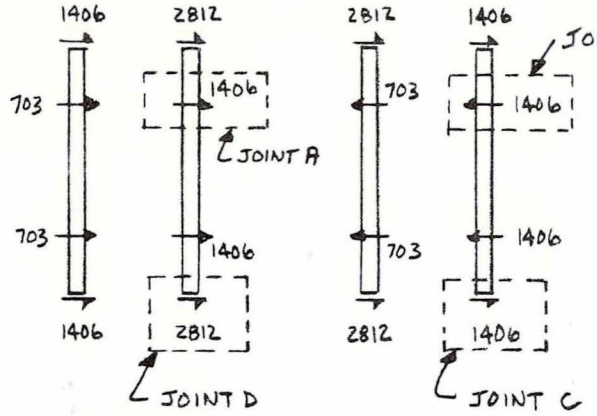

$$M.S._1 = \frac{\text{ALLOWABLE LOAD}}{\text{ACTUAL LOAD}} - 1$$

JOINT A

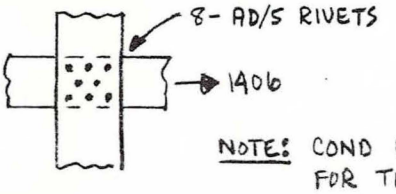

$$M.S._1 = \frac{8 \times 596}{1406} - 1 \longrightarrow M.S._1 = +2.4$$

NOTE: COND F LOADS ARE MORE CRITICAL FOR THIS JOINT. SEE P. 11

JOINT B

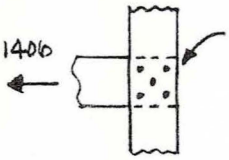

$$M.S._1 = \frac{5 \times 596}{1406} - 1 \longrightarrow M.S._1 = +1.12$$

JOINT C

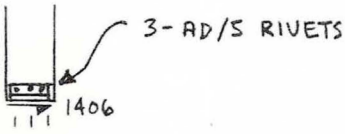

$$M.S._1 = \frac{3 \times 596}{1406} - 1 \longrightarrow M.S._1 = +.27$$

JOINT D

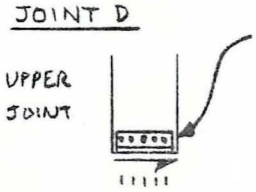

$$M.S._1 = \frac{5 \times 596}{2812} - 1 \longrightarrow M.S._1 = +.06$$

CALC	GRJ	1-28-75	REVISED	DATE
CHECK				
APR				
APR				

STRESS ANALYSIS FOR INTERNAL CHANNELS

AEROSPACE & DEFENSE GROUP
GOVERNMENT & AERONAUTICAL PRODUCTS DIVISION

EWA No	TYPE No	PAGE 12

HT-51 REV 11/71

ANALYSIS OF VERTICAL ANGLES ON SIDE SKIN (SEE P. 7)

PANEL B (SEE P. 7) — CRITICAL VERTICAL ANGLE {CLEAR VERTICAL SPAN = ℓ = 20"}

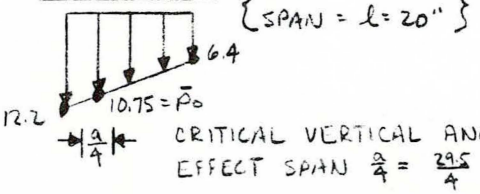

CRITICAL VERTICAL ANGLE SUPPORTS EFFECT SPAN $\frac{a}{4} = \frac{29.5}{4} = 7.38"$

BENDING MOMENT SUPPORTED BY VERTICAL ANGLE

$M = \frac{1}{8} w \ell^2 = \frac{1}{8}(\bar{P}_o \times \frac{a}{4})(\ell)^2 = \frac{1}{8}(10.75 \times 7.38)(20)^2$

M = 3967 IN-LBS ULT ✓

BENDING STRESS

$f_b = \frac{Mc}{I} = \frac{3967 \times .175}{.28}$

f_b = 24,794 PSI ULT ✓

MATERIAL (L & ⌐¬)

6061-T6 ALUM
F_{tu} = 43,000 PSI
RIVETS - AD/6 (D = $\frac{3}{16}$")
TENSILE STRENGTH = 800 LBS

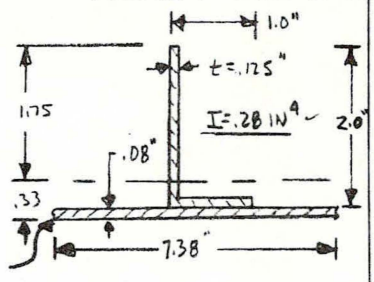

$M.S._1 = \frac{43,000}{24,794} - 1$

$M.S._1 = +.73$ ✓

ANALYSIS OF HORIZONTAL ⌐¬ SECTIONS ON TOP SKIN

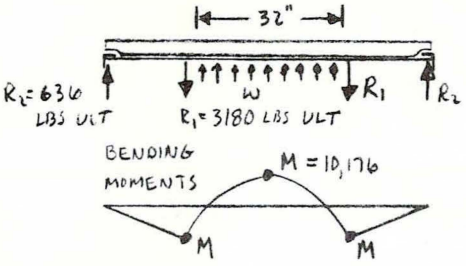

BENDING MOMENT

$M = \frac{1}{16} w \ell^2 = \frac{1}{16}(159)(32)^2$

M = 10,176 IN-LBS ULT ✓

BENDING STRESS

$f_b = \frac{Mc}{I} = \frac{10176 \times .80}{.22}$

f_b = 37,004 PSI ULT ✓

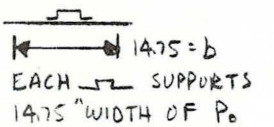

EACH ⌐¬ SUPPORTS 14.75" WIDTH OF P_o

$\omega = p_o b = 10.8 \times 14.75$

ω = 159 LBS/IN ULT

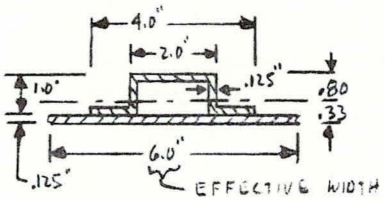

I = .22 IN⁴ ✓

RIVET ANALYSIS FOR R_1 = 3180 LBS TENSION
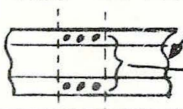
$M.S._1 = \frac{6 \times 800}{3180} - 1$

$M.S._1 = +.51$

$M.S._1 = \frac{43,000}{37,004} - 1$

$M.S._1 = +.16$ ✓

CALC	GRJ	1-13-75	REVISED	DATE
CHECK				
APR				
APR				

STRESS ANALYSIS FOR VERTICAL ANGLES ON SIDE SKIN AND HORIZONTAL ⌐¬ SECTIONS ON TOP SKIN

AEROSPACE & DEFENSE GROUP
GOVERNMENT & AERONAUTICAL PRODUCTS DIVISION

EWA No	TYPE No	PAGE 13

HT-51 REV 11/71

P = ULT DOWNWARD INERTIAL RETARDANT FORCE

P = 1.5 x 3.0 g's x 20,000 LBS

P = 90,000 LBS ULT

APPLIED LOADS ON TANK WITH DOORS REMOVED

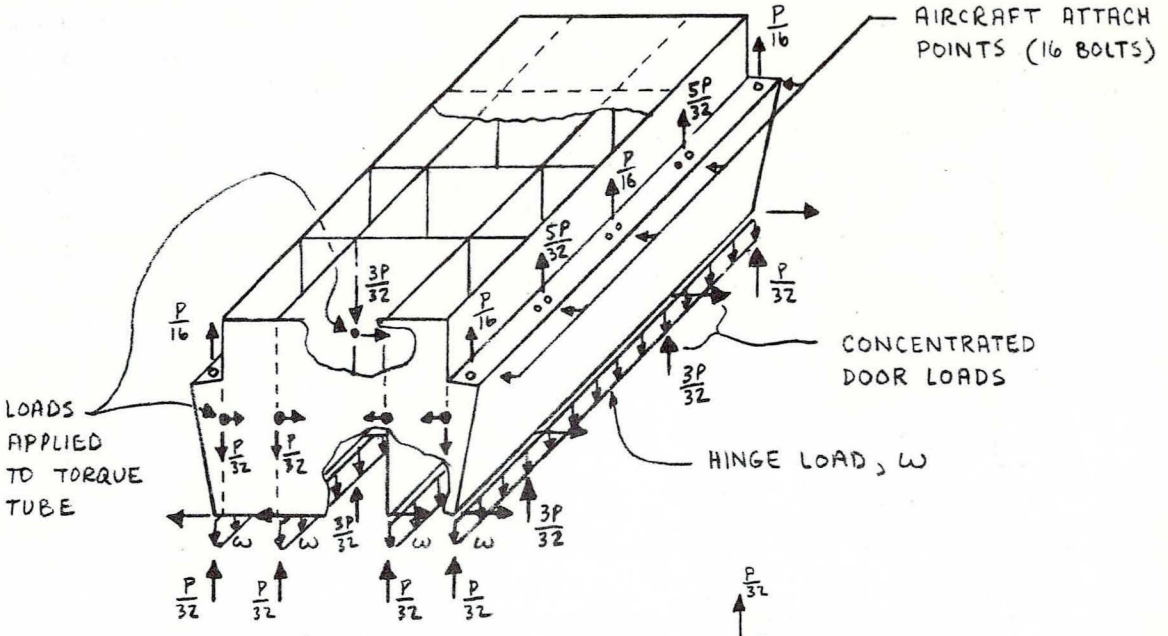

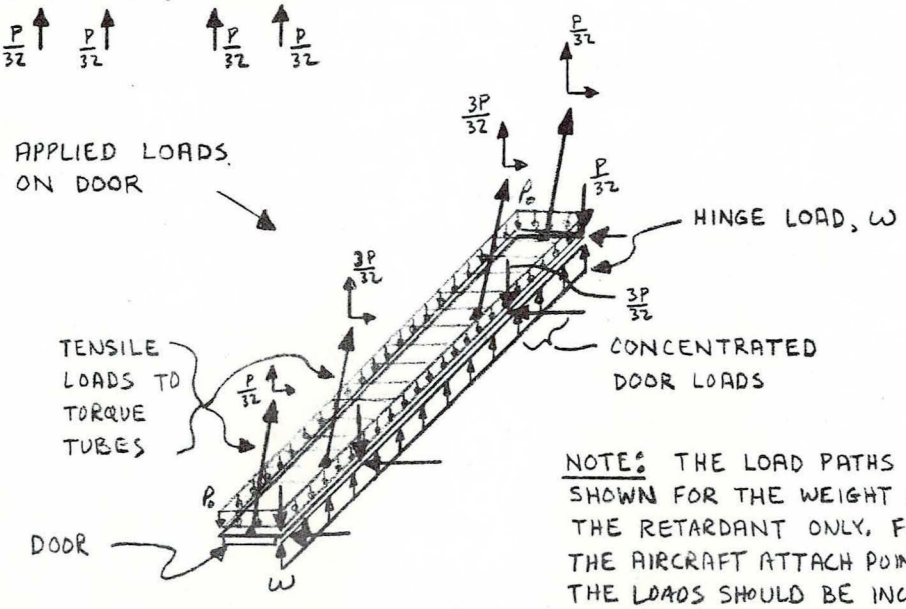

NOTE: THE LOAD PATHS ARE SHOWN FOR THE WEIGHT OF THE RETARDANT ONLY. FOR THE AIRCRAFT ATTACH POINTS, THE LOADS SHOULD BE INCREASED TO ACCOUNT FOR STRUCTURE WEIGHT.

CALC	GRJ	1-20-75	REVISED	DATE
CHECK				
APR				
APR				

LOAD PATHS FOR COND D

AEROSPACE & DEFENSE GROUP
GOVERNMENT & AERONAUTICAL PRODUCTS DIVISION

EWA No	TYPE No	PAGE 14

HT-51 REV 11/71

MATERIAL:

6061-T6 ALUM
F_{tu} = 43,000 PSI
F_{su} = 27,000 PSI

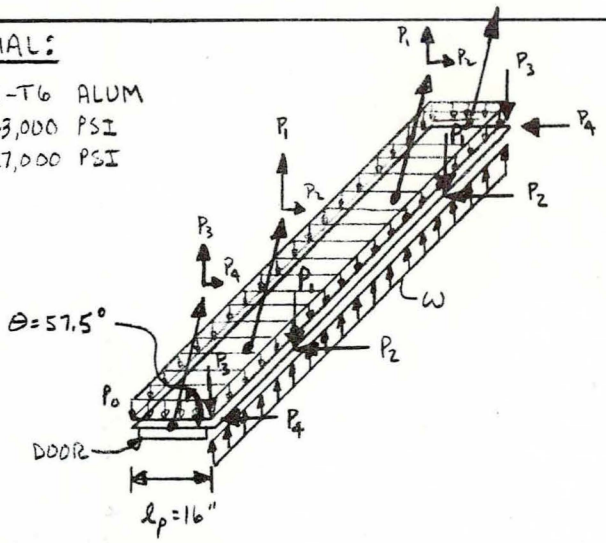

ULT LOADS FOR COND D

P_o = 11.9 PSI (P.5)

$\omega = P_o \ell_p = 11.9 \times 16$

ω = 190 LBS/IN

$P_1 = \frac{3}{32} P = \frac{3}{32}(90{,}000)$ {SEE P.14}

P_1 = 8438 LBS ULT

$P_2 = P_1 / \tan\theta = 8438/1.57$

P_2 = 5375 LBS ULT

$P_3 = \frac{P}{32} = 90{,}000/32$ {SEE P.14}

P_3 = 2813 LBS ULT

$P_4 = P_3 / \tan\theta = 2813/1.57$

P_4 = 1792 LBS ULT

P_{max} = 15.5 PSI ULT (COND A - P.5)

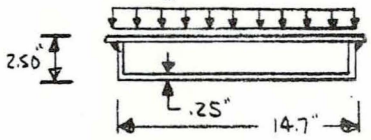

NOTE: THE MAX PRESSURE ON THE DOOR OCCURS DURING COND "A" (P_{max} = 15.5 PSI). HOWEVER, THIS IS A LOCALIZED PRESSURE WHICH OCCURS ONLY AT THE FWD END OF COMPARTMENTS 2,5,18. FOR OVERALL DOOR DESIGN, COND D GOVERNS BECAUSE THE PRESSURE (P_o = 11.9 PSI) ACTS UNIFORMLY ON ALL DOORS.

CHECK LOCALIZED BENDING IN TOP PLATE

$M = \frac{1}{8} P_{max} \ell^2$

$= \frac{1}{8}(15.5)(14.7 - 2\times.25)^2$

M = 391 IN-LBS/IN ULT

$f_b = \frac{6M}{t^2} = \frac{6\times391}{(.25)^2}$

f_b = 37,536 PSI ULT → $M.S. = \frac{43{,}000}{37{,}536} - 1$

M.S. = +.15

CHECK SHEAR STRESS DUE TO TORQUE

$T_{max} = \frac{2}{3} P_1 \frac{\ell_p}{2} = \frac{2}{3}(8438)\frac{16}{2}$

T_{max} = 45,000 IN-LBS ULT

$q = \frac{T_{max}}{2A} = \frac{45{,}000}{2(2.25\times1445)}$ {SHEAR FLOW}

q = 692 LBS/IN ULT

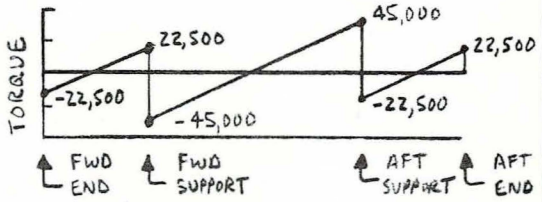

$f_s = \frac{q}{t} = \frac{692}{.25}$ → f_s = 2768 PSI ULT → $M.S. = \frac{27{,}000}{2768} - 1$ → M.S. = LARGE

CALC	GRJ	1-20-75	REVISED	DATE
CHECK				
APR				
APR				

DOOR ANALYSIS

AEROSPACE & DEFENSE GROUP
GOVERNMENT & AERONAUTICAL PRODUCTS DIVISION

EWA No	TYPE No	PAGE 15

HT-51 REV 11/71

DOOR SUPPORT

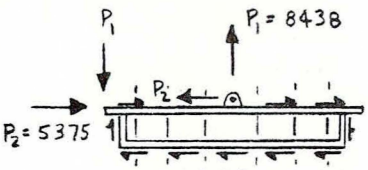

INTERMEDIATE SUPPORT SEE P. 15

{INCLUDES BOTH SIDES OF SUPPORT 1.5×692}

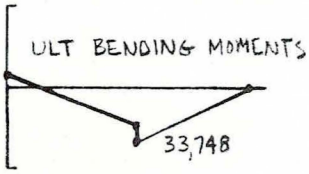

WEB ATTACHED TO SKIN WITH 6 - $\frac{1}{4}$" BOLTS

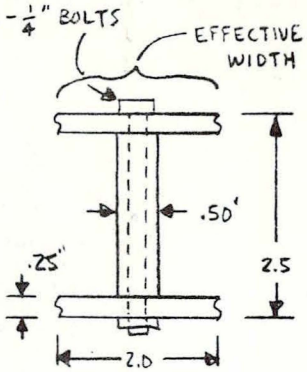

$I = I_{WEB} + 2A_{FLANGE}\left(\frac{d-t}{2}\right)^2$

$= \frac{.5}{12}(2)^3 + 2(.25\times 2.0)(1.125)^2$

$I = 1.60\ IN^4$ ✓

BENDING STRESS

$f_b = \frac{Mc}{I} = \frac{33,748 \times 1.25}{1.6}$

$f_b = 26,366$ PSI ULT ✓

$M.S. = \frac{43,000}{26,366} - 1$

$M.S. = +.63$ ✓

SHEAR STRESS IN BOLTS {MS9490-3B, F_s = 75,000 PSI}

$12P_s = qs$ → P_s = SHEAR IN BOLT; s = DISTANCE AT WHICH SHEAR FLOW ACTS

$P_s = \frac{1038}{12}(2\times 14.45 + 2\times 2.25)$

$P_s = 2889$ LBS ULT ✓

$f_s = P_s/A_s = 2889/(\pi .125^2)$ (SHEAR STRESS)

$f_s = 58,854$ PSI ULT ✓

$M.S. = \frac{75,000}{58,854} - 1$

$M.S. = +.27$ ✓

LUG ANALYSIS

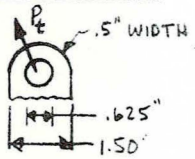

$P_t = \sqrt{P_1^2 + P_2^2} = \sqrt{8438^2 + 5375^2}$

$P_t = 10,005$ LBS ULT

TENSILE STRESS AT HOLE IN LUG

$f_t = \frac{P_t}{A} = \frac{10,005}{.5(1.5-.625)}$

$f_t = 22,869$ PSI ULT ✓

$M.S. = \frac{43,000}{22,869} - 1$

$M.S. = +.88$ ✓

CALC	GRJ	1-28-75	REVISED	DATE
CHECK				
APR				
APR				

DOOR ANALYSIS (CONT)

AEROSPACE & DEFENSE GROUP
GOVERNMENT & AERONAUTICAL PRODUCTS DIVISION

EWA No	TYPE No	PAGE 16

HT-51 REV 11/71

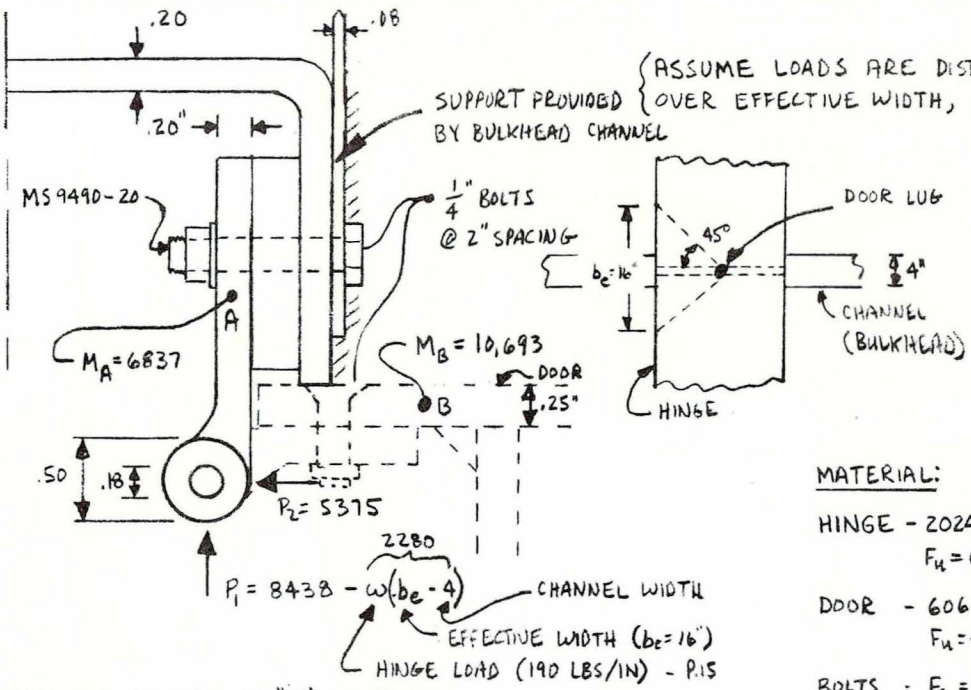

MATERIAL:

HINGE - 2024-T4 ALUM
F_u = 60,000 PSI

DOOR - 6061-T6 ALUM
F_u = 43,000 PSI

BOLTS - F_s = 75,000 PSI

BENDING STRESS AT "A" IN HINGE

$M_A = (8438 - 2280) \times .15" + 5375 \times 1.1" = 6837$ IN-LBS ULT ✓

$f_b = \frac{4M}{bt^2} = \frac{4 \times 6837}{16 \times .20^2}$

f_b = 42,731 PSI ULT ✓

M.S. = $\frac{60,000}{42,731} - 1$

M.S. = +.40 ✓

BENDING STRESS AT "B" IN DOOR

$M_B = (8438 - 2280) \times 1.3" + 5375 \times .5" = 10,693$ IN-LBS ULT ✓

$f_b = \frac{4M}{bt^2} = \frac{4 \times 10,693}{16 \times .25^2}$

f_b = 42,772 PSI ULT ✓

M.S. = $\frac{43,000}{42,772} - 1$

M.S. = +.01 ✓

SHEAR STRESS IN BOLTS

8 BOLTS EFFECTIVE IN VERTICAL SHEAR

$f_s = P/A_s = (8438 - 2280)/(8\pi \cdot .125^2)$

f_s = 15,681 PSI ULT ✓

M.S. = $\frac{75,000}{15,681} - 1$

M.S. = +3.8 ✓

CALC	GRJ	1-29-75	REVISED	DATE
CHECK				
APR				
APR				

DOOR HINGE ANALYSIS

AEROSPACE & DEFENSE GROUP
GOVERNMENT & AERONAUTICAL PRODUCTS DIVISION

EWA No	TYPE No	PAGE 17

HT-51 REV 11/71

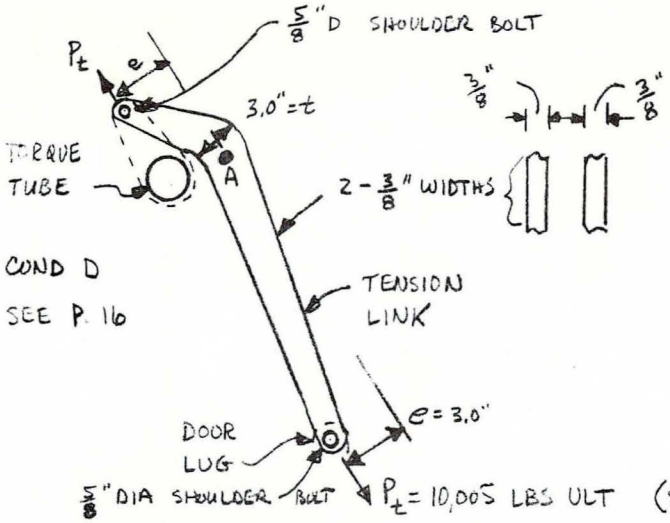

MATERIAL:

LINK 6061-T6 ALUM
F_u = 43,000 PSI

BOLT F_s = 75,000 PSI

FIND STRESS IN LINK AT "A"

$$f_t = \frac{6M}{bt^2} + \frac{P_t}{bt} = \frac{6 \times (10{,}005 \times 3")}{(2 \times \frac{3}{8}) \times (3.0)^2} + \frac{10{,}005}{(2 \times \frac{3}{8}) \times (3.0)}$$

$$= 26{,}680 + 4447$$

f_t = 31,127 PSI ULT ✓

$$M.S. = \frac{43{,}000}{31{,}127} - 1$$

M.S. = +.38 ✓

SHEAR STRESS IN SHOULDER BOLTS

$f_s = P_t / A_s = 10{,}005 / (2\pi \cdot .3125^2)$ (DOUBLE SHEAR)

f_s = 16,306 PSI ULT ✓

$$M.S. = \frac{75{,}000}{16{,}306} - 1$$

M.S. = +3.6 ✓

CALC	GRJ	1-29 75	REVISED	DATE
CHECK				
APR				
APR				

TENSION LINK ANALYSIS

AEROSPACE & DEFENSE GROUP
GOVERNMENT & AERONAUTICAL PRODUCTS DIVISION

EWA No	TYPE No	PAGE 18

HT-51 REV 11/71

PLAN VIEW

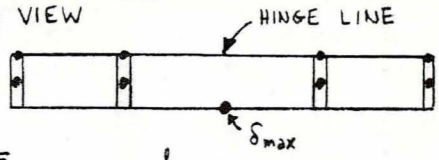

COND D ⇒ p_o = 11.9 PSI – P.5

ULT TORQUE SEE P.14

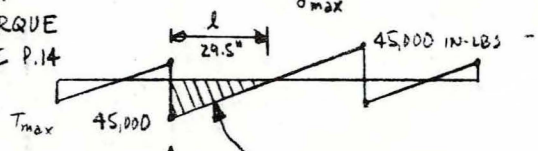

FIND ROTATION FROM SUPPORT TO MID SPAN, θ_{max}

ASSUME NO ROTATION AT SUPPORT

CROSS-SECTION OF DOOR

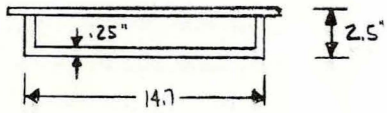

$$K = \frac{4A^2t}{S} = \frac{4(14.45 \times 2.25)^2 \times .25}{2(14.45+2.25)}$$ {ROARK P. 195}

$K = 31.6\ IN^4$

FIND ROTATION AT MID-SPAN, θ_{max}

$$\theta_{max} = \frac{\bar{T}\ell}{KG}$$

WHERE $\bar{T} = \frac{T_{max}}{2} = 22{,}500$
$\ell = 29.5"$
$K = 31.6"$
$G = 3.8 \times 10^6$

(θ_{max} FROM ROARK – P. 195)

$$= \frac{22{,}500 \times 29.5}{31.6 \times 3.8 \times 10^6}$$

$\theta_{max} = .00553$ RADIANS ULT

FIND DEFLECTION AT MID-SPAN, δ_{max}

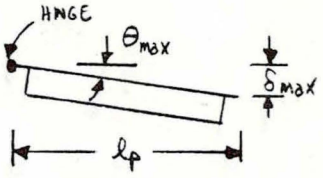

$$\delta_{max} = \theta_{max}\, \ell_p$$

$$= .00553 \times 16"$$

$\delta_{max} = .088"$ (DUE TO ULT PRESSURE)

$\delta_{max} = .059"$ (DUE TO LIMIT PRESSURE)

CALC	GRJ	1-24-75	REVISED	DATE
CHECK				
APR				
APR				

DOOR DEFLECTION ANALYSIS FOR COND D

AEROSPACE & DEFENSE GROUP
GOVERNMENT & AERONAUTICAL PRODUCTS DIVISION

EWA No	TYPE No	PAGE 19

HT-51 REV 11/71

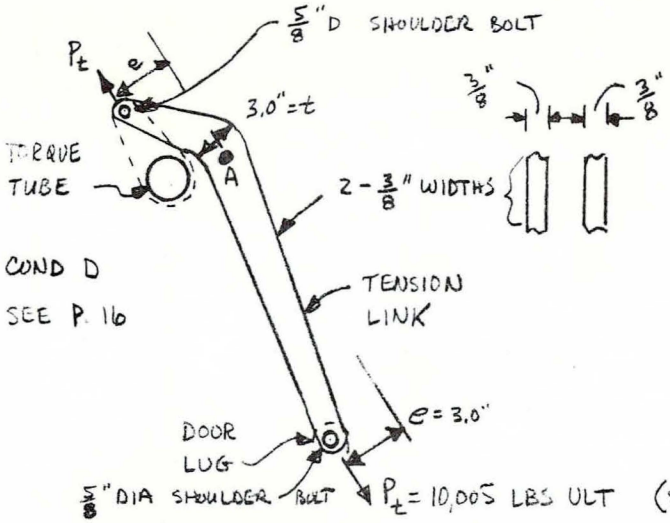

MATERIAL:

LINK 6061-T6 ALUM
F_u = 43,000 PSI

BOLT F_s = 75,000 PSI

FIND STRESS IN LINK AT "A"

$$f_t = \frac{6M}{bt^2} + \frac{P_t}{bt} = \frac{6 \times (10{,}005 \times 3")}{(2 \times \frac{3}{8}) \times (3.0)^2} + \frac{10{,}005}{(2 \times \frac{3}{8}) \times (3.0)}$$

$$= 26{,}680 + 4447$$

f_t = 31,127 PSI ULT ✓

$$M.S. = \frac{43{,}000}{31{,}127} - 1$$

M.S. = +.38 ✓

SHEAR STRESS IN SHOULDER BOLTS

$f_s = P_t / A_s = 10{,}005 / (2\pi \cdot .3125^2)$ (DOUBLE SHEAR)

f_s = 16,306 PSI ULT ✓

$$M.S. = \frac{75{,}000}{16{,}306} - 1$$

M.S. = +3.6 ✓

CALC	GRJ	1-29 75	REVISED	DATE
CHECK				
APR				
APR				

TENSION LINK ANALYSIS

AEROSPACE & DEFENSE GROUP
GOVERNMENT & AERONAUTICAL PRODUCTS DIVISION

EWA No	TYPE No	PAGE 18

HT-51 REV 11/71

FORWARD & AFT BULKHEADS

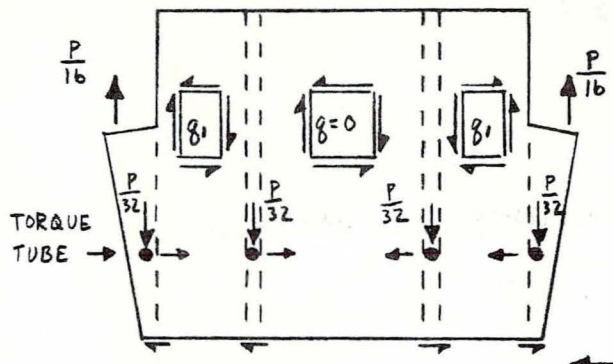

DOORS REMOVED

P = 90,000 LBS ULT

SEE P. 14

NOTE: THE LOADS SHOWN ARE FOR THE RETARDANT ONLY. FOR THE STRESS ANALYSIS OF THE ATTACH POINTS, THE LOADS WILL BE INCREASED TO ACCOUNT FOR THE STRUCTURE WEIGHT.

THE HINGE LOADS (SEE P. 14) ARE "BEAMED" TO THE BULKHEADS AND THEY CANCEL OUT THE VERTICAL CONCENTRATED DOOR LOADS (SEE P. 14)

$q_1 = \left(\frac{P}{32}\right) / \text{TOTAL DEPTH} = \frac{90{,}000}{32 \times 60}$

$q_1 = 47$ LBS/IN ULT

INTERMEDIATE BULKHEADS

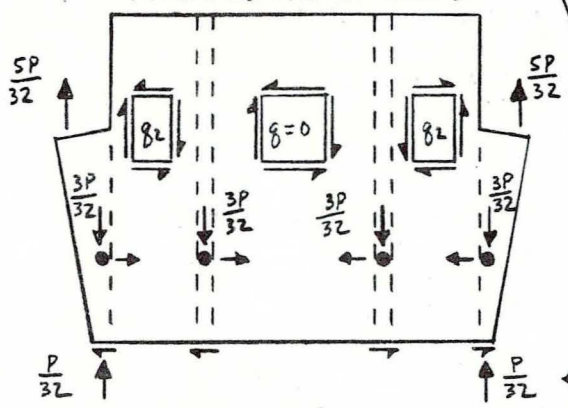

IT IS ASSUMED THE CENTER PARTITION DOES NOT DISTRIBUTE ANY OF THE INTERNAL HINGE LOADS TO THE SUPPORTS, SO THE CONCENTRATED DOOR LOADS ARE COMPLETELY CANCELED. A PORTION OF THE EXTERNAL HINGE LOADS IS TRANSFERRED DIRECTLY TO THE CENTER SUPPORTS (ATTACH POINTS), SO THE CONCENTRATED DOOR LOADS ARE NOT COMPLETELY CANCELED.

$q_2 = \frac{3P}{32} / \text{TOTAL DEPTH} = \frac{3 \times 90{,}000}{32 \times 60}$

$q_2 = 141$ LBS/IN ULT

CENTER PARTITION

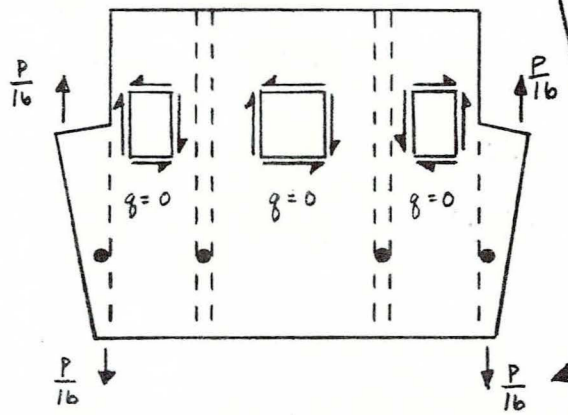

A PORTION OF THE EXTERNAL HINGE LOADS IS TRANSFERRED DIRECTLY TO THE SUPPORT.

THE PARTITION CARRIES NO SHEAR.

CALC	GRJ	1-25-75	REVISED	DATE
CHECK				
APR				
APR				

BULKHEAD LOADS FOR COND D

AEROSPACE & DEFENSE GROUP
GOVERNMENT & AERONAUTICAL PRODUCTS DIVISION

EWA No	TYPE No	PAGE 20

HT-51 REV 11/71

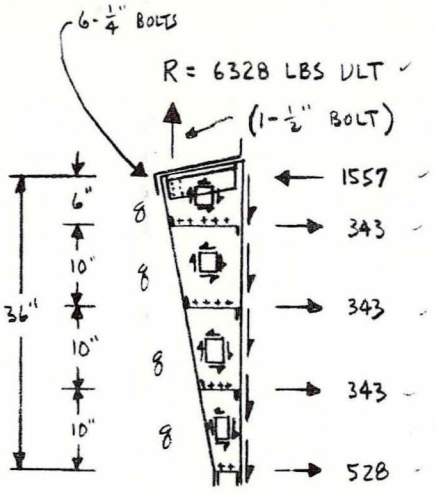

FROM P. 14, R IS GIVEN FOR THE WEIGHT OF THE RETARDANT ONLY. TO INCLUDE THE WEIGHT OF THE STRUCTURE, IT MUST BE INCREASED BY 12.5%

$$R = 1.125\,\frac{P}{16} = 1.125\,\frac{90{,}000}{16}$$

$$\underline{R = 6328 \text{ LBS ULT}} \quad ✓$$

EQUAL SHEAR FLOW, q, IN ALL PANELS

$$q = \frac{R}{L} = \frac{6328}{36}$$

$$\underline{q = 176 \text{ LBS/IN ULT}} \quad ✓$$

OUTER SKIN ON FWD & AFT BULKHEADS IS CONTINUOUS. THEREFORE, THE HORIZONTAL LOADS ARE SIMPLY TRANSFERRED INTO THE OUTER SKIN.

OUTER SKIN ⇒ 6061-T6 ALUM, $t = .063"$, $F_{CRIT} = \frac{\pi^2 k_s E}{12(1-\nu^2)}\left(\frac{t}{b}\right)^2$

$$= \frac{\pi^2 10(10^3)}{12(1-.3^2)}\left(\frac{.063}{10}\right)^2$$

$$\underline{F_{CRIT} = 3587 \text{ PSI}} \quad ✓$$

FIND SHEAR STRESS DUE TO SHEAR FLOW

$$f_s = q/t = 176/.063$$

$$\underline{f_s = 2794 \text{ PSI ULT}} \quad ✓$$

$$M.S. = \frac{3587}{2794} - 1$$

$$\underline{M.S. = +.28} \quad ✓$$

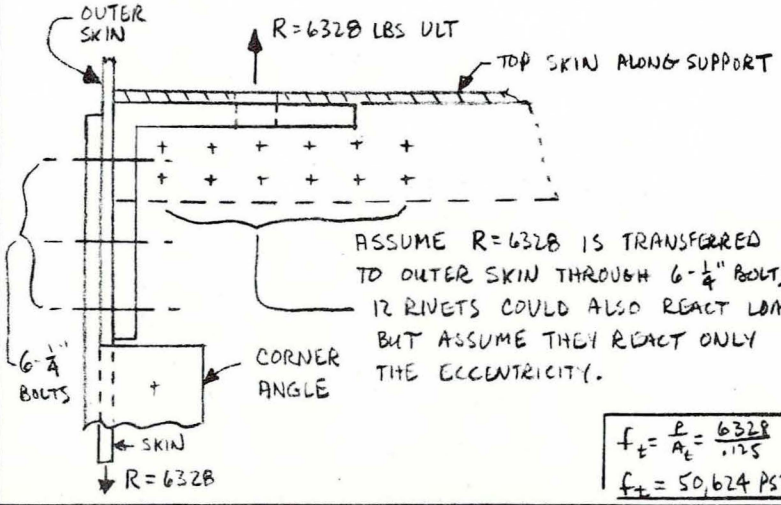
OUTER SKIN
R = 6328 LBS ULT
TOP SKIN ALONG SUPPORT
ASSUME R = 6328 IS TRANSFERRED TO OUTER SKIN THROUGH 6-¼" BOLTS. 12 RIVETS COULD ALSO REACT LOAD, BUT ASSUME THEY REACT ONLY THE ECCENTRICITY.
6-¼" BOLTS
CORNER ANGLE
SKIN
R = 6328

BEARING STRESS IN OUTER SKIN

6061-T6 ⇒ $F_{bru} = 90{,}000$ PSI

$$f_{br} = \frac{R}{A_{br}} = \frac{6328}{6\times.25\times.063} = \underline{66{,}963 \text{ PSI ULT}} \quad ✓$$

$$M.S. = \frac{90{,}000}{66{,}963} - 1 \Rightarrow \underline{M.S. = +.34} \quad ✓$$

SHEAR STRESS IN 6-¼" BOLTS

$$f_s = \frac{R}{A_s} = \frac{6328}{6\pi(.125)^2} = \underline{21{,}485 \text{ PSI ULT}}$$

$$M.S. = \frac{75{,}000}{21{,}485} - 1 \Rightarrow \underline{M.S. = +2.5}$$

TENSILE STRESS IN ½" ATTACH BOLT

$F_u = 160{,}000$ PSI

$$f_t = \frac{f}{A_t} = \frac{6328}{.125}$$

$$\underline{f_t = 50{,}624 \text{ PSI ULT}}$$

$$M.S. = \frac{160{,}000}{50{,}624} - 1$$

$$\underline{M.S. = +2.1} \quad ✓$$

CALC	GRJ	1-30-75	REVISED	DATE
CHECK				
APR				
APR				

ANALYSIS OF ATTACH POINTS AT END BULKHEADS FOR COND D

AEROSPACE & DEFENSE GROUP
GOVERNMENT & AERONAUTICAL PRODUCTS DIVISION

EWA No	TYPE No	PAGE 22

HT-51 REV 11/71

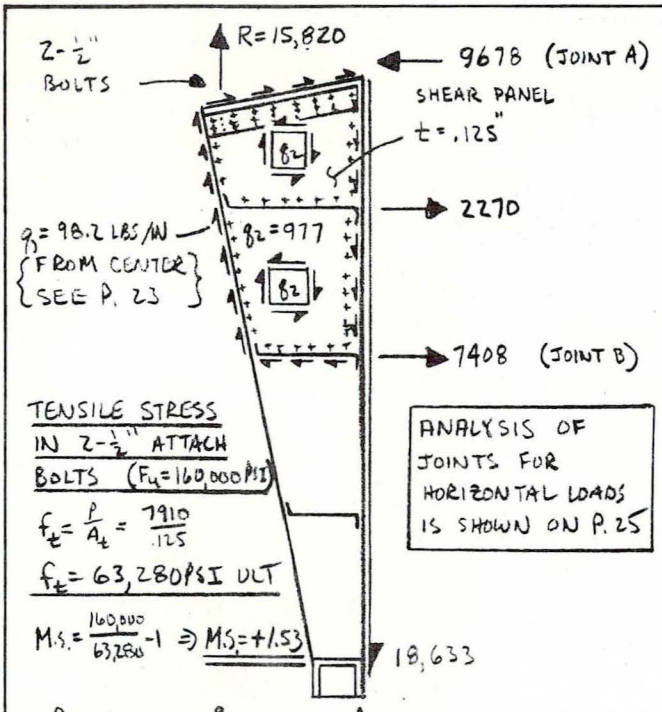

TENSILE STRESS IN 2-1/2" ATTACH BOLTS (F_{tu}=160,000 PSI)

$f_t = \frac{P}{A_t} = \frac{7910}{.125}$

f_t = 63,280 PSI ULT

$M.S. = \frac{160,000}{63,280} - 1 \Rightarrow M.S. = +1.53$

ANALYSIS OF JOINTS FOR HORIZONTAL LOADS IS SHOWN ON P. 25

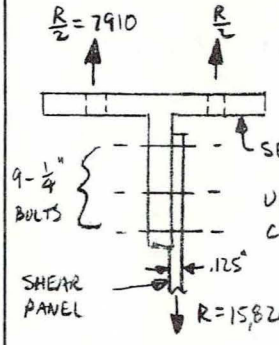

SEE P. 23 FOR GEOMETRY

ULT STRENGTH OF "T" CLIP = P_u = 22,500 LBS (P.23)

$M.S. = \frac{22,500}{15,820} - 1$

$M.S. = +.42$

SHEAR IN 9-1/4" BOLTS (F_s = 75,000 PSI)

$f_s = \frac{P}{A_s} = \frac{15,820}{9\pi(.125)^2}$ $\quad M.S. = \frac{75,000}{35,809} - 1$

f_s = 35,809 PSI ULT → $M.S. = +1.09$

BEARING IN SHEAR PANEL (F_{bru} = 90,000 PSI)

$f_{bru} = \frac{P}{A_{br}} = \frac{15,820}{9 \times .25 \times .025}$ $\quad M.S. = \frac{90,000}{56,249} - 1$

f_{bru} = 56,249 PSI ULT → $M.S. = +.59$

$R = 1.125 \times \frac{5}{32}(90,000)$ (SEE PP. 14, 20 & 22)

R = 15,820 LBS ULT

FIND SHEAR FLOW, q_2

$q_2 = \frac{15,820}{18"} + q = 879 + 98.2$

q_2 = 977 LBS/IN ULT

STRESS IN SHEAR PANEL (6061-T6)

$F_{CRIT} = \frac{\pi^2 k_s E}{12(1-\nu^2)}\left(\frac{t}{b}\right)^2 = \frac{\pi^2 10(10^3)}{12(1-.3^2)}\left(\frac{.125}{10}\right)^2$

F_{CRIT} = 14,122 PSI

$f_s = \frac{q_2}{t} = \frac{977}{.125}$ $\quad M.S. = \frac{14,122}{7816} - 1$

f_s = 7816 PSI ULT → $M.S. = +.81$

CHECK FASTENERS AROUND SHEAR PANEL

1/4" BOLTS @ 1.0" SPACING ⇒ 977 #/BOLT

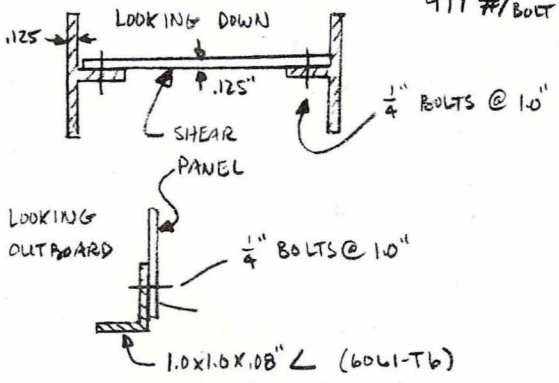

SHEAR IN BOLTS (F_s = 75,000 PSI)

$f_s = \frac{P}{A_s} = \frac{977}{\pi(.125)^2}$ $\quad M.S. = \frac{75,000}{19,903} - 1$

f_s = 19,903 PSI ULT → $M.S. = +2.8$

BEARING IN ANGLE (F_{bru} = 90,000 PSI)

$f_{bru} = \frac{P}{A_{br}} = \frac{977}{.25 \times .08}$ $\quad M.S. = \frac{90,000}{48,850} - 1$

f_{bru} = 48,850 PSI ULT → $M.S. = +.84$

CALC	GRJ	1-30-75	REVISED	DATE
CHECK				
APR				
APR				

ANALYSIS OF ATTACH POINTS AT INTERMEDIATE BULKHEADS FOR COND D

AEROSPACE & DEFENSE GROUP
GOVERNMENT & AERONAUTICAL PRODUCTS DIVISION

EWA No	TYPE No	PAGE 24

HT-51 REV 11/71

```
**********CALCULATION OF EFFECTIVE DOOR AREA.
      DX=VE*DELT
      IF(DQ) GO TO 180
      MAXDX=WD*SIN(A)
      HMAX=MAXDX*0.5
      TOTX=TOTX+DX
      IF(DX.GT.HMAX) GO TO 210
      IF(TOTX.GT.MAXDX) GO TO 200
      GO TO 190
*---------CONSIDER EFFECTIVE DOOR AREA = DOOR AREA.
  180 AE=AREAD
      GO TO 300
*---------DOOR RATE FAST ENOUGH NOT TO RESRICT FLOW.
  190 DELAE=DELT*COS(A)/(2.0*MAXDX)
      AE=AREAD*(1.0-DELAE)
      GO TO 300
*---------DOOR RATE RESTRICTING FLOW SOMEWHAT.
  200 DELAE=COS(A)/2.0
      AE=AREAD*(1.0-DELAE)
      GO TO 300
*---------DOOR RATE RESTRICTING FLOW.
  210 DELAE=0.0
      IF(A.GT.0.7854) GO TO 215
      ADIFF=A-ALAST
      IF(ADIFF.LE.0.0) GO TO 215
      DELAE=WD/2.0*COS(2.0*A)*ADIFF/VE
  215 AE=AREAD*(SIN(A)+DELAE)
      GO TO 310
  300 IF(DELAE.LT.0.005) DQ=.TRUE.
  310 IF(VE.LE.0.0) GO TO 405
**********CALCULATION OF CHANGE IN OUTPUT VOLUME (Q).
      Q=DX*AE
**********CALCULATION OF FLUID VELOCITY AT TOP (VZ).
      VZ=VE*AE/AREAT
      IF(VE.LE.0.0) GO TO 405
      P=-K*Q*Q
      P=P*VOL/(VOL+Q)
      VOL=VOL+Q
      H=H-VZ*DELT
      GAL=Q*7.481
      GALO=GALO+GAL
      PO=P*0.0069445
      RATE=GAL/DELT
      ALAST=A
      WRITE(9,400) T,H,VE,VZ,RATE,GALO,PO
  400 FORMAT(F4.2,F8.2,F9.2,F9.2,F10.2,F10.2,F10.3)
      IF(H.GT.0.0) GO TO 100
      STOP
  405 WRITE(9,410)
  410 FORMAT(///'PRESSURE=HEAD')
      STOP
      END
```

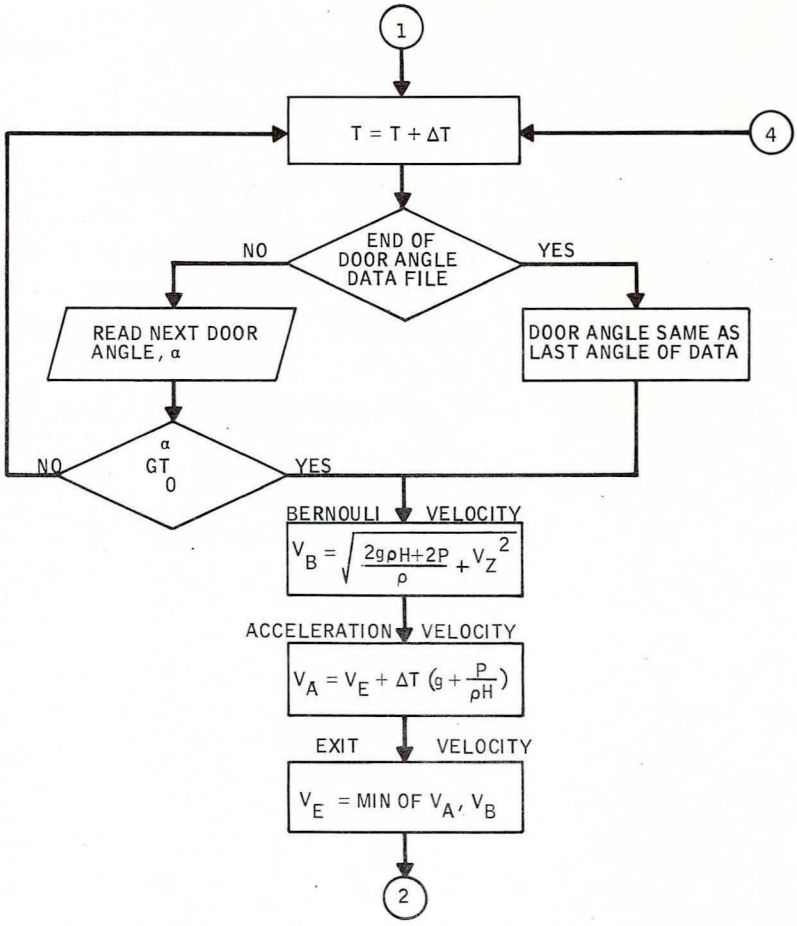
1
T = T + ΔT
4
END OF DOOR ANGLE DATA FILE
NO
YES
READ NEXT DOOR ANGLE, α
DOOR ANGLE SAME AS LAST ANGLE OF DATA
α GT 0
NO
YES
BERNOULI VELOCITY
$V_B = \sqrt{\frac{2g\rho H+2P}{\rho} + V_Z^2}$
ACCELERATION VELOCITY
$V_A = V_E + \Delta T \left(g + \frac{P}{\rho H}\right)$
EXIT VELOCITY
V_E = MIN OF V_A, V_B
2

FORWARD & AFT BULKHEADS

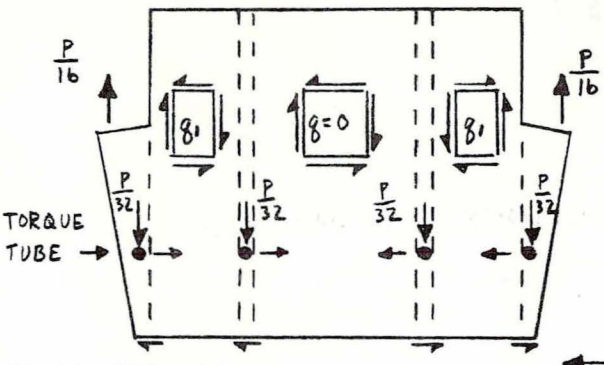

DOORS REMOVED

P = 90,000 LBS ULT

SEE P. 14

NOTE: THE LOADS SHOWN ARE FOR THE RETARDANT ONLY. FOR THE STRESS ANALYSIS OF THE ATTACH POINTS, THE LOADS WILL BE INCREASED TO ACCOUNT FOR THE STRUCTURE WEIGHT.

THE HINGE LOADS (SEE P. 14) ARE "BEAMED" TO THE BULKHEADS AND THEY CANCEL OUT THE VERTICAL CONCENTRATED DOOR LOADS (SEE P. 14)

$q_1 = (\frac{P}{32}) / \text{TOTAL DEPTH} = \frac{90{,}000}{32 \times 60}$

$q_1 = 47$ LBS/IN ULT

INTERMEDIATE BULKHEADS

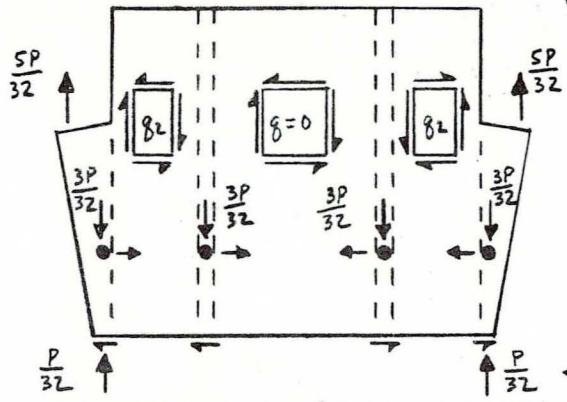

IT IS ASSUMED THE CENTER PARTITION DOES NOT DISTRIBUTE ANY OF THE INTERNAL HINGE LOADS TO THE SUPPORTS, SO THE CONCENTRATED DOOR LOADS ARE COMPLETELY CANCELED. A PORTION OF THE EXTERNAL HINGE LOADS IS TRANSFERRED DIRECTLY TO THE CENTER SUPPORTS (ATTACH POINTS), SO THE CONCENTRATED DOOR LOADS ARE NOT COMPLETELY CANCELED.

$q_2 = \frac{3P}{32} / \text{TOTAL DEPTH} = \frac{3 \times 90{,}000}{32 \times 60}$

$q_2 = 141$ LBS/IN ULT

CENTER PARTITION

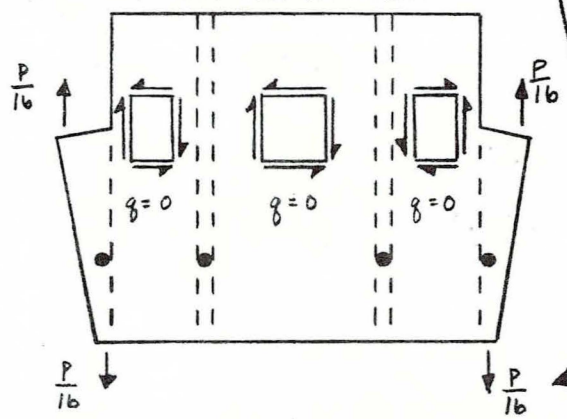

A PORTION OF THE EXTERNAL HINGE LOADS IS TRANSFERRED DIRECTLY TO THE SUPPORT.

THE PARTITION CARRIES NO SHEAR.

CALC	GRJ	1-25-75	REVISED	DATE
CHECK				
APR				
APR				

H

BULKHEAD LOADS FOR COND D

AEROSPACE & DEFENSE GROUP
GOVERNMENT & AERONAUTICAL PRODUCTS DIVISION

EWA No	TYPE No	PAGE 20

HT-51 REV 11/71

INTERMEDIATE BULKHEAD HAS MAX SHEAR FLOW, q_2 = 141 LBS/IN ULT (SEE P. 20)

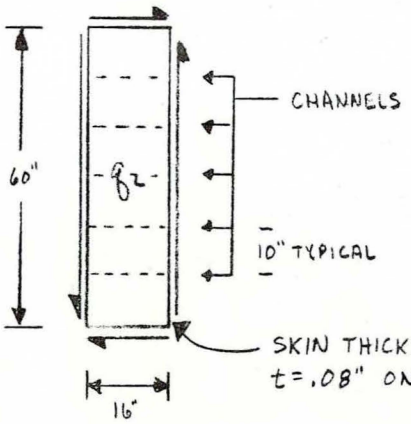

MATERIAL:

SKIN - 7075-T6 ALUM
F_s = 45,000 PSI
E = 10^7 PSI
RIVETS AD/5 (D = 5/16")
SHEAR STRENGTH = 596 LBS

FIND BUCKLING STRESS OF SKIN, F_{CRIT}

(LARGEST UNSUPPORTED SPAN IS 10" x 16")

$F_{CRIT} = \frac{\pi^2 K_s E}{12(1-\nu^2)} \left(\frac{t}{b}\right)^2$ (BRUHN - P. C5.6) $\frac{a}{b} = \frac{16}{10} = 1.6 \Rightarrow K_s = 7$

$= \frac{\pi^2 (7)\, 10^7}{12(1-.3^2)} \left(\frac{.08}{10}\right)^2$

F_{CRIT} = 4049 PSI ✓

SHEAR STRESS IN SKIN

$f_s = q_2/t = \frac{141}{2 \times .08}$

f_s = 881 PSI ULT ✓

M.S. = $\frac{4049}{881} - 1$

→ M.S. = + 3.6 ✓

FIND SHEAR FORCE PER RIVET, R_s

EACH SKIN HAS TWO ROWS OF RIVETS SPACED AT s = 1.25"

$R_s = q_2\left(\frac{s}{4}\right) = 141\left(\frac{1.25}{4}\right)$

R_s = 44.1 LBS PER RIVET ULT ✓

M.S. = $\frac{596}{44.1} - 1$

→ M.S. = + 12.5 ✓

NOTE: RIVET SPACING IS GOVERNED BY LEAKAGE REQUIREMENTS AND THE STRUCTURAL M.S. IS THEREFORE VERY LARGE

CALC	GRJ	1-27-75	REVISED	DATE
CHECK				
APR				
APR				

BULKHEAD SHEAR FLOW & RIVET ANALYSIS

AEROSPACE & DEFENSE GROUP
GOVERNMENT & AERONAUTICAL PRODUCTS DIVISION

EWA No	TYPE No	PAGE 21

HT-51 REV 11/71

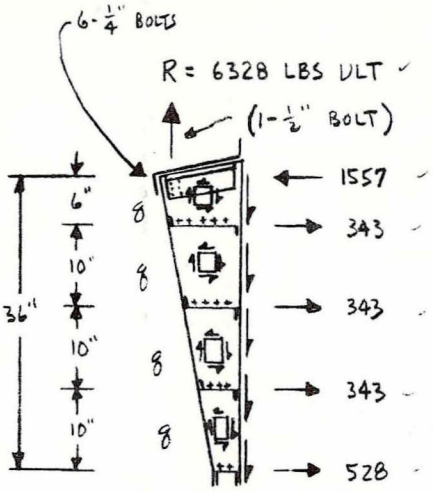

FROM P. 14, R IS GIVEN FOR THE WEIGHT OF THE RETARDANT ONLY. TO INCLUDE THE WEIGHT OF THE STRUCTURE, IT MUST BE INCREASED BY 12.5%

$$R = 1.125\,\frac{P}{16} = 1.125\,\frac{90{,}000}{16}$$

$$\underline{R = 6328 \text{ LBS ULT}} \quad ✓$$

EQUAL SHEAR FLOW, q, IN ALL PANELS

$$q = \frac{R}{L} = \frac{6328}{36}$$

$$\underline{q = 176 \text{ LBS/IN ULT}} \quad ✓$$

OUTER SKIN ON FWD & AFT BULKHEADS IS CONTINUOUS. THEREFORE, THE HORIZONTAL LOADS ARE SIMPLY TRANSFERRED INTO THE OUTER SKIN.

OUTER SKIN ⇒ 6061-T6 ALUM, $t = .063"$,

$$F_{CRIT} = \frac{\pi^2 K_s E}{12(1-\nu^2)}\left(\frac{t}{b}\right)^2 = \frac{\pi^2 10(10^3)}{12(1-.3^2)}\left(\frac{.063}{10}\right)^2$$

$$\underline{F_{CRIT} = 3587 \text{ PSI}} \quad ✓$$

FIND SHEAR STRESS DUE TO SHEAR FLOW

$$f_s = q/t = 176/.063$$

$$\underline{f_s = 2794 \text{ PSI ULT}} \quad ✓$$

$$M.S. = \frac{3587}{2794} - 1$$

$$\underline{M.S. = +.28} \quad ✓$$

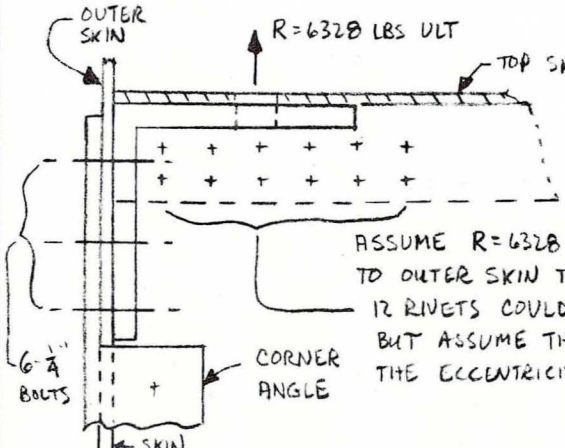
OUTER SKIN
R = 6328 LBS ULT
TOP SKIN ALONG SUPPORT
ASSUME R = 6328 IS TRANSFERRED TO OUTER SKIN THROUGH 6-¼" BOLTS. 12 RIVETS COULD ALSO REACT LOAD, BUT ASSUME THEY REACT ONLY THE ECCENTRICITY.
6-¼" BOLTS
CORNER ANGLE
SKIN
R = 6328

BEARING STRESS IN OUTER SKIN

6061-T6 ⇒ $F_{BRU} = 90{,}000$ PSI

$$f_{br} = \frac{R}{A_{br}} = \frac{6328}{6\times.75\times.063} = \underline{66{,}963 \text{ PSI ULT}} \quad ✓$$

$$M.S. = \frac{90{,}000}{66{,}963} - 1 \Rightarrow \underline{M.S. = +.34} \quad ✓$$

SHEAR STRESS IN 6-¼" BOLTS

$$f_s = \frac{R}{A_s} = \frac{6328}{6\pi(.125)^2} = \underline{21{,}485 \text{ PSI ULT}} \quad ✓$$

$$M.S. = \frac{75{,}000}{21{,}485} - 1 \Rightarrow \underline{M.S. = +2.5} \quad ✓$$

TENSILE STRESS IN ½" ATTACH BOLT

$F_{tu} = 160{,}000$ PSI

$$f_t = \frac{P}{A_t} = \frac{6328}{.125}$$

$$\underline{f_t = 50{,}624 \text{ PSI ULT}} \quad ✓$$

$$M.S. = \frac{160{,}000}{50{,}624} - 1$$

$$\underline{M.S. = +2.1} \quad ✓$$

CALC	GRJ	1-30-75	REVISED	DATE
CHECK				
APR				
APR				

ANALYSIS OF ATTACH POINTS AT END BULKHEADS FOR COND D

AEROSPACE & DEFENSE GROUP
GOVERNMENT & AERONAUTICAL PRODUCTS DIVISION

EWA No	TYPE No	PAGE 22

HT-51 REV 11/71

MATERIAL: ALUM

OUTER SKIN → 6061-T6 → E = 10^7 PSI
"T" CLIP → 7075-T6 → F_{tu} = 75,000 PSI
SHEAR PANEL → 7075-T6 → F_{bru} = 140,000 PSI

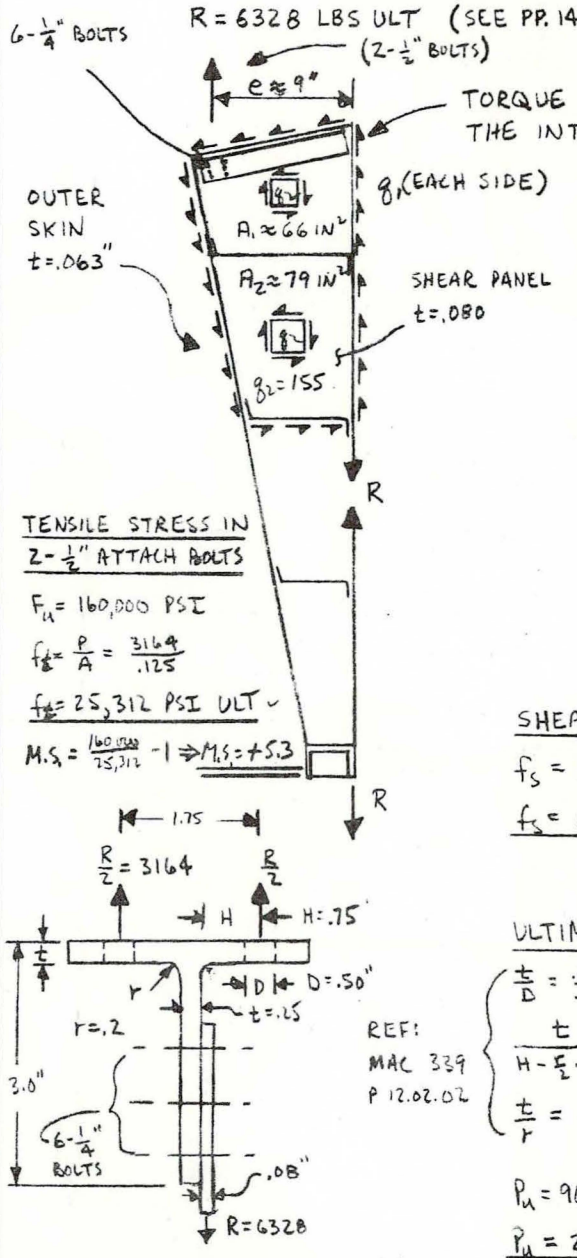

T = TORQUE TO EACH SUPPORT

$= \frac{1}{2} Re = \frac{1}{2}\ 6328 \times 9$

T = 28,476 IN-LBS ULT ✓

q_1 = SHEAR FLOW ON EACH SIDE

$= \frac{T}{2A} = \frac{28,476}{2(66+79)}$

q_1 = 98.2 LBS/IN ULT ✓

F_{CRIT} = BUCKLING STRESS (BRUHN)

$= \frac{\pi^2 K_s E}{12(1-\nu^2)} \left(\frac{t}{b}\right)^2 = \frac{\pi^2 6 (10^7)}{12(1-.3^2)} \left(\frac{.063}{10}\right)^2$

F_{CRIT} = 2152 PSI ✓ (FOR OUTER SKIN)

TENSILE STRESS IN 2-1/2" ATTACH BOLTS

F_{tu} = 160,000 PSI

$f_t = \frac{P}{A} = \frac{3164}{.125}$

f_t = 25,312 PSI ULT ✓

$M.S. = \frac{160,000}{25,312} - 1 \Rightarrow M.S. = +5.3$

SHEAR STRESS IN OUTER SKIN

$f_s = q/t = 98.2/.063$

f_s = 1559 PSI ULT ✓ → $M.S. = \frac{2152}{1559} - 1$ → M.S. = +.38

ULTIMATE STRENGTH OF "T" CLIP, P_u

REF: MAC 339 P 12.02.02

$\frac{t}{D} = \frac{.25}{.50} = .5$

$\frac{t}{H - \frac{t}{2} - \frac{D}{2}} = \frac{.25}{.75 - .10 - .25} = .625$ $\Rightarrow \frac{P_u}{D^2} = 90,000$

$\frac{t}{r} = \frac{.25}{.2} = 1.25$

$P_u = 90,000\ D^2 = 90,000 (.5)^2$

P_u = 22,500 LBS → $M.S. = \frac{22,500}{6328} - 1$ → M.S. = +2.5

R = 6328 IS REACTED BY 6-1/4" BOLTS

SHEAR STRESS IN 1/4" BOLTS: $f_s = R/A_1 = 6328/6\pi(.125)^2 = 21,485$ PSI ULT

$M.S. = \frac{75,000}{21,485} - 1 \Rightarrow M.S. = +2.5$ ✓

BEARING STRESS: $f_{br} = R/A_{br} = \frac{6328}{6 \times .25 \times .08} = 52,733$ PSI ULT ✓

$M.S. = \frac{140,000}{52,733} - 1 \Rightarrow M.S. = +1.65$

CALC	GRJ	1-30-75	REVISED	DATE
CHECK				
APR				
APR				

ANALYSIS OF ATTACH POINTS AT CENTER PARTITION FOR COND D

AEROSPACE & DEFENSE GROUP
GOVERNMENT & AERONAUTICAL PRODUCTS DIVISION

EWA No	TYPE No	PAGE 23

HT-51 REV 11/71

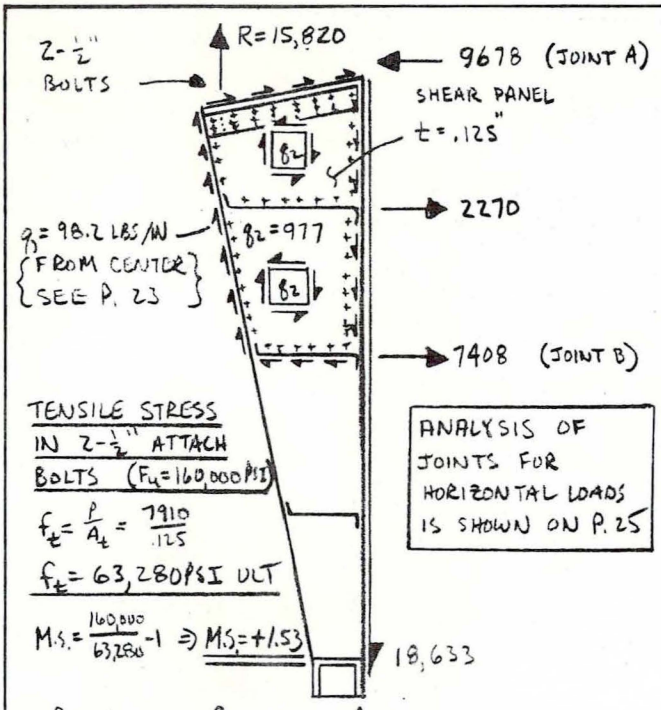

ANALYSIS OF JOINTS FOR HORIZONTAL LOADS IS SHOWN ON P. 25

$R = 1.125 \times \frac{5}{32}(90{,}000)$ (SEE PP. 14, 20 & 22)

$R = 15{,}820$ LBS ULT ✓

FIND SHEAR FLOW, q_2

$q_2 = \frac{15{,}820}{18"} + q = 879 + 98.2$

$q_2 = 977$ LBS/IN ULT ✓

STRESS IN SHEAR PANEL (6061-T6)

$F_{CRIT} = \frac{\pi^2 K_s E}{12(1-\nu^2)}\left(\frac{t}{b}\right)^2 = \frac{\pi^2 10(10^6)}{12(1-.3^2)}\left(\frac{.125}{10}\right)^2$ ✓

$F_{CRIT} = 14{,}122$ PSI ✓

$f_s = \frac{q_2}{t} = \frac{977}{.125}$ $\quad M.S. = \frac{14{,}122}{7816} - 1$

$f_s = 7816$ PSI ULT → M.S. = +.81 ✓

TENSILE STRESS IN 2-½" ATTACH BOLTS ($F_{tu} = 160{,}000$ PSI)

$f_t = \frac{P}{A_t} = \frac{7910}{.125}$

$f_t = 63{,}280$ PSI ULT

$M.S. = \frac{160{,}000}{63{,}280} - 1 \Rightarrow M.S. = +1.53$

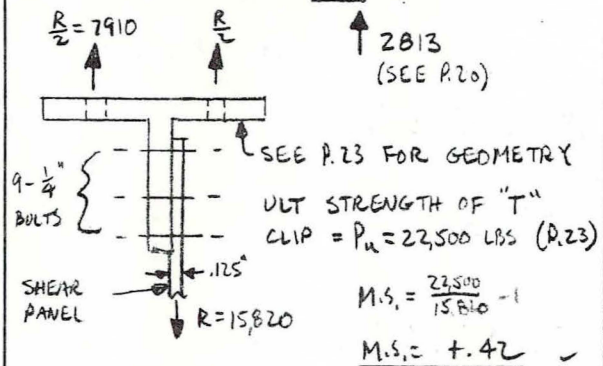

$M.S. = \frac{22{,}500}{15{,}820} - 1$

M.S. = +.42 ✓

SHEAR IN 9-¼" BOLTS ($F_s = 75{,}000$ PSI)

$f_s = \frac{P}{A_s} = \frac{15{,}820}{9\pi(.125)^2}$ $\quad M.S. = \frac{75{,}000}{35{,}809} - 1$

$f_s = 35{,}809$ PSI ULT ✓ → M.S. = +1.09 ✓

BEARING IN SHEAR PANEL ($F_{bru} = 90{,}000$ PSI)

$f_{bru} = \frac{P}{A_{br}} = \frac{15{,}820}{9 \times .25 \times .025}$ $\quad M.S. = \frac{90{,}000}{56{,}249} - 1$

$f_{bru} = 56{,}249$ PSI ULT → M.S. = +.59 ✓

CHECK FASTENERS AROUND SHEAR PANEL

¼" BOLTS @ 1.0" SPACING ⇒ 977 #/BOLT

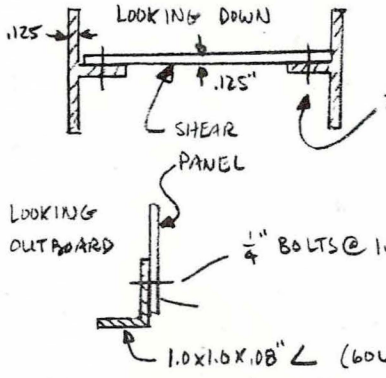

SHEAR IN BOLTS ($F_s = 75{,}000$ PSI)

$f_s = \frac{P}{A_s} = \frac{977}{\pi(.125)^2}$ $\quad M.S. = \frac{75{,}000}{19{,}903} - 1$

$f_s = 19{,}903$ PSI ULT ✓ → M.S. = +2.8

BEARING IN ANGLE ($F_{bru} = 90{,}000$ PSI)

$f_{bru} = \frac{P}{A_{br}} = \frac{977}{.25 \times .08}$ $\quad M.S. = \frac{90{,}000}{48{,}850} - 1$

$f_{bru} = 48{,}850$ PSI ULT ✓ → M.S. = +.84 ✓

CALC	GRJ	1-30-75	REVISED	DATE
CHECK				
APR				
APR				

ANALYSIS OF ATTACH POINTS AT INTERMEDIATE BULKHEADS FOR COND D

AEROSPACE & DEFENSE GROUP
GOVERNMENT & AERONAUTICAL PRODUCTS DIVISION

EWA No	TYPE No	PAGE 24

HT-51 REV 11/71

ANALYSIS OF JOINT A (SEE P. 24)

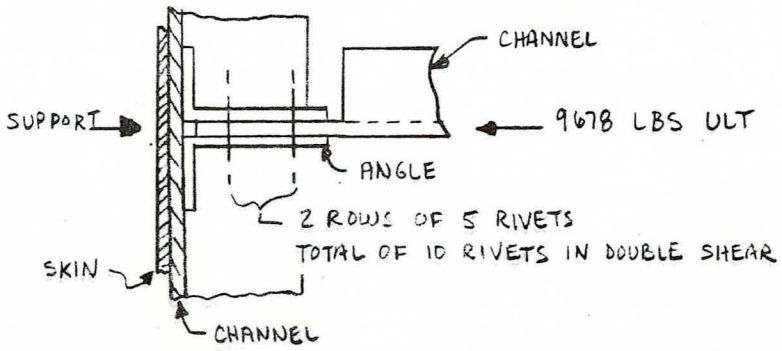

RIVETS - AD/5 ($D=\frac{5}{32}$)

SHEAR STRENGTH = 596 LBS

$M.S. = \frac{2 \times 10 \times 596}{9678} - 1$

$M.S. = +.23$ ✓

ANALYSIS OF JOINT B (SEE P. 24)

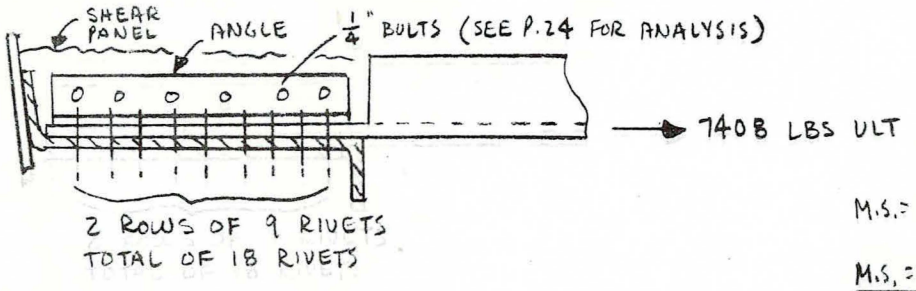

$M.S. = \frac{18 \times 596}{7408} - 1$

$M.S. = +.45$ ✓

CALC	GRJ	1-30-75	REVISED	DATE
CHECK				
APR				
APR				

ANALYSIS OF ATTACH POINTS AT INTERMEDIATE BULKHEADS FOR COND D

AEROSPACE & DEFENSE GROUP
GOVERNMENT & AERONAUTICAL PRODUCTS DIVISION

EWA No	TYPE No	PAGE 25 OF 25

HT-51 REV 11/71

APPENDIX B

FLOW RATE OFF-LINE PROGRAM LISTING AND PROGRAM FLOW

PROGRAM LISTING

```
      REAL K,LD,LT,LV,MAXDX
      LOGICAL DQ
      CALL DEFINE (1,6HPARAM )
      CALL DEFINE (2,5HDOOR )
***********INPUT PARAMETERS.
      READ(1,5) H,LD,WD,LT,WT,DV,LV,RHO,K,G,HT
    5 FORMAT(2X,F20.9/6(3X,F20.9/),4X,F20.9/2(2X,F20.9/),3X,F20.9)
***********OUTPUT TABLE HEADING.
      WRITE(9,10)
   10 FORMAT('TIME     HEAD      VEL       VEL       RATE',
     +'      VOLUME    PRESS'/'(SEC)   (FT)     EXIT      TOP',
     +'      GALS/SEC   OUT       PSI'/)
***********INITIAL VALUES AND CONSTANTS USED.
      P=0.0
      T=0.0
      DELT=0.02
      GALO=0.0
      VZ=0.0
      VE=0.0
      TOTX=0.0
      AREAT=WT*LT
      AREAD=WD*LD
      VOL=(HT-H)*AREAT
**********
      DQ=.FALSE.
      K=K/(DELT*DELT*DV**4.0)
      ALAST=0.0
      CONST=3.1416/180.0
**********
***********INCREMENT TIME ELAPSED.
  100 T=T+DELT
***********CALCULATE NEW DOOR ANGLE IN RADIANS
      IF(IEOF(2).EQ.1) GO TO 160
      READ(2,150) A
  150 FORMAT(F16.4)
      IF(A.LE.0.0) GO TO 100
      A=CONST*A
***********CALCULATE BERNOULI VELOCITY.
  160 RHOH=RHO*H
      X=2.0*(G*RHOH+P)/RHO
      X=X+VZ*VZ
      IF(X.LT.0.0) X=0.0
      VB=SQRT(X)
***********CALCULATE ACCELERATION VELOCITY.
      VA=VE+DELT*(G+P/RHOH)
***********EXIT VELOCITY IS SMALLER OF VA AND VB.
      VE=AMIN1(VB,VA)
```

```
**********CALCULATION OF EFFECTIVE DOOR AREA.
      DX=VE*DELT
      IF(DQ) GO TO 180
      MAXDX=WD*SIN(A)
      HMAX=MAXDX*0.5
      TOTX=TOTX+DX
      IF(DX.GT.HMAX) GO TO 210
      IF(TOTX.GT.MAXDX) GO TO 200
      GO TO 190
*---------CONSIDER EFFECTIVE DOOR AREA = DOOR AREA.
  180 AE=AREAD
      GO TO 300
*---------DOOR RATE FAST ENOUGH NOT TO RESRICT FLOW.
  190 DELAE=DELT*COS(A)/(2.0*MAXDX)
      AE=AREAD*(1.0-DELAE)
      GO TO 300
*---------DOOR RATE RESTRICTING FLOW SOMEWHAT.
  200 DELAE=COS(A)/2.0
      AE=AREAD*(1.0-DELAE)
      GO TO 300
*---------DOOR RATE RESTRICTING FLOW.
  210 DELAE=0.0
      IF(A.GT.0.7854) GO TO 215
      ADIFF=A-ALAST
      IF(ADIFF.LE.0.0) GO TO 215
      DELAE=WD/2.0*COS(2.0*A)*ADIFF/VE
  215 AE=AREAD*(SIN(A)+DELAE)
      GO TO 310
  300 IF(DELAE.LT.0.005) DQ=.TRUE.
  310 IF(VE.LE.0.0) GO TO 405
**********CALCULATION OF CHANGE IN OUTPUT VOLUME (Q).
      Q=DX*AE
**********CALCULATION OF FLUID VELOCITY AT TOP (VZ).
      VZ=VE*AE/AREAT
      IF(VE.LE.0.0) GO TO 405
      P=-K*Q*Q
      P=P*VOL/(VOL+Q)
      VOL=VOL+Q
      H=H-VZ*DELT
      GAL=Q*7.481
      GALO=GALO+GAL
      PO=P*0.0069445
      RATE=GAL/DELT
      ALAST=A
      WRITE(9,400) T,H,VE,VZ,RATE,GALO,PO
  400 FORMAT(F4.2,F8.2,F9.2,F9.2,F10.2,F10.2,F10.3)
      IF(H.GT.0.0) GO TO 100
      STOP
  405 WRITE(9,410)
  410 FORMAT(///'PRESSURE=HEAD')
      STOP
      END
```

PROGRAM FLOW

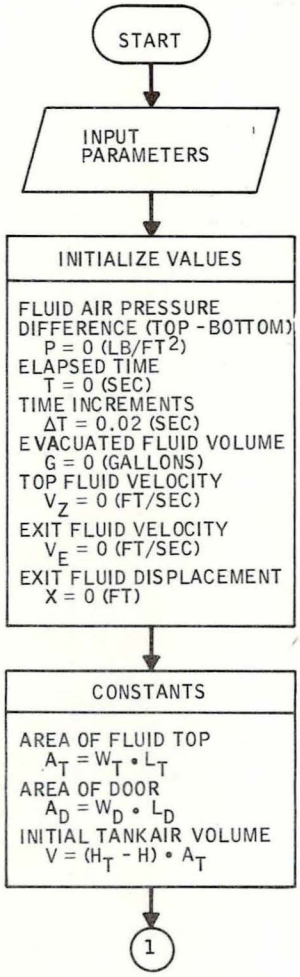

PARAMETERS			
H =		FT	HEAD HEIGHT
L_D =		FT	DOOR LENGTH
W_D =		FT	DOOR WIDTH
L_T =		FT	TANK LENGTH
W_T =		FT	TANK WIDTH
D_V =		FT	EQUIVALENT VENT DIAMETER
L_V =		FT	VENT LENGTH
ρ =	2.072	LB/FT^3	RETARDANT DENSITY
K =	0.0019275		COMBINATION OF CONSTANTS
g =	32.2	FT/SEC^2	GRAVITIONAL CONSTANT
H_T =		FT	TANK HEIGHT

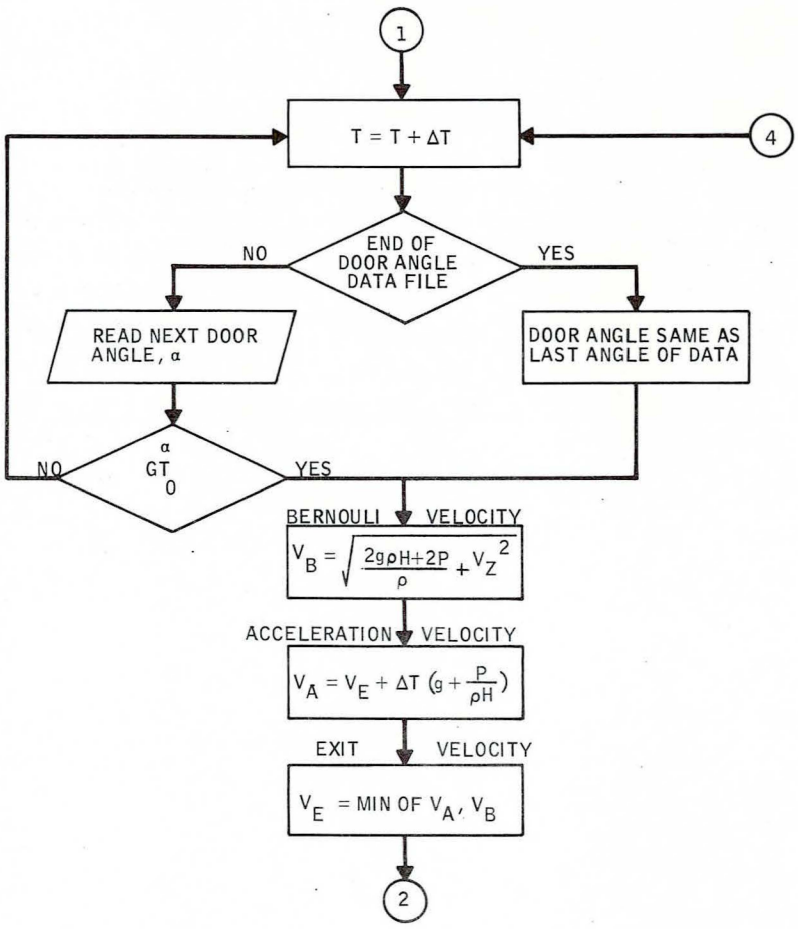
1
T = T + ΔT
4
END OF DOOR ANGLE DATA FILE
NO
YES
READ NEXT DOOR ANGLE, α
DOOR ANGLE SAME AS LAST ANGLE OF DATA
α GT 0
NO
YES
BERNOULI VELOCITY
$V_B = \sqrt{\frac{2g\rho H+2P}{\rho} + V_Z^2}$
ACCELERATION VELOCITY
$V_A = V_E + \Delta T \left(g + \frac{P}{\rho H}\right)$
EXIT VELOCITY
V_E = MIN OF V_A, V_B
2

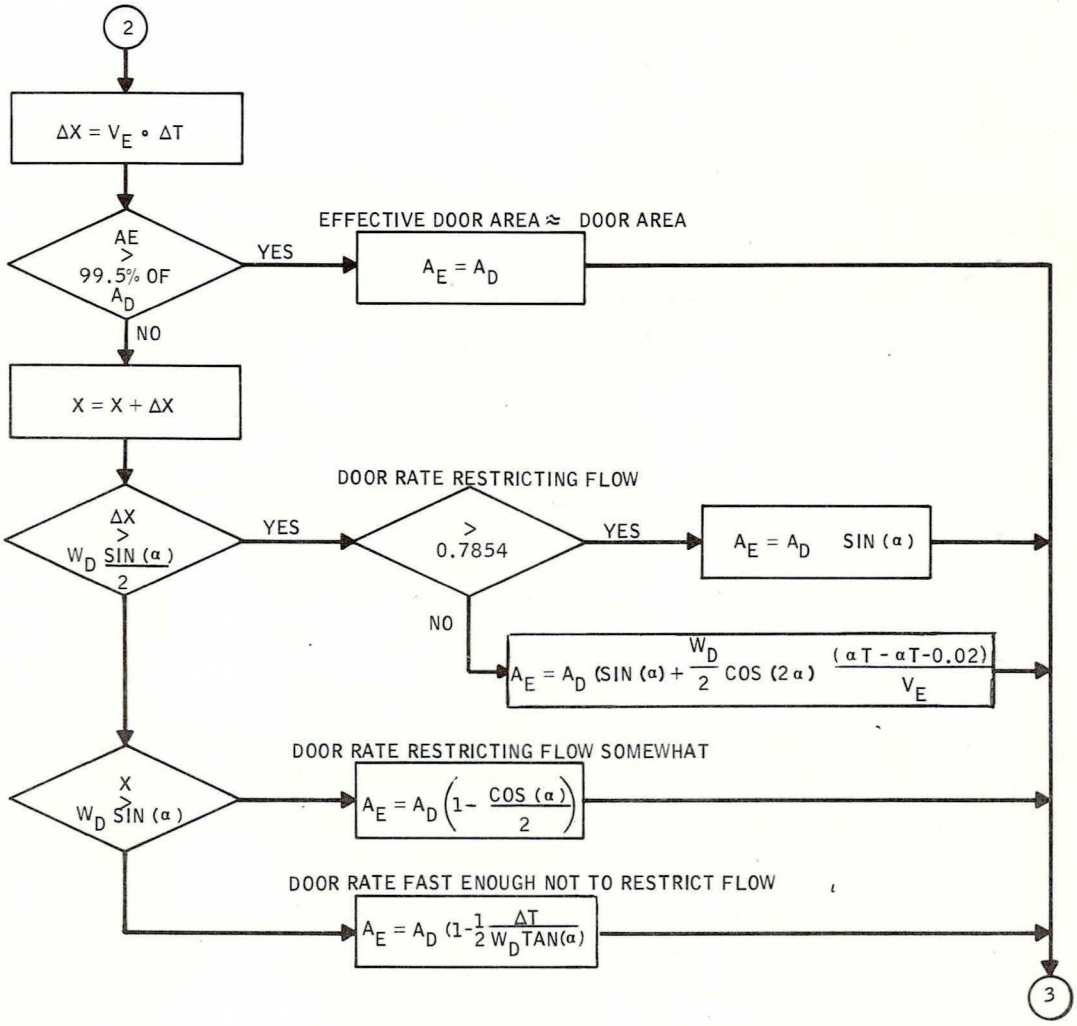
2
ΔX = V_E ∘ ΔT
AE > 99.5% OF A_D
YES
EFFECTIVE DOOR AREA ≈ DOOR AREA
A_E = A_D
NO
X = X + ΔX
ΔX > W_D SIN (α) / 2
YES
DOOR RATE RESTRICTING FLOW
> 0.7854
YES
A_E = A_D SIN (α)
NO
A_E = A_D (SIN (α) + W_D/2 COS (2α) (αT - αT-0.02) / V_E
X > W_D SIN (α)
DOOR RATE RESTRICTING FLOW SOMEWHAT
A_E = A_D (1 - COS (α) / 2)
DOOR RATE FAST ENOUGH NOT TO RESTRICT FLOW
A_E = A_D (1 - 1/2 ΔT / W_D TAN(α))
3

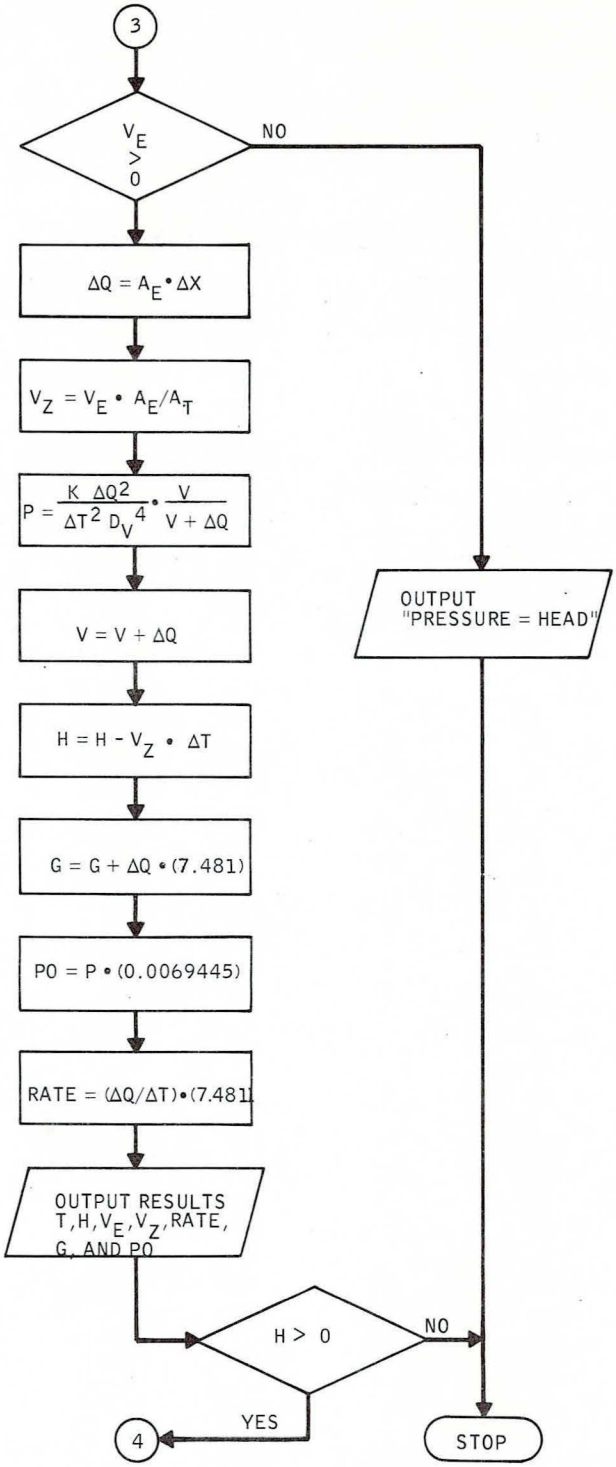
3
$V_E > 0$
NO
$\Delta Q = A_E \cdot \Delta X$
$V_Z = V_E \cdot A_E/A_T$
$P = \frac{K\ \Delta Q^2}{\Delta T^2\ D_V^4} \cdot \frac{V}{V + \Delta Q}$
$V = V + \Delta Q$
$H = H - V_Z \cdot \Delta T$
$G = G + \Delta Q \cdot (7.481)$
$PO = P \cdot (0.0069445)$
RATE = $(\Delta Q/\Delta T) \cdot (7.481$
OUTPUT RESULTS T,H,V_E,V_Z,RATE, G, AND PO
OUTPUT "PRESSURE = HEAD"
H > 0
NO
YES
4
STOP

Date	Drop Number	Retardant	Drop Height (Feet)	Drop Speed (knots)	Drop Size (Gallons)	Wind Speed (mph)	Wind Direction (Degrees)	Tanks	Doors and/ or drop	Config.	Door rate
10/7	1	PC	264.8	118.5	460	4.9	40R	5	2 & 3	C3-3/4	6
10/7	2	PC	256.3	113.0	460	1.8	115L	5	2 & 3	C3-3/4	6
10/7	3	PC	138.5	121.3	460	1.8	55L	5	2 & 3	C3-3/4	6
10/8	4	PC	131.1	123.8	460	3.1	10R	5	2 & 3	C3-3/4	6
10/8	5	PC	133.6	119.1	460	1.2	15R	5	2 & 3	C3-3/4	2
10/8	6	PC	142.1	119.3	460	1.8	168R	5	2	C3-1/4	2
10/8	7	Water	133.4	119.3	460	1.0	30R	5	2	C3-1/4	2
10/8	8	PC	133.3	119.0	460	5.6	78L	5	2	C3-1/4	6
10/8	9	PC	308.1	121.6	460	6.6	10L	5	2 & 3	C3-3/4	2
10/8	10	PC	135.9	129.8	460	10.8	8R	7,8,9	4	C1	2
10/12	11	PC	263.1	125.8	460	2.5	38R	5	2 & 3	C3-1/4	6
10/12	12	PC	323.8	128.9	460	1.9	20R	5	2 & 3	C3-1/4	2
10/12	13	Water	284.8	120.1	460	2.8	1R	5	2 & 3	C3-3/4	2
10/12	14	Water	262.8	122.3	460	4.6	18L	5	2 & 3	C3-3/4	2
10/12	15	Water	140.0	127.6	460	5.0	12L	5	2 & 3	C3-3/4	2

Date	Drop Number	Retardant	Drop Height (Feet)	Drop Speed (knots)	Drop Size (Gallons)	Wind Speed (mph)	Wind Direction (Degrees)	Tanks	Doors and/ or drop	Config.	Door rate
10/12	16	Water	122.2	122.0	460	4.6	25R	5	2 & 3	C3-3/4	6
10/12	17	Water	245.0	124.3	460	5.1	20L	5	2	C3-1/4	6
10/13	18	Water	283.4	113.8	460	3.3	170L	5	2 & 3	C3-3/4	6
10/13	19	Water	286.1	119.0	460	2.0	130L	5	2	C3-1/4	2
10/13	20	Water	288.7*	117.2	460	5.5	175L	5	2	C3-1/4	5
10/13	21	Water	141.4	116.4	460	3.0	128L	7,8,9	4	C1-4L:W	2
10/13	22	Water	141.6	120.2	230	2.8	175L	4	2 & 3	1L:W	6
10/14	23	Water	289.7	120.6	460	2.3	144L	7,8,9	4	C1-4L:W	2
10/14	24	Water	319.5	109.9	460	4.3	179L	1,4,7	1,2,3,4	C2-1L:W	1 & 4 2 2 & 3 6
10/14	25	PC	299.1	118.9	460	2.4	115L	1,4,7	1,2,3,4	C2-1L:W	1 & 4 2 2 & 3 6
10/14	26	PC	280.4	119.9	460	1.0	92L	7,8,9	4	C1-4L:W	2
10/14	27	Water	142.0	118.7	460	3.3	52L	5	2	C3-1/4	6
10/14	28	Water	321.2	118.6	460	2.8	53L	5	2	C3-1/4	2
10/14	29	Water	147.0	117.0	460	2.6	10L	3,6,9	1,2,3,4	C2-1L:W	1 & 4 2 2 & 3 6

*150-foot target

Date	Drop Number	Retardant	Drop Height (Feet)	Drop Speed (knots)	Drop Size (Gallons)	Wind Speed (mph)	Wind Direction (Degrees)	Tanks	Doors and/ or drop	Config.	Door rate
10/15	30	Water	292.1	120.5	460	1.3	12L	5	2 & 3	C3-1/2	6
10/15	31	Water	357.4	126.4	460	2.9	118L	5	2	C3-1/2	2
10/15	32	PC	154.9	116.9	460	3.3	102L	5	2	C3-1/2	6
10/15	33	PC	157.1	122.1	460	1.4	100R	5	2	C3-1/2	2
10/15	34	PC	392.9	130.4	460	3.9	152L	5	2 & 3	C3-full	2
10/15	35	PC	274.3	122.5	460	0.5	25R	5	2	C3-1/2	2
10/15	36	Water	264.2	125.6	460	1.6	35L	5	2 & 3	C3-full	2
10/16	37	PC	272.0	127.3	460	1.4	126L	5	2	C3-1/2	6
10/16	38	PC	353.4	122.6	460	3.0	80L	5	2 & 3	C3-full	6
10/16	39	Water	295.4	126.2	460	2.0	127L	5	2 & 3	C3-full	6
10/16	40	PC	136.1	123.8	460	1.2	118R	5	2 & 3	C3-full	6
10/16	41	PC	139.3	123.9	460	1.0	95L	5	2 & 3	C3-full	2
10/16	42	Water	159.9	127.0	460	1.7	60L	5	2	C3-1/2	6

Date	Drop Number	Retardant	Drop Height (Feet)	Drop Speed (knots)	Drop Size (Gallons)	Wind Speed (mph)	Wind Direction (Degrees)	Tanks	Doors and/ or drop	Config.	Door rate
10/17	43	Water	154.3	125.2	460	2.5	179L	5	2	C3-1/2	2
10/17	44	Water	139.7	126.2	460	0.9	65R	5	2 & 3	C3-full	6
10/17	45	Water	133.8	130.6	460	3.3	2R	5	2 & 3	C3-full	2
10/20	46	PC	275.0	130.4	460	1.2	33R	2 & 8	1 & 4	C4	2
10/20	47	Water	273.1	130.4	460	5.2	25L	2 & 8	1 & 4	C4	2
10/20	48	PC	288.6	139.2	460	2.3	7L	4 & 6	2 & 3	C6	6
10/20	49	Water	327.1	141.3	460	5.8	7L	4 & 6	2 & 3	C6	6
10/20	50	PC	140.3	134.8	460	7.2	8L	2 - 8	1 & 4	C4	2
10/20	51	Water	137.1	136.2	460	9.1	3L	2 - 8	1 & 4	C4	2
10/21	52	PC	277.4	125.2	460	2.8	179L	1,3,7,9	1 & 4	C5	2
10/21	53	Water	150.6	130.9	460	10.1	2R	1,3,7,9	1 & 4	C5	2
10/22	54	PC	142.3	114.5	460	10.0	170R	1,3,7,9	1 & 4	C5	2
0/22	55	PC	129.7	107.9	460	16.2	174R	7,8,9	4	C1	2
0/22	56	Water	130.5	120.1	460	13.0	173L	7,8,9	4	C1	2
0/22	57	PC	148.9	107.8	460	19.5	170R	5	2 & 3	C3	6

Date	Drop Number	Retardant	Drop Height (Feet)	Drop Speed (knots)	Drop Size (Gallons)	Wind Speed (mph)	Wind Direction (Degrees)	Tanks	Doors and/ or drop	Config.	Door rate
10/22	58	Water	125.0	100.3 *	460	19.3	160R	5	2 & 3	C3	6
10/23	59	Water	151.3	108.7 *	460	16.8	178R	1,3,7,9	1 & 4	C5	2
10/23	60	Water	128.7	142.5	460	18.7	172R	7,8,9	4	C1	2
10/23	61	PC	125.4	147.7	460	23.5	175L	7,8,9	4	C1	2
10/24	62	Water	286.2	126.5	460	2.5	179L	1,3,7,9	1 & 4	C5	2
10/24	63	Water	147.7	121.4	460	5.6	175R	4,6	2 & 3	C6	6
10/24	64	PC	130.2	118.5	460	8.8	172R	4,6	2 & 3	C6	6
10/24	65	PC	146.9	117.3	460	8.9	177L	3,6,9	1,2,3,4	C2	2 & 6
10/24	66	PC	324.7	163.9	460	1.0	178L	3,6,9	1,2,3,4	C2	2 & 6
10/24	67	PC	118.9	165.0	460	2.8	5L	3,6,9	1,2,3,4	C2	2 & 6
10/24	68	Water	254.8	161.6	460	1.3	18R	1,4,7	1,2,3,4	C2	2 & 6
10/24	69	PC	295.4	162.8	460	3.2	10R	5	2 & 3	C3	6
10/24	70	Water	306.7	166.8	460	2.8	42L	5	2 & 3	C3	6
10/27	71	PC	125.5	139.7	460	9.1	10R	7,8,9	4	C1	2
10/27	72	Water	115.9	139.8	460	11.2	5L	2,8	1 & 4	C4	2

*125-knot target

Date	Drop Number	Retardant	Drop Height (Feet)	Drop Speed (knots)	Drop Size (Gallons)	Wind Speed (mph)	Wind Direction (Degrees)	Tanks	Doors and/ or drop	Config.	Door rate
10/27	73	PC	128.1	134.6	460	7.0	1L	1,3,7,9	1 & 4	C5	2
10/27	74	Water	124.7	137.5	460	14.6	12R	1,3,7,9	1 & 4	C5	2
10/27	75	PC	102.5	132.4	460	13.0	19R	2 & 8	1 & 4	C4	2
10/27	76	Water	115.6	138.9	460	14.0	32R	7,8,9	4	C1	2
10/28	77	PC	282.7	160.1	460	1.3	156R	7,8,9	4	C1	2
10/28	78	Water	301.0	154.9	460	4.5	154L	7,8,9	4	C1	2
10/28	79	PC	271.0	159.9	460	5.4	176R	2 & 8	1 & 4	C4	2
10/28	80	Water	281.8	156.0	460	8.6	179R	2 & 8	1 & 4	C4	2
10/28	81	PC	274.9	155.4	460	8.8	179R	1,3,7,9	1 & 4	C5	2
10/28	82	PC	262.4	161.4	460	2.8	161L	4 & 6	2 & 3	C6	6
10/28	83	Water	282.2	159.0	460	1.0	29R	4 & 6	2 & 3	C6	6
10/28	84	Water	293.5	158.7	460	0.6	104R	1,3,7,9	1 & 4	C5	2
10/28	85	PC	116.7	171.3	460	4.5	52L	5	2 & 3	C3	6
10/29	86	Water	123.4	163.6	460	2.3	110L	4 & 6	2 & 3	C6	6
10/29	87	PC	115.5	158.6	460	1.1	141L	4 & 6	2 & 3	C6	6

Date	Drop Number	Retardant	Drop Height (Feet)	Drop Speed (knots)	Drop Size (Gallons)	Wind Speed (mph)	Wind Direction (Degrees)	Tanks	Doors and/ or drop	Config.	Door rate
10/29	88	PC	134.7	128.1	460	5.4	68L	4 & 6	2 & 3	C6	6
10/29	89	Water	123.2	173.6	460	8.4	6R	5	2 & 3	C3	6
10/29	90	Water	128.1	173.6	460	14.8	2R	3,6,9	1,2,3,4	C2	2-6-2
10/30	91	PC	124.8	136.9	460	5.3	2R	3,6,9	1,2,3,4	C2	2-6-2
10/30	92	Water	140.7	164.4	460	2.6	123R	3,6,9	1,2,3,4	C2	2-6-2
10/30	93	PC	128.7	122.7	460	10.7	173R	7,8,9	4	C1	2
10/30	94	PC	139.2	148.7	460	11.7	175R	3,6,9	1,2,3,4	C2	2-6-2
10/30	95	Water	144.3	116.8	460	12.5	170R	3,6,9	1,2,3,4	C2	2-6-2
10/31	96	PC	129.4	148.6	460	9.6	175R	2 & 8	1 & 4	C4	2
10/31	97	PC	132.5	147.8	460	14.0	162R	5	2 & 3	C3	6
10/31	98	Water	168.8	142.1	460	12.2	179L	4 & 6	2 & 3	C6	6
10/31	99	PC	128.9	164.7	460	1.7	130R	7,8,9	4	C4	2
11/1	100	PC	137.1	124.6	460	1.8	134L	7,8,9	4	C1	2
11/1	101	Water	134.6	160.4	460	1.1	120L	7,8,9	4	C1	2
11/1	102	PC	131.6	161.6	460	1.5	6L	2 & 8	1 & 4	C4	2

Date	Drop Number	Retardant	Drop Height (Feet)	Drop Speed (knots)	Drop Size (Gallons)	Wind Speed (mph)	Wind Direction (Degrees)	Tanks	Doors and/ or drop	Config.	Door rate
11/1	103	Water	127.0	164.1	460	2.0	18R	2 & 8	1 & 4	C4	2
11/1	104	Water	129.8	129.1	460	1.0	27L	2 & 8	1 & 4	C4	2
11/3	105	Water	305.5	129.1	235	1.5	155R	8	4	C16	2
11/3	106	PC	299.2	126.1	235	4.4	175L	8	4	C16	2
11/3	107	PC	334.7	125.4	345	3.3	150R	8 & 9	4	C17	2
11/3	108	Water	315.9	123.7	345	3.5	170R	8 & 9	4	C17	2
11/3	109	Water	324.0	131.2	690	3.3	165R	6 & 5	2 & 3	C11	6
11/4	110	Water	174.1	168.4	460	2.6	132L	5	2 & 3	C3	6
11/4	111	Water	322.4	125.4	920	2.4	178L	1,2,3,7,8,9	1 & 4	C9	2
11/4	112	PC	306.9	121.9	690	3.3	172L	5 & 6	2 & 3	C11	6
11/4	113	PC	283.0	92.8	460	4.0	118L	7,8,9	4	C1	2
11/4	114	PC	158.5	97	460	4.6	88L	7,8,9	4	C1	2
11/4	115	Water	331.7	106.8	460	2.5	145L	7,8,9	4	C1	2
11/4	116	Water	171.9	114.5	460	2.2	25L	7,8,9	4	C1	2
11/4	117	Water	165.4	183.3	460	2.0	2L	7,8,9	4	C1	2
11/4	118	Water	167.1	111.9	460	4.8	28R	5	2 & 3	C3	6

Date	Drop Number	Retardant	Drop Height (Feet)	Drop Speed (knots)	Drop Size (Gallons)	Wind Speed (mph)	Wind Direction (Degrees)	Tanks	Doors and/ or drop	Config.	Door rate
11/5	119	Water	343.6	112.7	460	5.5	10R	5	2 & 3	C3	6
11/5	120	PC	163.6 *	114.7	460	11.6	5R	5	2 & 3	C3	6
11/5	121	PC	144.5	172.3	460	8.3	10L	4 & 6	2 & 3	C6	6
11/5	122	Water	166.4	121.9	460	12.5	75L	4 & 6	2 & 3	C6	6
11/5	123	Water	153.4	167.8	460	6.8	8L	7,8,9	4	C1	2
11/6	124	Water	344.1	138.4	920	4.4	4R	4,5,6	2 & 3	C7	6
11/6	125	PC	348.2	197.3	460	10.9	15R	7,8,9	4	C1	2
11/6	126	PC	151.7	186.6	460	8.4	12R	7,8,9	4	C1	2
11/6	127	PC	162.3	136.1	460	6.6	2L	7,8,9	4	C1	6
11/7	128	Water	157.8	186.4	460	4.5	11L	5	2 & 3	C3	6
11/7	129	PC	315.7	131.0	460	2.4	12L	7,8,9	4	C1	6
11/7	130	Water	335.3	136.5	460	1.5	112L	7,8,9	4	C1	6
11/8	131	PC	329.3	179.9	460	.1	72R	5	2 & 3	C3	6
11/8	132	Water	153	113.2	460	6.8	178R	7,8,9	4	C1	6
11/8	133	Water	314.3	170.9	460	8.4	178R	7,8,9	4	C1	2

*300-foot target

Date	Drop Number	Retardant	Drop Height (Feet)	Drop Speed (knots)	Drop Size (Gallons)	Wind Speed (mph)	Wind Direction (Degrees)	Tanks	Doors and/ or drop	Config.	Door rate
11/11	134	Water	164.8	87.7	460	9.3	174R	5	2 & 3	C3	6
11/11	135	PC	161.2	90.5	460	12.2	172R	5	2 & 3	C3	6
11/11	136	Water	172.0	?	460	14.0	178R	7,8,9	4	C1	4
11/12	137	Water	345.8	123.4	460	3.2	92R	5	2 & 3	C3	3
11/12	138	Water	361.4	184.7	460	.1	105L	5	2 & 3	C3	6
11/12	139	Water	309.5	128.4	460	3.4	118L	5	2 & 3	C3	1
11/12	140	PC	307.1	126.4	460	2.1	85L	5	2 & 3	C3	1
11/12	141	PC	357.7	122.2	460	1.7	140R	5	2 & 3	C3	3
11/12	142	Water	174.1	121.2	460	.4	8R	5	2 & 3	C3	1
11/12	143	PC	173.7	182.6	460	.8	90L	5	2 & 3	C3	6
11/12	144	PC	317.6	125.7	460	1.6	35L	5	2 & 3	C3	7-1
11/12	145	Water	324.4	123.6	460	1.6	91L	5	2 & 3	C3	4
11/12	146	Water	329.8	126.3	460	3.3	161R	7,8,9	4	C1	4
11/13	147	PC	342.0	126.9	460	1.7	25R	5	2 & 3	C3	2
11/13	148	PC	337.3	104.0	460	1.0	135R	5	2 & 3	C3	(6)

Date	Drop Number	Retardant	Drop Height (Feet)	Drop Speed (knots)	Drop Size (Gallons)	Wind Speed (mph)	Wind Direction (Degrees)	Tanks	Doors and/ or drop	Config.	Door rate
11/13	149	PC	170.7	122.7	230	1.2	75L	8	4	C16	2
11/13	150	PC	331.4	130.6	460	1.0	13L	5	2 & 3	C3	4
11/13	151	Water	305.5	137.0	460	2.9	43L	5	2 & 3	C3	2
11/13	152	Water	172.1	131	460	2.2	3L	5	2 & 3	C3	2
11/13	153	Water	166.6	137.6	460	3.5	30R	5	2 & 3	C3	3
11/14	154	PC	339.2	130.8	460	2.0	47R	5	2 & 3	C3	6
11/14	155	PC	368.6	134.5	460	4.0	110L	5	2 & 3	C3	6
11/14	156	PC	377.3	179.2	460	6.9	161L	5	2 & 3	C3	6
11/14	157	PC	408.3	187.7	460	3.2	168L	5	2 & 3	C3	6
11/14	158	PC	370.2	187.1	460	2.6	179R	5	2 & 3	C3	6
11/14	159	PC	333.9	183.1	460	5.2	87R	5	2 & 3	C3	6
11/14	160	Fire-Trol	304.4	130.9	460	6.8	102L	5	2 & 3	C3	6
11/14	161	PC	336.8	186.4	460	.1	56L	5	2 & 3	C3	6
11/14	162	Water	301.4	128.4	460	1.3	70L	5	2 & 3	C3	6
11/19	163	.42 XA	334.5	129.2	460	3.4	170R	5	2 & 3	C3	6
11/19	164	.42 XA	313.5	122.9	460	4.4	135R	5	2 & 3	C3	6

Date	Drop Number	Retardant	Drop Height (Feet)	Drop Speed (knots)	Drop Size (Gallons)	Wind Speed (mph)	Wind Direction (Degrees)	Tanks	Doors and/ or drop	Config.	Door rate
11/19	165	931LC	350.8	124	460	1.2	150L	5	2 & 3	C3	6
11/19	166	931LC	342.0	133.9	460	2.4	15L	5	2 & 3	C3	6
11/19	167	Water	308.2	132.1	1035	10.2	7R	5,6,8,9	2,3,4	C18	2-6
11/19	168	1.60 XA	317.7	137.5	460	6.9	7R	5	2 & 3	C3	6
11/19	169	1.60 XA	340.6	133.0	460	4.5	18R	5	2 & 3	C3	6
11/20	170	PC	165.3	114.1	345	5.6	179R	7 & 8	4	C17	2
11/20	171	PC	324.2	118.6	460	5.5	175R	7,8,9	4	C1	4
11/20	172	PC	172.4	113.4	460	6.5	172L	7,8,9	4	C1	4
11/20	173	PC	175.9	116.0	460	9.5	168L	5	2 & 3	C3	1
11/20	174	Water	164.3	114.9	460	8.1	175L	5	2 & 3	C3	4
11/21	175	PC	325.0	120.6	460	3.1	170R	4,5,6	2 & 3	C13	6
11/21	176	PC	323.9	117.6	460	5.2	167R	2,5,8	1,2,3,4	C14	2-6
11/21	177	PC	173.1	120.5	460	5.9	173L	5	2 & 3	C3	6
11/21	178	PC	158.9	120.4	460	5.1	154R	5	2 & 3	C3	4
11/21	179	Water	336.4	119.8	920	6.2	177L	2,5,8	1,2,3,4	C10	2-6
11/21	180	PC	168.1	116.7	460	6.3	178L	5	2 & 3	C3	3

Date	Drop Number	Retardant	Drop Height (Feet)	Drop Speed (knots)	Drop Size (Gallons)	Wind Speed (mph)	Wind Direction (Degrees)	Tanks	Doors and/ or drop	Config.	Door rate
11/21	181	PC	195.6	117	460	6.8	172L	5	2 & 3	C3	2
11/21	182	PC	159.0	117.1	460	4.9	175R	5	2 & 3	C3	7/1
11/21	183	PC	321.7	117.2	920	4.0	168L	4,5,6	2 & 3	C7	6
11/21	184	Water	324.7	119.0	1380	1.7	122L	4,5,6 7,8,9	2,3,4	C19	6-2
11/22	185	PC	310.6	124.2	460	1.7	70L	1,2,3,4, 5,6,7,8,9	1,2,3,4	C15	2-6
11/22	186	PC	356.2	118.2	460	6.0	160L	4,5	2 & 3	C11	6
11/22	187	PC	167.4	118.0	690	6.9	157R	5,6	2 & 3	C11	6
11/22	188	Water	178.2	120.5	690	3.0	138R	5,6	2 & 3	C11	6
11/22	189	PC	353.6	126.5	460	3.5	73L	5,8	2,3,4	C12	6-2
11/22	190	PC	332.8	116.6	920	4.8	158R	4,5,6	2 & 3	C7	1
11/22	191	Water	352.0	117.1	920	3.7	178L	1,2,3 7,8,9	1 - 4	C9	6
11/24	192	Water	314.5	135.5	1840	2.3	150R	1,2,3,4, 5,6,7,8,9	1,2,3,4	C15	2-6
11/24	193	Water	339.3	129.0	960	.5	18R	4,5,6	2 & 3	C7	4
11/24	194	PC/FT	324.7	129.9	960	1.1	115R	1,2,3 7,8,9	1 & 4	C9	6
11/24	195	PC	338.4	127	960	3.2	171R	4,5,6	2 & 3	C7	4

Date	Drop Number	Retardant	Drop Height (Feet)	Drop Speed (knots)	Drop Size (Gallons)	Wind Speed (mph)	Wind Direction (Degrees)	Tanks	Doors and/ or drop	Config.	Door rate
11/24	196	Water	286.5	124.1	960	2.8	164L	1,4,7 3,6,9	1,2,3,4	C8	2 - 6
11/24	197	Water	161.8	122.4	960	1.2	44R	4,5,6	2 & 3	C7	6
11/25	198	Water	173.2	81.9 *	460	15.3	170R	5	2 & 3	C3	6 - 1
11/26	199	PC	163.8	136.1	460	8.9	8R	1,2,3,4, 5,6,7,8,9	1,2,3,4	C15	2 - 6
11/29	200	PC	167.1	128.7	460	5.3	40R	4,5,6	2 & 3	C13	6
11/29	201	PC	165.2	133.6	460	5.5	15R	2,5,8	1,2,3,4	C14	2 - 6
11/29	202	Water	170.4	135.1	460	14.4	10R	2,5,8	1,2,3,4	C14	2 - 6
12/1	203	PC	169.9	115.6	460	3.5	174R	4,5	2 & 3	C11	6
12/1	204	PC	177.0	118.4	460	7.2	178L	2,5	1,2,3	C12	2 - 6
12/1	205	Water	329.6	118.7	460	5.6	179R	2,5	1,2,3	C12	2 - 6
12/1	206	PC	333.7	117.0	1840	11.3	178R	all	all	C15	2 - 6
12/1	207	Water	318.8	110.0	460	6.2	168R	all	1,2,3,4	C15	2 - 6
12/2	208	Water	341.2	126.1	460	.1	140R	4,5,6	2 & 3	C13	6
12/2	209	Water	339.4	127.4	460	1.0	162L	2,5,7	1,2,3,4	C14	2 - 6
12/2	210	Water	321.0	123.6	460	2.6	178L	4,5	2 & 3	C11	6
12/2	211	Water	164.0	122.2	460	.5	178L	4,5	2 & 3	C11	6

*125-knot target

Date	Drop Number	Retardant	Drop Height (Feet)	Drop Speed (knots)	Drop Size (Gallons)	Wind Speed (mph)	Wind Direction (Degrees)	Tanks	Doors and/ or drop	Config.	Door rate
12/2	212	Water	164.7	124.4	460	1.4	52R	all	all	C15	2 - 6
12/2	213	Water	176.3	131.3	460	1.8	81R	5,8	2,3,4	C12	2 - 6
12/2	214	Water	190.0	119.8	460	2.4	80L	4,5,6	2 & 3	C13	6
12/2	215	PC XA	337.2	127.7	1380	4.0	50R	1,2,3, 4,5,6	1,2,3	C19	2 - 6
12/2	216	PC XA	338.3	128.6	690	4.2	40R	4,5	2 & 3	C11	6
12/2	217	Water	384.0	135.7	690	3.3	22R	4,5	2 & 3	C11	6
12/3	218	PC XA	349.3	127.3	1035	.1	100R	5,6,8,9	2,3,4	C18	2 - 6
12/3	219	PC XA	333.2	125.1	920	4.7	160L	4,5,6	2 & 3	C7	2
12/3	220	PC XA	314.6	126.0	920	2.6	105L	1,2,3 7,8,9	1 & 4	C9	2
12/3	221	Water	336.2	125.5	460	3.5	158L	7,8,9	4	C1	6
12/3	222	Water	348.6	124.5	920	1.4	145L	4,5,6	2 & 3	C7	1
12/3	223	PC XA	310.5	120.0	920	3.0	128L	2,5,8	1,2,3,4	C10	2 - 6
12/3	224	PC XA	322.0	124.9	920	1.5	108R	1,4,7 3,6,9	1,2,3,4	C8	2 - 6
12/3	225	Water	328.3	121.7	920	1.1	140R	4,5,6	2 & 3	C7	2
12/6	226	PC XA	346.4	130.1	920	3.1	174L	1,2,3 7,8,9	1 & 4	C9	6

Date	Drop Number	Retardant	Drop Height (Feet)	Drop Speed (knots)	Drop Size (Gallons)	Wind Speed (mph)	Wind Direction (Degrees)	Tanks	Doors &/ or Drop	Config.	Door Rate
12/6	227	PC XA	316.8	126.8	460	3.6	174R	5	2,3	C3	7/1
12/6	228	PC XA	175.1	122.8	460	6.1	172R	5	2,3	C3	7/1
12/6	229	Water	176.4	121.5	230	7.4	165R	8	4	C16	2
12/6	230	Water	321.5	119.1	460	6.8	153L	5	2 & 3	C3	7/1
12/6	231	Water	180.1	125.3	460	7.3	148L	5	2 & 3	C3	7/1
12/6	232	PX/FT	325.2	122.4	920	6.0	170L	1,2,3 7,8,9	1 & 4	C9	6
12/6	233	PC XA	154.7	101.4	460	4.8	158L	5	2 & 3	C3	6
12/12	234	FT 100	331.9	?	460	8.6	176L	5	2 & 3	C3	6
12/12	235	FT 100	323.2	?	460	12.5	177R	5	2 & 3	C3	6
12/12	236	PC XA	163.1	?	920	20.3	178R	4,5,6	2 & 3	C7	1
12/12	237	PC XA	176.6	?	920	16.8	175R	4,5,6	2 & 3	C7	2
12/12	238	FT 931	173.4	107.7 *	460	16.8	176R	5	2 & 3	C3	6
12/13	239	FT 100	345.0	134.7	460	4.9	38R	5	2 & 3	C3	6
12/13	240	FT 100	350.4	131.6	460	4.4	20R	5	2 & 3	C3	6
12/13	241	FT 100	333.2	123.3	460	2.2	67R	5	2 & 3	C3	6
12/13	242	PC XA	459.8	119.1	920	1.0	80R	4,5,6	2 & 3	C7	6
12/15	243	PC XA	523.1	128,5	460	.1	70L	5	2 & 3	C3	6
12/15	244	Water	526.8	123.3	920	4.7	175R	4,5,6	2 & 3	C7	6
12/15	245	Water	161.5	114.7	460	5.2	174L	5	2 & 3	C3	6

*125-knot target

TEST MATRIX NO. 1

FLOW RATE STUDY - CENTRAL TANK (2L x W)

BASIS: The variables that control flow rate and thus the ground distribution pattern from a fixed size tank are the exit area, and the door opening rate.

PHOS-CHEK XA

Drop No. (Wind Speed)

	EXIT AREA							
	.25		.50		.75		1.00	
DROP HEIGHT	RATE 6	RATE 2	RATE 6	RATE 2	RATE 6	RATE 2	RATE 6	RATE 2
150 FEET	8 (5.6)	6 (1.8)	32 (3.3)	33 (1.4)	3 (1.8) 4 (3.1)	5 (1.2)	40 (1.2)	41 (1.0)
300 FEET	11 (2.5)	12 (1.9)	37 (1.4)	35 (0.5)	2 (1.8) 1 (4.9)	9 (6.6)	38 (3.0)	34 (3.9)

WATER

	EXIT AREA							
	.25		.50		.75		1.00	
DROP HEIGHT	RATE 6	RATE 2	RATE 6	RATE 2	RATE 6	RATE 2	RATE 6	RATE 2
150 FEET	27 (3.3)	7 (1.0)	42 (1.7)	43 (2.5)	16 (4.6)	15 (5.0)	44 (0.9)	45 (3.3)
300 FEET	17 (5.1)	19 (2.0) 28 (2.8)	30. (1.3)	31 (2.9)	18 (3.3)	13 (2.8) 14 (4.6)	39 (2.0)	36 (1.6)

Note: The number in parenthesis indicates wind velocity for that particular drop.

TEST MATRIX NUMBER 2

CONFIGURATION STUDIES

BASIS: The shape of the tank as it relates to pattern development will be studied in this series. Currently the simulation models do not make a distinction on these variables, and the determination of the ground pattern arises thru the flow rate function. Two separate drops with the same total flow rate function are represented by the same simulation, whatever the geometry. Since the flow rate depends on configuration this experimental study will examine configuration and measure the effect of flowrate (flow rate is held constant) to see how pattern development is affected.

PHOS-CHEK XA

DROP HEIGHT (FEET)	AIRCRAFT VELOCITY (KNOTS)	CONFIGURATION C_1	C_2	C_3	C_4	C_5	C_6
		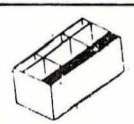	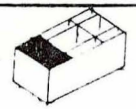	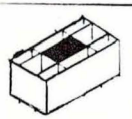	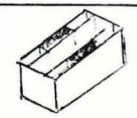	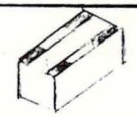	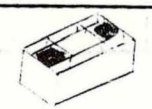
150	125	Drop No. (Wind Speed) 10 (10.8) 93 (10.7) 65 (8.9) 55 (16.2) 100 (1.8) 91 (5.3)		40 (1.2) 57 (19.5)	50 (7.2)	54 (10.0)	64 (8.8) 88 (5.4)
	160	71 (9.1) 61 (23.5) 67 (2.8) 99 (1.7) 94 (11.7)		85 (4.5) 97 (14.0)	75 (13.0) 96 (9.6) 102 (1.5)	73 (7.0)	87 (1.1) 121 (8.3)
300	125	26 (1.0)	25 (2.4)	38 (3.0) 154 (2.0) 155 (4.0)	46 (1.2)	52 (2.8)	48 (2.3)
	160	77 (1.3)	66 (1.0)	69 (3.2)	79 (5.4)	81 (8.8)	82 (2.8)

WATER

150	125	21 (3.0) 56 (13.0)	29 (2.6) 95 (12.5)	44 (0.9) 58 (19.3)	51 (9.1) 104 (1.0)	53 (10.1) 59 (16.8)	63 (5.6) 122 (12.5)
	160	76 (14.0) 123 (6.8) 60 (18.7) 101 (1.1)	90 (14.8) 92 (2.6)	89 (8.4) 111 (2.4)	72 (11.2) 103 (2.0)	74 (14.6)	86 (2.3) 98 (12.0)
300	125	23 (2.3)	24 (4.3)	162 (1.3) 39 (2.0)	47 (5.2)	62 (2.5)	49 (5.8)
	160	78 (4.5)	68 (1.3)	70 (2.8)	80 (8.6)	84 (0.6)	83 (1.0)

TEST MATRIX NUMBER 3
1000 Gallon Load Size Series

The objective of this matrix was to provide additional information on configuration and separation

Phos-Chek XA

Drop No. (Wind Speed)

Configuration	C7				C8	C9		C10
	Tanks 4,5,6				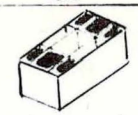 Tanks 1,4,7,3,6,9	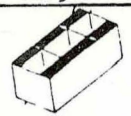 Tanks 1,2,3,7,8,9		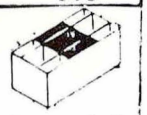 Tanks 2,5,8
Door rate	6	4	2	1	6	2	6	6
Drop Height 150			237 (16.8)	236 (20.3)				
300	183 (4.0)	195 (3.2)	219 (4.7)	190 (4.8)	224 (1.5)	220 (2.6)	194 (1.1)* 226 (3.1) 232 (6.0)**	223 (3.0)
500	242 (1.0)							

Water

* 194 Special PC and FT 100
** 232 Special PC and FT 931

Configuration	C7				C8	C9		C10
Door rate	6	4	2	1	6	2	6	6
Drop Height 150	197 (1.2)							
300	124 (4.4)	193 (0.5)	225 (1.1)	222 (1.4)	196 (2.8)	111 (2.4)	191 (3.7)	179 (6.2)
500	244 (4.7)							

TEST MATRIX NUMBER 4
Head Height Effect Study - 460 Gallons

Phos-Chek XA

Drop No. (Wind Speed)

Drop Height (Feet)	2/3 head		1/2 head		1/4 head
	C11 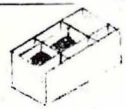 Tanks 4&5	C12 Tanks 2&5	C13 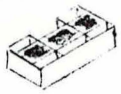 Tanks 4,5,6	C14 Tanks 2,5,8	C15 All Tanks
150	203 (3.5)	204 (7.2)	200 (5.3)	201 (5.5)	199 (8.9)
300	186 (6.0)	189 (3.5)	175 (3.1)	176 (5.2)	185 (1.7)

Water

Drop Height (Feet)	2/3 head		1/2 head		1/4 head
	C11	C12	C13	C14	C15
150	211 (0.5)	213 (1.8)	214 (2.4)	202 (14.4)	212 (1.4)
300	210 (2.6)	205 (5.6)	208 (0.1)	209 (1.0)	207 (6.2)

The objective of this matrix was to evaluate the effect of downloading, or tanks designed with short height, on pattern formation

TEST MATRIX NUMBER 5
LOAD SIZE TEST SERIES

Phos-Chek XA

Drop No. (Wind Speed)

Drop Height (Feet)	Load Size (Gallons) 230 C16 Tank 8 or 2	345 C17 Tanks 7 &8 or equivalent	460 C1 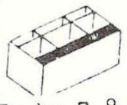 Tanks 7,8,9 or 1,2,3	690 C11 Tanks 5,6 or 4,5	920 C7 Tanks 4,5,6	1035 C18 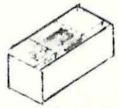 Tanks 5,6,8,9 or equivalent	1380 C19 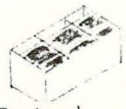 Tanks 4 -- 9 or equivalent	1840 C15 All Tanks
150	149 (1.2)	170 (5.6)	93 (10.1) 10 (10.8) 55 (16.2)	187 (6.9)				
300	106 (4.4)	107 (3.3)	26 (1.0)	112 (3.3) 216 (4.2)	183 (4.0)	218 (0.1)	215 (4.0)	206 (11.3)

Water

Drop Height (Feet)	Load Size (Gallons) 230 C16	345 C17	460 C1	690 C11	920 C7	1035 C18	1380 C19	1840 C15
150	229 (7.4)		21 (3.0) 56 (13.0)	188 (3.0)	197 (1.2)			
300	105 (1.5)	108 (3.5)	23 (2.3)	217 (3.3) 109 (3.3)	124 (4.4)	167 (10.2)	184 (1.7)	192 (2.3)

The objective of this matrix was to assess the effect of quantity on pattern performance

TEST MATRIX NUMBER 6
AIR SPEED TEST MATRIX (460 Gallon Drops)

Phos-Chek XA

Drop No. (Wind Speed)

Drop Height (Feet)	Configuration and Air speed (knots)							
	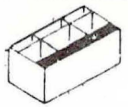 C1, Rate 2				C3, Rate 6			
	100	125	160	180	100	125	160	180
150	114 (4.6)	10 (10.8) 55 (16.3) 93 (10.7) 100 (1.8)	61 (23.5) 71 (9.1) 99 (1.7)	126 (8.4)	135 (12.2) 233 (4.8)	40 (1.2) 57 (19.5)	85 (4.5) 97 (14.0)	143 (0.8)
300	113 (4.0)	26 (1.0)	77 (1.3)	125 (10.9)	120 (11.6) 148 (1.0)	38 (3.0)	69 (2.8)	159 (5.2) 131 (0.1) 161 (0.1) 156 (6.9) 157 (3.2) 158 (2.6)

Water

Drop Height (Feet)	Configuration and Air Speed (knots)							
	C1				C3			
	100	125	160	180	100	125	160	180
150	116 (2.2)	21 (3.0)	60 (18.7) 76 (14.0) 101 (1.1)	117 (2.0)	118 (4.8) 134 (9.5)	44 (0.9) 58 (19.3)	89 (8.4) 110 (2.6) (leak)	128 (4.5)
300	115 (2.5)	23 (2.3)	78 (4.5)	133 (8.4)	119 (11.6)	39 (2.0)	70 (2.8)	138

The objective of this matrix was to ascertain the effect of velocity on configurational differences in pattern generation

TEST MATRIX NUMBER 7
ADDITIONAL DOOR RATE STUDIES (460 Gallons)

Phos-Chek XA

Drop No. (Wind Speed)

Drop Height (Feet)	Configuration and door rate											
	C3					C1			C3 Dual Door Rate			
	1	2	3	4	6	2	4	6	7-1			
150	173 (9.5)	181 (6.8)	180 (6.3)	178 (3.1)	40 (1.2) 57 (19.5) 177 (5.9)	10 (10.8) 55 (16.3) 93 (10.7)	172 (6.5)	127 (6.6)	182 (4.9) 228 (6.1)	(not dual door rate)		
300	140 (2.1)	147 (1.7)	141 (1.7)	150 (1.0)	38 (3.0)	26 (1.0)	171 (5.5)	129 (2.4)	144 (1.6) 227 (3.6)	(Not dual door rate)		

Water

Drop Height (Feet)	Configuration and door rate											
	C3					C1			C3 Dual Door Rate			
	1	2	3	4	6	2	4	6	7-1			
150	142 (2.4)	152 (2.2)	153 (3.5)	174 (8.1)	245 (5.2)	21 (3.0) 56 (13.0)	136 (14.0)	132 (6.8)	231 (7.3)	198 (5.3)		
300	139 (3.4)	151 (2.9)	137 (3.2)	145 (1.6)	39 (2.0) 162 (1.3)	23 (2.3)	146 (3.3)	221 (3.5) 130 (1.5)	230 (6.8)			

TEST MATRIX NUMBER 8

SHOCK-HYDRODYNAMICS--RETARDANT RHEOLOGICAL PROPERTIES
TANK C5, DOOR RATE 6, 460 GALLONS, 300 FOOT DROP HEIGHT

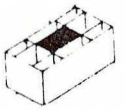

All Drops in Config. C3

Retardant	Drop Number	Drop Height (Feet)	Aircraft Speed (Knots)	Wind Speed (mph)	Wind Direction (Degrees)
Phos-Chek XA	154	300 339.2	125 130.8	2.0	47R
Phos-Chek XA	155	300 368.6	125 134.5	4.0	110L
Phos-Chek XA	156	300 377.8	180 179.2	6.9	161L
Phos-Chek XA	157	300 408.8	180 187.7	3.2	168L
Phos-Chek XA	158	300 370.2	180 187.1	2.6	179R
Phos-Chek XA	159	300 339.2	180 183.1	5.2	87R
Phos-Chek XA	161	300 336.8	180 186.4	0.1	56L
Fire-Trol 100	160	300 304.4	125 130.9	6.8	102L
Water	162	300 301.4	125 128.4	1.3	70L
Fire-Trol 931L	165	300 350.8	125 124.0	1.2	150L
Fire-Trol 931L	166	300 342.0	125 133.9	2.4	15L
Phos-Chek .42 XA	163	300 334.5	125 129.3	3.4	170R
Phos-Chek .42 XA	164	300 313.5	125 122.9	4.4	135R
Phos-Chek 1.60 XA	168	300 317.5	125 137.5	6.9	7R
Phos-Chek 1.60 XA	169	300 340.6	125 133.0	4.5	18R

Thesis/
Reports
SWANSON,
D.H.

Experimental tank and Grating Systems

This report is published as a part of a program to improve fire control technology, specifically through the use of fire retardant chemicals and delivery systems whose chemical and/or design characteristics are tailored to fuel and fire situation needs. This program is being conducted at the Northern Forest Fire Laboratory. Information or questions regarding these studies should be directed to the

Northern Forest Fire Laboratory
Drawer G
Missoula, Montana 59801

Use of trade or film names* is for vendor information only and does not constitute endorsement by the U.S. Department of Agriculture of any commercial product or service

* Phos-Chek is a registered trademark of the Monsanto Co